Millstone Power Station Unit 3
Safety Analysis Report

Chapter 4: Reactor

CHAPTER 4—REACTOR

Table of Contents

CHAPTER 4—REACTOR
Table of Contents (Continued)

CHAPTER 4—REACTOR
Table of Contents (Continued)

CHAPTER 4—REACTOR
Table of Contents (Continued)

CHAPTER 4—REACTOR
Table of Contents (Continued)

CHAPTER 4—REACTOR
Table of Contents (Continued)

CHAPTER 4—REACTOR
Table of Contents (Continued)

CHAPTER 4—REACTOR

List of Tables

NOTE: REFER TO THE CONTROLLED PLANT DRAWING FOR THE LATEST REVISION.

CHAPTER 4—REACTOR

List of Figures

NOTE: REFER TO THE CONTROLLED PLANT DRAWING FOR THE LATEST REVISION.

CHAPTER 4-REACTOR
List of Figures (Continued)

NOTE: REFER TO THE CONTROLLED PLANT DRAWING FOR THE LATEST REVISION.

CHAPTER 4-REACTOR
List of Figures (Continued)

NOTE: REFER TO THE CONTROLLED PLANT DRAWING FOR THE LATEST REVISION.

CHAPTER 4-REACTOR
List of Figures (Continued)

CHAPTER 4 – REACTOR

4.1   SUMMARY DESCRIPTION

This chapter describes: 1) the mechanical components of the reactor and reactor core, including the fuel rods and fuel assemblies, 2) the nuclear design, and 3) the thermal-hydraulic design.

The initial reactor core was composed of an array of 193 fuel assemblies identical in mechanical design, but different in fuel enrichment. Within each fuel assembly, for the initial core, all fuel was of the same enrichment. Three different enrichments were employed in the first core. These enrichments were 2.42 (Region 1), 2.90 (Region 2), and 3.40 (Region 3) weight percent. Subsequent reactor cores used fuel with enrichments as noted in Table 4.1-1.

A fuel assembly from any region is composed of 264 fuel rods in a 17 by 17 square array. The center position in the fuel assembly is reserved for incore instrumentation. The remaining 24 positions in the fuel assembly have guide thimbles for the rod cluster control assemblies (RCCA's). The guide thimbles are joined to the bottom nozzles of the fuel assembly and also serve to support the fuel grids. The fuel grids, including the intermediate flow mixers (IFMs), consist of an "egg-crate" arrangement of interlocked straps that maintain lateral spacing between the rods. The straps have spring fingers and dimples which grip and support the fuel rods. The middle grids also have coolant-mixing vanes. The fuel rods consist of slightly enriched uranium, in the form of cylindrical pellets of uranium dioxide, contained in Zircaloy-4, ZIRLO, or Optimized ZIRLO tubing. The tubing is plugged and seal-welded at the ends to encapsulate the fuel. All fuel rods are pressurized internally with helium during fabrication to reduce clad creep down during operation and thereby to increase fatigue life.

Depending on the position of the assembly in the core, the guide thimbles are used for RCCAs, neutron source assemblies, or burnable absorber assemblies (used in Cycles 1 and 2). If none of these are required, the guide thimbles may be fitted with plugging devices to limit bypass flow or left open.

The bottom nozzle is a box-like structure which serves as the lower structural element of the fuel assembly and directs the coolant flow distribution to the assembly. The top nozzle assembly serves as the upper structural element of the fuel assembly and provides a partial protective housing for the RCCA or other components.

The RCCA's consist of 24 absorber rods fastened at the top end to a common hub or spider assembly. Each absorber rod consists of an alloy of silver-indium-cadmium (Ag-In-Cd). The initial reactor core used RCCA's with hafnium as the neutron absorber. All hafnium RCCA's were removed at the end of Cycle 4. Ag-In-Cd RCCA's are clad in stainless steel, chromed stainless steel or stainless steel with an ion-nitrided surface treatment. The RCCA's are used to control relatively rapid changes in reactivity and to control the axial power distribution.

The reactor core is cooled and moderated by light water at conditions as noted in Table 4.1-1. Soluble boron in the moderator/coolant serves as a neutron absorber. The concentration of boron is varied to control reactivity changes that occur relatively slowly, including the effects of fuel

burnup and transient xenon. Burnable absorbers assemblies were employed in the reactor core in Cycles 1 and 2 to limit the amount of soluble boron required and thereby to maintain the desired negative reactivity coefficients. Starting in Cycle 3, burnable absorbers have been in the form of a boron coating on some fuel pellets called integral fuel burnable absorbers (IFBA).

The nuclear design analyses establish the core locations for fresh and reinserted fuel assemblies and define design parameters, such as fuel enrichments and boron concentration in the coolant. The nuclear design analyses establish that the reactor core and the reactor control system satisfy all design criteria, even if the highest reactivity worth RCCA is in the fully withdrawn position. The core has inherent stability against diametral and azimuthal power oscillations. Axial power oscillations which may be induced by load changes and resultant transient xenon may be suppressed by the use of control rods (RCCA's).

The thermal-hydraulic design analyses establish that adequate heat transfer is provided between the fuel clad and the reactor coolant. The thermal design takes into account local variations in dimensions, power generation, flow distribution, and mixing. The mixing vanes incorporated in the fuel assembly spacer grid design and IFMs induce additional flow-mixing between the various flow channels within a fuel assembly as well as between adjacent assemblies.

The performance of the core is monitored by fixed neutron detectors outside of the core, movable neutron detectors within the core, and thermocouples at the outlet of selected fuel assemblies. The ex-core nuclear instrumentation provides input to automatic control functions.

Table 4.1-1 presents the principal nuclear, thermal-hydraulic, and mechanical design parameters of Millstone 3.

The analytical techniques employed in the core design are tabulated in Table 4.1-2. The mechanical loading conditions considered for the core internals and components are tabulated in Table 4.1-3. Specific or limiting loads considered for design purposes of the various components are listed as follows: fuel assemblies in Section 4.2.1.5 and neutron absorber rods, burnable absorbers, neutron source rods, and thimble plug assemblies in Section 4.2.1.6. The dynamic analyses, input forcing functions, and response loadings for the control rod drive system and reactor vessel internals are presented in Sections 3.9N.4 and 3.9N.5. The effects of fuel densification have been evaluated with the methods described in Sections 4.2.1.2 and 4.4.2.11.

TABLE 4.1-1 REACTOR DESIGN PARAMETER TABLE

MPS-3

Thermal and Hydraulic Design Parameters

1.	Reactor core heat output (MWt)	3709****
2.	Reactor core heat output (10^6 Btu/hr)	12,656****
3.	Heat generated in fuel (percent)	97.4
4.	System pressure, nominal (psia)	2,250
5.	System pressure, minimum steady state (psia)	2,200
6.	Minimum departure from nuclear boiling ratio for design transients	See Table 4.4-4
7.	DNB correlation	WRB-2M *

Coolant Flow

8.	Total thermal flow rate (10^6 lb/hr)	135.5
9.	Effective flow rate for heat transfer (10^6 lb/hr)	123.9
10.	Effective flow area for heat transfer (ft^2):	
	Full core of RFA / RFA-2 fuel	51.1
11.	Average velocity along fuel rods (ft/sec):	
	Full core of RFA / RFA-2 fuel	14.5
12.	Average inlet mass velocity (10^6 lb/hr-ft^2):	
	Full core of RFA / RFA-2 fuel	2.42

Coolant Temperature

13.	Nominal inlet (°F)	555.8
14.	Average rise in vessel (°F)	67.4
15.	Average rise in core (°F)	72.9
16.	Average in core (°F)	594.7
17.	Average in vessel (°F)	589.5

Heat Transfer

18.	Active heat transfer, surface area (ft^2)	59,700
19.	Average heat flux (Btu/hr-ft^2)	206,500
20.	Maximum heat flux for normal operation (Btu/hr-ft^2)	526,100
21.	Average linear power (kW/ft)	5.92 **

TABLE 4.1-1 REACTOR DESIGN PARAMETER TABLE (CONTINUED)

22.	Peak linear power for normal operation (kW/ft)	15.09****
23.	Peak linear power resulting from overpower transients/operator errors, assuming a maximum overpower of 121 percent (kW/ft)	22.6
24.	Heat flux hot channel factor (F_Q)	2.548 ***
25.	Peak fuel central temperature for prevention of centerline melt (°F)	4,700

Core Mechanical Design Parameters

26.	Design	RCC canless 17 x 17
27.	Number of fuel assemblies	193
28.	UO_2 rods per assembly	264
29.	Rod pitch (in.)	0.496
30.	Overall dimensions (in.)	8.426 x 8.426
31.	Fuel weight (MTU) (Typical)	87.8
32.	Clad weight (lb) (Typical)	45,300
33.	Number of grids per assembly	12 (RFA/RFA-2) [#]
34.	Loading technique	Low Leakage

Fuel Rods

35.	Number	50,952
36.	Outside diameter (in.)	0.374
37.	Diametral gap (in.)	0.0065
38.	Clad thickness (in.)	0.0225
39.	Clad material	Zircaloy-4 (Regions 1 through 6)
		ZIRLO (Regions 7 through 17)
		Optimized ZIRLO (Beginning with Region 18)

Fuel Pellets

40.	Material	UO_2 sintered
41.	Density, percent of theoretical	95.0 Regions 1 - 5
		95.5 Regions 6 and later
42.	Diameter (in.)	0.3225
43.	Length (in.)	

TABLE 4.1-1 REACTOR DESIGN PARAMETER TABLE (CONTINUED)

Enriched

Square - Regions 1-3	0.530
Standardized - Beginning with Region 4	0.387

Axial Blanket

Original - Regions 5-6	0.545
Annular - Regions 7-10	0.462
Annular - Beginning with Region 11	0.500

Rod Cluster Control Assemblies

44.	Neutron absorber	Ag-In-Cd
45.	Cladding material	Type 304 SS-cold worked
		(with or without chrome plating) – Westinghouse design
		Type 316L SS
		(with ion-nitrided surface treatment) – AREVA design
46.	Clad thickness	0.0185
47.	Number of clusters, full length / part length	61/-
48.	Number of absorber rods per cluster	24

Core Structure

49.	Core barrel, I.D./O.D.(in.)	148.0 / 152.5
50.	Reactor vessel shielding	Neutron panel design
51.	Baffle thickness (in.)	0.875

Structure Characteristics

52.	Core diameter, equivalent (in.)	132.7
53.	Core height, active fuel (in.) (Cold nominal)	144

Reflector Thickness and Composition

54.	Top, water plus steel (in) (approximate)	10
55.	Bottom, water plus steel (in.) (approximate)	10
56.	Side, water plus steel (in.) (approximate)	15
57.	H_2O/U molecular ratio core, lattice, cold	2.39

Fuel Enrichment (weight percent)

58.	Region 1	2.42
59.	Region 2	2.90
60.	Region 3	3.40

TABLE 4.1-1 REACTOR DESIGN PARAMETER TABLE (CONTINUED)

61.	Regions 4A/4B	3.5 / 3.8
62.	Regions 5A/5B	4.1 / 4.5
63.	Regions 6A/6B	4.2 / 4.5
64.	Region 7	4.4
65.	Region 8	4.6
66.	Regions 9A / 9B	4.4 / 4.8
67.	Regions 10A / 10B	4.4 / 4.8
68.	Regions 11A / 11B	4.2 / 4.7
69.	Regions 12A / 12B / 12C	4.7 / 4.95 / 4.95
70.	Regions 13A / 13B	4.0 / 4.95
71.	Regions 14A / 14B	4.7 / 4.95
72.	Beginning with Region 15 (Cycle 13)	The reload region is a 'split-batch' with typical fuel assembly enrichments of 4.10 and 4.95 weight percent.

NOTES:

* The ABB-NV and WLOP Correlations are used for analyses in which the WRB-2M correlation is not applicable. W-3 may also be used where WRB-2M is not applicable.

** Based on an average active fuel stack height of 143.7 in.

*** This is the maximum value of F_Q for normal operation using ASTRUM to support MUR operation.

****Values correspond to a Rated Thermal Power (RTP) of 3709 MWt. Thermal-hydraulic analyses considered a bounding RTP of 3712 MWt.

Includes the protective bottom grid (P–grid) (Regions 9–16) or Robust Protective Grid (RPG) (starting with Region 17) which is a feature of the RFA/RFA–2.

TABLE 4.1-2 ANALYTICAL TECHNIQUES IN CORE DESIGN

Analysis	Technique	Computer Code	Section Referenced
Mechanical design of core internals loads, deflections, and stress analysis	Static and Dynamic Modeling	MULTIFLEX, FORCE 2, LATFORC, finite element, structural analysis code, and others	3.7(N).2.1
			3.9N.2
			3.9N.3
Fuel rod design			
Full performance characteristics (temperature, internal pressure, clad stress, etc.)	Semi-empirical thermal model of fuel rod with consideration of fuel density, changes, heat transfer, fission gas release, etc.	Westinghouse fuel rod design model	4.2.1.1
			4.2.3.2
			4.2.3.3
			4.3.3.1
			4.4.2.11
Nuclear design			
1. Cross sections and group constants	Microscopic data; macroscopic constants for homogenized core regions	Modified ENDF/B-VII library Casmo5	4.3.3.2
			4.3.3.2
2. X-Y and X-Y-Z power distributions, fuel depletion critical boron concentrations, X-Y and X-Y-Z xenon distributions, reactivity coefficients	Multi-group nodal theory	Simulate5	4.3.3.3

TABLE 4.1-2 ANALYTICAL TECHNIQUES IN CORE DESIGN

	Analysis	Technique	Computer Code	Section Referenced
3.	Axial power distributions, control rod worths, and axial xenon distribution	Multi-group nodal theory	Simulate5	4.3.3.3
4.	Criticality of reactor and fuel assemblies	3-D Monte Carlo theory	AMPX system of codes, KENO-Va.	4.3.2.6
5.	Vessel irradiation	Multi-group spatial dependent transport theory	DOT	4.3.2.8
Thermal-hydraulic design				
1.	Steady state	Subchannel analysis of local fluid conditions in rod bundles, including inertial and cross-flow resistance terms, solution progresses from corewide to hot assembly to hot channel	VIPRE-D	4.4.4.5.2
2.	Transient	Subchannel analysis of local fluid conditions based on time dependent system conditions	VIPRE-D	4.4.4.5.4

TABLE 4.1-3 DESIGN LOADING CONDITIONS FOR REACTOR CORE COMPONENTS

1.   Fuel assembly weight and core component weights, (BPs, sources, plugging devices).

2.   Fuel assembly spring forces and core component spring forces.

3.   Internals weight.

4.   Control rod trip (equivalent static load).

5.   Differential pressure.

6.   Spring preloads.

7.   Coolant flow forces (static).

8.   Temperature gradients.

9.   Differences in thermal expansion.

   a.   Due to temperature differences

   b.   Due to expansion of different materials.

10.   Interference between components.

11.   Vibration (mechanically or hydraulically induced).

12.   One or more loops out of service.

13.   All operational transients listed in Table 3.9N–1.

14.   Pump overspeed.

15.   Seismic loads (Operating Basis Earthquake and Safe Shutdown Earthquake).

16.   Blowdown forces (due to cold and hot leg break).

4.2   FUEL SYSTEM DESIGN

Plant conditions for design are divided into four categories in accordance with their anticipated frequency of occurrence and risk to the public: Condition I - Normal Operation; Condition II - Incidents of Moderate Frequency; Condition III - Infrequent Incidents; Condition IV - Limiting Faults. Chapter 15 describes bases and plant operation and events involving each condition.

The reactor is designed so that its components meet the following performance and safety criteria:

1.   The mechanical design of the reactor core components and their physical arrangement, together with corrective actions of the reactor control, protection, and emergency cooling systems (when applicable), ensure that:

   a.   Fuel damage will not occur during Condition I and Condition II events. (Fuel damage, as used here, is defined as penetration of the fission product barrier, i.e., the fuel rod clad.) It is not possible, however, to preclude a very small number of rod failures. These failures are within the capability of the plant cleanup system and are consistent with plant design bases.

   b.   The reactor can be brought to a safe state following a Condition III event with only a small number of fuel rods damaged, although sufficient fuel damage might occur to preclude immediate resumption of operation. (In any case, the fraction of fuel rods damaged must be limited so as to meet the dose guidelines of 10 CFR 50.67).

   c.   The reactor can be brought to a safe state and the core can be kept subcritical with acceptable heat transfer geometry following transients arising from Condition IV events.

2.   Fuel assemblies are designed to withstand loads induced during shipping, handling, and core loading without exceeding the criteria of Section 4.2.1.5.

3.   Fuel assemblies are designed to accept control rod insertions to provide the required reactivity control for power operations and reactivity shutdown conditions.

4.   All fuel assemblies have provisions for the insertion of incore instrumentation necessary for plant operation.

5.   The reactor internals, in conjunction with the fuel assemblies and incore control components, direct reactor coolant through the core to achieve acceptable flow distribution and to restrict bypass flow to assure heat transfer performance requirements for all modes of operation. Other thermal and hydraulic design concerns such as fuel uplift, crud deposition, and fuel clad temperatures are discussed in Section 4.4.

4.2.1   DESIGN BASES

For the 17 x 17 STD, V5H, RFA/RFA-2 fuel assemblies, Next Generation Fuel (NGF) Lead Test Assemblies (LTAs), and 17 x 17 RFA-2 with AXIOM fuel cladding LTAs the fuel rod and fuel assembly design bases are established to satisfy the general performance and safety criteria presented in Section 4.2.

The fuel rods from Regions 1 through 4 are designed for a rod pellet burnup of approximately 50,000 megawatt days per metric ton of uranium (MWD/MTU) in the fuel cycle equilibrium condition. Starting from fuel Region 5, the design peak rod burnup is increased to approximately 60,000 MWD/MTU.

The detailed fuel rod design establishes parameters that include pellet size and density, clad/pellet diametral gap, gas plenum size, and helium prepressurization level. The design also considers effects such as fuel density changes, fission gas release, clad creep, and other physical properties which vary with burnup. The fuel rods are designed to prevent excessive fuel temperatures (Section 4.2.1.2), excessive internal rod gas pressures (Section 4.2.1.3) due to fission gas releases, and excessive cladding stresses, strains, and strain fatigue (Section 4.2.1.1). This is achieved by designing the fuel rods so that the conservative design bases in the following subsections are satisfied during Condition I and Condition II events over the fuel lifetime. For each design basis, the performance of the limiting fuel rod must not exceed the limits specified by the design basis.

Integrity of the fuel assembly structure is ensured by setting limits on stresses and deformations due to various loads and by preventing the assembly structure from interfering with the functioning of other components. Three types of loads are considered:

1.   Nonoperational loads such as those due to shipping and handling

2.   Normal and abnormal loads defined for Conditions I and II

3.   Abnormal loads defined for Conditions III and IV

The design bases for the incore control components are described in Section 4.2.1.6.

Other supplemental fuel design criteria/limits are given in References 4.2-21 and 4.2-22.

4.2.1.1   Cladding

1.   Materials and Mechanical Properties

Zircaloy-4, ZIRLO or Optimized ZIRLO tubing combine neutron economy (low absorption cross section); high corrosion resistance to coolant, fuel, and fission products; and high strength and ductility at operating temperatures. Optimized ZIRLO fuel rod cladding is implemented because it provides improved corrosion resistance as compared to ZIRLO. Optimized ZIRLO fuel rod cladding has a lower tin content than ZIRLO and the thermal and mechanical processing of the cladding

has also been optimized. The resulting material has mechanical properties similar to ZIRLO, while offering improved resistance to general corrosion. The reduced corrosion of Optimized ZIRLO cladding extends the operational capability of the cladding. Reference 4.2-6 documents the operating experience with Zicaloy-4, ZIRLO or Optimized ZIRLO tubing as a clad material. Information on the material's chemical and mechanical properties of the cladding is given in References 4.2-15 and 4.2-23. Reference 4.2-31 describes the optimization of the material composition of the licensed material ZIRLO to an Optimized (low tin) ZIRLO composition used in the cladding of the NGF LTAs (Region 12C). Optimized ZIRLO was implemented for full-region applications starting with Region 18. Reference 4.2-36 describes the Westinghouse cladding corrosion model that is used to analyze the corrosion of ZIRLO and Optimized ZIRLO cladding as part of the fuel rod design analysis.

The AXIOM alloy used in the fuel cladding of the AXIOM LTAs (Region 21) has a reduced tin content as compared to Optimized ZIRLO which leads to an increased reduction in corrosion. Further optimization in the thermal and mechanical processing for the AXIOM alloy as well as additional alloying elements results in improved hydrogen pickup.

2.   Stress-strain Limits

    a.   Clad Stress - The clad stresses under Conditions I and II are less than the Zicaloy-4, ZIRLO or Optimized ZIRLO tubing yield stress, with due consideration of temperature and irradiation effects. While the clad has some capability for accommodating plastic strain, the yield stress has been accepted as a conservative design basis.

    b.   Clad Tensile Strain - The total tensile creep strain is less than 1 percent from the unirradiated condition. The cluster tensile strain during a transient is less than 1 percent from the pretransient value. This limit is consistent with proven practice Reference 4.2-6.

    Alternatively, clad stress can be evaluated by applying the following NRC approved cladding stress criteria (Reference 4.2-35):

        i.   The maximum cladding stress intensities, excluding pellet cladding interaction, but accounting for cladding corrosion as a loss of load carrying metal, is less than the stress limit, as defined based on the ASME Code, Section III calculations.

        ii.   The one-percent transient clad strain criterion is met.

        iii.   An additional steady-state clad strain criterion based on the total (plastic plus elastic strain) is met.

iv.   No centerline fuel melting occurs.

v.   The effect of the plastic deformation is accounted for in all fuel rod design criteria as appropriate.

3.   Vibration and Fatigue

a.   <u>Strain Fatigue</u> - The cumulative strain fatigue cycles are less than the design strain fatigue life. This basis is consistent with proven practice Reference 4.2-6.

b.   <u>Vibration</u> - Potential fretting wear due to vibration is prevented, assuring that the stress-strain limits are not exceeded during design life. Fretting of the clad surface can occur due to flow-induced vibration between the fuel rods and fuel assembly grid springs. Vibration and fretting forces vary during the fuel life due to clad diameter creepdown combined with grid spring relaxation.

4.   Chemical Properties

Chemical properties of the cladding are discussed in References 4.2-15 and 4.2-23.

4.2.1.2   Fuel Material

1.   Thermal-physical Properties

Fuel pellet temperatures - The center temperature of the hottest pellet is below the melting temperature of the UO_2 melting point of 5,080°F (Reference 4.2-15, unirradiated and decreasing by 58°F per 10,000 MWD/MTU). While a limited amount of center melting can be tolerated, the design conservatively precludes center melting. A calculated fuel centerline temperature of 4,700°F has been selected as an overpower limit to ensure no fuel melting. This provides sufficient margin for uncertainties as described in Section 4.4.2.9.

The normal design density of the fuel is 95 percent of theoretical. Additional information on fuel properties is given in Reference 4.2-15.

2.   Fuel Densification and Fission Product Swelling

The design bases and models used for fuel densification and swelling are provided by References 4.2-7 and 4.2-21.

3.   Chemical Properties

Reference 4.2-15 indicates that no adverse chemical interactions occur between the fuel and its adjacent material.

4.2.1.3   Fuel Rod Performance

    1.   Fuel Rod Methods and Models

          The basic fuel rod methods and models and the ability to predict operating characteristics are given by References 4.2-19, 4.2-21, 4.2-23, 4.2-32, 4.2-34, 4.2-36 and Section 4.2.3.

    2.   Mechanical Design Limits

          Cladding collapse shall be precluded during the fuel rod design lifetime. The models described by Reference 4.2-25 are used for this evaluation.

          The rod internal gas pressure remains below the value which causes the fuel/clad diametral gap to increase due to outward cladding creep during steady state operation. Rod pressure is also limited such that extensive departure from nucleate boiling (DNB) propagation does not occur during normal operation or any accident event. Reference 4.2-14 shows that the DNB propagation criteria are satisfied.

4.2.1.4   Spacer Grids

    1.   Mechanical Limits and Materials Properties

          The grid component strength criteria are based on experimental tests. The allowable limit (P) is established as the lower 95 percent confidence in the true mean at BOL condition at 600°F. If P is exceeded, the core must maintain a geometry amenable to cooling. As an integral part of the fuel assembly structure, the grids satisfy the applicable fuel assembly design bases and limits defined in Section 4.2.1.5.

          The grid material and chemical properties are given by Reference 4.2-15. ZIRLO grid material and chemical properties are covered by Reference 4.2-23. Reference 4.2-31 describes the optimization of the material composition of the licensed material ZIRLO to an Optimized (low tin) ZIRLO composition used in the mid-grids and Intermediate Flow Mixing grids (Fins) of the NGF LTAs.

    2.   Vibration and Fatigue

          The grids provide sufficient fuel rod support to limit fuel rod vibration and maintain clad fretting wear to within acceptable limits (defined in Section 4.2.1.1).

4.2.1.5   Fuel Assembly

    1.   Structural Design

As previously discussed in Section 4.2.1, the structural integrity of the fuel assemblies is ensured by setting design limits on stresses and deformations due to various nonoperational, operational, and accident loads. These limit bases are applied to the design and evaluation of the top and bottom nozzles, guide thimbles, grids, and thimble joints.

The design bases for evaluating the structural integrity of the fuel assemblies are:

a.   Nonoperational - 4g axial and 6g lateral loading with dimensional stability.

b.   For the normal operating and upset conditions, the fuel assembly component structural design criteria are established for the two primary material categories, namely austenitic stainless steels and Zircaloy/ZIRLO. The stress categories and strength theory presented in the American Society of Mechanical Engineers (ASME) Boiler and Pressure Vessel Code, Section III, are used as a general guide. The maximum shear-theory (Tresca criterion) for combined stresses determines the stress intensities for the austenitic stainless steel components. The stress intensity is defined as the numerically largest difference between the various principal stresses in a three dimensional field. The allowable stress intensity value for austenitic stainless steel, such as nickel-chromium-iron alloys, is given by the lowest of the following:

1.   One-third of the specified minimum tensile strength or two-thirds of the specified minimum yield strength at room temperature;

2.   One-third of the tensile strength or 90 percent of the yield strength at temperature but not to exceed two-thirds of the specified minimum yield strength at room temperature.

The stress limits for the austenitic stainless steel components are given below. All stress nomenclature is per the ASME Code, Section III.

Stress Intensity Limits

Categories	Limit
General primary membrane stress intensity	Sm
Local primary membrane stress intensity	1.5 Sm
Primary membrane plus bending stress intensity	1.5 Sm
Total primary plus secondary stress intensity	3.0 Sm

The Zircaloy/ZIRLO structural components consist of grids, guide thimble, and fuel tubes and are, in turn, subdivided into two categories because of material differences and functional requirements. Fuel tube design criteria is discussed in Section 4.2.1.1. The maximum shear theory evaluates the guide thimble design. For conservative purposes, the Zircaloy/ZIRLO unirradiated properties define stress limits.

3.   Abnormal loads during Conditions III or IV - worst cases represented by combined seismic and blowdown loads.

    a.   Deflections of component failures cannot interfere with the reactor shutdown or emergency cooling of the fuel rods.

    b.   The fuel assembly structural component stresses under faulted conditions are evaluated using primarily the methods outlined in Appendix F of the ASME Code, Section III. Since the current analytical methods utilize elastic analysis, the stress allowables are defined as the smaller value of 2.4 Sm or 0.70 S for primary membrane and 3.6 Sm or 1.05 S for primary membrane plus primary bending. For the austenitic stainless steel fuel assembly components, the stress intensity is defined in accordance with the rules described in the previous section for normal operating conditions. For the Zircaloy/ZIRLO components the stress intensity limits are set at two-thirds of the material yield strength, S at reactor operating temperature. This results in Zircaloy/ZIRLO stress limits being smaller than 1.6 S or 0.70 S for primary membrane and 2.4 S or 1.05 S for primary membrane plus bending. For conservative purposes, the Zircaloy/ZIRLO unirradiated properties are used to define the stress limits.

        The material and chemical properties of the fuel assembly components are given by Reference 4.2-15. Section 4.2.3.4 discusses the spacer grid crush testing. ZIRLO grid material and chemical properties are covered by Reference 4.2-23.

    c.   Thermal-hydraulic design is discussed in Section 4.4.

The implementation of Reference 4.2-30 for Cycle 10 is a change to the fuel evaluation methodolgy, which replaces the hydrogen content design criterion for fuel assembly structural components with a structural component stress criterion that accounts for material thinning due to corrosion. The implementation of Reference 4.2-36 in Cycle 17 provides the revised cladding corrosion model to analyze ZIRLO and Optimized ZIRLO cladding in the fuel rod design analysis on a cycle-specific basis.

4.2.1.6   Incore Control Components

The control components are subdivided into permanent and temporary devices.

The permanent components are the rod cluster control assemblies and secondary neutron source assemblies. The temporary components are the burnable poison assemblies and the primary neutron source assemblies which are normally used only in the initial core and thimble plug assemblies.

Materials are selected for compatibility in a pressurized water reactor environment, for adequate mechanical properties at room and operating temperatures, for resistance to adverse property changes in a radioactive environment, and for compatibility with interfacing components. Material properties are given in Reference 4.2-15. Identical absorber material (Ag-In-Cd) is utilized by both Westinghouse and AREVA and the properties are applicable to both vendor's designs. ZIRLO grid material and chemical properties are covered by Reference 4.2-23.

The design bases for each of the mentioned components are given in the following subsections.

1.   Absorber Rods

For Conditions I and II the stress categories and strength theory presented in the ASME Boiler and Pressure Vessel Code, Section III, Subsection NG-3000, are used as a general guide in the design of the control rod cladding.

Design conditions which are considered under the ASME Code, Section III are as follows:

a.   External pressure equal to the reactor coolant system operating pressure with appropriate allowance for overpressure transients

b.   Wear allowance equivalent to 1,000 reactor trips

c.   Bending of the rod due to a misalignment in the guide tube

d.   Forces imposed on the rods during rod drop

e.   Loads imposed by the accelerations of the control rod drive mechanism

f.   Radiation exposure during maximum core life

The absorber material temperature does not exceed its melting temperature - 1,454°F for silver-indium-cadmium (Ag-In-Cd) absorber material or 3,913°F for hafnium (Reference 4.2-15).

g.   Temperature effects at operating conditions

2.   Burnable Absorber Rods

Burnable absorber rods were used only in Cycles 1 and 2.

For Conditions I and II the stress categories and strength theory presented in the ASME Boiler and Pressure Vessel Code, Section III, Subsection NB-3000, are used as a general guide in the design of the burnable poison cladding. For abnormal loads during Conditions III and IV, code stresses are not considered limiting.

Failure of the burnable absorber rods during these conditions must not interfere with reactor shutdown or cooling of the fuel rods.

The burnable poison absorber material is nonstructural. The structural elements of the burnable absorber rod maintain the absorber geometry even if the absorber material is fractured. The rods are designed to maintain the absorber material below its softening temperature (1,492°F for reference 12.5 weight percent boron rods). (Borosilicate glass is the absorber material used in burnable absorber rods. The softening temperature, as defined in the ASTM C 338, is 1,510 ±18°F). In addition, the structural elements prevent excessive slumping.

3.   Neutron Source Rods

The neutron source rods withstand the following conditions:

a.   The external pressure equal to the reactor coolant system operating pressure with appropriate allowance for overpressure transients

b.   An internal pressure equal to the pressure generated by released gases over the source rod life

4.   Thimble Plug Assembly

The thimble plug assembly restricts bypass flow through thimbles not occupied by absorber, source, or burnable absorber rods.

The thimble plug assemblies:

a.   Accommodate the differential thermal expansion between the fuel assembly and the core internals

b.   Maintain positive contact with the fuel assembly and the core internals

c.   Limit the flow through each occupied thimble to acceptable design value

4.2.1.7   Surveillance Program

Section 4.2.4.5 and Sections 8 and 23 of Reference 4.2-13, discuss the ongoing testing and fuel surveillance operational experience program to verify the adequacy of the fuel performance and design bases. Fuel surveillance and testing results are used to improve fuel rod design and manufacturing processes and to be sure that design bases and safety criteria are satisfied.

4.2.2   DESIGN DESCRIPTION

Each fuel assembly is a 17 x 17 lattice consisting of 264 fuel rods, 24 guide thimble tubes, and one instrumentation thimble tube arranged within a supporting structure. The instrumentation thimble is located in the center position and provides a channel for insertion of an incore neutron detector, if the fuel assembly is located in an instrumented core position. The guide thimbles provide channels for insertion of either a rod cluster control assembly, a neutron source assembly, or a thimble plug assembly, depending on the position of the particular fuel assembly in the core. Figure 4.2–1 shows a cross section of the fuel assembly array, and Figure 4.2–2 shows a fuel assembly full-length view. The fuel rods are loaded into the fuel assembly structure so that there is clearance between the fuel rod ends and the top and bottom nozzles.

Fuel assemblies are installed vertically in the reactor vessel and stand upright on the lower core plate, which is fitted with alignment pins to locate and orient each assembly. After all fuel assemblies are set in place, the upper support structure is installed. Alignment pins, built into the upper core plate, engage and locate the upper ends of the fuel assemblies. The upper core plate then bears downward against the hold-down springs on the top nozzle of each fuel assembly to hold the fuel assemblies in place.

Improper orientation of fuel assemblies within the core is prevented by the use of an indexing hole in one corner of the top nozzle top plate. The assembly is oriented with respect to the handling tool and the core by means of a pin which is inserted into this indexing hole. Visual confirmation of proper orientation is also provided by an engraved identification number on the opposite corner clamp.

In this section, information is provided related to the fuel assembly designs and the history of their implementation. In summary, the evolution of fuel assembly designs has been:

- 17 x 17 Standard (STD) fuel assembly – initial core

- Vantage 5H (V5H) – starting in Cycle 4

- V5H with rotated grids – starting in Cycle 5

- Robust Fuel Assembly (RFA) – starting in Cycle 7

- RFA with redesigned mid-grids (RFA–2) – starting in Cycle 10

- Next Generation Fuel (NGF) Lead Test Assembly Program – Cycles 10 to 12

- RFA-2 with Robust Protective Grid and Standardized Debris Filter Bottom Nozzle – starting in Cycle 15

- RFA-2 with Westinghouse Integral Nozzle (WIN) top nozzle - starting in Cycle 18

- AXIOM fuel cladding Lead Test Assembly Program - Cycles 19 through 21

Reactor design parameters, including a history of fuel enrichments and information specific to the RFA/RFA–2 design, are provided in Table 4.1-1.

The initial reactor core (Cycle 1) was entirely comprised of Westinghouse 17 x 17 Standard (STD) fuel assemblies. The initial core contained Region 1, Region 2, and Region 3 fuel assemblies which were identical in mechanical design but different in enrichment. Tables 4.1-1 and 4.3-3 provide fuel assembly and fuel rod information for the initial core.

The Region 4 (Cycle 2) and Region 5 (Cycle 3) fuel products were also of the Westinghouse 17 x 17 STD design but they were considered as transition designs, gradually incorporating the various improvements of the Vantage 5 Hybrid (V5H) fuel assembly design (see below).

The Vantage 5 Hybrid (V5H) fuel assembly was used starting in Region 6 (Cycle 4). This design employed many improvements over the fuel assemblies used in the first core such as (1) standardized (chamfered) fuel pellets, (2) a reconstitutable top nozzle (RTN), (3) debris filter bottom nozzle (DFBN), (4) zircaloy mid-span structural grids, (5) high burnup capability, (6) integral fuel burnable absorbers (IFBA), (7) axial blankets, and (8) intermediate flow mixer grids. These features are discussed in more detail in later sections.

The V5H design was further improved for Region 7 (Cycle 5) by: (1) the use of ZIRLO to replace much of the Zircaloy-4, (2) the use of enriched B-10 in the IFBA and (3) the use of annular axial blankets. Recaging of 48 of the 84 Region 7 fuel assemblies was performed prior to use in the core, whereby the odd numbered mixing vane grids were rotated 90° in the clockwise direction. Therefore, grid #3 and each of the three intermediate flow mixer (IFM) grids were rotated. This modification was performed to minimize the susceptibility of these fuel assemblies to flow-induced vibration. The V5H design for Region 8 (Cycle 6) included minor mechanical modifications to the V5H fuel assembly and the mixing vane grid rotation was implemented on all 84 fuel assemblies.

The Robust Fuel Assembly (RFA) was used starting in Region 9 (Cycle 7). The mechanical design of the Region 9 (RFA) fuel assemblies is the same as that of the Region 8 (V5H) fuel assemblies, except for the following improvements: (1) RFA design features, (2) 3-tab top and bottom Inconel grids, (3) protective bottom grid, (4) composite cast top nozzle, and (5) longer top

and bottom grooved fuel rod end plugs. A description of each of these fuel design improvements follows:

1. The RFA design features include a thicker wall guide thimble tube, thicker wall instrumentation tube, Modified Low Pressure Drop (LPD) mid-grids, and Modified Intermediate Flow Mixer (IFM) grids.

    Guide thimble and instrumentation tube wall thickness is increased to improve stiffness and mitigate Incomplete Rod Insertion (IRI). The major diameter section OD is increased from 0.474 inch to 0.482 inch while the ID is maintained at 0.442 inch. The dashpot section OD is increased from 0.430 inch to 0.439 inch while the ID is maintained at 0.397 inch. With the thicker guide thimble tube, the cross-sectional area is increased by 26% in the major diameter section and by 29% in the dashpot section.

    The Modified LPD and Modified IFM grids are described in transmittals to the U.S. NRC (Kitchen, Liparulo). Since the RFA has a thicker guide thimble tube (0.482 inch OD), the Modified LPD mid-grid will also be embossed (radial) to accept the larger tube OD. In addition, the sleeve and the sleeve notch on the strap will also be larger to provide clearance for the larger diameter guide thimble tube. This improvement also addresses high thimble tube loading forces during skeleton fabrication. The Modified LPD grids and the Modified IFM grids no longer required mid-grid rotations.

2. The top and bottom Inconel grids have changed from a single twist tab at the center of the inner-to-outer strap joint to a 3-tab inner-to-outer joint configuration. The 3-tab design has one smaller twist tab and two additional tabs at the top and bottom of the strap. This change is intended to improve the structural integrity and enhance the anti-snag resistance of the top and bottom grids.

3. Debris mitigating features in the RFA include a protective bottom grid and modified fuel rod end plugs. The protective bottom grid is a partial height grid similar in configuration to the mid-grid, but fabricated of Inconel without mixing vanes. It is positioned on the top plate of the bottom nozzle. The grooved fuel rod end plug is an elongated version of the current fuel rod end plug design and extends through the protective bottom grid to the bottom grid. This longer fuel rod end plug design ensures that any debris trapped by the protective bottom grid can only fret against a solid end plug instead of the fuel rod cladding.

    Hydraulic testing indicates that the design of the protective bottom grid and the elongated end plug causes no significant effect on fuel assembly hydraulic performance (Brown). In addition to the debris mitigation feature, the protective grid also provides increased support to the fuel rods.

4. A composite cast top nozzle is included in the RFA as a manufacturing process change. The new design includes a single casting that replaces the machined top

plate/enclosure/pad weldment. The adapter plate, thimble hole and flow patterns remain unchanged. The new top nozzle is functionally identical to the original design.

5.   In conjunction with the protective grid and the new elongated bottom end plug (see Item 3 above), the fuel rod top end plug was elongated and fitted with an external gripper to assist in positioning the fuel rod during fabrication and also to facilitate fuel rod removal during reconstitution. The pre-welded design of the fuel rod top and bottom end plugs has been changed to include a groove around the circumference of the plug for the feed region. The improved top and bottom end plugs allow a greater depth of weld penetration.

The mechanical design of the Region 11 (Cycle 9) RFA is essentially the same as that of the Region 9 and 10 fuel assemblies, but also included:

1.   Top nozzle instrumentation tube plug elimination,

2.   Bead blasted Inconel-718 top nozzle spring screws and revised spring screw design,

3.   Longer fuel tube design,

4.   Longer guide tube and instrumentation tubes and V+2 leaf spring,

5.   Intermediate Flow Mixer Grids (IFMs) strap item reduction,

6.   Shorter top end plug without gripper, and

7.   Longer plenum spring.

A description of each of these RFA fuel design improvements in Region 11 follows.

1.   The elimination of the top nozzle instrumentation plug is a design change that reduces the total number of component parts required to fabricate and assemble a 17 x 17 fuel assembly. The new design eliminates the instrumentation plug that has to be welded into a counterbore in the top nozzle adapter plate and replaces it with a blind hole with a small weep hole that is machined into the top nozzle adapter plate. The purpose of this change is for a manufacturing process improvement to increase manufacturing flexibility. The design change meets all functional and design requirements specified for the top nozzle and does not adversely affect the form, fit or function of the fuel assembly.

2.   Changes have been made to the Inconel top nozzle spring screw to increase resistance to primary water stress corrosion cracking (PWSCC). The spring screw is bead blasted (shot peened) in the shank-to-thread area to create an even layer of metal in residual compressive stress which will inhibit the initiation and

propagation of PWSCC cracks. Dimensional changes have been made to increase the radius in the shank-to-thread area in order to decrease stress concentration. Finally, the material was changed from Inconel Alloy 600 to precipitation hardened Inconel-718 to increase yield and tensile strength.

3.   The fuel tube length has been increased slightly to increase plenum volume and thus provide additional margin to the rod internal pressure limit at high burnup.

4.   Compared to the current ZIRLO fuel assembly, the guide tube and instrumentation tube are slightly longer. As part of the increase in fuel rod length, as discussed in Section 2.1.3, the fuel assembly overall length had to be increased slightly to accommodate the fuel rod growth. The design change meets all current design criteria for high burnup operations. In addition, the leaf spring design has been changed to accommodate the longer fuel assembly length and the pre-load has been eliminated to improve the loading on the top nozzle spring screws.

5.   A generic product change is being implemented in the IFM grid strap for all 17 x 17 fuel designs. This product change involves elimination of half of the IFM inner strap configurations. The primary reason for this change is to improve the manufacturing process of the IFM grid design. There will be no impact on the grid performance or on safety analyses.

6.   Incorporation of the shorter top end plug results in a slight fuel rod length reduction to provide additional growth margin. Elimination of the gripper is of no consequence to design or manufacturing.

7.   Since the fuel tube has been lengthened, the plenum spring has been increased slightly to accommodate the added fuel tube length. The increased plenum spring free length still maintains the same 4g design criterion as the previous design fuel regions.

Starting with Region 12 (Cycle 10) a version of the Robust Fuel Assembly, called RFA–2, was used which included mid–grids with a revised design. The RFA–2 mid–gird is designed to provide increased margin to fuel rod fretting wear while maintaining the performance of the RFA in areas such as DNB and pressure drop. The design differences and similarities between the RFA Region 11 (Cycle 9) and the RFA–2 are summarized as follows:

1.   Changes were made to the profiles of the springs and dimples in the mid–grids (6 mid–grids per fuel assembly) of the RFA–2 fuel assembly resulting in an increase in the spring-to-fuel rod contact area and the dimple-to-fuel rod contact area as compared to the RFA. Additionally, the spring and dimple slots (i.e., the cut-outs in the grid strap material) were revised so that the overall cell stiffness for the RFA–2 is equivalent to or lower than that of the RFA. Further discussion is provided in Section 4.2.2.2.4.

2.   There is no change to the fuel assembly length or envelope or to the fuel rod design in the 17 x 17 RFA–2 design as compared to the RFA.

3.   The Inconel top, bottom and protective bottom grids and the ZIRLO IFM grids are not changed in the 17 x 17 RFA–2 design as compared to the RFA.

4.   There is no change to the Removable Top Nozzle (RTN), the Debris Filter Bottom Nozzle (DFBN), or the ZIRLO thimble and instrument tubes in the 17 x 17 RFA–2 design as compared to the RFA.

A Lead Test Assembly (LTA) program was initiated in Cycle 10 which involved eight Next Generation Fuel (NGF) fuel assemblies. The eight LTAs were first inserted in the Cycle 10 core and all eight LTAs were subsequently inserted in the Cycle 11 core for a second cycle of operation. For Cycle 12, five of the LTAs were inserted for a third cycle of operation while the remaining three LTAs were discharged to the spent fuel pool. The purpose of the LTA program was to demonstrate the mechanical performance of the NGF fuel assemblies with respect to improved resistance to corrosion and grid-to-rod fretting, resistance to fuel assembly bowing and improved flow mixing. The LTA program involved only the Cycle 10, 11, and 12 cores. No NGF fuel assemblies are installed in Cycle 13 and beyond.

The mechanical design of the RFA–2 fuel assembly that is used starting with Region 17 (Cycle 15) is essentially the same as that of the Region 12 through 16 (Cycle 10-14) RFA–2 design with the following two exceptions:

1.   Starting with Region 17 (Cycle 15) the Standardized Debris Filter Bottom Nozzle (SDFBN) replaces the DFBN which has been used since Cycle 4 (Region 6). The SDFBN was developed for Westinghouse 17x17 fuel. It is designed in order to eliminate manufacturing variability, primarily in the drilling of the flow holes, between the sub-suppliers providing the SDFBN to Westinghouse. This, in turn, will result in a loss coefficient for this product that is the same and independent of sub-supplier. Additionally, the side skirt communication flow holes that are present in the DFBN have been eliminated in the SDFBN as a means of improving the debris mitigation performance of the bottom nozzle.

Testing by Westinghouse has demonstrated that the SDFBN has no adverse affect on thermal hydraulic performance, either with respect to the pressure drop or with respect to DNB. However, until a full core of the SDFBN is implemented, there will be a small transition core DNB penalty because of the slightly lower loss coefficient of the SDFBN as compared to the current DFBN in the resident fuel assemblies.

2.   Starting with Region 17 (Cycle 15) the Robust Protective Grid (RPG) replaces the protective bottom grid which has been used since Cycle 7 (Region 9). The RPG was developed by Westinghouse as a result of observed failures in the protective bottom grids, as noted in Post Irradiation Exams (PIE) performed at several different plants. It was determined that the observed failures were the result of two

primary issues; 1) fatigue failure within the protective grid itself at the top of the end strap and 2) stress corrosion cracking (SCC) primarily within the rod support dimples.

The RPG implements design changes that include: 1.) increasing the maximum nominal height of the grid, 2.) increasing the ligament length and the radii of the ligament cutouts, and 3.) the use of four additional spacers to help support the grid. Additionally, the nominal height of the RPG was increased, as compared to the protective bottom grid, to allow "V-notch" window cutouts to be added which will minimize flow-induced vibration caused by vortex shedding at the trailing edge of the inner grid straps.

The design changes incorporated into the RPG design help address the issues of fatigue failures and failures due to SCC. It was determined that the changes noted above do not adversely impact the thermal-hydraulic performance of the RPG as there is no change to the loss coefficient. In addition, the RPG retains the original function of the protective bottom grid as a debris mitigation feature.

Starting with Region 18 (Cycle 16), Optimized ZIRLO replaces ZIRLO as the fuel rod cladding product. Optimized ZIRLO is incorporated to further reduce the fuel clad corrosion rate while maintaining the composition and physical properties, such as mechanical strength, similar to standard ZIRLO. The RFA-2 guide thimbles, instrumentation tubes, structural mid-grids, and IFMs continue to be fabricated with ZIRLO.

Starting with Region 20 (Cycle 18), the Westinghouse Integral Nozzle (WIN) top nozzle replaces the Reconstitutable Top Nozzle (RTN). The WIN design is a proactive change made to reduce the potential for holddown spring screw failures in the top nozzle by eliminating the holddown spring screw. The springs are held in the nozzle by a machined pocket and a tack welded pin pushed through the pocket and springs. The WIN design also eliminates the use of left and right-hand springs in favor of a same-hand spring. Aside from the changes listed above, there are no mechanical, nuclear, or thermal hydraulic differences between the WIN and RTN designs. The change to the WIN top nozzle has no effect on handling or movement of the assembly.

Starting with Region 21 (Cycle 19), a Lead Test Assembly (LTA) program is initiated with the insertion of eight (8) 17 x 17 RFA-2 fuel assemblies with AXIOM fuel rod cladding. The LTAs are of the same design as the resident fuel except for the use of AXIOM fuel cladding in place of Optimized ZIRLO cladding. The purpose of the LTA program is to demonstrate the fuel rod performance of the AXIOM cladding.

4.2.2.1   Fuel Rods

The fuel rods consist of uranium dioxide ceramic pellets contained in slightly cold worked Zicaloy-4, ZIRLO or Optimized ZIRLO tubing which is plugged and seal-welded at the ends to encapsulate the fuel. A schematic of the fuel rod is shown on Figure 4.2–3. The fuel pellets are right circular cylinders consisting of slightly enriched uranium dioxide powder which has been compacted by cold pressing and then sintered to the required density. The ends of each pellet are

dished slightly to allow greater axial expansion at the center of the pellets. There are several different types of fuel pellets with variations in enrichment, dimensions and geometry. IFBA enriched fuel pellets are coated with a boride absorber. The axial blanket is a six inch (approximate) stack of natural or slightly enriched fuel pellets (solid or annular) located at the top and bottom of the fuel stack in each fuel rod.

Void volume and clearances are provided within the rods to accommodate fission gases released from the fuel, differential thermal expansion between the clad and the fuel, and fuel density changes during irradiation. Shifting of the fuel within the clad during handling or shipping prior to core loading is prevented by a stainless steel helical spring which bears on top of the fuel. At assembly, the pellets are stacked in the clad to the required fuel height. The spring is then inserted into the top end of the fuel tube and the end plugs pressed into the ends of the tube and welded. All fuel rods are internally pressurized with helium during the welding process in order to minimize compressive clad stresses and prevent clad flattening under coolant operating pressures.

The fuel rods are prepressurized and designed so that: the internal gas pressure mechanical design limit given in Section 4.2.1.3 is not exceeded, the cladding stress-strain limits (Section 4.2.1.1) are not exceeded for Condition I and II events, and clad flattening will not occur during the fuel core life. The amount of prepressurization varies depending on fuel type.

Limited substitutions of Zircaloy-4, ZIRLO or stainless steel filler rods for fuel rods may be used. Fuel assemblies in this configuration are analyzed in accordance with Reference 4.2-24 and shown by test or cycle-specific reload analyses to comply with all fuel safety design bases.

As discussed in Section 4.2.2, the RFA, used for the first time in Region 9 (Cycle 7) implements the protective grid which includes an elongated bottom end plug. In the RFA design, the fuel rod top end plug was elongated and fitted with an external gripper to assist in positioning the fuel rod during fabrication and also to facilitate fuel rod removal during reconstitution. The pre-welded design of the fuel rod top and bottom end plugs has been changed to include a groove around the circumference of the plug for the feed region.

Starting with Region 10, the fuel rod top end plug has been shortened, by the elimination of the external gripper, to provide additional fuel rod growth margin.

4.2.2.2   Fuel Assembly Structure

The fuel assembly structure consists of a bottom nozzle, top nozzle, guide thimbles and grids, as shown on Figure 4.2–2.

4.2.2.2.1   Bottom Nozzle

The bottom nozzle serves as a bottom structural element of the fuel assembly and directs the coolant flow distribution to the assembly. The square nozzle is fabricated from type 304 stainless steel and consists of a perforated plate, skirt and four angle-legs with bearing plates, as shown on Figure 4.2–2. The legs and skirt form a plenum for the inlet coolant flow to the fuel assembly. The plate also prevents accidental downward ejection of the fuel rods from the fuel assembly. The

bottom nozzle is fastened to the fuel assembly guide tubes by locked screws which penetrate the nozzle and mate with a threaded plug in each guide tube. The screw is prevented from loosening by a stainless steel thimble screw with locking cup.

There are three types of bottom nozzles; the standard design, the debris filter bottom nozzle (DFBN) and the Standardized Debris Filter Bottom Nozzle (SDFBN). The DFBN was introduced with the Region 5 fuel. The relatively large flow holes in the standard design were replaced with a new pattern of smaller flow holes in the DFBN. Tests to measure pressure drop and demonstrate structural integrity have been performed to verify that the DFBN is totally compatible with the standard design. Additionally, the DFBN is lower in height than the standard design to accommodate high burnup fuel.

Coolant flows from the plenum in the bottom nozzle upward through the penetrations in the plate to the channels between the fuel rods. The penetrations in the plate are positioned between the rows of the fuel rods.

Axial loads (hold-down) imposed on the fuel assembly and the weight of the fuel assembly are transmitted through the bottom nozzle to the lower core plate. Indexing and positioning of the fuel assembly is controlled by alignment holes in two diagonally opposite bearing plates which mate with locating pins in the lower core plate. Lateral loads on the fuel assembly are transmitted to the lower core plate through the locating pins.

As discussed in Section 4.2.2, the RFA was used for the first time in Region 9 (Cycle 7) and this fuel assembly design included the protective bottom grid which is positioned on the top plate of the DFBN. Starting with Region 17 (Cycle 15), the SDFBN and RPG replace the DFBN and the protective bottom grid.

4.2.2.2.2   Top Nozzle

The top nozzle assembly functions as the upper structural element of the fuel assembly in addition to providing a partial protective housing for the rod cluster control assembly or other components. They are installed in the guide thimble tubes. The top nozzle assembly consists of an adapter plate, enclosure, top plate, and pads. The top nozzle assembly comprises holddown springs, pins or screws, and clamps located on the top plate as shown on Figure 4.2–2. The springs and spring screws are made of Inconel 718 and 600, respectively, whereas other components of the top nozzle are made of type 304/304L stainless steel.

There are three types of top nozzles-the standard design, the Reconstitutable Top Nozzle (RTN), and the Westinghouse Integral Nozzle (WIN). The RTN has a groove in each thimble through-hole in the nozzle plate to facilitate attachment and removal. Additionally, the RTN is shorter than the standard design to accommodate high burnup fuel. The RTN was introduced with the Region 5 fuel. The WIN uses a different design than the RTN for attaching the holddown springs to the top nozzle. In the WIN design, the spring clamps are machined directly into the nozzle casting to create spring pockets integral to the nozzle. The tail end of the holddown spring pack slides into a blind pocket machined into the top nozzle casting. Instead of using a holddown spring screw, the spring pack is held in place by a retaining pin pushed vertically through the

pocket and springs. The pin is tack welded to the top nozzle to secure it in position. The WIN was introduced with the Region 20 fuel.

The square adapter plate is provided with round penetrations and semicircular ended slots to permit the flow of coolant upward through the top nozzle. Other round holes are provided to accept inserts which are locked into internal grooves in the adapter plate at their upper ends using a lock tube and mechanically attached to the thimble tubes at the lower ends. The ligaments in the plate cover the tops of the fuel rods and prevent their upward ejection from the fuel assembly. The enclosure is a box-like structure which sets the distance between the adapter plate and the top plate. The top plate has a large square hole in the center to permit access for the control rods and the control rod spiders. Holddown springs are mounted on the top plate and are retained by clamps and either spring screws or retaining pins located at two diagonally opposite corners. On the other two corners integral pads are positioned which contain alignment holes for locating the upper end of the fuel assembly.

As discussed in Section 4.2.2, the RFA, used for the first time in Region 9 (Cycle 7) will also contain a new composite cast top nozzle as a manufacturing process change. The new top nozzle is functionally identical to the original design.

As noted in Section 4.2.2, improvements to the top nozzle incorporated for Region 10 have also been incorporated into subsequent batches through Batch 19. The top nozzle instrument tube plug has been eliminated, the top nozzle spring screws have been improved to increase their resistance to primary water stress corrosion cracking (PWSCC), and the leaf springs have been changed to accommodate the slightly longer fuel assembly length.

As noted in Section 4.2.2, the WIN includes mechanical changes from the RTN designed to improve the structural integrity of the top nozzle in response to observed stress corrosion cracking of the top nozzle holddown spring screws and failure of the spring screw clamp. The holddown spring modification increases fuel assembly integrity and eliminates the potential for loose parts.

4.2.2.2.3   Guide Thimbles and Instrument Tube

The guide thimbles are structural members which also provide channels for the control rods, neutron absorber rods, burnable poison rods, neutron source, or thimble plug assemblies. Each thimble is fabricated from Zircaloy or ZIRLO tubing having two different diameters. The tube diameter at the top section provides the annular area necessary to permit rapid control rod insertion during a reactor trip. Holes are provided on the thimble tube above the dashpot to reduce the rod drop time. The lower portion of the guide thimble is swaged to a smaller diameter to reduce diametral clearances and produce a dashpot action near the end of control rod travel during normal trip operation. The dashpot is closed at the bottom by means of an end plug with a small flow port to avoid fluid stagnation in the dashpot volume during normal operation. The top end of the guide thimble is fastened to an insert by three expansion swages. The insert fits into and is locked into the top nozzle adapter plate using a lock tube. The lower end of the guide thimble is fitted with an end plug which is then fastened into the bottom nozzle by a locked screw.

Fuel rod support grids are fastened to the guide thimble assemblies to create an integrated structure. Because the Inconel grid and the Zircaloy or ZIRLO thimble cannot be welded, the mechanical fastening technique as depicted on Figures 4.2–6 and 4.2–7 are used for the top and bottom grids in a fuel assembly. Midgrids and IFM grids are fastened as shown in Figures 4.2–4 and 4.2–5.

An expanding tool is inserted into the inner diameter of the thimble tube at the elevation of the grid sleeves that have been previously attached to the grid assembly. The four-lobed tool forces the thimble and sleeve outward to a predetermined diameter, thus joining the two components.

The top grid-to-thimble attachment is shown on Figure 4.2–6. The stainless steel sleeves are brazed into the Inconel grid assembly. The guide thimbles are fastened to the long sleeves. The top Inconel grid sleeve, top nozzle insert and thimble tube are joined together using a three bulge joint mechanical attachment as shown in Figure 4.2–6.

The bottom grid assembly is joined to the assembly (Figure 4.2–7). The stainless steel insert is spot-welded to the bottom grid and later captured between the guide thimble end plug and the bottom nozzle by means of a stainless steel thimble screw.

The described methods of grid fastening are standard and have been used successfully since the introduction of Zircaloy guide thimbles in 1969.

The central instrumentation tube of each fuel assembly is constrained by seating in a counterbore in the bottom nozzle at its lower end and is expanded at the top and mid grids in the same manner as the previously described expansion of the guide thimbles to the grids. The tube is a constant diameter and guides the incore neutron detectors.

The guide thimbles and instrument tube used on the V5H fuel assemblies are slightly reduced in diameter to accept the thicker Zircaloy/ZIRLO grids and slightly increased in length to allow more space for fuel rod growth at high burnup. The reduced diameter thimbles on the V5H fuel assembly still provides sufficient clearance for the core compartments in use at Millstone 3.

As discussed in Section 4.2.2, the RFA, used for the first time in Region 9 (Cycle 7) will also implement an increased wall thickness in the guide thimbles and instrumentation tubes to improve stiffness and mitigate Incomplete Rod Insertion (IRI).

4.2.2.2.4   Grid Assemblies

The fuel rods (Figure 4.2–2) are supported at intervals along their length by grid assemblies which maintain the lateral spacing between the rods. Each fuel rod is supported within each grid by the combination of support dimples and springs. The grid assembly consists of individual slotted straps assembled and interlocked into an egg-crate arrangement with the straps permanently joined at their points of intersection. The straps contain spring fingers, support dimples, and mixing vanes.

The grid material is Inconel 718 on the 17 x 17 STD fuel assembly and both Inconel and Zircaloy or ZIRLO on the V5H and RFA. The magnitude of the grid restraining force on the fuel rod is set high enough to minimize possible fretting, without overstressing the cladding at the points of contact between the grids and fuel rods. The grid assemblies also allow axial thermal expansion of the fuel rods without imposing restraint sufficient to develop buckling or distortion of the fuel rods.

Two types of grid assemblies are used in each 17 x 17 STD fuel assembly. One type, with mixing vanes projecting from the edges of the straps into the coolant stream, is used in the high heat flux region of the fuel assemblies to promote mixing of the coolant. The other type, located at the ends of the assembly, does not contain mixing vanes on the internal straps. The outside straps on all grids contain mixing vanes which, in addition to their mixing function, aid in guiding the grids and fuel assemblies past projecting surfaces during handling, and during loading and unloading of the core.

The V5H fuel assemblies use three types of grids; Inconel nonmixing vane grids at the top and bottom, Zircaloy or ZIRLO mixing vane grids, and Zircaloy or ZIRLO IFM grids. See Figure 4.2–2 for the grid arrangement. The IFMs are located in the three uppermost spans between the Zircaloy or ZIRLO mixing vane structural grids and incorporate a similar mixing vane array. Their prime function is mid-span flow mixing in the hottest fuel assembly spans.

The IFM grids are not designed to be structural members. The outer strap configuration was designed similar to mid-span grids to preclude grid hang-up and damage during fuel handling. Additionally, the grid envelope is smaller which further minimizes the potential for damage and reduces calculated forces seismic/LOCA events. A callable geometry is therefore assured at the IFM grid elevation as well as at the structural grid elevation.

As discussed in Section 4.2.2, the RFA, used for the first time in Region 9 (Cycle 7), implemented the Modified Low Pressure Drop (LPD) mid-grids, the Modified Intermediate Flow Mixer (IFM) grids, and the protective bottom grid which is a debris mitigating feature.

The mechanical design of the RFA-2 fuel assembly design introduced in Region 12 is the same as the previous cycle RFA designs except for the use of a modified mid-grid to improve resistance to fuel rod fretting. The new mid-grid design has been demonstrated to exhibit improved resistance to fuel rod fretting without significantly affecting any other thermal-hydraulic or mechanical performance. The overall width of the mid-grid springs and local width of the dimples are larger in the RFA-2 design versus the RFA.

4.2.2.3   Incore Control Components

Reactivity control is provided by neutron absorbing rods and a soluble chemical neutron absorber (boric acid). The boric acid concentration is varied to control long term reactivity changes including:

1.   Fuel depletion and fission product buildup

2.   Cold to hot, zero power reactivity change

3.   Reactivity change produced by intermediate term fission products such as xenon and samarium

4.   Burnable absorber depletion

The chemical and volume control system is discussed in Chapter 9.

The rod cluster control assemblies (RCCAs) provide reactivity control for:

1.   Shutdown

2.   Reactivity changes due to coolant temperature changes in the power range

3.   Reactivity changes associated with the power coefficient of reactivity

4.   Reactivity changes due to void formation

A negative moderator temperature coefficient throughout the entire cycle is desirable to reduce possible deleterious effects of a positive coefficient during loss of coolant or loss-of-flow accidents. The first fuel cycle contains more excess reactivity than subsequent cycles due to the loading of all fresh (unburned) fuel. Since soluble boron alone is insufficient to ensure a negative moderator coefficient, burnable absorbers are also used.

The RCCAs and their control drive mechanisms are the only moving parts in the reactor. Figure 4.2–8 illustrates the rod cluster control and control rod drive mechanism assembly, in addition to the arrangement of these components in the reactor, relative to the interfacing fuel assembly and guide tubes. In the following paragraphs, each reactivity control component is described in detail. The control rod drive mechanism assembly is described in Section 3.9N.4.

The neutron source assemblies provide a means of monitoring the core during periods of low neutron activity. The thimble plug assemblies limit bypass flow through those fuel assembly thimbles which do not contain control rods, burnable absorber rods, or neutron source rods.

4.2.2.3.1   Full Length Rod Cluster Control Assembly (RCCA)

The Rod Cluster Control Assemblies (RCCAs) used at Millstone Unit 3 have been provided by Westinghouse and AREVA (now known as Framatome). The AREVA RCCAs are functionally equivalent to the Westinghouse RCCAs (Reference 4.2-33) and a core configuration of RCCAs can be made up of all Westinghouse RCCAs, all AREVA RCCAs or any combination of both.

The RCCAs are divided into two categories: control and shutdown. The control groups compensate for reactivity changes due to variations in the operating conditions of the reactor, i.e., power and temperature variations. Two nuclear design criteria have been employed for selection of the control group. First, the total reactivity worth must be adequate to meet the nuclear

requirements of the reactor. Second, because the rods may be partially inserted at power operation, the total power peaking factor should be low enough to ensure that the power capability is met. The control and shutdown group provides adequate shutdown margin.

An RCCA is comprised of a group of individual neutron absorber rods fastened at the top end to a common spider assembly (Westinghouse, Figure 4.2–9a; AREVA, Figure 4.2–9b). The absorber material used in the control rods is silver-indium-cadmium alloy (Ag-In-Cd) which is essentially "black" to thermal neutrons and has sufficient additional resonance absorption to significantly increase their worth. The absorber materials are in the form of bars which are sealed in stainless steel tubes (Westinghouse, Figure 4.2–10; AREVA, Figure 4.2–9b) which may or may not have a wear resistant coating. Sufficient diametric and end clearance is provided to accommodate relative thermal expansions. The bottom plugs are made bullet-nosed to reduce the hydraulic drag during reactor trip and to guide smoothly into the dashpot section of the fuel assembly guide thimbles.

The overall length is such that when the assembly is withdrawn through its full travel the tips of the absorber rods remain engaged in the guide thimbles so that alignment between rods and thimbles is always maintained. Since the rods are long and slender, they are relatively free to conform to small misalignments with the guide thimble.

4.2.2.3.1.1 Westinghouse RCCA

The spider assembly is in the form of a central hub with radial vanes containing cylindrical fingers from which the absorber rods are suspended. Handling detents for connection to the drive rod assembly are machined into the upper end of the hub. A coil spring inside the spider body absorbs the impact energy at the end of the trip insertion. The radial vanes are joined to the hub by tack welding and brazing, and the fingers are joined to the vanes by brazing. A center post which holds the spring and its retainer is threaded into the hub within the skirt and welded to prevent loosening in service.

All components of the spider assembly are made from types 304 and 308 stainless steel except for the retainer, which is 17-4 PH material, and the springs, which are Inconel 718 alloy. The Westinghouse absorber rods use a type 304 stainless steel cladding. Westinghouse RCCAs received in 1991 and later utilize chrome plated cladding to improve wear resistance. The material used in the absober rod end plugs is type 308 stainless steel. The design stresses used for the type 308 material are the same as those defined in the ASME Code, Section III, for type 304 stainless steel. At room temperature the yield and ultimate stresses per ASTM 580 are exactly the same for the two alloys. In view of the similarity of the alloy composition, the temperature dependence of strength for the two materials is also assumed to be the same. The allowable stresses used as a function of temperature are listed in Table I-1.2 of Section III of the ASME Code. The fatigue strength for the type 308 material is based on the S-N curve for austenitic stainless steels on Figures I-9.2 of Section III.

The absorber rods are fastened securely to the spider. The rods are first threaded into the spider fingers and then pinned to maintain joint tightness, after which the pins are welded in place. The

end plug below the pin position is designed with a reduced section to permit flexing of the rods to correct for small operating or assembly misalignments.

4.2.2.3.1.2   AREVA RCCA

The AREVA RCCA spider is a single piece casting made of CF3 stainless steel. The coil spring material within the AREVA spider is Inconel 718 alloy and the retainer is 17-4 PH material.

The AREVA absorber rods use a type 316L stainless steel cladding with an ion-nitrided surface treatment to improve wear resistance. The absorber material is in the form of two solid bars, with the shorted lower end bar having a reduced diameter to allow for radiation induced swelling.

The AREVA absober rods are fastened securely to the spider. They are first pinned to the spider, with a pin tack welded to the spider to set its position, and then a nut is screwed onto the top of the rod and tack welded to the spider to prevent rotation of the nut.

4.2.2.3.2   Burnable Absorber Assembly and Integral Fuel Burnable Absorbers (IFBA)

Burnable absorber assemblies were only used in Cycles 1 and 2; IFBA has been used since.

Each burnable absorber assembly consists of burnable absorber rods attached to a hold-down assembly. A burnable absorber assembly is shown on Figure 4.2–11. When needed for nuclear considerations, burnable absorber assemblies are inserted into selected thimbles within fuel assemblies.

The absorber rods consist of borosilicate glass tubes contained within type 304 stainless steel tubular cladding which is plugged and seal welded at the ends to encapsulate the glass. The glass is also supported along the length of its inside diameter by a thin wall tubular inner liner. The top end of the liner is open to permit the diffused helium to pass into the void volume and the liner overhangs the glass. The liner has an outward flange at the bottom end to maintain the position of the liner with the glass. A typical burnable absorber rod is shown in longitudinal and transverse cross sections on Figure 4.2–11.

The absorber rods in each fuel assembly are grouped and attached together at the top end of the rods to a hold down assembly by a flat perforated retaining plate which fits within the fuel assembly top nozzle and rests on the adapter plate.

The retaining plate and the absorber rods are held down and restrained against vertical motion through a spring pack which bears against the plate and is compressed by the upper core plate when the reactor upper internals assembly is lowered into the reactor. This arrangement ensures that the absorber rods cannot be ejected from the core by flow forces. Each rod is permanently attached to the base plate by a nut which is lock-welded into place.

The cladding in the burnable absorber rods is slightly cold worked type 304 stainless steel. All other structural materials are types 304 or 308 stainless steel except for the springs which are

Inconel 718. The borosilicate glass tube provides sufficient boron content to meet the criteria discussed in Section 4.3.1.

Integral fuel burnable absorbers (IFBA) consists of a thin ZrB_2 coating on some of the fuel pellets. The height of the ZrBr coating, the total number used in the core, and the placement pattern are determined for each cycle of operation. IFBAs offer advantages in that burnable absorber assemblies handling is avoided during refueling and there are a greater number of available locations within a fuel assembly to position the absorber.

4.2.2.3.3   Neutron Source Assembly

The purpose of the neutron source assemblies is to provide a base neutron level to ensure that the ex-core neutron detectors are operational and responding to core multiplication neutrons. The neutron source assemblies also permit detection of changes in the core multiplication factor during core fuel loading, and approach to criticality. This can be done since the multiplication factor is related to an inverse function of the detector count rate. Changes in the multiplication factor can be detected during addition of fuel assemblies while loading the core, changes in control rod positions, and changes in boron concentration.

Three types of neutron source assemblies have been utilized at Millstone Unit 3. These are: 1.) the Primary Source Assembly (PSA), 2.) the single encapsulated Secondary Source Assembly (SSA), and 3.) the double-encapsulated SSA.

The PSAs contain one primary source rod and a number of burnable absorber rods. The single encapsulated SSAs contain a symmetrical grouping of four secondary source rods. The double-encapsulated SSAs contain a symmetrical grouping of six secondary source rods. The neutron source assemblies contain a hold-down assembly identical to that of the burnable poison assembly. The PSA is shown on Figure 4.2–13. The single-encapsulated and double-encapsulated SSAs are shown on Figure 4.2–14a and Figure 4.2–14b, respectively.

The rods in the PSAs contain a radioactive material that spontaneously emits neutrons during initial core loading, reactor startup, and initial operation of the first core. After the rods in the PSAs decay beyond the desired neutron flux level, neutrons are then supplied by the SSAs. The rods in the SSAs contain a stable material that must be activated during reactor operation. The activation results in the subsequent release of neutrons.

The cladding of the rods for both the PSAs and SSAs is slightly cold worked type 304 stainless steel. The rods in the PSAs contain capsules of californium (Pu-Be, possible alternate) source material and alumina spacer to position the source material within the cladding. The rods in the single-encapsulated SSAs contain Sb-Be pellets stacked to a height of approximately 97 inches while the rods in the double-encapsulated SSAs contain Sb-Be pellets stacked to a height of approximately 88 inches. The rods in each assembly are permanently fastened at the top end to a hold-down assembly. All other structural materials are constructed of type 304 or 308 stainless steel except for the springs that are Inconel 718.

For the first core (Cycle 1), PSAs were placed in the reactor to provide a positive neutron count of at least two counts per second on the source range detectors attributable to core neutrons. The detectors, called source range detectors, are used primarily when the core is subcritical and during special subcritical modes of operation. In total, four source assemblies were installed in the Cycle 1 reactor core: two PSAs and two SSAs. The SSAs were of the single-encapsulated design. The PSAs were removed after Cycle 1.

The double-encapsulated SSA design was first used in Cycle 6. The double-encapsulated SSA design provides additional margin against failure of the source rod cladding and the subsequent leakage of source material. Cycle 6 also constituted last use of the singe-encapsulated SSA design (2 SSA pairs were loaded).

The number and placement of secondary source assemblies in reload cycles is determined as part of the Reload Safety Evaluation process. Neutron source assemblies, when used, are employed in pairs on opposite sides of the core. The neutron assemblies are inserted into the rod cluster control guide thimbles in fuel assemblies in select unrodded locations.

4.2.2.3.4   Thimble Plug Assembly

Thimble plug assemblies limit bypass flow through the rod cluster control guide thimbles in fuel assemblies which do not contain either control rods, source rods, or burnable absorber rods.

The removal of all thimble plugs was allowed for Cycles 3 and 4. However, beginning with Cycle 5 the installation of thimble plugs and the resulting increase in core flow rate is credited analytically to provide additional DNB margin.

The thimble plug assemblies consist of a flat base plate with short rods suspended from the bottom surface and a spring pack assembly (Figure 4.2–15). The 24 short rods, called thimble plugs, project into the upper ends of the guide thimbles to reduce the bypass flow. Each thimble plug is permanently attached to the base plate by a nut which is locked to the threaded end of the plug. Similar short rods are also used on the source assemblies and burnable absorber assemblies to plug the ends of all vacant fuel assembly guide thimbles. When in the core, the thimble plug assemblies interface with both the upper core plate and with the fuel assembly trip nozzles by resting on the adapter plate. The spring pack is compressed by the upper core plate when the upper internals assembly is lowered into place.

All components in the thimble plug assembly, except for the springs, are constructed from type 304 or 308 stainless steel. The springs are Inconel 718.

4.2.3   DESIGN EVALUATION

The fuel assemblies, fuel rods, and incore control components are designed to satisfy the performance and safety criteria of Section 4.2, the mechanical design bases of Section 4.2.1, and other interfacing nuclear and thermal-hydraulic design bases specified in Sections 4.3 and 4.4.

Effects of Conditions II, III, IV or anticipated transients without trip on fuel integrity are presented in Chapter 15 or supporting topical reports.

The initial step in fuel rod design evaluation for a region of fuel is to determine the limiting rod(s). Limiting rods are defined as those rods whose predicted performance provides the minimum margin to each of the design criteria. For a number of design criteria, the limiting rod is the lead burnup rod of a fuel region. In other instances, it may be the maximum power or the minimum burnup rod. For the most part, no single rod is limiting with respect to all design criteria.

After identifying the limiting rod(s), a worst-case performance analysis is performed which considers the effects of rod operating history, model uncertainties, and dimensional variations. To verify adherence to the design criteria, the evaluation considers the effects of postulated transient power changes during operation consistent with Conditions I and II. These transient power increases can affect both rod average and local power levels. Parameters considered include rod internal pressure, fuel temperature, clad stress, clad strain, and clad corrosion (oxidation and hydrogen pickup). In fuel rod design analyses, these performance parameters provide the basis for comparison between expected fuel rod behavior and the corresponding design criteria limits.

Fuel rod and assembly models used for the performance evaluations are documented and maintained under an appropriate control system. Materials properties used in the design evaluations are given in Reference 4.2-15.

4.2.3.1   Cladding

1.   Vibration and wear

Fuel rod vibrations are flow induced. The effect of the vibration on the fuel assembly and individual fuel rods is minimal. The cyclic stress range associated with deflections of such small magnitude is insignificant and has no effect on the structural integrity of the fuel rod.

The reaction force on the grid supports due to rod vibration motions is also small and is much less than the spring preload. Firm fuel clad spring contact is maintained. No significant wear of the clad or grid supports is expected during the life of the fuel assembly, based on out-of-pile flow tests, performance of similarly designed fuel in operating reactors, and design analyses.

Clad fretting and fuel vibration has been experimentally investigated, as shown in Reference 4.2-9.

2.   Fuel rod internal pressure and cladding stresses

A burnup dependent fission gas release model is used in determining the internal gas pressures as a function of irradiation time. The plenum height within the fuel rod has been designed to ensure that the maximum internal pressure of the fuel rod will not exceed the value which would cause: (1) the fuel/clad diametral gap to

increase during steady state operation, and (2) extensive DNB propagation to occur.

The clad stresses at a constant local fuel rod power are low. Compressive stresses are created by the pressure differential between the coolant pressure and the rod internal gas pressure. Because of the prepressurization with helium, the volume average effective stresses are always less than approximately 10,000 psi at the pressurization level used in this fuel rod design. Stresses due to the temperature gradient are not included in this average effective stress because thermal stresses are, in general, negative at the clad inside diameter and positive at the clad outside diameter and their contribution to the clad volume average stress is small. Furthermore, the thermal stress decreases with time during steady state operation due to stress relaxation. The stress due to pressure differential is highest in the minimum power rod at the beginning of life due to low internal gas pressure and the thermal stress is highest in the maximum power rod due to steep temperature gradient.

The internal gas pressure at beginning of life for the initial core is approximately 1,400 psia for a typical lead burnup fuel rod. The total tangential stress at the clad inside diameter at beginning of life is approximately 14,400 psi compressive (approximately 13,000 psi due to ΔP and approximately 1,400 due to ΔT) for a low power rod, operating at 5 kW/ft and approximately 12,000 psi compressive (8,500 psi due to ΔP and approximately 3,500 psi due to ΔT) for a high power rod operating at 15 kW/ft. However, the volume average effective stress at beginning of life is between approximately 8,000 psi (high power rod) and approximately 10,000 psi (low power rod). These stresses are substantially below even the unirradiated clad strength (55,500 psi) at a typical clad mean operating temperature of 700°F.

Tensile stresses could be created once the clad has come in contact with the pellet. These stresses would be induced by the fuel pellet swelling during irradiation. Swelling of the fuel pellet can result in small clad strains (< 1 percent) for expected discharge burnups, but the associated clad stresses are very low because of clad creep (thermal- and irradiation-induced). The 1 percent strain criterion is extremely conservative for fuel-swelling driven clad strain because the strain rate associated with solid fission products swelling is very slow. A detailed discussion on fuel rod performance is given in Section 4.2.3.3.

3.   Materials and chemical evaluation

Zicaloy-4, ZIRLO or Optimized ZIRLO tubing has a high corrosion resistance to coolant, fuel, and fission products. As shown in Reference 4.2-6, there is considerable pressurized water reactor operating experience on the capability of Zircaloy/ZIRLO as a clad material. Controls on fuel fabrication specify maximum moisture levels to preclude clad hydriding.

ZIRLO fuel rod cladding was used in the feed fuel assemblies from Cycle 5 (Region 7) to Cycle 15 (Region 17). Optimized ZIRLO fuel rod cladding was used starting with Cycle 16 (Region 18). Both ZIRLO and Optimized ZIRLO have improved resistance to corrosion above the Zircaloy-4 used previously. References 4.2-23 and 4.2-31 provide discussions related to the material properties of ZIRLO and Optimized ZIRLO.

Metallographic examination of irradiated commercial fuel rods have shown occurrences of fuel/clad chemical interaction. Reaction layers of < 1 mil in thickness have been observed between fuel and clad at limited points around the circumference. Metallographic data indicate that this interface layer remains very thin even at high burnup. Thus, there is no indication of propagation of the layer and eventual clad penetration.

Stress corrosion cracking is another postulated phenomenon related to fuel/clad chemical interaction. Out-of-pile tests have shown that in the presence of high clad tensile stresses, large concentrations of iodine can chemically attack the Zircaloy tubing and lead to eventual clad cracking. Extensive post-irradiation examination has produced no conclusive in-pile evidence that this mechanism is operative in commercial fuel.

Reference 4.2-36 describes the Westinghouse cladding corrosion model that is used to analyze the corrosion of ZIRLO and Optimized ZIRLO cladding as part of the fuel rod design analysis.

4. Rod bowing

   Reference 4.2-12, presents the model used for evaluation of fuel rod bowing. Additional discussion on rod bowing is provided in Section 4.2.3.3 (Item 5) and Section 4.4.2.2.5.

5. Consequences of power-coolant mismatch

   This subject is discussed in Chapter 15.

6. Creep collapse and creepdown

   This subject and the associated irradiation stability of cladding have been evaluated using the models described in References 4.2-25 and 4.2-31. It has been established that the design basis of no clad collapse during planned core life can be satisfied by limiting fuel densification and by having a sufficiently high initial rod internal pressure.

7. Irradiation Stability of the Cladding

Testing of irradiated Zircaloy-4 is provided in References 4.2-15 and 4.2-23 for ZIRLO and Optimized ZIRLO. Pressurized water reactor operating experience on the capability of Zicaloy-4, ZIRLO or Optimized ZIRLO tubing as a cladding material is summarized in Reference 4.2-6.

8.   Cycling and Fatigue

A comprehensive review of the available strain fatigue models was conducted by Westinghouse as early as 1968. This review included the Langer-O'Donnell model, the Yao-Munse model and the Manson-Halford model. Upon completion of this review and using the results of the Westinghouse experimental progrms discussed below, it was concluded that the approach defined by Langer-O'Donnell would be retained and the empirical factors of their correlation modified in order to conservatively bound the results of the Westinghouse testing program.

The Westinghouse testing program was subdivided into the following subprograms:

1.   A rotating bend fatigue experiment on unirradiated Zircaloy-4 specimens at room temperature and at 725°F. Both hydrided and nonhydrided Zircaloy-4 cladding were tested.

2.   A biaxial fatigue experiment in gas autoclave on unirradiated Zircaloy-4 cladding, both hydrided and nonhydrided.

3.   A fatigue test program on irradiated cladding from the CVS and Yankee Core V conducted at Battelle Memorial Institute.

The results of these test programs provided information on different cladding conditions including the effects of irradiation, of hydrogen levels and of temperature.

The design equations followed the concept for the fatigue design criterion according to the ASME Boiler and Pressure Vessel Code, Section III.

It is recognized that a possible limitation to the satisfactory behavior of the fuel rods in a reactor which is subjected to daily load follow is the failure of the cladding by low cycle strain fatigue. During their normal residence time in reactor, the fuel rods may be subjected to approximately 1000 cycles with typical changes in power level from 50 to 100 percent of their steady state values.

The assessment of the fatigue life of the fuel rod cladding is subject to a considerable uncertainty due to the difficulty of evaluating the strain range which results from the cyclic interaction of the fuel pellets and cladding. This difficulty arises, for example, from such highly unpredictable phenomenon as pellet cracking, fragmentation and relocation. Nevertheless, since early 1968, this

particular phenomenon has been investigated analytically and experimentally. Strain fatigue tests on irradiated and nonirradiated hydrided Zr-4 claddings were performed, which permitted a definition of a conservative fatigue life limit and recommendation on a methodology to treat the strain fatigue evaluation of the Westinghouse reference fuel rod designs.

It is believed that the final proof of the adequacy of a given fuel rod design to meet the load follow requirements can only come from incore experiments performed on actual reactors. Experience in load follow operation dates back to early 1970 with the load follow operation of the Saxton reactor. Successful Load follow operation has been performed on Reactor A (> 400 load follow cycles) and Reactor B (> 500 load follow cycles). In both cases, there was no significant coolant activity increase that could be associated with the load follow mode of operation.

4.2.3.2 Fuel Materials Considerations

Sintered, high density uranium dioxide fuel reacts only slightly with the clad, at core operating temperatures and pressures. In the event of clad defects, the high resistance of uranium dioxide to attack by water protects against fuel deterioration although limited fuel erosion can occur. As has been shown by operating experience and extensive experimental work, the thermal design parameters conservatively account for changes in the thermal performance of the fuel elements due to pellet fracture which may occur during power operation. The consequences of defects in the clad are greatly reduced by the ability of uranium dioxide to retain fission products including those which are gaseous or highly volatile. Observations from several operating Westinghouse pressurized water reactors, Reference 4.2-13 have shown that, under irradiation, fuel pellets can densify to higher than manufactured values. Fuel densification and subsequent settling of the fuel pellets can result in local and distributed gaps in the fuel rods. Fuel densification has been minimized by improvements in the fuel manufacturing process and by specifying a nominal 95 percent initial fuel density.

The evaluation of fuel densification effects and their consideration in fuel design are described in References 4.2-7 and 4.2-21. The treatment of fuel swelling and fission gas release are described in Reference 4.2-21.

The effects of waterlogging on fuel behavior are discussed in Section 4.2.3.3.

4.2.3.3 Fuel Rod Performance

In the calculation of the steady state performance of a nuclear fuel rod, the following interacting factors must be considered:

1. Clad creep and elastic deflection

2. Pellet density changes, thermal expansion, gas release, and thermal properties as a function of temperature and fuel burnup

3.   Internal pressure as a function of fission gas release, rod geometry, and temperature distribution

These effects are evaluated by the fuel rod design model described in References 4.2-21 and 4.2-34, accounting for time dependent fuel densification and clad creep. With these interacting factors considered, the model determines the fuel rod performance characteristics for a given rod geometry, power history, and axial power shape. In particular, internal gas pressure, fuel and clad temperatures, and clad deflections are calculated. The fuel rod is divided into several axial sections and radially into a number of annular zones. Fuel density changes are calculated separately for each segment. The effects are integrated to obtain the internal rod pressure. The initial rod internal pressure is selected to delay fuel/clad mechanical interaction and to avoid the potential for flattened rod formation. It is limited, however, by the design criteria for the rod internal pressure (Section 4.2.1.3). The gap conductance between the pellet surface and the clad inner diameter is calculated as a function of the composition, temperature, and pressure of the gas mixture, and the gap size of contact pressure between clad and pellet. After computing the fuel temperature for each pellet annular zone, the fractional fission gas release is assessed using an empirical model derived from experimental data in Reference 4.2-21. The total amount of gas released is based on the average fractional release within each axial and radial zone and the gas generation rate which in turn is a function of burnup. Finally, the gas released is summed over all zones and the pressure is calculated. The code shows good agreement in fit for a variety of published and proprietary data on fission gas release, fuel temperatures, and clad deflections in Reference 4.2-21. These data include variations in power, time, fuel density, and geometry.

1.   Fuel/cladding mechanical interaction

One factor in fuel element duty is potential mechanical interaction of fuel and clad. This fuel/clad interaction produces cyclic stresses and strains in the clad, and these, in turn, consume clad fatigue life. The reduction of fuel/clad interaction is therefore a goal of design. The technology for using prepressurized fuel rods in Westinghouse pressurized water reactors has been developed to further this objective.

The gap between the fuel and clad is initially sufficient to prevent hard contact between the two. However, during power operation a gradual compressive creep of the clad onto the fuel pellet occurs due to the external pressure exerted on the rod by the coolant. Clad compressive creep eventually results in the fuel/clad contact. Once fuel/clad contact occurs, changes in power level result in changes in clad stresses and strains. By using prepressurized fuel rods to partially offset the effect of the coolant external pressure, the rate of clad creep toward the surface of the fuel is reduced. Fuel rod prepressurization delays the time at which fuel/clad contact occurs and hence significantly reduces the extent of cyclic stresses and strains experienced by the clad both before and after fuel/clad contact. These factors result in an increase in the fatigue life margin of the clad and lead to greater clad reliability. If gaps should form in the fuel stacks, clad flattening will be prevented by the rod prepressurization so that the flattening time will be greater than the fuel core life.

A two dimensional (r, θ) finite element model has been established to investigate the effects of radial pellet cracks on stress concentrations in the clad (Reference 4.2-18). Stress concentration, herein, is defined as the difference between the maximum clad stress in the θ–direction and the mean clad stress. The first case has the fuel and clad in mechanical equilibrium and as a result the stress in the clad is close to zero. In subsequent cases the pellet power is increased in steps and the resultant fuel thermal expansion imposes tensile stress in the clad. In addition to uniform clad stresses, stress concentrations develop in the clad adjacent to radial cracks in the pellet. These radial cracks have a tendency to open during a power increase but the frictional forces between fuel and clad oppose the opening of these cracks and result in localized increases in clad stress. As power is further increased, large tensile stresses exceed the ultimate tensile strength of UO_2, and additional cracks in the fuel are created which limit the magnitude of the stress concentration in the clad.

As part of the standard fuel rod design analysis, the maximum stress concentration evaluated from finite element calculations is added to the volume averaged effective stress in the clad as determined from one dimensional stress/strain calculations. The resultant clad stress is then compared to the temperature-dependent yield stress in order to ensure that the stress/strain criteria are satisfied.

Transient Evaluation Method

Pellet thermal expansion due to power increases is considered the only mechanism by which significant stresses and strains can be imposed on the clad. Power increases in commercial reactors can result from fuel shuffling (e.g., region 3 positioned near the center of the core for cycle 2 operation after operating near the periphery during cycle 1), reactor power escalation following extended reduced power operation, and full-length control rod movement. In the mechanical design model, lead rods are depleted using best estimate power histories as determined by core physics calculations. During burnup, the amount of diametral gap closure is evaluated based upon the pellet expansion cracking model, clad creep model, and fuel swelling model. At various times during the depletion, the power is increased locally on the rod to the burnup dependent attainable power density as determined by core physics calculations. The radial, tangential, and axial clad stresses resulting from the power increase are combined into a volume average effective clad stress.

The Von Mises criterion or the ASME methodology calculated clad stress (Reference 4.2-35) is used to determine if the clad yield stress has been exceeded. This criterion states that an isotropic material in multiaxial stress begins to yield plastically when the effective stress exceeds the yield stress as determined by an axial tensile test. The yield stress correlation is that for irradiated cladding, since fuel/clad interaction occurs at high burnup. In applying this criterion, the effective stress is increased by an allowance which accounts for stress concentrations in the clad adjacent to radial cracks in the pellet, prior to the comparison with the yield

stress. This allowance was evaluated using a two dimensional (r,θ) finite element model. The ASME clad stress methodology utilizes the unirratdiated clad yield strength in the analysis discussed in Section 4.2.1.1.

Slow transient power increases can result in large clad strains without exceeding the clad yield stress because of clad creep and stress relaxation. Therefore, in addition to the yield stress criterion, a criterion on allowable clad strain is necessary. Based upon high strain rate burst and tensile test data on irradiated tubing, 1 percent strain was determined to be a conservative lower limit on irradiated clad ductility and thus adopted as a design criterion (Reference 4.2-18).

A comprehensive review of the available strain-fatigue models was conducted by Westinghouse as early as 1968. This included the Langer-O'Donnell model (Reference 4.2-1), the Yao-Munse model, and the Manson-Halford model. Upon completion of this review and using the results of the Westinghouse experimental programs discussed below, it was concluded that the approach defined in Reference 4.2-1 would be retained and the empirical factors of their correlation modified in order to conservatively bound the results of the Westinghouse testing program.

The Langer-O'Donnell empirical correlation has the following form:

$$S_a = \frac{E}{4\sqrt{N_f}} ln\left[\frac{100}{100 - RA}\right] + S_e$$

where:

$S_a = 1/2E\Delta^\varepsilon_t$ = pseudo-stress amplitude which causes failure in N_f cycles (lb/in^2)

Δ^ε_t = total strain range (in/in)

E = Young's Modulus (lb/in^2)

RA = effective reduction in area at fracture in a uniaxial tensile test (percent)

S_e = effective endurance limit (lb/in^2)

Both RA and S_e are empirical constants which depend on the type of material, the temperature, and irradiation conditions.

The Westinghouse testing program was subdivided into the following subprograms:

a. A rotating bend fatigue experiment on unirradiated Zircaloy-4 specimens at room temperature and at 725°F. Both hydrided and nonhydrided Zircaloy-4 cladding were tested.

b.   A biaxial fatigue experiment in a gas autoclave on unirradiated Zircaloy-4 cladding both hydrided and nonhydrided.

c.   A fatigue test program on irradiated cladding from the Carolina-Virginia Tube Reactor and Yankee Core V conducted at Battelle Memorial Institute (Reference 4.2-18).

The results of these test programs provided information on different cladding conditions, including the effect of irradiation, hydrogen level, and temperature.

The design equations followed the concept for the fatigue design criterion according to the ASME Code, Section III, namely:

a.   The calculated pseudo-stress amplitude (S_a) has to be multiplied by a factor of 2 in order to obtain the allowable number of cycles (N_f).

b.   The allowable cycles for a given S_a is 5 percent of N_f, or a safety factor of 20 on cycles.

The lesser of the two allowable number of cycles is selected. The cumulative fatigue life fraction is then computed as:

$$\sum_{1}^{k} \frac{n_k}{N_{fk}} \leq 1$$

where:

n_k = number of cycles of mode k

N_{fk} = number of allowable cycles

It is recognized that a possible limitation to the satisfactory behavior of the fuel rods in a reactor which is subjected to daily load follow is the failure of the clad by low-cycle strain fatigue. During their normal residence time in reactor, the fuel rods may be subjected to approximately 1,000 cycles with typical changes in power level from 50 to 100 percent of their steady state values.

The assessment of the fatigue life of the fuel rod clad is subject to a considerable uncertainty due to the difficulty of evaluating the strain range which results from the cyclic interaction of the fuel pellets and clad. This difficulty arises, for example, from such highly unpredictable phenomena as pellet cracking, fragmentation, and relocation. Nevertheless, since early 1968, this particular phenomenon has been investigated analytically and experimentally (Reference 4.2-1). Strain fatigue tests on irradiated and nonirradiated hydrided

Zircaloy-4 claddings were performed which permitted a definition of a conservative fatigue life limit and recommendation for a methodology to treat the strain fatigue evaluation of the Westinghouse reference fuel rod designs (Reference 4.2-18).

It is believed that the final proof of the adequacy of a given fuel rod design to meet the load follow requirements can come only from incore experiments performed on actual reactors. Experience in load follow operation dates back to early 1970 with the load follow operation of the Saxton reactor. Successful load follow operation has been performed on reactor A (approximately 400 load follow cycles) and reactor B (>500 load follow cycles). In both cases, there was no significant coolant activity increase that could be associated with the load follow mode of operation.

2.   Irradiation experience

Westinghouse fuel operational experience is presented in Reference 4.2-6. Additional test assembly and test rod experience are given in Sections 8 and 23 of Reference 4.2-13.

3.   Fuel and cladding temperature

The methods used for evaluation of fuel rod temperatures are presented in Section 4.4.2.11.

4.   Waterlogging

Local cladding deformations typical of waterlogging bursts have never been observed in commercial Westinghouse fuel. (Waterlogging damage of a previously defected fuel rod has occasionally been postulated as a mechanism for subsequent rupture of the cladding. Such damage has been postulated as a consequence of a power increase on a rod after water has entered such a rod through a clad defect of appropriate size. Rupture is postulated upon power increase if the rod internal pressure increase is excessive due to insufficient venting of water to the reactor coolant.) Experience has shown that the small number of rods which have acquired clad defects, regardless of primary mechanism, remain intact and do not progressively distort or restrict coolant flow. In fact, such small defects are normally observed through reductions in coolant activity to be progressively closed upon further operation due to the buildup of zirconium oxide and other substances. Secondary failures which have been observed in defected rods are attributed to hydrogen embrittlement of the cladding. Post-irradiation examinations point to the hydriding failure mechanism rather than a waterlogging mechanism; the secondary failures occur as axial cracks in the cladding and are similar regardless of the primary failure mechanism. Such cracks do not result in flow blockage or increase the effects of any postulated transients.

More information is provided in Reference 4.2-2.

5.   Potentially damaging temperature effects during transients

The fuel rod experiences many operational transients (intentional maneuvers) during its residence in the core. A number of thermal effects must be considered when analyzing the fuel rod performance.

The clad can be in contact with the fuel pellet at some time in the fuel lifetime. Clad/pellet interaction occurs if the fuel pellet temperature is increased after the clad is in contact with the pellet. Clad/pellet interaction is discussed in Section 4.2.3.3.

The potential effects of operation with waterlogging fuel are discussed in Section 4.2.3.3 which concludes that waterlogging is not a concern during operational transients.

Clad flattening, as shown in Reference 4.2-11 has been observed in some operating power reactors. Thermal expansion (axial) of the fuel rod stack against a flattened section of clad could cause failure of the clad. This is no longer a concern because clad flattening is precluded during the fuel residence in the core (Section 4.2.3.1).

Potential differential thermal expansion between the fuel rods and the guide thimbles during a transient is considered in the design. Excessive bowing of the fuel rods is precluded because the grid assemblies allow axial movement of the fuel rods relative to the grids. Specifically, thermal expansion of the fuel rods is considered in the grid design so that axial loads imposed on the fuel rods during a thermal transient will not result in excessively bowed fuel rods.

6.   Fuel element burnout and potential energy release

As discussed in Section 4.4.2.2, the core is protected from DNB over the full range of possible operating conditions. In the extremely unlikely event that DNB should occur, the clad temperature will rise due to the steam blanketing at the rod surface and the consequent degradation in heat transfer. During this time there is a potential for chemical reaction between the cladding and the coolant. However, because of the relatively good film boiling heat transfer following DNB, the energy release resulting from this reaction is insignificant compared to the power produced by the fuel.

7.   Coolant flow blockage effects on fuel rods

This evaluation is presented in Section 4.4.4.7.

4.2.3.4   Spacer Grids

The reactor core coolant flow channels were established and maintained by the fuel assembly structure composed of grids and guide thimbles. The lateral spacing between fuel rods is provided and controlled by the support dimples of adjacent grid cells. Contact of the fuel rods on the dimples is maintained through the clamping force of the grid springs. Lateral motion of the fuel rods is opposed by the spring force and the internal moments generated between the spring and the support dimples.

Time history numerical integration techniques were used to analyze the fuel assembly responses resulting from the lateral safe shutdown earthquake (SSE) and the most limiting main coolant pipe break accident, LOCA. The reactor vessel motions resulting from the transient loading were asymmetric with respect to the geometrical center of the reactor core. The complete fuel assembly core finite element model was employed to determine the fuel assembly deflections and grid impact forces.

A comparison of the seismic (SSE) response spectrum of the reactor vessel supports versus the response spectrum of the time history indicated that the time history spectrum generally enveloped the plant design spectrum with the exception of a small frequency range at the second mode of the fuel assembly. The seismic analyses performed for a number of plants indicated that the maximum impact response was, in general, influenced by the acceleration level of the input forcing function at the fuel assembly fundamental mode. Thus, the data in seismic time histories corresponding to the design envelope were conservatively used for the fuel evaluation.

The reactor core finite element model consisting of the maximum number of fuel assemblies across the core diameter was used. The maximum number of fuel assemblies across the core for Millstone 3 is fifteen 17 x 17 8-grid fuel assemblies arranged in a planar array. Gapped elements simulated the clearances between the peripheral fuel assemblies and the baffle plates. IFM grids are not structural components and are not included.

The fuel assembly essential dynamic properties, such as the fuel assembly vibration frequencies, mode shapes, and mass distribution were presented in the finite element model. The time history motions for the upper and lower core plates and the motions for the core barrel at the upper core plate elevation were simultaneously introduced into the simulated core model. The analytical procedures, the fuel assembly and core modeling, and the methodology are detailed in References 4.2-8 and 4.2-17. The time history inputs representing the SSE motions and the coolant pipe rupture transients were obtained from the time history analyses of the reactor vessel internals. Grid crush tests and results of seismic and LOCA evaluations indicate the grids maintain a geometry that is capable of being cooled under the worst-case accident, Condition IV event.

4.2.3.4.1   Grid Analysis

The maximum grid impact forces for both the seismic accident and asymmetric LOCA occur at the peripheral fuel assembly locations adjacent to the baffle wall. The maximum grid impact forces result from postulated LOCA and seismic loadings, and are required to be less than the allowable grid crush strength. A calculation of the maximum LOCA and seismic grid impact

forces, combined using the square root sum of the squares method in accordance with SRP 4.2, Appendix A, demonstrated that the maximum value is below the allowable grid strength.

Later studies of Zircaloy and ZIRLO spacer grids crush strengths are contained in References 4.2-20 and 4.2-23.

The grid strength was established experimentally. It was based on the 95 percent confidence level on the true mean as taken from the distribution of measurements.

4.2.3.4.2   Nongrid Component Analyses

The stresses induced in the various fuel assembly nongrid components were calculated. The calculations were based on the maximum responses obtained from the most limiting LOCA and seismic accident conditions. The fuel assembly axial forces resulting from the LOCA accident were the primary sources of stresses in the thimble guide tube and the fuel assembly nozzles. The induced stresses in the fuel rods result from the relative deflections during the simulated seismic and LOCA accidents. The fuel rod stresses were generally small. The combined seismic and LOCA induced stresses of the various fuel assembly components presented in Table 4.2-1 were expressed as a percentage of the allowable limit. Consequently, the fuel assembly components are structurally acceptable under the postulated accident design conditions for Millstone 3.

4.2.3.5   Fuel Assembly

4.2.3.5.1   Stresses and Deflections

The fuel assembly component stress levels are limited by the design. For example, stresses in the fuel rod due to thermal expansion and Zircaloy irradiation growth are limited by the relative motion of the rod as it slips over the grid spring and dimple surfaces. Clearances between the fuel rod ends and nozzles are provided so that Zircaloy irradiation growth does not result in rod end interferences. The growth of ZIRLO and Optimized ZIRLO is expected to be about half that of Zircaloy-4. Stresses in the fuel assembly caused by tripping of the rod cluster control assembly have little influence on fatigue because of the small number of events during the life of an assembly. Assembly components and prototype fuel assemblies made from production parts have been subjected to structural tests to verify that the design bases requirements are met.

The fuel assembly design loads for shipping have been established at 4g axial and 6g lateral. Accelerometers are permanently placed into the shipping cask to monitor and detect fuel assembly accelerations that would exceed the criteria. Past history and experience have indicated that loads which exceed the allowable limits rarely occur. Exceeding the limits requires reinspection of the fuel assembly for damage. Tests on various fuel assembly components, such as the grid assembly, sleeves, inserts, and structure joints, have been performed to ensure that the shipping design limits do not result in impairment of fuel assembly function. Seismic analysis of the fuel assembly is presented in Reference 4.2-8.

4.2.3.5.2   Dimensional Stability

A prototype fuel assembly has been subjected to column loads in excess of those expected in normal service and faulted conditions (Reference 4.2-8).

No interference with control rod insertion into thimble tubes will occur during a postulated LOCA transient due to fuel rod swelling, thermal expansion, or bowing. In the early phase of the transient following the coolant break, the high axial loads, which could be generated by the difference in thermal expansion between fuel clad and thimbles, are relieved by slippage of the fuel rods through the grids. The relatively low drag force restraint on the fuel rods will induce only minor thermal bowing, which is insufficient to close the fuel rod-to-thimble tube gap.

Reference 4.2-8 shows that the fuel assemblies will maintain a geometry amenable to cooling during a combined seismic and double-ended LOCA.

4.2.3.6   Reactivity Control Assembly and Burnable Absorber Rods

1.   Internal pressure and cladding stresses during normal, transient, and accident conditions

The designs of the burnable absorber and source rods provide a sufficient cold void volume to accommodate the internal pressure increase during operation. This is not a concern for the absorber rod because no gas is released by the absorber material.

For the burnable absorber rod used in Cycles 1 and 2, the use of glass in tubular form provides a central void volume along the length of the rods (Figure 4.2–11). For the source rods, a void volume is provided within the rod in order to limit the internal pressure increase until end of life (Figures 4.2–13 and 4.2-14).

The stress analysis of these rods assumes 100 percent gas release to the rod void volume in addition to the initial pressure within the rod.

During normal transient and accident conditions the void volume limits the internal pressures to values which satisfy the criteria in Section 4.2.1.6. These limits are established not only to ensure that peak stresses do not reach unacceptable values, but also limit the amplitude of the oscillatory stress component in consideration of the fatigue characteristics of the materials.

Rod, guide thimble, and dashpot flow analyses indicate that the flow is sufficient to prevent coolant boiling within the guide thimble. Therefore, clad temperatures at which the clad material has adequate strength to resist coolant operating pressures and rod internal pressures are maintained.

2.   Thermal stability of the absorber material, including phase changes and thermal expansion

The radial and axial temperature profiles within the source and absorber rods have been determined by considering gap conductance, thermal expansion, neutron or gamma heating of the contained material as well as gamma heating of the clad.

The maximum temperatures of the Ag-In-Cd or hafnium control rod absorber material were calculated and found to be significantly less than the respective material melting point and occur axially at only the highest flux region. The thermal expansion properties of the absorber material and the phase changes are discussed in Reference 4.2-15 for the Ag-In-Cd and hafnium materials. Identical absorber material (Ag-In-Cd) is utilized by both Westinghouse and AREVA and the material properties are applicable to both vendor's designs.

The maximum temperature of the borosilicate glass used in Cycles 1 and 2 was calculated to be about 1300 °F and takes place following the initial rise to power. As the operating cycle proceeds, the glass temperature decreases for the following reasons:

a.   Reduction in power generation due to boron-10 depletion

b.   Better gap conductance as the helium produced diffuses to the gap

c.   External gap reduction due to borosilicate glass creep

Sufficient diametral and end clearances have been provided in the neutron absorber, burnable absorber, and source rods to accommodate the relative thermal expansions between the enclosed material and the surrounding clad and end plug.

3.   Irradiation stability of the absorber material, taking into consideration gas release and swelling

The irradiation stability of the absorber material is discussed in Reference 4.2-15 for Ag-In-Cd and hafnium. Irradiation produces no deleterious effects in the absorber material.

As mentioned in Item 1 above, gas release is not a concern for the control rod material because no gas is released by the absorber material. Sufficient diametral and end clearances are provided to accommodate swelling of the absorber material. Identical absorber material (Ag-In-Cd) is utilized by both Westinghouse and AREVA and the material properties are applicable to both vendor's designs.

Based on experience with the borosilicate glass used in Cycles 1 and 2, and on nuclear and thermal calculations, gross swelling or cracking of the glass tubing is not expected during operation. Some minor creep of the glass at the hot spot could occur, but would continue only until B-10 depletion and helium gap closure by creep had lowered the glass temperature to values which cause negligible creep. The wall thickness of the inner liner is sized to provide adequate support in the

event of slumping and to collapse locally before rupture of the exterior cladding if unexpected large volume changes, due to swelling or cracking, should occur. The ends of the inner liner are open to allow helium, which diffuses out of the glass to occupy the central void.

4.   Potential for chemical interaction, including possible waterlogging rupture

The structural materials selected have good resistance to irradiation damage and are compatible with the reactor environment.

Corrosion of the materials exposed to the coolant is quite low, and proper control of chloride and oxygen in the coolant prevents the occurrence of stress corrosion. The potential for the interference with rod cluster control movement due to possible corrosion phenomena is very low.

Waterlogging rupture is not a failure mechanism associated with Westinghouse designed control rods. However, a breach of the cladding for any postulated reason does not result in serious consequences. Both the silver-indium-cadmium and hafnium absorber material are relatively inert and would remain remote from high coolant velocity regions. Rapid loss of material resulting in significant loss of reactivity control material would not occur. Bettis test results (Reference 4.2-15) concluded that additions of indium and cadmium to silver, in the amounts to form the Westinghouse absorber material composition, result in small corrosion rates. There is extensive U.S. Naval reactor experience with unclad hafnium as an absorber material and its corrosion resistance has been excellent; in fact, it has been reported to be superior to Zircaloy-2 with respect to corrosion resistance (Reference 4.2-15). Ag-In-Cd RCCAs were introduced in Cycle 3.

The consequences of a clad breach in the burnable absorber cladding would be small. It is anticipated that upon clad breach, the borosilicate glass would be leached by the coolant water and that localized power peaking of a few percent would occur; no design criteria would be expected to be violated.

4.2.4   TESTING AND INSPECTION PLAN

4.2.4.1   Quality Assurance Program: Westinghouse

The quality assurance program plan of the Energy Systems Business Unit is summarized in References 4.2-5 and 4.2-10 and the Quality Management System.

The program provides for control over all activities affecting product quality, commencing with design and development and continuing through procurement, materials handling, fabrication, testing and inspection, storage, and transportation. The program also provides for the indoctrination and training of personnel and for the auditing of activities affecting product quality through a formal auditing program.

Westinghouse drawings and product, process, and material specifications identify the inspections to be performed.

4.2.4.2   Quality Control: Westinghouse

Quality control philosophy is generally based on the following inspections being performed to a 95 percent confidence that at least 95 percent of the product meets specification.

1.   Fuel System Components and Parts

The characteristics inspected depend upon the component parts, and the quality control program includes dimensional and visual examinations, check audits of test reports, material certification, and nondestructive examination, such as x-ray, ultrasonic (UT), leak detection, and gamma scan.

All material used in the Millstone Unit 3 core is accepted and released by Quality Control.

2.   Pellets

Inspection is performed for characteristics such as diameter, density, length, and squareness of ends. Additional visual inspections are performed for cracks, chips, and surface conditions according to approved standards.

Density is determined as a percent of theoretical density using a geometric technique. Pellet hydrogen and chemical analyses are performed for each blend lot throughout pellet production.

3.   Rod Inspection

Fuel rod, control rodlet, burnable poison and source rod inspection consists of the following nondestructive examination techniques and methods, as applicable:

a.   Leak testing - Each rod is tested using a calibrated mass spectrometer, with helium being the detectable gas.

b.   Enclosure welds - All nonfuel weld enclosures are x-rayed. All fuel rod welds are UT- or x-ray-inspected. X-rays are taken in accordance with Westinghouse specifications meeting the requirements of ASTM-E-142.

c.   Dimensional - All rods are dimensionally inspected prior to final release. The requirements include such items as length, camber, girth weld diameter, and visual appearance utilizing approved standards.

d.   Plenum dimensions - All fuel and nonfuel rods are inspected by gamma scan, fluoroscope, or other approved methods.

e.   Pellet-to-pellet gaps - All fuel rods are inspected by fluoroscope, gamma scanning, or other methods.

f.   All of the fuel rods are active gamma scanned to verify enrichment control prior to acceptance for assembly loading. In addition, coated fuel is passive scanned to verify enrichment control in the coated portion (IFBA) of the fuel stack.

g.   Traceability - Traceability of rods and associated rod components is established by Quality Control.

4.   Assemblies

Each fuel rod, control rod, burnable poison and source rod assembly is inspected for compliance with drawing and/or specification requirements. Other incore control component inspection and specification requirements are given in Section 4.2.4.3.

5.   Other Inspections

The following inspections are performed as part of the routine inspection operation:

a.   Tool and gauge inspection and control, including calibration to primary and/or secondary working standards are performed at prescribed intervals on all serialized inspection and functional gages. Complete records are kept of calibration and conditions of tools and resultant product dispositions.

b.   Audits are performed of inspection activities and records to ensure that prescribed methods are followed and that records are correct and properly maintained.

c.   Surveillance inspection, where appropriate, and audits of outside contractors are performed to ensure conformance with specified requirements.

6.   Process Control

To prevent the possibility of mixing enrichments during fuel manufacture and assembly, strict enrichment segregation and other process controls are exercised.

The UO_2 powder is kept in closed containers. The contents are fully identified both by descriptive tagging and through a computer monitoring system. An identification tag that provides traceability is affixed to the containers before transfer to powder storage. Isotopic content is confirmed by analysis.

Powder withdrawal from storage can be made by only one authorized group, which directs the powder to the correct pellet production line. All pellet production lines are physically separated from each other and pellets of only a single nominal enrichment are produced in a given production line or a segregated part of the line at any given time.

Finished pellets are placed on trays identified with the contract and enrichment and transferred to segregated storage carts within the confines of the pelleting area. Samples from each pellet lot are tested for isotopic content and impurity levels prior to acceptance by Quality Control. Physical barriers prevent mixing of pellets of different nominal enrichments in this storage area. Unused powder and substandard pellets are returned to storage in the original containers, except for material from axial blanket rods.

Loading of pellets into the clad is performed on dedicated production lines. One rod design is loaded on a line at a time.

Each fuel rod is uniquely serialized with a traceability code which also identifies the contract and enrichment. The end plugs are inserted and then welded to seal the rod. The fuel rod remains coded and traceable even after installation in the fuel assembly.

At the time of installation into an assembly, a matrix is generated to identify each rod in its position within a given assembly. The top nozzle is inscribed with a permanent unique identification number providing traceability to the fuel contained within the assembly.

Similar traceability is provided for burnable poison, source rods, and control rodlets, as required.

4.2.4.3   Incore Control Component Testing and Inspection

Tests and inspections are performed on each reactivity control component to verify the mechanical characteristics. In the case of the full length rod cluster control assembly, prototype testing has been conducted and both manufacturing test/inspections and functional testing at the plant site are performed.

During the component manufacturing phase, the following requirements apply to the reactivity control components to ensure proper functioning during reactor operation:

1.   All materials are procured to specifications to attain the desired standard of quality.

2.   Westinghouse, because of the manner of their manufacture, requires that a spider from each braze lot is proof tested by applying a 5,000 pound load to the spider body. This proof load provides a ending moment at the spider body approximately

equivalent to 1.4 times the load caused by the acceleration imposed by the control rod drive mechanism.

3.   Both manufacturers, AREVA and Westinghouse, require:

- All rods are checked for integrity by the methods described in Section (3) Rod Inspection).

- To ensure proper fit up with the fuel assembly, the rod cluster control, burnable poison, and source assemblies are installed in the fuel assembly and checked for binding in the dry condition.

The RCCAs were functionally tested, following initial core loading but prior to criticality, to demonstrate reliable operation of the assemblies. The initial functional test is typically more rigorous then the subsequent confirmatory testing required by the Technical Specifications. The test results confirmed that the functional requirements of the RCCAs were met.

To demonstrate continuous free movement of the RCCAs and to ensure acceptable core power distributions during operations, partial movement checks are performed on every RCCA, as required by the technical specifications. In addition, periodic drop tests of the full length RCCAs are performed at each refueling shutdown to demonstrate continued ability to meet trip time requirements.

If an RCCA cannot be moved by its mechanism, adjustments in the boron concentration ensure that adequate shutdown margin would be achieved following a trip. Thus, inability to move one rod cluster control assembly can be tolerated. More than one inoperable rod cluster control assembly could be tolerated, but would impose additional demands on the plant operator. Therefore, the number of inoperable RCCAs has been limited to one.

4.2.4.4   Tests and Inspections by Others: Westinghouse

If any tests and inspections are to be performed on behalf of Westinghouse, Westinghouse will review and approve the quality control procedures, inspection plans, etc., to be used to ensure that they are equivalent to the description provided in Sections 4.2.4.1 through 4.2.4.3 and are performed properly to meet all Westinghouse requirements.

4.2.4.5   In-Service Surveillance

Westinghouse has extensive experience with the use of 17 x 17 fuel assemblies in other operating plants. This experience is summarized in Reference 4.2-6, which is periodically updated to provide the most recent information on operating plant. There are no plans to provide a specific in-service surveillance program for this plant.

Surveillance of fuel and reactor performance will be routinely conducted at Millstone 3. Methods will be employed during operation to detect the occurrence of fuel rod failures. Specifically,

reactor coolant chemistry samples and radiochemical analysis will be routinely performed to identify the existence of any fuel rod failures.

Reactor coolant chemistry samples are routinely trended for indications of fuel performance. Fuel inspections may be conducted depending on the results of this operational monitoring or any special projects ongoing which could impact the fuel. These inspections may be performed by one or more means available at the time through commercial contractors as judged necessary by plant management. To the extent practicable, leaking fuel assemblies/rods will be excluded from the operating cores.

4.2.4.6　On-Site Inspection

Detailed written procedures are used by the station staff for the post shipment inspection of all new fuel and associated components, such as control rods, plugs, and inserts. Fuel handling procedures specify the sequence in which handling and inspection takes place.

Loaded fuel containers, when received on-site, are externally inspected to ensure that labels and markings are intact and that seals are unbroken. After the containers are opened, the shock indicators attached to the suspended internals are inspected to determine if movement during transit exceeded design limitations.

Following removal of the fuel assembly from the container in accordance with detailed procedures, the fuel assembly polyethylene wrapper is examined for evidence of damage. The polyethylene wrapper is then removed and a visual inspection of the entire bundle is performed.

Westinghouse control rod assemblies are normally shipped in fuel assemblies and are inspected via detailed, written procedures prior to core load. The control rod assembly is withdrawn from the fuel assembly to ensure free and unrestricted movement. The exposed section is then visibly inspected for mechanical integrity, replaced in the fuel assembly and stored with the fuel assembly. AREVA RCCAs are shipped separately from the Westinghouse provided fuel assemblies. Following acceptable receipt inspection, the AREVA RCCAs are normally placed in fuel assemblies.

4.2.4.7　Testing and Inspection Plan: AREVA RCCAs

4.2.4.7.1　Quality Assurance Program

AREVA engineering specifications require that core components be fabricated under an approved quality control program. This includes shop quality control procedures, which are audited by AREVA quality assurance personnel. In addition, special process procedures are approved by AREVA design personnel as required by the procurement documents.

AREVA manufactures core components under a controlled manufacturing system, which includes complimentary written procedures and inspection provisions. Extensive attention is given to processing details to ensure a reliable, reproducible, quality product.

4.2.4.7.2   Quality Control

The fabrication activities are supported and monitored by quality control. Additional inspections are performed routinely along with the required inspection program to further assure the quality of the final product.

4.2.4.7.3   Onsite Inspection

AREVA provides documentation for the inspection of reload assemblies manufactured and delivered by AREVA. The post-shipment inspections of new fuel assemblies and insert components performed by the station described in Section 4.2.4.6 are also applicable to AREVA components.

4.2.5   REFERENCES FOR SECTION 4.2

4.2-1   O'Donnell, W.J. and Langer, B.F. 1964. Fatigue Design Basis for Zircaloy Components. Nuclear Science and Engineering, 20, 1-12.

4.2-2   Stephan, L. A. 1970. The Effects of Cladding Material and Heat Treatment on the Response of Waterlogged UO_2 Fuel Rods to Power Bursts. IN-ITR-111.

4.2-3   Western New York Nuclear Research Center Correspondence With the U.S. Atomic Energy Commission on February 11 and August 27, 1971, Docket No. 50-57

4.2-4   Westinghouse Energy System Business Unit Quality Management System.

4.2-5   WCAP-7800, Revision 6-A, 1983, "Nuclear Fuel Division Quality Assurance Program Plan."

4.2-6   WCAP-8183 (Latest Revision), "Operational Experience with Westinghouse Cores."

4.2-7   WCAP-8218 P-A (Proprietary) and WCAP-8219-A (Non proprietary) 1975, Hellman, J. M. (Ed.), "Fuel Densification Experimental Results and Model for Reactor Application."

4.2-8   WCAP-8236 (Proprietary) and WCAP-8288 (Non proprietary) 1973, Gesinski, L. and Chiang, D., "Safety Analysis of the 17 x 17 Fuel Assembly for Combined Seismic and Loss-of-Coolant Accident."

4.2-9   WCAP-8278 (Proprietary) and WCAP-8279 (Non proprietary) 1974, Demario, E. E., "Hydraulic Flow Test of the 17 x 17 Fuel Assembly."

4.2-10 WCAP-8370, Revision 10-A, 1983, "Westinghouse Energy System Business Unit Quality Assurance Program Plan."

4.2-11 WCAP-8377 (Proprietary) and WCAP-8381 (Non proprietary) 1974, George, R. A.; Lee, Y. C.; and Eng, G. H., "Revised Clad Flattening Model."

4.2-12 WCAP-8691, Revision 1 (Proprietary) and WCAP-8692, Revision 1 (Non- proprietary) 1979, Skaritka, Jr., (Ed.), "Fuel Rod Bow Evaluation."

4.2-13 WCAP-8768, Revision 2, 1978, Eggleston, F. R. "Safety-Related Research and Development for Westinghouse Pressurized Water Reactors, Program Summaries, Winter 1977 - Summer 1978."

4.2-14 WCAP-8963 (Proprietary) 1976 and WCAP-8964 (Non proprietary) 1977, Risher, D. et al., "Safety Analysis for the Revised Fuel Rod Internal Pressure Design Basis."

4.2-15 WCAP-9179, Revision 1 (Proprietary) and WCAP-9224 (Non proprietary) 1978, Beaumont, M.D., et al., "Properties of Fuel and Core Component Materials and Appendix A, 1980 Hofnium."

4.2-16 Western New York Nuclear Research Center Correspondence With the U.S. Atomic Energy Commission on February 11 and August 27, 1971, Docket No. 50-57.

4.2-17 WCAP-9401-P-A (Proprietary) and WCAP-9402-A (Non-proprietary) 1981, Davidson, S. L., et al., "Verification Testing and Analysis of the 17 x 17 Optimized Fuel Assembly."

4.2-18 WCAP-9500-A, 1982, Davidson, S. L., "Reference Core Report - 17 x 17 Optimized Fuel Assembly."

4.2-19 WCAP-10125, 1985, Davidson, S. L. (Ed.), et al., "Extended Burnup Evaluation of Westinghouse Fuel."

4.2-20 WCAP-10444-P-A, 1985, Davidson, S. L., "VANTAGE 5 Fuel Assembly Reference Core Report and Addendum 2-A, 1988, VANTAGE 5H Fuel Assembly".

4.2-21 WCAP-10851-P-A, 1988, Weiner, R. A." Improved Fuel Performance Models for Westinghouse Fuel Rod Design and Safety Evaluations."

4.2-22 WCAP-12488-A, 1994, Davidson, S. L., "Westinghouse Fuel Criteria Evaluation Process."

4.2-23 WCAP-12610-P-A, 1995, Davidson, S. L. and Ryan, T. L., "VANTAGE + Fuel Assembly Reference Core Report."

4.2-24 WCAP-13060-P-A, 1993, Slagle, W. H., "Westinghouse Fuel Assembly Reconstitution Evaluation Methodology."

4.2-25 WCAP-13589-A, 1995, Kersting, P. J. et al., "Assessment of Clad Flattening and Densification Power Spike Factor Elimination in Westinghouse Nuclear Fuel."

4.2-26 Brown, U. L., "Generic Safety Evaluation for Performance Plus Fuel Features," SECL-92-305, April 5, 1994.

4.2-27 Kitchen, T. J., "Generic Safety Evaluation for 17x17 Standard Robust Fuel Assembly (17x17 STD RFA)," SECL-98-056, Revision 0, September 30, 1998.

4.2-28 Liparulo, N. J. (Westinghouse) letter to Lyons, J. E. (NRC), "Transmittal of Response to NRC Request for Information on Wolf Creek Fuel Design Modifications," NSD-NRC-97-5189, June 30, 1997.

4.2-29 Liparulo, N. J. (Westinghouse) letter to Jones, R. C. (NRC), "Transmittal of Presentation Material from NRC/Westinghouse Fuel Design Change Meeting on April 15, 1996," NSD-NRC-96-4964, April 22, 1996.

4.2-30 WCAP-12488-A, Addendum 1-A, Revision 1, 2002. Addendum to WCAP-12488-A, "Revision to Design Criteria."

4.2-31 WCAP-12610-P-A and CENPD-404-P-A, Addendum 1-A, Rev. 0, July 2006, P. Schueren & H.H. Shah, "Optimized ZIRLO^{TM}."

4.2-32 Sepp, H.A. (Westinghouse) letter to Wermiel, J. (NRC), "Fuel Criterion Evaluation Process (FCEP) Notification of the RFA-2 Design, Revision 1," LTR-NRC-02-55, November 13, 2002.

4.2-33 Thomas, G. A. (AREVA) Letter to Sterner, R. W. (Dominion), "Millstone Unit 3 RCCA Safety Analysis," FAB08-353, July 28, 2008.

4.2-34 WCAP-15063-P-A, Revision 1, with Errata, Foster, J.P. and Siderer, S., "Westinghouse Improved Performance Analysis and Design Model (PAD 4.0)," July 2000.

4.2-35 WCAP-10125-P-A, Addendum 1-A, Revision 1-A, Davidson, S.L. (Ed.), et al., "Extended Burnup Evaluation of Westinghouse Fuel," May 2005.

4.2-36 WCAP-12610-P-A & CENPD-404-P-A, Addendum 2-A, Lenahan R., et al., "Westinghouse Clad Corrosion Model for ZIRLO and Optimized ZIRLO," October 2013.

TABLE 4.2-1 FUEL ASSEMBLY COMPONENT STRESSES

(Percent of Allowable)

Component	Uniform Stresses (Direct/Membrane)	Combined Stresses (Membrane + Bending)
Thimble	94.1	85.3
Fuel Rod *	38.5	32.1
Top Nozzle Plate	**	**
Bottom Nozzle Plate	**	**
Bottom Nozzle Leg	**	**

NOTES:

*   Including primary operating stresses.

**   Mechanical Testing performed to assure component structural integrity requirements are met.

FIGURE 4.2–1 FUEL ASSEMBLY CROSS SECTION 17 X 17
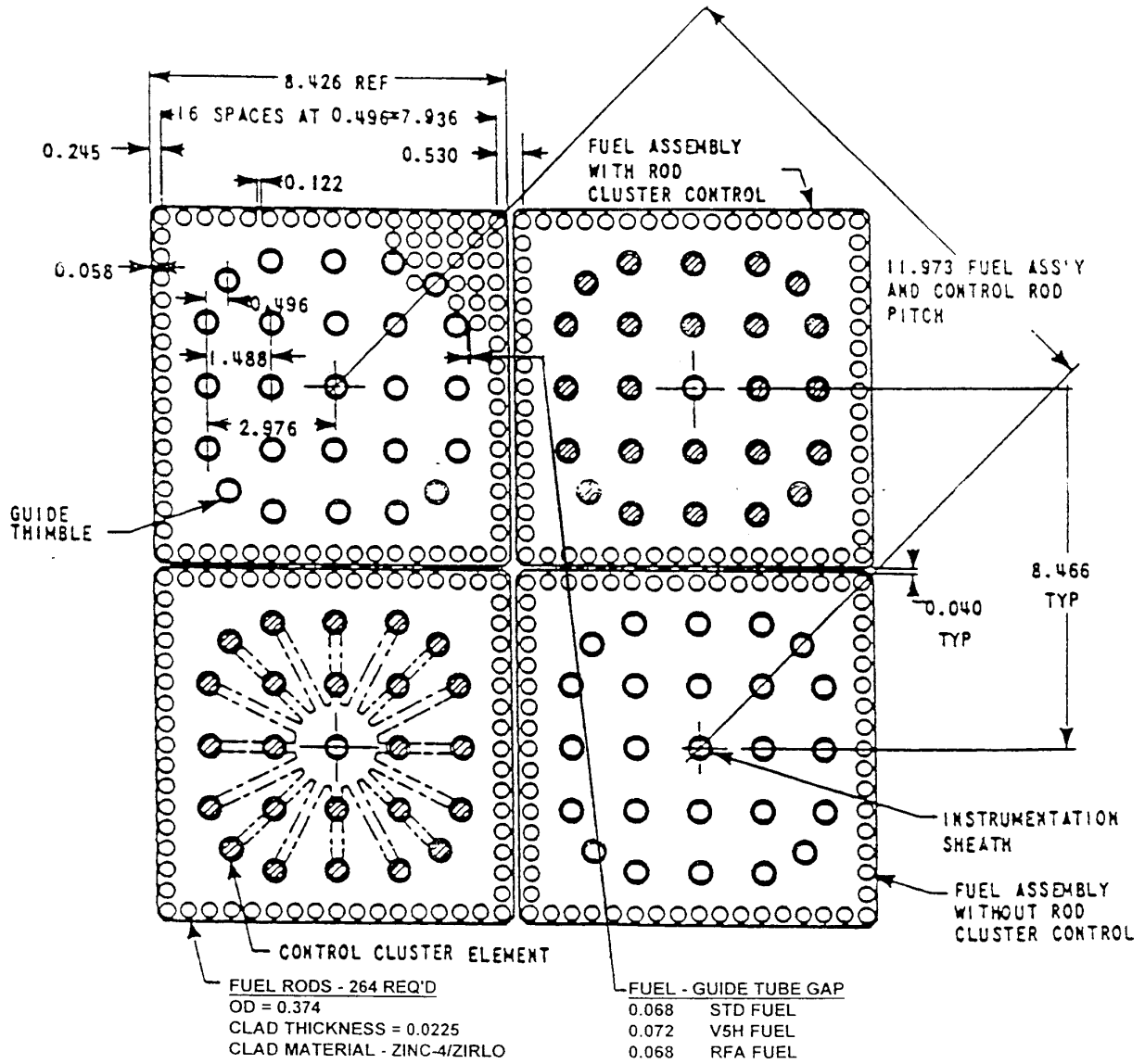
NOTE:
ALL DIMENSIONS ARE IN INCHES

FIGURE 4.2–2 COMPARISON OF THE 17 X 17 V5H FUEL ASSEMBLY AND THE 17 X 17 STANDARD FUEL ASSEMBLY

REGION 6
17X17 VANTAGE 5H FUEL ASSEMBLY
(W/ INTERMEDIATE FLOW MIXERS)

159.775 (ZIRLO)
159.975 (zirc-4)

3.470 (Zirc-4)
3.475 (ZIRLO)

2.383

151.100 (ZIRLO)
152.200 (Zirc-4)

17X17 RECONSTITUTABLE STD FUEL ASSEMBLY

159.915

3.47   2.383

152.160
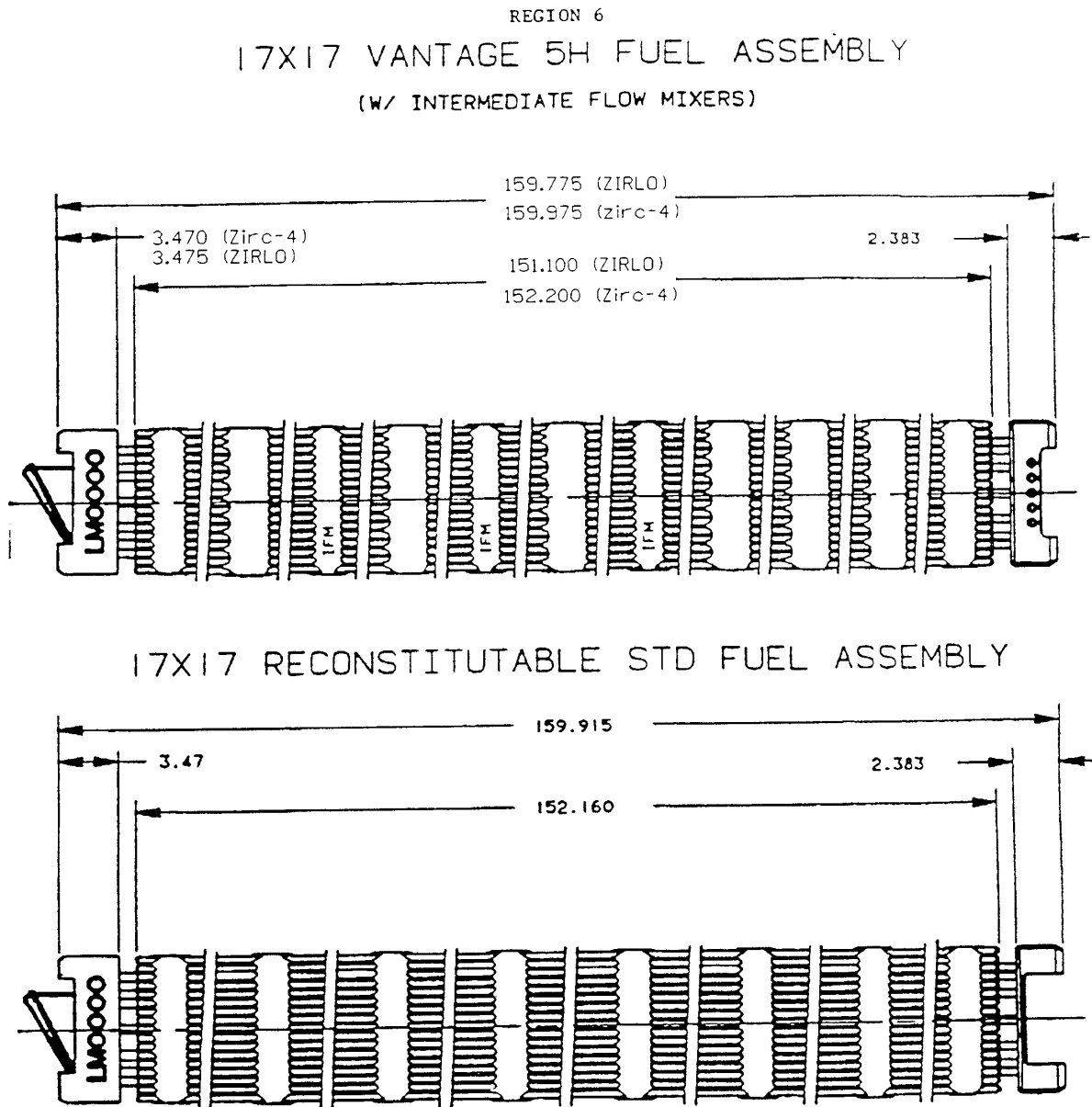
FIGURE 4.2–3 17 X 17 VANTAGE 5-H FUEL ROD ASSEMBLY

DIM	17 x 17 V5H	
	Zirc-4	ZIRLO
A	152.200	152.100
B	7.350	7.340
C	144.00	144.00
DIA D	0.329	0.329
DIA E	0.374	0.374

DIMENSIONS ARE IN INCHES

BOTTOM END PLUG SHOWS
INTERNAL GRIP TYPE
FOR V5-H FUEL RODS

TOP   DIA E   DIA D   BOTTOM

DIM B
PLENUM

DIM C
FUEL STACK LENGTH

DIM A
FUEL ROD LENGTH
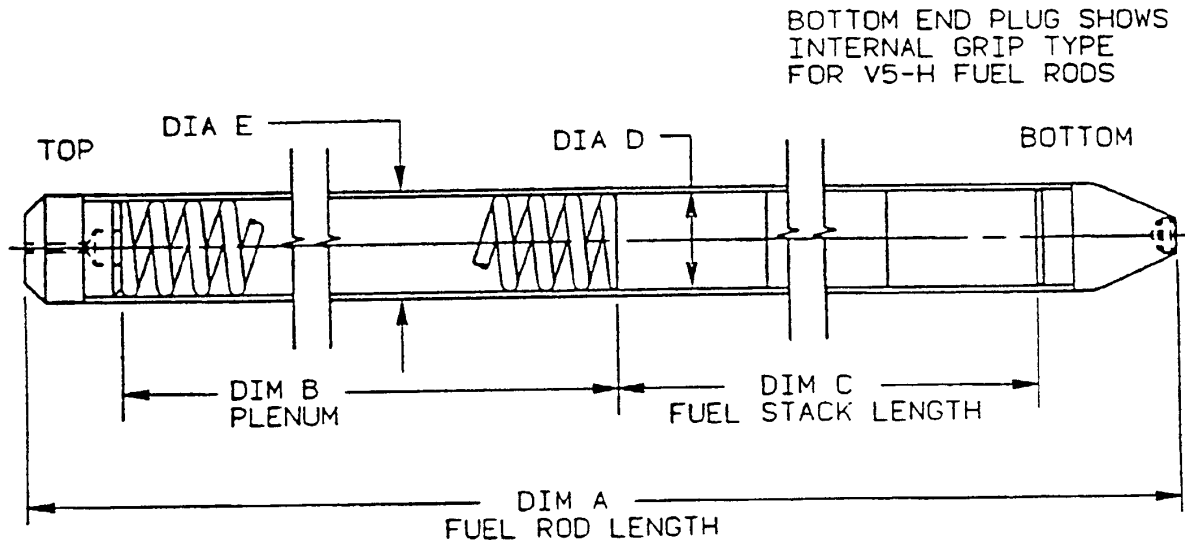
FIGURE 4.2–4 PLAN VIEW
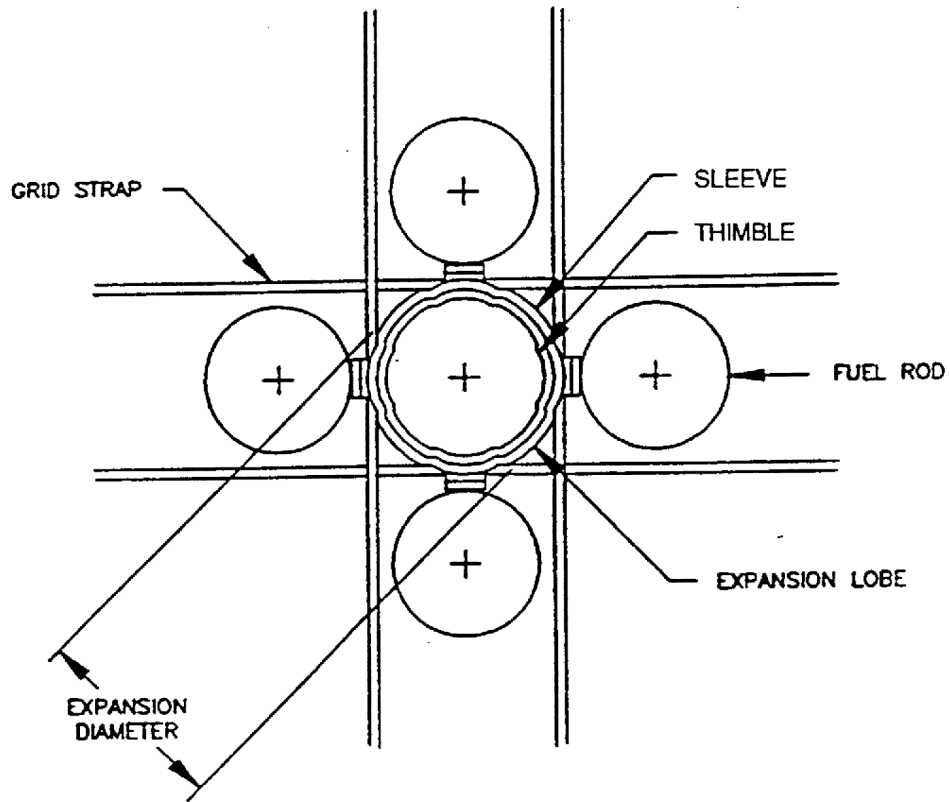
V5H FUEL ASSEMBLY

IFM AND MID GRID EXPANSION JOINT DESIGN

FIGURE 4.2–5 GRID TO THIMBLE ATTACHMENT JOINTS

GUIDE THIMBLE TUBE

MIXING VANE

IFM GRID

.475

IFM GRID SLEEVE

WELD

EXPANSION LOBE

GUIDE THIMBLE TUBE

MIXING VANE

MID GRID

1.500

MID GRID SLEEVE

WELD

EXPANSION LOBE
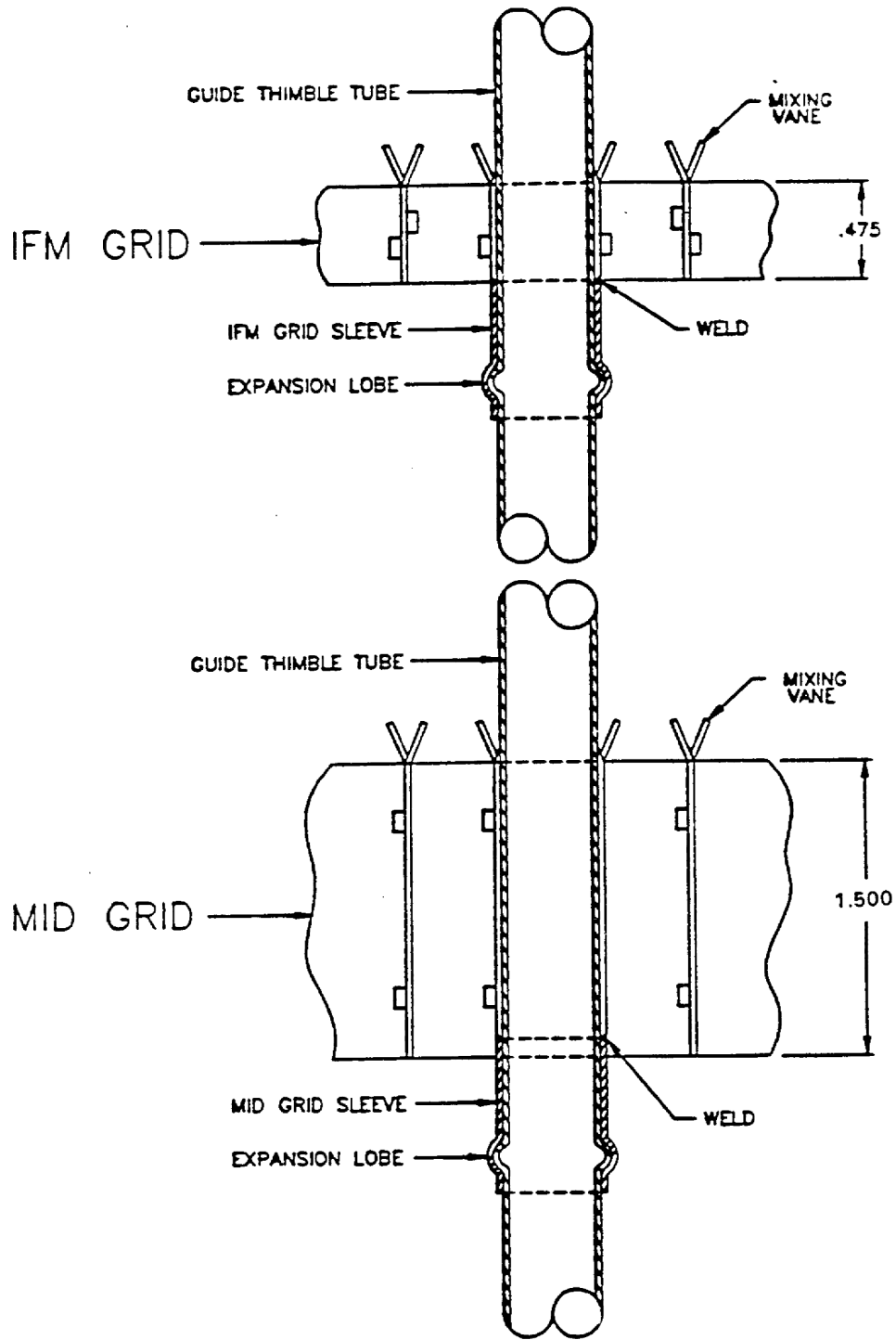
V5H FUEL ASSEMBLY

DIMENSIONS ARE IN INCHES (NOMINAL)

FIGURE 4.2–6 THIMBLE/INSERT/TOP GRID SLEEVE BULGE JOINT GEOMETRY

LOCK TUBE

ADAPTOR PLATE

GROOVE

ADAPTOR PLATE THRU HOLE

NOZZLE INSERT

E   E

BULGE JOINTS (4 LOBES EACH)

THIMBLE TUBE

TOP GRID

TOP GRID SLEEVE

SECTION E—E

(TYPICAL)

UNASSEMBLED
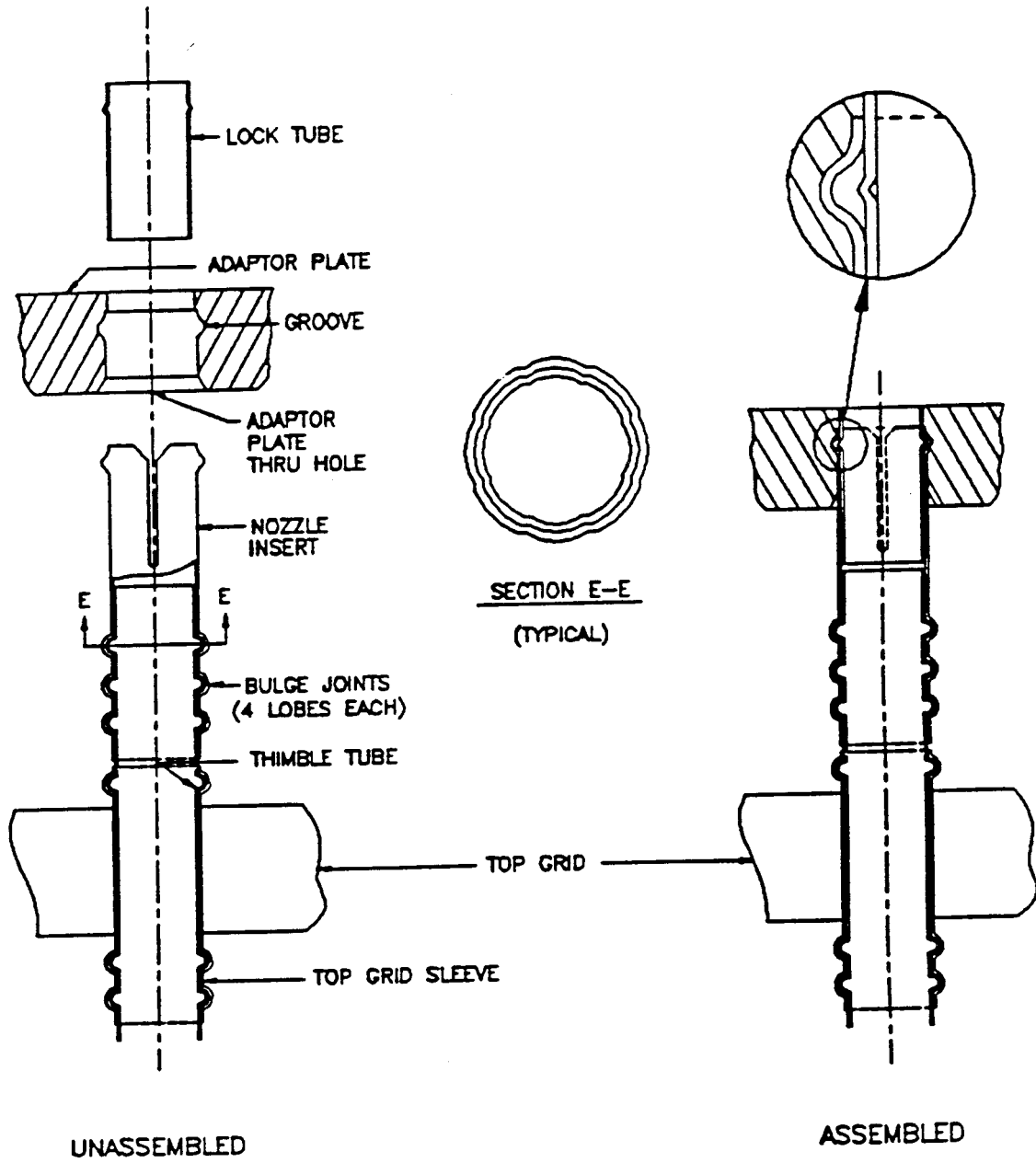
ASSEMBLED

V5H FUEL ASSEMBLY

FIGURE 4.2–7 GUIDE THIMBLE TO BOTTOM NOZZLE JOINT
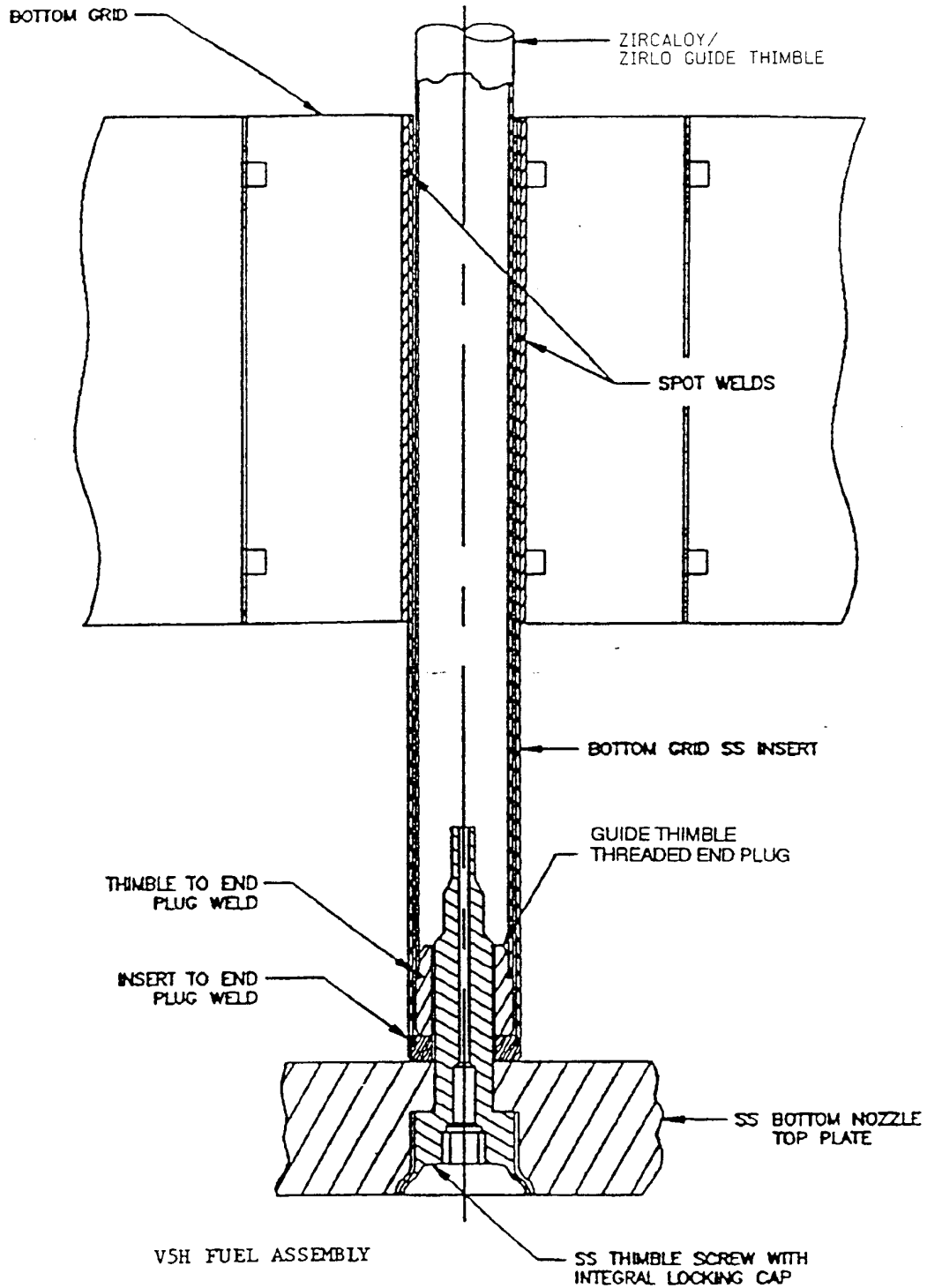
FIGURE 4.2–8 ROD CLUSTER CONTROL AND DRIVE ROD ASSEMBLY WITH INTERFACING COMPONENTS
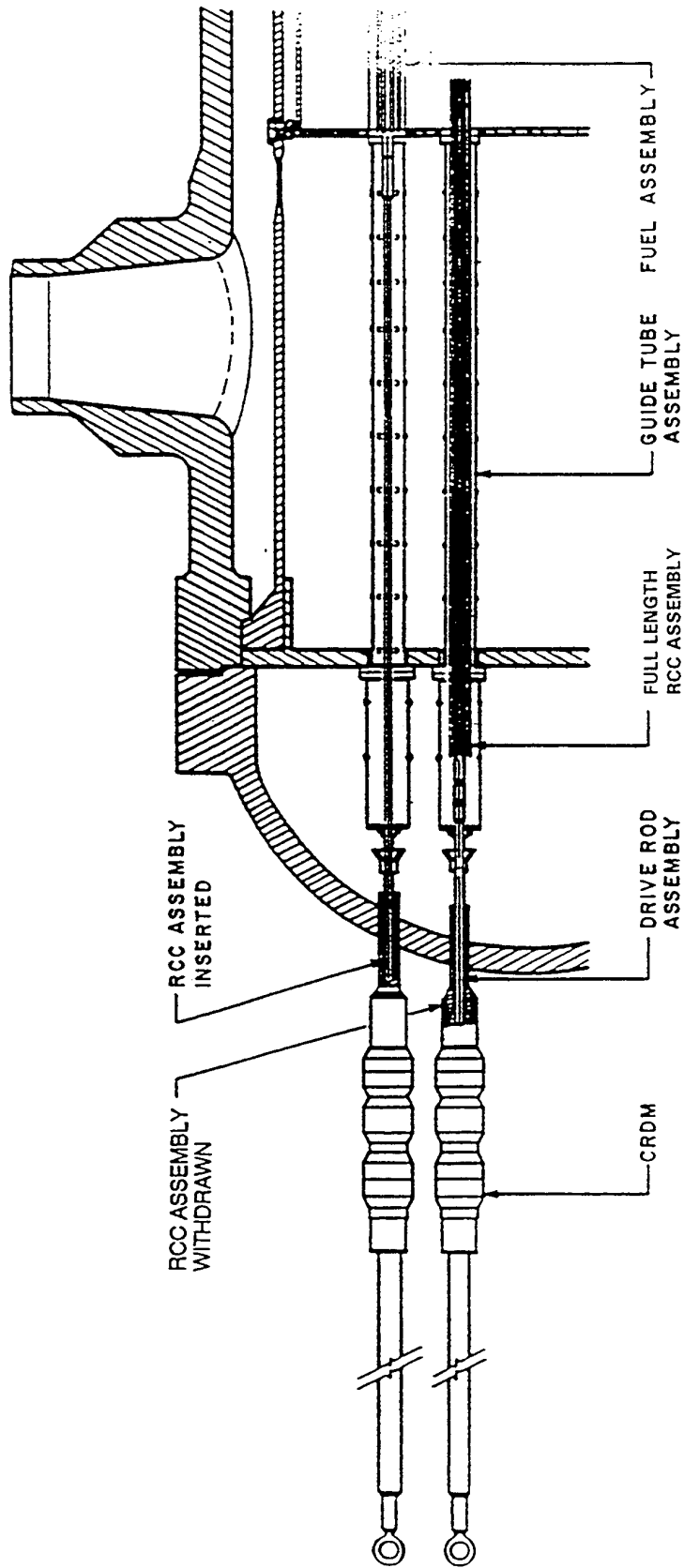
FIGURE 4.2–9 DELETED BY FSARCR PKG FSC 08-MP3-027

FIGURE 4.2–9A FULL LENGTH ROD CLUSTER CONTROL ASSEMBLY (WESTINGHOUSE)
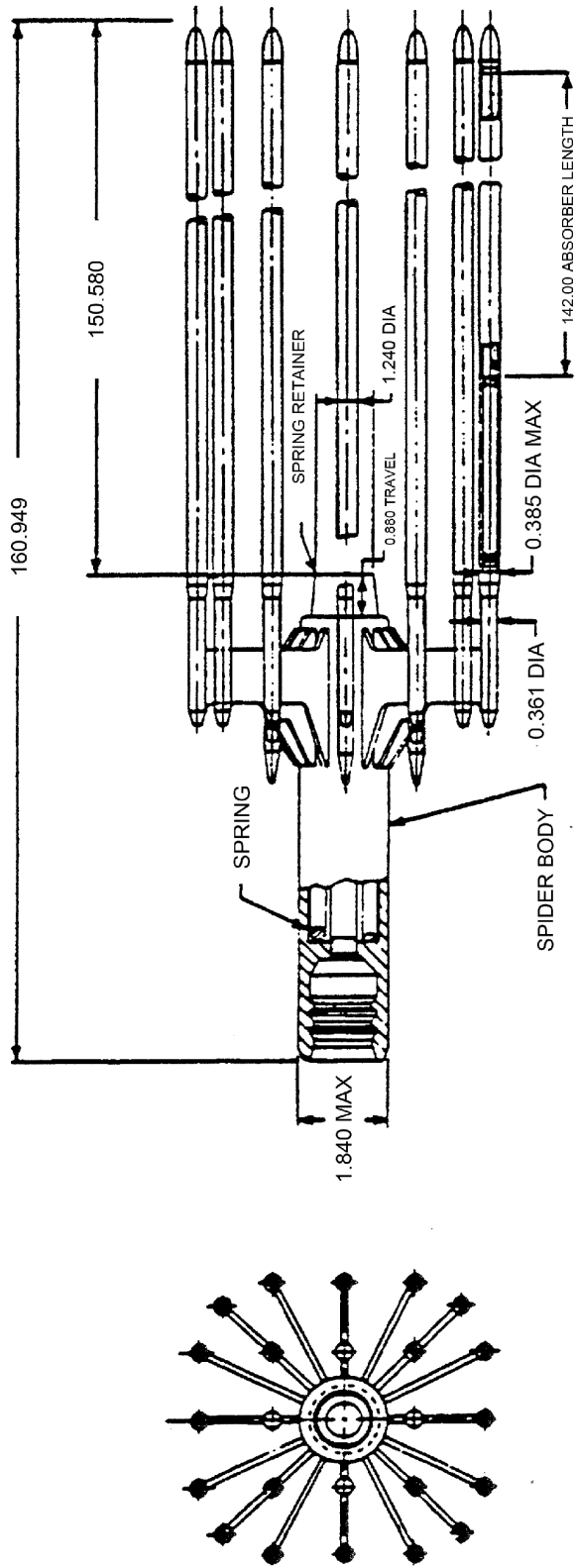
FIGURE 4.2–9B FULL LENGTH ROD CLUSTER CONTROL ASSEMBLY AND ABSORBER ROD (AREVA)
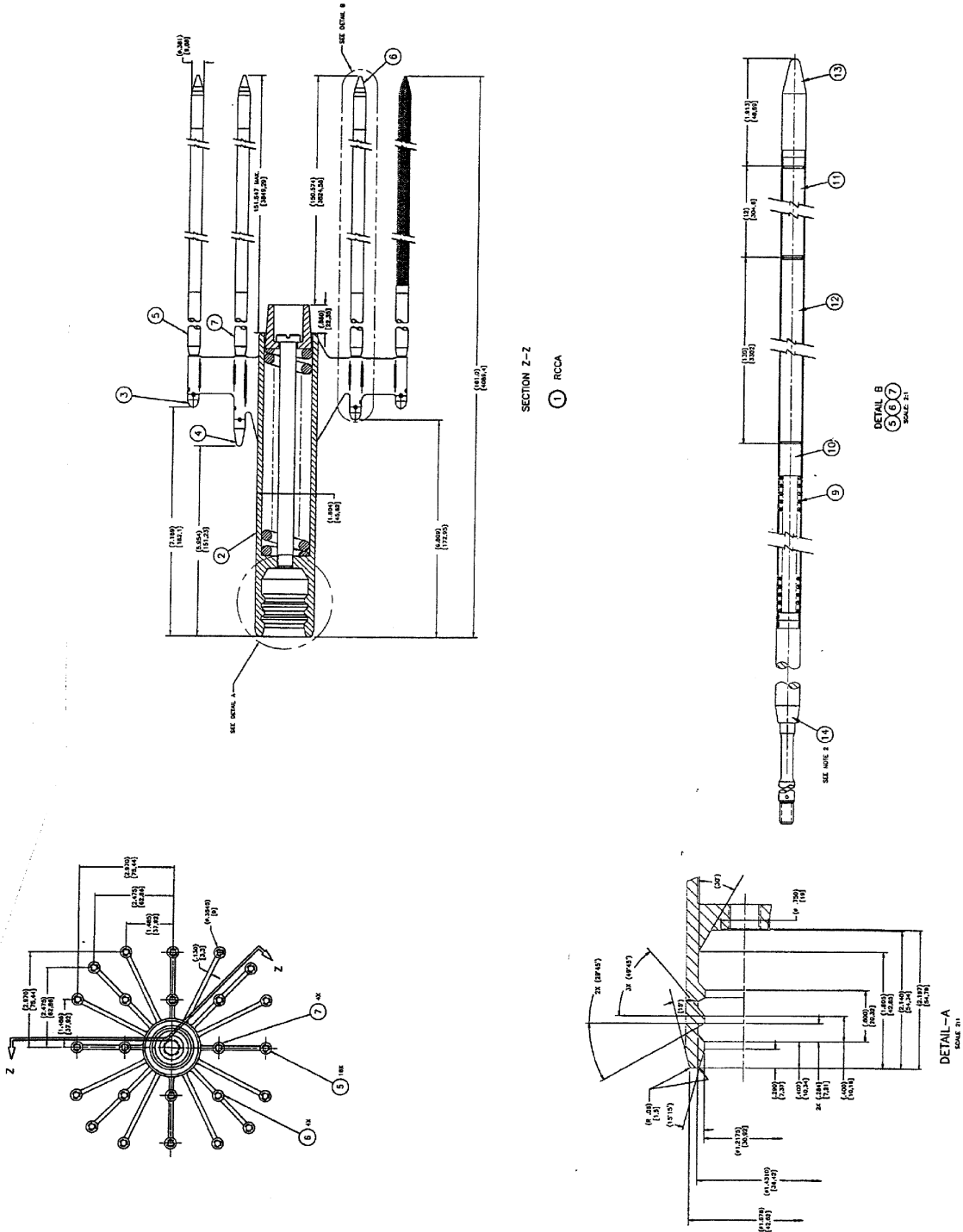
FIGURE 4.2–10 ABSORBER ROD (WESTINGHOUSE)
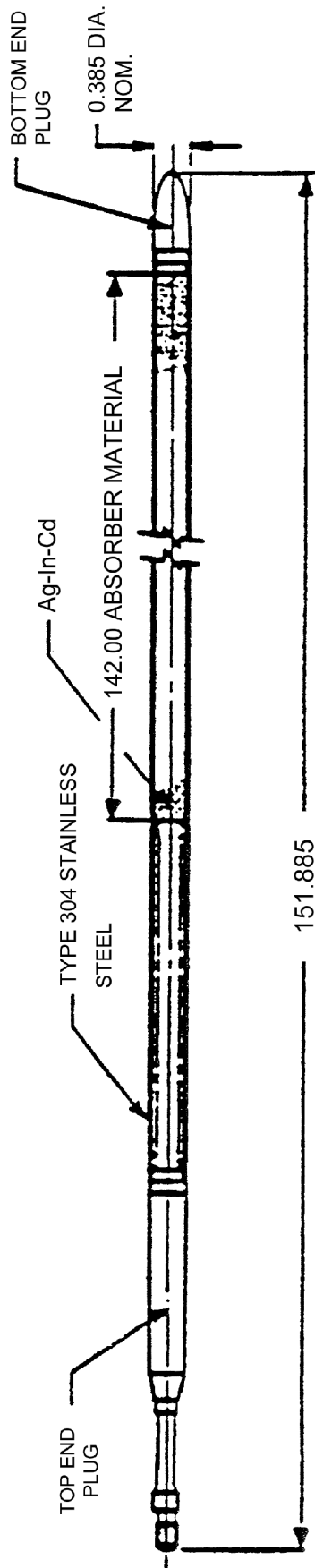
FIGURE 4.2–11 BURNABLE ABSORBER ASSEMBLY
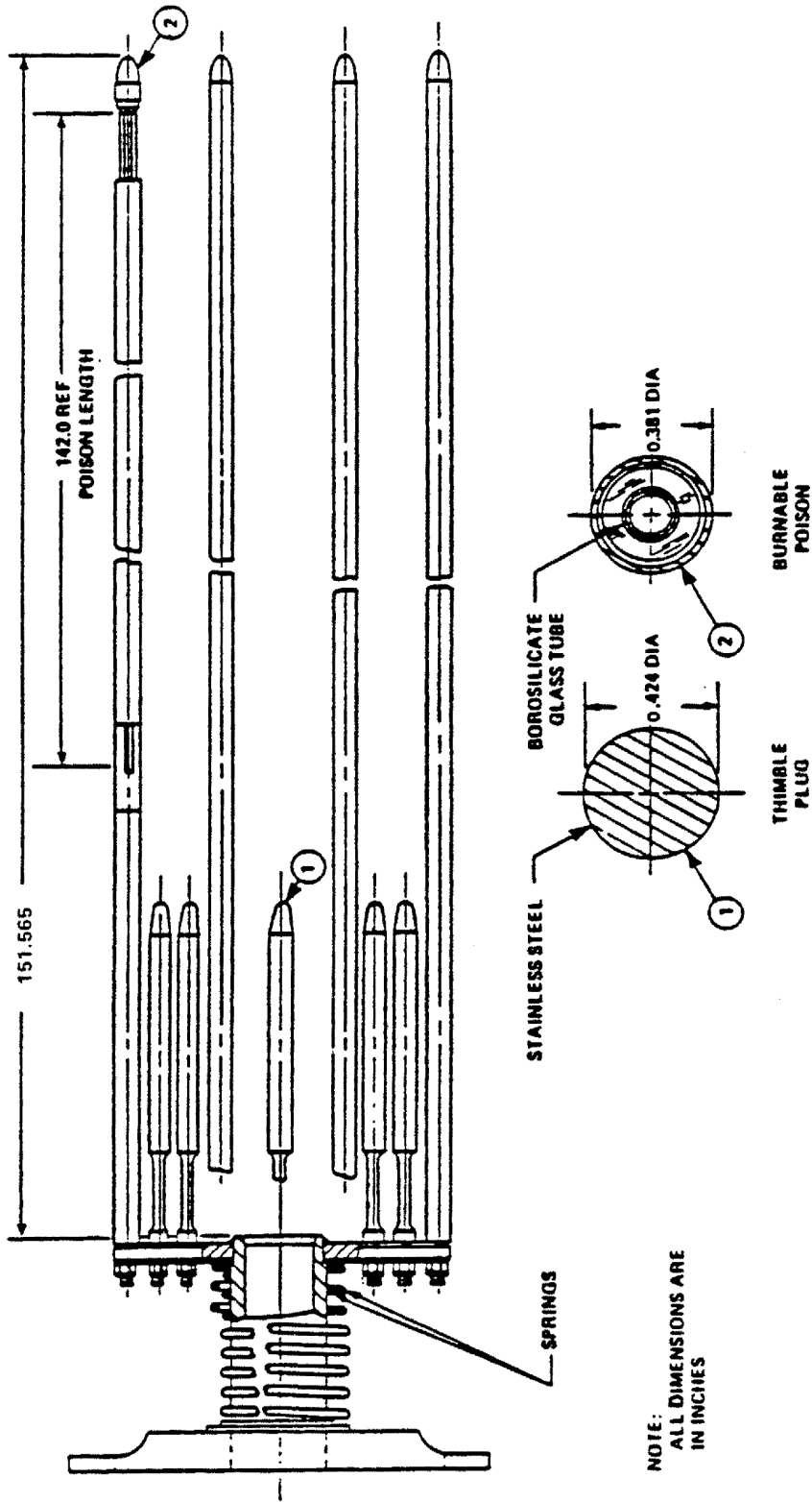
FIGURE 4.2–12 NOT USED

FIGURE 4.2–13 PRIMARY SOURCE ASSEMBLY

NOTE
ALL DIMENSIONS ARE IN INCHES
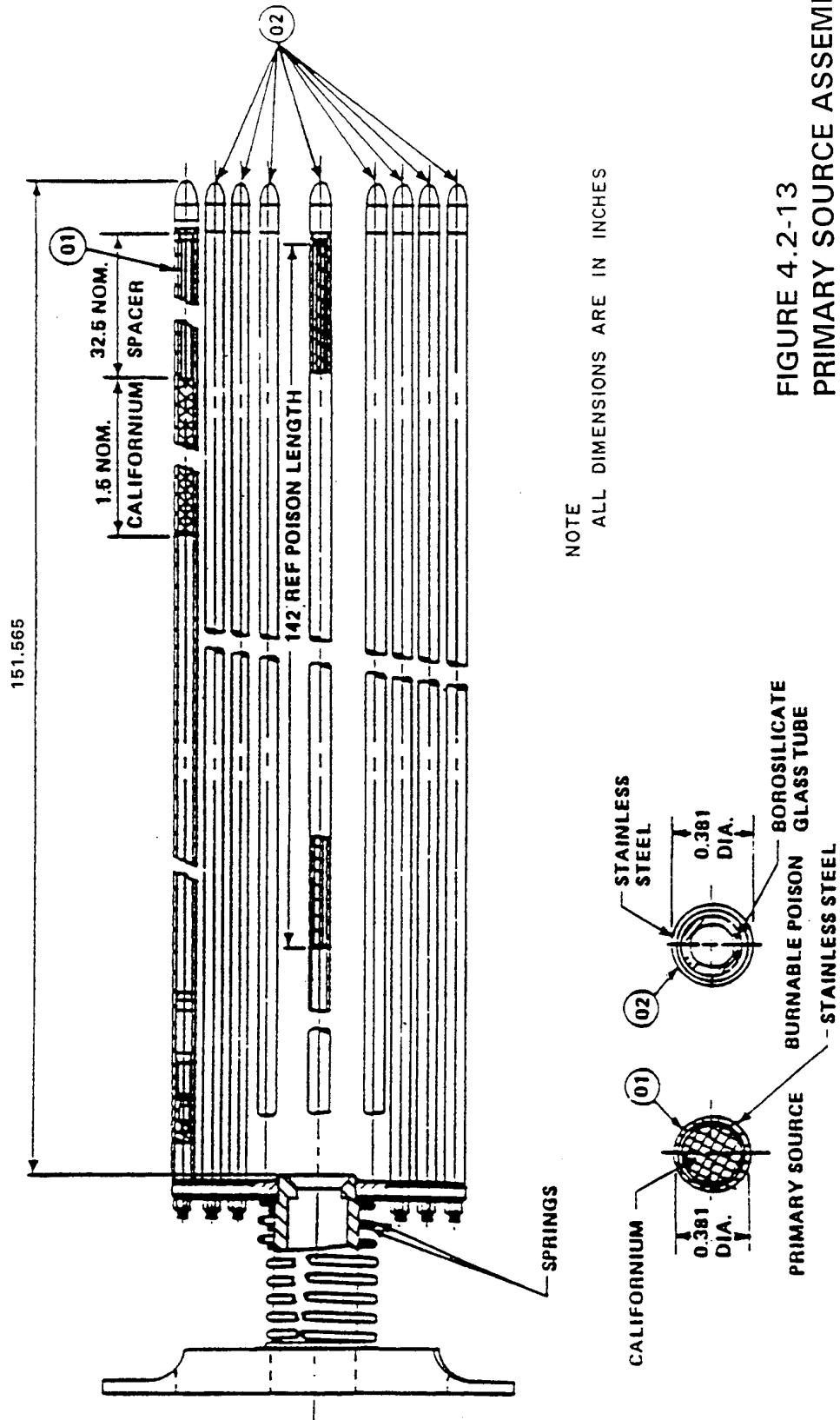
FIGURE 4.2-13
PRIMARY SOURCE ASSEMBLY

FIGURE 4.2–14 NOT USED

FIGURE 4.2–14A SINGLE ENCAPSULATED SECONDARY SOURCE ASSEMBLY

FIGURE 4.2-14B
DOUBLE ENCAPSULATED
SECONDARY SOURCE ASSEMBLY
MILLSTONE NUCLEAR POWER STATION
UNIT 3
FINAL SAFETY ANALYSIS REPORT
CAD FILE: 4214b.dgn/4214b.clt

FIGURE 4.2–14B DOUBLE ENCAPSULATED SECONDARY SOURCE ASSEMBLY

FIGURE 4.2-14B
DOUBLE ENCAPSULATED
SECONDARY SOURCE ASSEMBLY
MILLSTONE NUCLEAR POWER STATION
UNIT 3
FINAL SAFETY ANALYSIS REPORT
CAD FILE: 4214b.dgn/4214b.clt
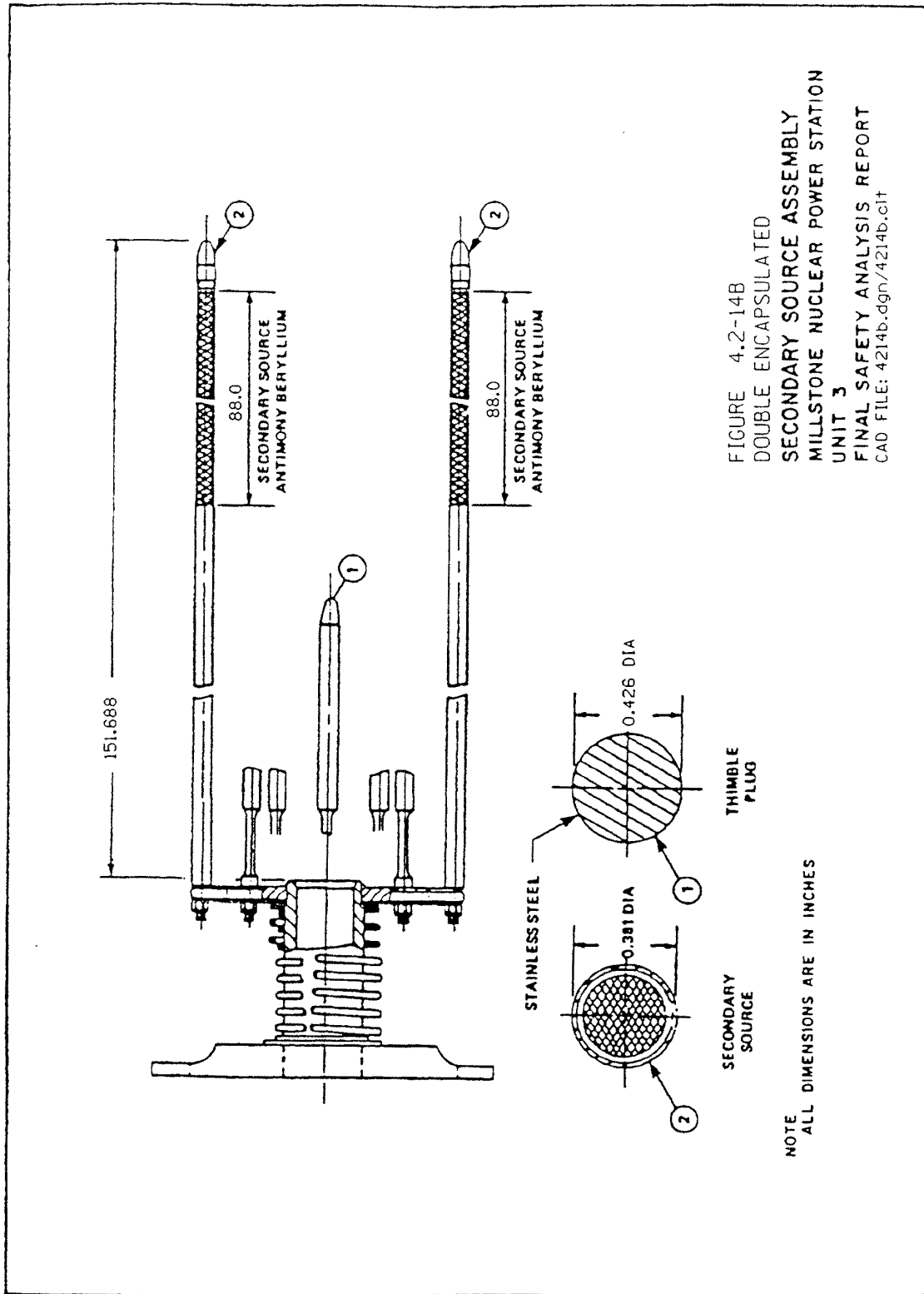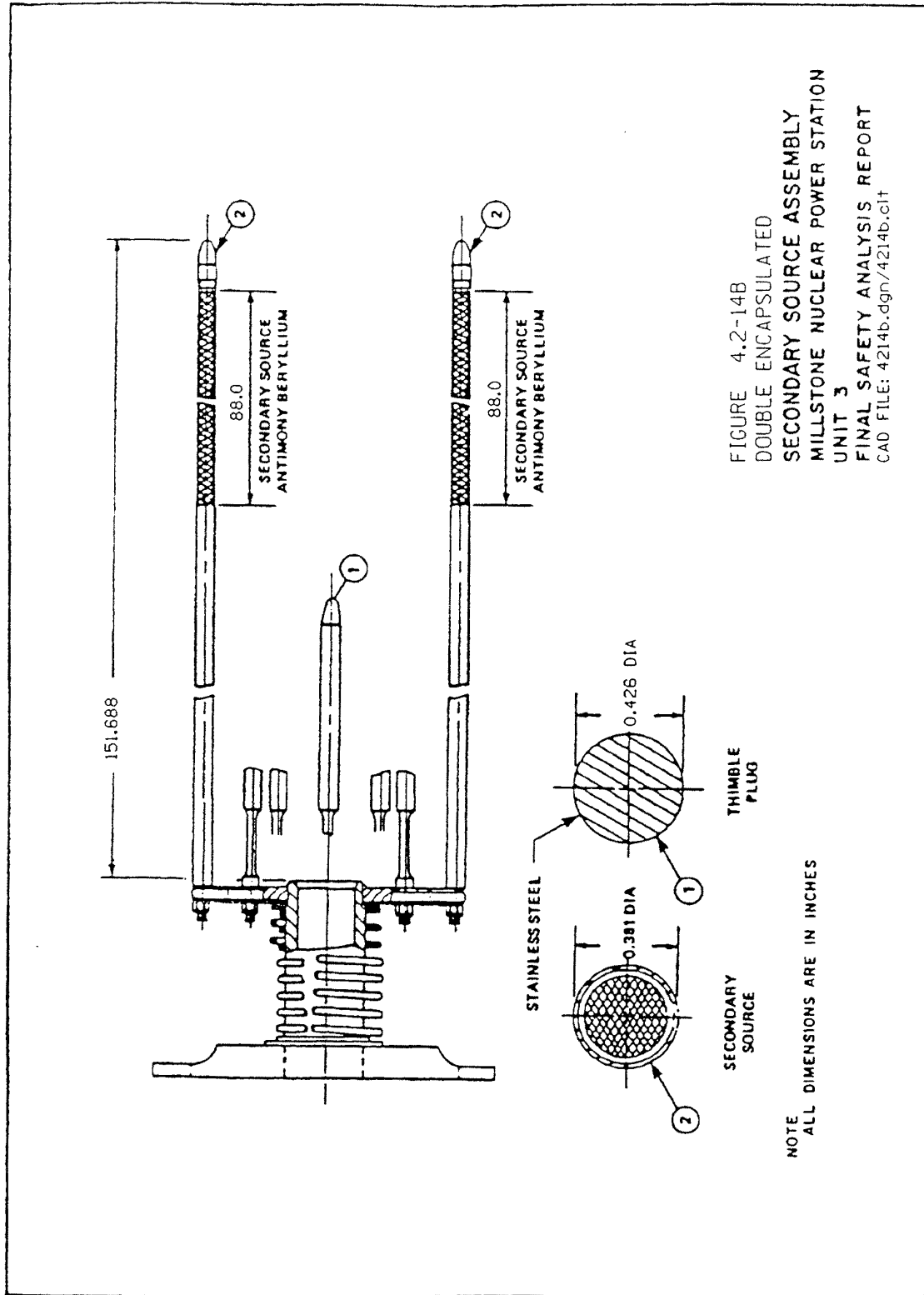
FIGURE 4.2–15 THIMBLE PLUG ASSEMBLY
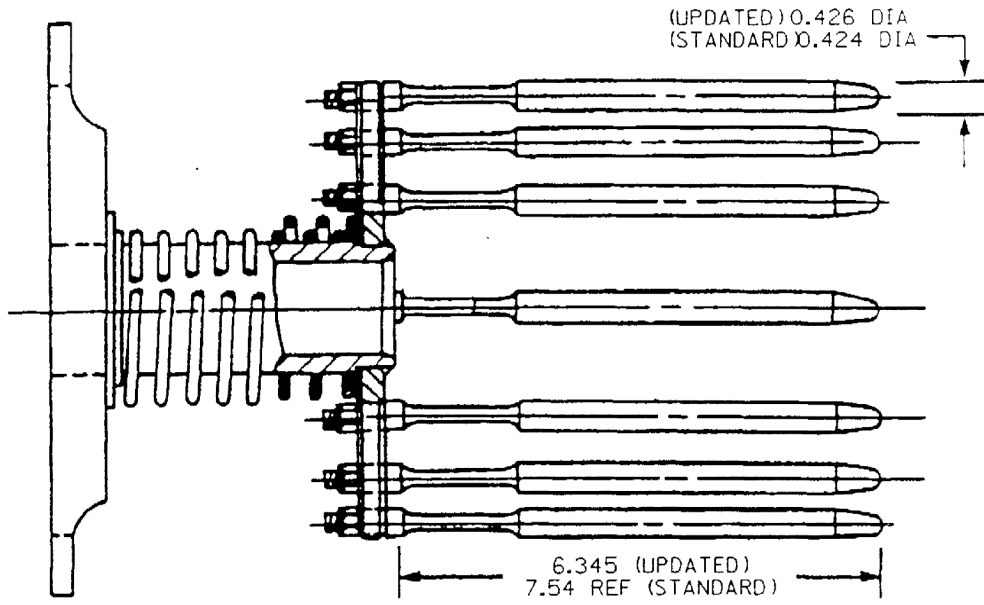
NOTE:
  ALL DIMENSIONS ARE IN INCHES

4.3   NUCLEAR DESIGN

4.3.1   DESIGN BASES

This section describes the design bases and functional requirements used in the nuclear design of the fuel and reactivity control system and relates these design bases to the General Design Criteria (GDC) presented in 10 CFR 50, Appendix A. Where applicable, supplemental criteria, such as the "Final Acceptance Criteria for Emergency Core Cooling Systems," are addressed. But, before discussing the nuclear design bases, it is appropriate to briefly review the four major categories ascribed to conditions of plant operation.

The full spectrum of plant conditions is divided into four categories, in accordance with the anticipated frequency of occurrence and risk to the public:

1.   Condition I - Normal Operation

2.   Condition II - Incidents of Moderate Frequency

3.   Condition III - Infrequent Faults

4.   Condition IV - Limiting Faults

In general, the Condition I occurrences are accommodated with margin between any plant parameter and the value of that parameter which would require either automatic or manual protective action. Condition II incidents are accommodated with, at most, a shutdown of the reactor with the plant capable of returning to operation after corrective action. Fuel damage (fuel damage, as used here, is defined as penetration of the fission product barrier, i.e., the fuel rod clad) is not expected during Condition I and Condition II events. It is not possible, however, to preclude a very small number of rod failures. These are within the capability of the CVCS and are consistent with the plant design basis.

Condition III incidents do not cause more than a small fraction of the fuel elements in the reactor to be damaged, although sufficient fuel element damage might occur to preclude immediate resumption of operation. The release of radioactive material due to Condition III incidents is not sufficient to interrupt or restrict public use of those areas beyond the exclusion boundary area. Furthermore, a Condition III incident does not, by itself, generate a Condition IV fault or result in a consequential loss of function of the reactor coolant or reactor containment barriers.

Condition IV occurrences are faults that are not expected to occur but are defined as limiting faults which must be designed against. Condition IV faults do not cause a release of radioactive material that exceed the limits of 10 CFR 50.67.

The core design power distribution limits related to fuel integrity are met for Condition I occurrences through conservative design and maintained by the action of the control system. The requirements for Condition II occurrences are met by providing an adequate protection system

which monitors reactor parameters. The control and protection systems are described in Chapter 7, and the consequences of Condition II, III, and IV occurrences are given in Chapter 15.

4.3.1.1   Fuel Burnup

Basis

A limitation on initial installed excess reactivity or average discharge burnup is not required other than as is quantified in terms of other design bases, such as core negative reactivity feedback and shutdown margin, as discussed below.

Discussion

Fuel burnup is a measure of fuel depletion which represents the integrated energy output of the fuel (MWD/MTU) and is a convenient means for quantifying fuel exposure criteria.

The core design lifetime or design discharge burnup is achieved by installing sufficient initial excess reactivity in each fuel region and by following a fuel replacement program (such as that described in Section 4.3.2) that meets all safety related criteria in each cycle of operation.

Initial excess reactivity installed in the fuel, although not a design bases, must be sufficient to maintain core criticality of full power operating conditions throughout cycle life with equilibrium xenon, samarium, and other fission products present. The end of design cycle life is defined to occur when the chemical shim concentration is essentially zero with control rods present to the degree necessary for operational requirements (e.g., the controlling bank at the "bite" position). In terms of chemical shim boron concentration, this represents approximately 10 ppm with no control rod insertion.

4.3.1.2   Negative Reactivity Feedback (Reactivity Coefficient)

Basis

The fuel temperature coefficient will be negative, and the moderator temperature coefficient of reactivity will be non-positive at 100 percent power, less than or equal to a linear ramp from 0 pcm/°F at 100 percent power to +5.0 pcm/°F at 70 percent power, and less than or equal to +5.0 pcm/°F below 70 percent power, thereby providing negative reactivity feedback characteristics at full power. The design basis meets GDC-11.

Discussion

When compensation for a rapid increase in reactivity is considered, there are two major effects. These are the resonance absorption effects (Doppler) associated with changing fuel temperature and the neutron spectrum and reactor composition change effects resulting from changing moderator density. These basic physics characteristics are often identified by reactivity coefficients. The use of slightly enriched uranium ensures that the Doppler coefficient of reactivity is negative. This coefficient provides the most rapid reactivity compensation. The core

is also designed to have an overall moderator temperature coefficient of reactivity which is non-positive at 100 percent power, less than or equal to a linear ramp from 0 pcm/°F at 100 percent power to +5.0 pcm/°F at 70 percent power, and less than or equal to +5.0 pcm/°F below 70 percent power. At full power coolant temperature or void content provides another, slower compensatory effect. The moderator temperature coefficient above can be achieved through use of fixed burnable absorbers and/or control rods which decrease concentration of soluble boron while maintaining reactivity control.

Restrictions on burnable absorbers content (quantity and distribution) are not applied as a design basis other than as they relate to accomplishment of a non-positive moderator temperature coefficient which is within the limits stated above as discussed in Section 4.3.2.

4.3.1.3   Control of Power Distribution

Basis

The nuclear design basis is that, with at least 95 percent confidence level:

1.   The fuel will be operated at less than or equal to 15.09 kW/ft, or 15.15 kW/ft after accounting for 0.4% calorimetric error uncertainty allowance.

2.   Under abnormal conditions, including the maximum overpower condition, the fuel peak power will not cause melting, as defined in Section 4.4.1.2.

3.   The fuel will not operate with a power distribution that violates the departure from nuclear boiling (DNB) design basis (as discussed in Section 4.4.1) under Condition I and II events, including the maximum overpower condition.

4.   Fuel management will be such as to produce values of fuel rod power and burnup consistent with the assumptions in the fuel rod mechanical integrity analysis of Section 4.2.

The above basis meets GDC-10.

Discussion

Calculations of extreme power shapes which affect fuel design limits are performed with proven methods and frequently verified with measurements from operating reactors. The conditions, under which limiting power shapes are assumed to occur, are conservatively chosen with regard to any permissible operating state.

Even though there is good agreement between calculated peak power and measurements, a nuclear uncertainty (Section 4.3.2.2.1) is applied to the calculated peak local power. Such a margin is provided both for the analyses for normal operating states and for anticipated transients.

4.3.1.4   Maximum Controlled Reactivity Insertion Rate

Basis

The maximum reactivity insertion rate due to withdrawal of rod cluster control assemblies or by boron dilution is limited by plant design, hardware, and basic physics. During normal operation, the maximum controlled reactivity insertion rate is limited. The maximum reactivity change rate for accidental withdrawal of two control banks is set such that the peak linear heat rate and departure from nucleate boiling ratio limitations are not challenged. This satisfies GDC-25.

The maximum reactivity worth of control rods and the maximum rates of reactivity insertion employing control rods are limited to preclude rupture of the coolant pressure boundary or disruption of the core internals to a degree which would impair core cooling capacity due to a rod withdrawal or ejection accident (see Chapter 15).

Following any Condition IV event (rod ejection, steamline break, etc.) the reactor can be brought to the shutdown condition and the core will maintain acceptable heat transfer geometry. This satisfies GDC-28.

Discussion

Reactivity addition associated with an accidental withdrawal of a control bank (or banks) is limited by the maximum rod speed (or travel rates) and by the worth of the bank(s). For this reactor, the maximum control rod speed is documented in Section 7.7.1.2.1.

The reactivity change rates are conservatively calculated, assuming unfavorable axial power and xenon distributions. The typical peak xenon burnout rate is significantly lower than the maximum reactivity addition rate for normal operation and for accidental withdrawal of two banks.

4.3.1.5   Shutdown Margins

Basis

Minimum shutdown margin, as specified in the Technical Specifications, is required in all operating modes, in the hot standby shutdown condition, and in the cold shutdown condition.

In all analyses involving reactor trip, the single, highest worth rod cluster control assembly is postulated to remain untripped in its full-out position (stuck rod criterion). This satisfies GDC-26.

Discussion

Two independent reactivity control systems are provided: control rods and soluble boron in the coolant. The control rod system can compensate for the reactivity effects of the fuel and water temperature changes accompanying power level changes over the range from full-load to no-load. In addition, the control rod system provides the minimum shutdown margin under Condition I events and is capable of making the core subcritical rapidly enough to prevent exceeding

acceptable fuel damage limits (very small number of rod failures), assuming that the highest worth control rod is stuck out upon trip.

The boron system can compensate for all xenon burnout reactivity changes and will maintain the reactor in the cold shutdown condition. Thus, backup and emergency shutdown provisions are provided by a mechanical and a chemical shim control system which satisfies GDC-26.

Basis

When fuel assemblies are in the pressure vessel and the vessel head is not in place, k_{eff} will be maintained at or below 0.95 by control rods and soluble boron. Further, the fuel will be maintained sufficiently subcritical that removal of all rod cluster control assemblies will not result in criticality.28

Discussion

10 CFR 50.68(b)(4) specifies that K_{eff} willbe maintained ≤ 0.95 in the spent fuel storage racks when flooded with borated water, and K_{eff} will be maintained < 1.0 when this area is flooded with unborated water. Also, in the normally dry new fuel storage racks K_{eff} will be maintained ≤ 0.98 assuming optimum moderation. No criterion is given for the refueling and transfer operation. However, a 5 percent margin, which is consistent with spent fuel storage and new fuel storage, is adequate for the controlled and continuously monitored operations involved.

The boron concentration required to meet the refueling shutdown criteria is specified in the Technical Specifications. Verification of this shutdown criteria, including uncertainties, is achieved using standard design methods, such as the Casmo5 and Simulate5 codes. The subcriticality of the core is continuously monitored as described in the Technical Specifications.

4.3.1.6   Stability

Basis

The core will be inherently stable to power oscillations at the fundamental mode. This satisfies GDC-12.

Spatial power oscillations within the core with a constant core power output, should they occur, can be reliably and readily detected and suppressed.

Discussion

Oscillations of the total power output of the core, from whatever cause, are readily detected by the loop temperature sensors and by the nuclear instrumentation. The core is protected by these systems, and a reactor trip would occur if power unacceptably increased, preserving the design

margins to fuel design limits. The stability of the turbine/steam generator/core systems and the reactor control system is such that total core power oscillations are not normally possible. The redundancy of the protection circuits ensures an extremely low probability of exceeding design power levels.

The core is designed so that diametral and azimuthal oscillations due to spatial xenon effects are self-damping, and no operator action or control action is required to suppress them. The stability to diametral oscillations is so great that this excitation is highly improbable. Convergent azimuthal oscillations can be excited by prohibited motion of individual control rods. Such oscillations are readily observable and alarmed, using the excore long ion chambers. Indications are also continuously available from incore thermocouples and loop temperature measurements. Movable incore detectors can be activated to provide more detailed information. In all proposed cores, these horizontal plane oscillations are self-damping by virtue of reactivity feedback effects designed into the core.

However, axial xenon spatial power oscillations may occur late in core life. The control bank and excore detectors are provided for control and monitoring of axial power distributions.

Assurance that fuel design limits are not exceeded is provided by reactor Overpower ΔT and Overtemperature ΔT trip functions which use the measured axial power imbalance as an input. Detection and suppression of xenon oscillations are discussed in Section 4.3.2.7.

4.3.1.7 Anticipated Transients Without SCRAM

The effects of anticipated transients with failure to trip are not considered in the design bases of the plant. Analysis has shown that the likelihood of such a hypothetical event is negligibly small. Furthermore, analysis of the consequences of hypothetical failure to trip following anticipated transients has shown that no significant core damage would result, system peak pressures would be limited to acceptable values, and no failure of the reactor coolant system would result (WCAP-8330, Reference 4.3-40). A description of the Anticipated Transient Without Scram Mitigation System Actuation Circuitry (AMSAC) is provided in Section 7.8.

4.3.2 DESCRIPTION

4.3.2.1 Nuclear Design Description

The reactor core consists of a specified number of fuel rods which are held in bundles by spacer grids and top and bottom fittings. The fuel rods are constructed of cylindrical Zircaloy-4, ZIRLO or Optimized ZIRLO tubes containing UO_2 fuel pellets. The bundles, known as fuel assemblies, are arranged in a pattern which approximates a right circular cylinder.

Each fuel assembly contains a 17 x 17 rod array composed of 264 fuel rods, 24 rod cluster control thimbles, and an incore instrumentation thimble. Figure 4.2–1 shows a cross-sectional view of a 17 x 17 fuel assembly and the related rod cluster control locations. Further details of the fuel assembly are given in Section 4.2.

For initial core loading, the fuel rods within a given assembly have the same uranium enrichment in both the radial and axial planes. Fuel assemblies of three different enrichments are used in the initial core loading to establish a favorable radial power distribution. Figure 4.3–1 shows the fuel loading pattern to be used in the first core. Two regions consisting of the two lower enrichments are interspersed so as to form a checkerboard pattern in the central portion of the core. The third region is arranged around the periphery of the core and contains the highest enrichment. The enrichments for Millstone 3 are shown in Table 4.3-1.

A typical reload core loading pattern will be a low-leakage pattern in order to achieve an increased cycle length and a reduced fluence at the periphery of the core. The exact reloading pattern, initial and final positions of assemblies, and the number of fresh assemblies and their placement are dependent on the energy requirement for the next cycle and burnup and power histories of the previous cycles. The figures presented throughout Section 4.3.2, unless designated otherwise, show typical values for normal 4-loop operation.

The core average enrichment is determined by the amount of fissionable material required to provide the desired core lifetime and energy requirements. The physics of the burnout process is such that operation of the reactor depletes the amount of fuel available due to the absorption of neutrons by the U-235 atoms and their subsequent fission. In addition, the fission process results in the formation of fission products, some of which readily absorb neutrons. These effects, depletion, and the buildup of fission products, are partially offset by the buildup of plutonium from the non-fission absorption of neutrons in U-238, as shown on Figure 4.3–2 for a typical 17 x 17 fuel assembly. Therefore, at the beginning of any cycle, a reactivity reserve equal to the depletion of the fissionable fuel and the buildup of fission product poisons over the specified cycle life must be "built" into the reactor. This excess reactivity is controlled by removable neutron absorbing material in the form of boron dissolved in the primary coolant and burnable absorbers.

The concentration of the soluble neutron absorber is varied to compensate for reactivity changes due to fuel burnup, fission product poisoning, including xenon and samarium, burnable absorbers depletion, and the cold-to-operating moderator temperature change. Using its normal makeup path, the chemical and volume control system (CVCS) is typically capable of inserting negative reactivity at a rate of approximately 30 pcm/min when the reactor coolant boron concentration is 1,000 ppm and approximately 35 pcm/min when reactor coolant boron concentration is 100 ppm. If the emergency boration path is used, the CVCS is typically capable of inserting negative reactivity at a rate of approximately 65 pcm/min when the reactor coolant concentration is 1,000 ppm and approximately 75 pcm/min when the reactor coolant boron concentration is 100 ppm. The peak burnout rate for xenon is typically 25 pcm/min (Section 9.3.4 discusses the capability of the CVCS to counteract xenon decay). The actual cycle dependent analysis performed to confirm the adequate boration flow from the CVCS employs reload-specific design information and is a coordinated analysis among several design groups. The methods employed are described in WCAP-14441 (Reference 4.3-41). Rapid transient reactivity requirements and safety shutdown requirements are met with control rods.

As the boron concentration is increased, the moderator temperature coefficient becomes less negative. The use of a soluble boron alone would result in a positive moderator coefficient at

beginning-of-life. Therefore, burnable absorber rods are used in the first core to sufficiently reduce the soluble boron concentration to ensure that the moderator temperature coefficient is negative at power operating conditions. Later reactor cores may use burnable absorbers in the form of rodded assemblies or IFBA (see Section 4.2.2.3.2). During operation, the absorber content in these rods is depleted, thus adding positive reactivity to offset some of the negative reactivity from fuel depletion and fission product buildup. The depletion rate of the burnable absorber rods is not critical since chemical shim is always available and flexible enough to cover any possible deviations in the expected burnable absorber depletion rate.

Figure 4.3–3 is a plot of typical core depletion with and without burnable absorbers. Note that even at end-of-life conditions, some residual absorber remains resulting in a net decrease in the first cycle lifetime.

In addition to reactivity control, the burnable absorbers are strategically located to provide a favorable radial power distribution. Figure 4.3–4 shows the typical burnable absorber distributions within a fuel assembly for assemblies with IFBA. The initial core burnable absorber loading pattern is shown on Figure 4.3–5. A typical reload core using IFBA is shown on Figure 4.3–5a.

Tables 4.3-1 through 4.3-3 contain summaries of the reactor core design parameters for the first fuel cycle, including reactivity coefficients, delayed neutron fraction, and neutron lifetimes. Sufficient information is included to permit an independent calculation of the nuclear performance characteristics of the core.

4.3.2.2   Power Distributions

The accuracy of power distribution calculations has been confirmed through approximately 1,000 flux maps during some 20 years of operation under conditions very similar to those expected. Details of this confirmation are given in WCAP-7308 (Reference 4.3-2) and in Section 4.3.2.2.7.

4.3.2.2.1   Definitions

Power distributions are quantified in terms of hot channel factors. These factors are a measure of the peak pellet power within the reactor core and the total energy produced in a coolant channel, relative to the total reactor power output, and are expressed in terms of quantities related to the nuclear or thermal design, namely:

Power density is the thermal power produced per unit volume of the core (kW/liter).

Linear power density is the thermal power produced per unit length of active fuel (kW/ft). Since fuel assembly geometry is standardized, this is the unit of power density most commonly used. For all practical purposes, it differs from kW/liter by a constant factor which includes geometry and the fraction of the total thermal power which is generated in the fuel rod.

Average linear power density is the total thermal power produced in the fuel rods divided by the total active fuel length of all rods in the core.

Local heat flux is the heat flux at the surface of the cladding ($BTU/ft^2/hr$). For nominal rod parameters, this differs from linear power density by a constant factor.

Rod power or rod integral power is the length integrated linear power density in one rod (kW).

Average rod power is the total thermal power produced in the fuel rods divided by the number of fuel rods (assuming all rods have equal length).

The hot channel factors used in the discussion of power distributions in this section are defined as follows:

F_Q, heat flux hot channel factor, is defined as the maximum local heat flux on the surface of a fuel rod divided by the average fuel rod heat flux, allowing for manufacturing tolerances on fuel pellets and rods, and allowing for measurement conservatism.

F^Q_N, nuclear heat flux hot channel factor, is defined as the maximum local fuel rod linear power density divided by the average fuel rod linear power density, assuming nominal fuel pellet and rod parameters.

F^E_Q, engineering heat flux hot channel factor, is the allowance on heat flux required for manufacturing tolerances. The engineering factor allows for local variations in enrichment, pellet density and diameter, surface area of the fuel rod, and eccentricity of the gap between pellet and clad. Statistically combined, the net effect is a factor of 1.03 to be applied to fuel rod surface heat flux.

$F^N_{\Delta H}$, nuclear enthalpy rise hot channel factor, is defined as the ratio of the integral of linear power along the rod with the highest integrated power to the average rod power.

Manufacturing tolerances, hot channel power distribution, and surrounding channel power distributions are explicitly treated in the calculation of the DNBR described in Section 4.4.

It is convenient for the purposes of discussion to define subfactors of F_Q. However, design limits are set in terms of the total peaking factor.

F_Q = Total peaking factor or heat flux hot channel factor

= (Maximum kW/ft) ÷ (Average kW/ft

= $F^N_Q \times F^E_Q \times F^N_U$

= $F^N_{XY} \times F^N_Z \times F^E_Q \times F^N_U$

where:

F^N_Q and F^E_Q are defined above

F^N_U = factor for measurement conservatism to be 1.05 is employed.

F^N_{XY} = ratio of peak power density to average power density in the horizontal plane of peak local power

F^N_Z = ratio of the power per unit core height in the horizontal plane of peak local power to the average value of power per unit core height. If the plane of peak local power coincides with the plane of maximum power per unit core height, the F^N_Z is the core average axial peaking factor.

4.3.2.2.2   Radial Power Distributions

The power shape in horizontal sections of the core at full power is a function of the fuel assembly and burnable absorber loading patterns, the control rod pattern, and the fuel burnup distribution. Thus, at any time in the cycle, a horizontal section of the core can be characterized as unrodded or with group D control rods. These two situations, combined with burnup effects, determine the radial power shapes which can exist in the core at full power. Typical values of F^N_{XY} are the radial factors (BOL to EOL) given in Table 4.3-2, Sheet 2. The effect on radial power shapes of power level, xenon, samarium, and moderator density effects are also considered but these are quite small. The effect of nonuniform flow distribution is negligible. While radial power distributions in various planes of the core are often illustrated, since the moderator density is proportioned to enthalpy, the core radial enthalpy rise distribution, as determined by the integral of power up each channel, is of greater interest.

Since the position of the hot channel varies from time to time, a single reference radial design power distribution is selected for DNB calculations. This reference power distribution is conservatively chosen to concentrate power in one area of the core, minimizing the benefits of flow redistribution. Assembly powers are normalized to core average power. The radial power distribution within a fuel rod and its variation with burnup as utilized in thermal calculations and fuel rod design is discussed in Section 4.4.

4.3.2.2.3   Assembly Power Distributions

Since the detailed power distribution surrounding the hot channel varies from time to time, a conservatively flat radial assembly power distribution is assumed in the DNB analysis, described in Section 4.4, with the rod of maximum integrated power artificially raised to the design value of $F^N_{\Delta H}$. Care is taken in the nuclear design of all fuel cycles and all operating conditions to ensure that a flatter assembly power distribution does not occur with limiting values of $F^N_{\Delta H}$.

4.3.2.2.4   Axial Power Distributions

The shape of the power profile in the axial, or vertical, direction is largely under the control of the operator through either the manual operation of the control rods or automatic motion of rods responding to manual operation of the CVCS. Nuclear effects which cause variations in the axial power shape include moderator density, Doppler effect on resonance absorption, spatial distribution of xenon, and burnup. Automatically controlled variations in total power output and full length rod motion are also important in determining the axial power shape at any time. Signals are available to the operator from the excore ion chambers, which are long ion chambers outside the reactor vessel running parallel to the axis of the core. Separate signals are taken from the top and bottom halves of the chambers. The difference between top and bottom signals from each of four pairs of detectors is displayed on the control panel and called the flux difference, ΔI. Calculations of the core average peaking factor for many plants and measurements from operating plants under many operating situations are associated with either ΔI or axial offset in such a way that an upper bound can be placed on the peaking factor. For these correlations, axial offset is defined as:

$$\text{axial offset} = (\phi_t - \phi_b) \div (\phi_t + \phi_b)$$

and ϕ_t and ϕ_b are the top and bottom detector readings.

The applicability of the separability assumption is ensured through extensive three dimensional calculations of possible rodded conditions. As an example, Figure 4.3–17 compares the axial power distribution for several assemblies at different distances from inserted control rods with the core average distribution.

The only significant difference from the average occurs in the low power peripheral assemblies, thus confirming the validity of the separability assumption.

4.3.2.2.5   Local Power Peaking

Fuel densification, which has been observed to occur under irradiation in several operating reactors, causes the fuel pellets to shrink both axially and radially. The pellet shrinkage combined with random hang-up of fuel pellets can result in gaps in the fuel column when the pellets below the hung-up pellet settle in the fuel rod. Axial gaps greater than 0.5 inches can lead to cladding collapse which can then result in significant flux and power spiking. A quantitative measure of the local power peaking which results from pellet densification is represented by the power spike factor S(Z), where Z is the axial location in the core.

Past creep collapse methods have assumed that pellet hang-up occurs and an axial gap exists in all fuel rods within a reactor core. The size of the gap is estimated from conservative early-in-life fuel densification as determined from out-of-reactor sintering tests described in Regulatory Guide 1.126. The size of the axial gap also determines the magnitude of the power spike factor applied to Westinghouse fuel designs. In WCAP-13589-A (Reference 4.3-3), it has been demonstrated that no large axial gaps, i.e., > 0.3 inches, form in current Westinghouse fuel designs. In the WCAP submittal, it was also shown that axial gaps less than 0.5 inches do not result in cladding

collapse, and that these types of gaps are associated with relatively small power spikes of 1% or less. As a result, application of a power spike factor to account for fuel densification effects is no longer necessary for Westinghouse fuel designs.

4.3.2.2.6   Limiting Power Distributions

According to the ANSI classification of plant conditions (Chapter 15), Condition I occurrences are those which are frequently or regularly expected in the course of power operation, maintenance, or maneuvering of the plant. As such, Condition I occurrences are accommodated with margin between any plant parameter and the value of that parameter which would require either automatic or manual protective action. Inasmuch as Condition I occurrences frequently or regularly occur, they must be considered from the point of view of affecting the consequences of fault conditions (Conditions II, III, and IV). In this regard, analysis of each fault condition described is generally based on a conservative set of initial conditions corresponding to the most adverse set of conditions which can occur during Condition I operation.

The list of steady state and shutdown conditions, permissible deviations, and operational transients is given in Chapter 15. Implicit in the definition of normal operation is proper and timely action by the reactor operator. That is, the operator follows recommended operating procedures for maintaining appropriate power distributions and takes any necessary remedial actions when alerted to do so by the plant instrumentation. Thus, as stated above, the worst or limiting power distribution which can occur during normal operation is to be considered as the starting point for analysis of Conditions II, III, and IV events.

Improper procedural actions or errors by the operator are assumed in the design as occurrences of moderate frequency (Condition II). Some of the consequences which might result are discussed in Chapter 15. Therefore, the limiting power shapes which result from such Condition II events are those power shapes which deviate from the normal operating condition at the recommended axial offset band, e.g., due to lack of proper action by the operator during a xenon transient following a change in power level brought about by control rod motion. Power shapes which fall in this category are used for determination of the reactor protection system setpoints so as to maintain margin to overpower or DNB limits.

The means for maintaining power distributions within the required hot channel factor limits are described in the Technical Specifications. The calculations used to establish the limits on core power distribution are described in Reference 4.3-43. All of the nuclear effects which influence the radial and/or axial power distributions throughout core life for various modes of operation, including load follow, reduced power operation, and axial xenon transients are considered.

The steady state nuclear design calculations are done for normal flow with the same mass flow in each channel and flow redistribution effects neglected. The effect of flow redistribution is explicitly calculated where it is important in the DNB analysis of accidents. The effect of xenon on radial power distribution is small but is included as part of the normal design process.

The core average axial profile can experience significant changes which can rapidly occur as a result of rod motion and load changes and more slowly due to xenon distribution. For the study of

points of closest approach to axial power distribution limits, several thousand cases are examined. Since the properties of nuclear design dictate what axial shapes can occur, boundaries on the limits of interest can be set in terms of the parameters which are readily observed on the plant. Specifically, the nuclear design parameters which are significant to the axial power distribution analysis are:

1.   Core power level.

2.   Core height.

3.   Coolant temperature and flow.

4.   Coolant temperature program as a function of reactor power.

5.   Fuel cycle lifetimes.

6.   Rod bank worths.

7.   Rod bank overlaps.

Normal operation of the plant assumes compliance with the following conditions:

1.   Control rods in a single bank move together with no individual rod insertion differing by more than 12 steps (indicated) from the bank demand position.

2.   Control banks are sequenced with overlapping banks.

3.   The full length control bank insertion limits are not violated.

4.   Axial power distribution control procedures, which are given in terms of flux difference control and control bank position, are observed.

The axial power distribution procedures referred to above are part of the required operating procedures which are followed in normal operation. Briefly, they require control of the axial offset (flux difference divided by fractional power) at all power levels within a permissible operating band.

The operational restriction on axial flux difference, also known as delta-I, is reflected in the Relaxed Power Distribution Control (RPDC) (Reference 4.3-43) analysis performed for each reload core. The objective of an RPDC analysis is to determine acceptable delta-I band limits that provide assurance that margin to all applicable design bases criteria is maintained. Since the RPDC delta-I band is an analysis output quantity, axial shapes which adequately bound the potential delta-I range must be generated. These axial shapes include the effect of all potential combinations of the key parameters such as burnup, control rod position, xenon distribution, and power level. The methods for generating these shapes (outlined in Reference 4.3-43) involve the use of the 3D Simulate5 Code (References 4.3-43, 4.3-44) to generate the xenon distributions that

bound the desired analytical delta-I operating space. This is accomplished by using either the xenon free oscillation or axial offset search methods. Both methods produce xenon distributions more severe than those typically experienced during normal operation including load follow maneuvers. These xenon distributions combined with power levels from 50% to 100% power and control rod insertions governed by the rod insertion limits are used to produce the axial power distributions for the RPDC normal operation analysis.

The envelope drawn over the calculated normalized max (F_Q (Z) x Power) points on Figure 4.3–21, as specified in the Technical Specifications, represents an upper bound envelope on local power density versus elevation in the core. The calculated values have been increased by the nuclear uncertainty factor F^N_U of 1.05 for conservatism and a factor of 1.03 for the engineering factor F^E_Q. It should be emphasized that this envelope is a conservative representation of the bounding values of local power density. Expected values are considerably smaller.

Allowing for fuel densification effects, the average linear power at 3709 MW is 5.92 kW/ft. From Figure 4.3–21, the conservative upper bound value of normalized local power density, including uncertainty allowances, is 2.548, corresponding to a full power peak linear power of 15.09 kW/ft, or 15.15 kW/ft after accounting for 0.4% calorimetric error uncertainty allowance.

Condition II or abnormal operation which may be the result of system malfunctions or operator errors and create reactor conditions that fall outside the bounds of normal operation established by the LOCA and LOFA precondition analysis, must be analyzed under RPDC. The RPDC analysis examine the most limiting Condition II events (control rod withdrawl, excessive heat removal, and erroneous boration/dilution) to confirm the Overtemperature Delta-T (OTDT) setpoints have been conservatively calculated and that margin to the fuel design limits is maintained.

The required Overpower ΔT and Overtemperature ΔT reactor trip setpoints as a function of power and flux difference are cycle dependent. The peak power density which can occur in the core assuming reactor trip at the Overpower ΔT reactor trip setpoint is less than that required for center-line melt including uncertainties. Similarly, assuming the reactor is tripped at the Overtemperature ΔT setpoint, the minimum DNBR during events for which the Overtemperature ΔT provides protection will be greater than the safety analysis limit value.

F_Q can be increased with decreasing power, as shown in the Technical Specifications. Increasing $F^N_{\Delta H}$ with decreasing power is permitted by the DNB protection setpoints and allows radial power shape changes with rod insertion to the insertion limits, as described in Section 4.4.4.3. The allowance for increased $F^N_{\Delta H}$ permitted is cycle-dependent and is shown in the Core Operating Limits Report. The worst values generally occur when the rods are assumed to be at their insertion limits. These $F^N_{\Delta H}$ are taken as input to the thermal hydraulic analysis as described in Section 4.4.4.3.1.

When a situation is possible in normal operation which could result in local power densities in excess of those assumed as the precondition for a subsequent hypothetical accident, but which

would not itself cause fuel failure, administrative controls and alarms are provided for returning the core to a safe condition. These alarms are described in detail in Chapter 7.

4.3.2.2.7   Experimental Verification of Power Distribution Analysis

This subject is discussed in depth in WCAP-7308 (Reference 4.3-2). A summary of this report is given below. It should be noted that power distribution related measurements are incorporated into the evaluation of calculated power distribution information, using an incore instrumentation processing code described in WCAP-8498 (Reference 4.3-9). The measured versus calculational comparison is normally performed periodically throughout the cycle lifetime of the reactor, as required by Technical Specifications.

In a measurement of the heat flux hot channel factor, F_Q, with the movable detector system described in Section 7.7.1 and 4.4.6, the following uncertainties have to be considered:

1.   Reproduciblity of the measured signal.

2.   Errors in the calculated relationship between detector current and local flux.

3.   Errors in the calculated relationship between detector flux and peak rod power some distance from the measurement thimble.

The appropriate allowance for category 1 above has been quantified by repetitive measurements made with several inter-calibrated detectors by using the common thimble features of the incore detector system. This system allows more than one detector to access any thimble. Errors in category 2 above are quantified to the extent possible, by using the detector current measured at one thimble location to predict fluxes at another location, which is also measured. Local power distribution predictions are verified in critical experiments on arrays of rods with simulated guide thimbles, control rods, burnable poisons, etc. These critical experiments provide quantification of errors of categories 1 and 3 above.

WCAP-7308 (Reference 4.3-2) describes critical experiments performed at the Westinghouse Reactor Evaluation Center and measurements taken on two Westinghouse plants with incore systems of the same type as used in the Millstone 3 plant. The report concludes that the uncertainty associated with F_Q (heat flux) is 3.9 percent at the 95 percent confidence level with only 5 percent of the measurements greater than the inferred value. This is the equivalent of 1.645 limit on a normal distribution and is the uncertainty to be associated with a full core flux map with movable detectors reduced with a reasonable set of input data incorporating the influence of burnup on the radial power distribution. The uncertainty is usually rounded up to 5 percent.

In comparing measured power distributions (or detector currents) with calculations for the same operating conditions, it is not possible to isolate the detector reproducibility. Thus, a comparison between measured and predicted power distributions has to include some measurement error. Such a comparison is given on Figure 4.3–24 for one of the maps used in WCAP-7308 (Reference 4.3-2). Since the first publication of WCAP-7308 (Reference 4.3-2), hundreds of

maps have been taken on these and other reactors. The results confirm the adequacy of the 5 percent uncertainty allowance on the calculated F_Q.

A similar analysis for the uncertainty in $F^N_{\Delta H}$ (rod integral power) measurements results in an allowance of 3.65 percent at the equivalent of 1.645 confidence level. For historical reasons, an eight percent uncertainty factor is allowed in the nuclear design calculational basis; that is, the predicted rod integrals at full power must not exceed the design $F^N_{\Delta H}$ less 8 percent.

A measurement in the second cycle of a 121 assembly, 12 foot, core is compared with a simplified one dimensional core average axial calculation on Figure 4.3–25. This calculation does not give explicit representation to the fuel grids.

The accumulated data on power distributions in actual operation is basically of three types:

1. Much of the data is obtained in steady state operation at constant power in the normal operating configuration.

2. Data with unusual values of axial offset are obtained as part of the excore detector calibration exercise which is performed monthly.

3. Special tests have been performed in load follow and other transient xenon conditions which have yielded useful information on power distributions.

These data are presented in detail in WCAP-7912-P-A (Reference 4.3-8). Figure 4.3–26 contains a summary of measured values of F_Q as a function of axial offset for five plants from that report.

4.3.2.2.8   Testing

An extensive series of physics tests will be performed on the first core. These tests and the criteria for satisfactory results are described in Chapter 14. Since not all limiting situations can be created at BOL, the main purpose of the tests is to provide a check on the calculational methods used in the predictions for the conditions of the test. Tests performed at the beginning of each reload cycle are limited to verification of the selected safety- related parameters of the reload design.

4.3.2.2.9   Monitoring Instrumentation

The adequacy of instrument numbers, spatial deployment, required correlations between readings and peaking factors, calibration, and errors are described in WCAP-7308 (Reference 4.3-2); WCAP-7811 (Reference 4.3-6); and WCAP-7912-P-A (Reference 4.3-8). The relevant conclusions are summarized in Sections 4.3.2.2.7 and 4.4.6.

Provided the limitations given in Section 4.3.2.2.6 on rod insertion and flux difference are observed, the excore detector system provides adequate online monitoring of power distributions. Further details of specific limits on the observed rod positions and flux difference are given in the Technical Specifications, together with a discussion of their bases.

Limits for alarms, reactor trip, etc., are given in the Technical Specifications Descriptions of the systems provided are given in Section 7.7.

4.3.2.3   Reactivity Coefficients

The kinetic characteristics of the reactor core determine the response of the core to changing plant conditions or to operator adjustments made during normal operation, as well as the core response during abnormal or accidental transients. These kinetic characteristics are quantified in reactivity coefficients. The reactivity coefficients reflect the changes in the neutron multiplication due to varying plant conditions, such as power, moderator or fuel temperatures, or pressure or void conditions, although the latter are relatively unimportant in the Millstone 3 reactor. Since reactivity coefficients change during the life of the core, ranges of coefficients are employed in transient analysis to determine the response of the plant throughout life. The results of such simulations and the reactivity coefficients used are presented in Chapter 15. The reactivity coefficient is calculated on a core wide basis using 3D neutronics methods. The effect of radial and axial power distribution on core average reactivity coefficients are explicitly accounted for. The spatial effects are accentuated in some transient conditions, for example, in the postulated rupture of the main steam line and rupture of a rod cluster control assembly mechanism housing, as described in Sections 15.1.5 and 15.4.8.

The analytical methods and calculational models used in calculating the reactivity coefficients are given in Section 4.3.3. These models have been confirmed through extensive testing of many cores similar to the plant described herein; results of these tests are discussed in Section 4.3.3.

Quantitative information for calculated reactivity coefficients, including fuel Doppler coefficient, moderator coefficients (density, temperature, pressure, and void), and power coefficient is given in the following sections.

4.3.2.3.1   Fuel Temperature (Doppler) Coefficient

The fuel temperature (Doppler) coefficient is defined as the change in reactivity per degree change in effective fuel temperature and is primarily a measure of the Doppler broadening of U-238 and Pu-240 resonance absorption peaks. Doppler broadening of other isotopes is also considered but their contribution to the Doppler effect is small. An increase in fuel temperature increases the effective resonance absorption cross-sections of the fuel and produces a corresponding reduction in reactivity.

The fuel temperature coefficient is calculated by performing multi-group calculations, using Simulate5, Reference 4.3-44. Fuel temperatures are calculated as discussed in Section 4.3.3.1.

A typical Doppler temperature coefficient is shown on Figure 4.3–27 as a function of the effective fuel temperature (at BOL and EOL conditions). The effective fuel temperature is lower than the volume averaged fuel temperature, since the neutron flux distribution is non-uniform through the pellet and gives preferential weight to the surface temperature. A typical Doppler-only contribution to the power coefficient, defined later, is shown on Figure 4.3–28 as a function of relative core power. The integral of the differential curve on Figure 4.3–28 is the Doppler

contribution to the power defect and is shown on Figure 4.3–29 as a function of relative power. The Doppler coefficient becomes more negative as a function of life as the Pu-240 content increases, thus increasing the Pu-240 resonance absorption, but the overall value becomes less negative since the fuel temperature changes with burnup. The upper and lower limits of Doppler coefficient used in accident analyses are given in Chapter 15.

4.3.2.3.2   Moderator Coefficients

The moderator coefficient is a measure of the change in reactivity due to a change in specific coolant parameters, such as density, temperature, pressure, or void. The coefficients so obtained are moderator density, temperature, pressure, and void coefficients.

Moderator Density and Temperature Coefficients

The moderator temperature (density) coefficient is defined as the change in reactivity per degree change in the moderator temperature. Generally, the effects of the changes in moderator density, as well as the temperature, are considered together.

The soluble boron used in the reactor as a means of reactivity control also has an effect on moderator density coefficient, since the soluble boron poison density, as well as the water density, is decreased when the coolant temperature rises. A decrease in the soluble poison density introduces a positive component in the moderator coefficient. If the concentration of soluble poison is large enough, the net value of the coefficient may be positive. With the burnable poison rods present, however, the initial hot boron concentration is sufficiently low that the moderator temperature coefficient is nonpositive at 100 percent power, less than or equal to a linear ramp from 0 pcm/°F at 100 percent power to +5.0 pcm/°F at 70 percent power, and less than or equal to +5.0 pcm/°F below 70 percent power. The effect of control rods is to make the moderator coefficient more negative since the thermal neutron mean free path, and hence the volume affected by the control rods increases with an increase in temperature.

With burnup, the moderator coefficient becomes more negative, primarily as a result of boric acid dilution, but also to a significant extent from the effects of the buildup of plutonium and fission products.

The moderator coefficient is calculated for a range of plant conditions by performing multi-group calculations, in which the moderator temperature (and density) is varied by about 5°F about each of the mean temperatures. The moderator temperature coefficient is shown as a function of core temperature and boron concentration for a typical unrodded and rodded core on Figures 4.3–30 through 4.3–32. The temperature range covered is from cold (68°F) to about 600°F. The contribution due to Doppler coefficient (because of change in moderator temperature) has been subtracted from these results. Figure 4.3–33 shows the hot, full power moderator temperature coefficient for a typical core plotted as a function of first cycle lifetime for the just critical boron concentration condition based on the design boron letdown condition.

The moderator coefficients presented here are calculated on a corewide basis, since they are used to describe the core behavior in normal and accident situations when the moderator temperature changes can be considered to affect the entire core.

Moderator Pressure Coefficient

The moderator pressure coefficient relates the change in moderator density, resulting from a reactor coolant pressure change, to the corresponding effect on neutron production. This coefficient is of much less significance in comparison with the moderator temperature coefficient.

A change of 50 psi in pressure has approximately the same effect on reactivity as a one-half degree change in moderator temperature This coefficient can be determined from the moderator temperature coefficient by relating change in pressure to the corresponding change in density. The moderator pressure coefficient is negative over a portion of the moderator temperature range at BOL ≤ (-0.004 pcm/psi, BOL) but is always positive at operating conditions and becomes more positive during life (+0.3 pcm/psi, EOL).

Moderator Void Coefficient

The moderator void coefficient relates the change in neutron multiplication to the presence of voids in the moderator. In a pressurized water reactor, this coefficient is not very significant because of the low void content in the coolant. The core void content is less than one-half of 1 percent and is due to local or statistical boiling. The void coefficient typically varies from 50 pcm/percent void at BOL and at low temperatures to -250 pcm/percent void at EOL and at operating temperatures. The void coefficient at operating temperature becomes more negative with fuel burnup.

4.3.2.3.3   Power Coefficient

The combined effect of moderator temperature and fuel temperature change as the core power level changes is the total power coefficient and is expressed in terms of reactivity change per percent power change. A typical power coefficient at BOL and EOL conditions is given on Figure 4.3–34.

It becomes more negative with burnup, reflecting the combined effect of moderator and fuel temperature coefficients with burnup. The power defect (integral reactivity effect) at BOL and EOL is given on Figure 4.3–25.

4.3.2.3.4   Comparison of Calculated and Experimental Reactivity Coefficients

Reference 4.3-44 describes the comparison of calculated and experimental reactivity coefficients in detail.

Experimental evaluation of the reactivity coefficients will be performed during the physics startup tests described in Chapter 14.

4.3.2.3.5   Reactivity Coefficients Used in Transient Analysis

Table 4.3-2 gives the limiting values, as well as the best estimate values, for reactivity coefficients. The limiting values are used as design limits in the transient analysis. The exact values of the coefficient used in the analysis depend on whether the transient of interest is examined at the BOL or EOL, whether the most negative or the most positive (least negative) coefficients are appropriate, and whether spatial non-uniformity must be considered in the analysis. Conservative values of coefficients, considering various aspects of analysis, are used in the transient analysis This is described in Chapter 15.

The reactivity coefficients shown on Figures 4.3–27 thru 4.3–35 are typical best estimate values calculated for a first cycle. The limiting values, shown in Table 4.3-2, are chosen to encompass the best estimate reactivity coefficients, including the uncertainties given in Section 4.3.3.3 over appropriate operating conditions calculated for the first cycle and the expected values for the subsequent cycles. The most positive, as well as the most negative, values are selected to form the design basis range used in the transient analysis. A direct comparison of the best estimate and design limit values shown in Table 4.3-2 can be misleading since, in many instances, the most conservative combination of reactivity coefficients is used in the transient analysis even though the extreme coefficients assumed may not simultaneously occur at the conditions assumed in the analysis. The need for a reevaluation of any accident in a subsequent cycle is contingent upon whether or not the coefficients for that cycle fall within the identified range used in the analysis presented in Chapter 15 with due allowance for the calculational uncertainties given in Section 4.3.3.3. Control rod requirements are given in Table 4.3-3 for the core described and for a hypothetical equilibrium cycle, since these are markedly different. These latter numbers are provided for information only since refueling specifications for subsequent cycles have not yet been established. The actual values used for any given cycle's safety analysis are properly documented in the Reload Safety Analysis Checklist. This document is jointly reviewed by several organizations participating in the fuel design, characterization, safety analysis and operating recommendations which are supplied to MP-3 via approved design and operating documents.

4.3.2.4   Control Requirements

To ensure the shutdown margin stated in Technical Specifications under conditions where a cooldown to ambient temperature is required, concentrated soluble boron is added to the coolant Boron concentrations for several core conditions are listed in Table 4.3-2. For all core conditions, including refueling, the boron concentration is well below the solubility limit. The rod cluster control assemblies are employed to bring the reactor to the hot shutdown condition. The minimum required shutdown margin is given in the Technical Specifications.

The ability to accomplish the shutdown for hot conditions is demonstrated in Table 4.3-3 by comparing the difference between the rod cluster control assembly reactivity available with an allowance for the worst stuck rod with that required for control and protection purposes. The shutdown margin includes an allowance of 10 percent of analytic uncertainties (see Section 4.3.2.4.9). The largest reactivity control requirement appears at the EOL when the

moderator temperature coefficient reaches its peak negative value as reflected in the larger power defect.

The control rods are required to provide sufficient reactivity to account for the power defect from full power to zero power and to provide the required shutdown margin. The reactivity addition resulting from power reduction consists of contributions from Doppler, moderator temperature, flux redistribution, and reduction in void content, as discussed below.

4.3.2.4.1   Doppler

The Doppler effect arises from the broadening of U-238 and Pu-240 resonance cross-sections with an increase in effective pellet temperature. This effect is most noticeable over the range of zero power to full power due to the large pellet temperature increase with power generation.

4.3.2.4.2   Variable Average Moderator Temperature

When the core is shut down to the hot, zero power condition, the average moderator temperature changes from the equilibrium full load value determined by the steam generator and turbine characteristics (steam pressure, heat transfer, tube fouling, etc.) to the equilibrium no-load value, which is based on the steam generator shell side design pressure. The nuclear fuel design procedures require that the change in temperature is conservatively increased by an appropriate amount to account for the control dead band and measurement errors documented in the cycle dependent RSAC.

Since the moderator coefficient is negative for most of the cycle, there is a reactivity addition with power reduction. The moderator coefficient becomes more negative as the fuel depletes because the boron concentration is reduced. This effect is the major contributor to the increased requirement at EOL.

4.3.2.4.3   Redistribution

During full power operation, the coolant density decreases with core height, and this, together with partial insertion of the control rods, results in less fuel depletion near the top of the core. Under steady state conditions, the relative power distribution will be slightly asymmetric toward the bottom of the core. On the other hand, at hot zero power conditions, the coolant density is uniform up the core, and there is no flattening due to Doppler. The result will be a flux distribution which, at zero power, can be skewed toward the top of the core. The reactivity insertion due to the skewed distribution is calculated with an allowance for effects of xenon distribution.

4.3.2.4.4   Void Content

A small void content in the core is due to nucleate boiling at full power. The void collapse coincidental with power reduction makes a small reactivity contribution.

4.3.2.4.5   Rod Insertion Allowance

At full power, the control bank is operated within a prescribed band of travel to compensate for small changes in boron concentration, changes in temperature, and very small changes in the xenon concentration not compensated for by a change in boron concentration. When the control bank reaches either limit of this band, a change in boron concentration is required to compensate for additional reactivity changes. Since the insertion limit is set by a rod travel limit, a conservatively high calculation of the inserted worth is made which exceeds the normally inserted reactivity.

4.3.2.4.6   Installed Excess Reactivity for Depletion

Excess reactivity is installed at the beginning of each cycle to provide sufficient reactivity to compensate for fuel depletion and fission product building throughout the cycle. This reactivity is controlled by the addition of soluble boron to the coolant and by burnable poisons. The soluble boron concentration for several core configurations, the unit boron worth, and burnable poison worth are given in Tables 4.3-1 and 4.3-2. Since the excess reactivity for burnup is controlled by soluble boron and/or burnable poisons, it is not included in control rod requirements.

4.3.2.4.7   Xenon and Samarium Poisoning

Changes in xenon and samarium concentrations in the core occur at a sufficiently slow rate, even following rapid power level changes, that the resulting reactivity change can be controlled by changing the soluble boron concentration (also see Section 4.3.2.4.16).

4.3.2.4.8   pH Effects

Changes in reactivity due to a change in coolant pH, if any, are sufficiently small in magnitude and occur slowly enough to be controlled by the boron system. Further details are provided in Cermak et al. (Reference 4.3-12).

4.3.2.4.9   Experimental Confirmation

The capability of the methods described in Section 4.3.3 to model all aspects of reactivity control has been directly demonstrated versus comparisons with measured data as described in Reference 4.3-44.

4.3.2.4.10 Control

Core reactivity is controlled by means of a chemical poison dissolved in the coolant, rod cluster control assemblies, and burnable absorber rods, as described below.

4.3.2.4.11 Chemical Poison

Boron in solution as boric acid is used to control relatively slow reactivity changes associated with:

1.   The moderator temperature defect in going from cold shutdown at ambient temperature to the hot operating temperature at zero power.

2.   The transient xenon and samarium poisoning, such as that following power changes or changes in rod cluster control position.

3.   The reactivity effects of fissile inventory depletion and buildup of long-life fission products.

4.   The burnable absorber depletion.

The boron concentrations for various core conditions are presented in Table 4.3-2.

4.3.2.4.12 Rod Cluster Control Assemblies

The number of rod cluster control assemblies is shown in Table 4.3-1. The rod cluster control assemblies are used for shutdown and control purposes to offset fast reactivity changes associated with:

1.   The required shutdown margin in the hot zero power, stuck rods condition.

2.   The reactivity compensation as a result of an increase in power above hot zero power (power defect, including Doppler, and moderator reactivity changes).

3.   Unprogrammed fluctuations in boron concentration, coolant temperature, or xenon concentration (with rods not exceeding the allowable rod insertion limits).

4.   Reactivity ramp rates resulting from load changes.

The allowed control bank reactivity insertion is limited at full power to maintain shutdown capability. As the power level is reduced, control rod reactivity requirements are also reduced, and more rod insertion is allowed. The control bank position is monitored, and the operator is notified by an alarm if the limit is approached. The determination of the insertion limit uses conservative xenon distributions and axial power shapes. In addition, the rod cluster control assembly withdrawal pattern determined from these analyses is used in determining power distribution factors and in determining the maximum worth of an inserted rod cluster control assembly ejection accident. For further discussion, refer to the Technical Specifications on rod insertion limits.

Power distribution, rod ejection, and rod misalignment analyses are based on the arrangement of the shutdown and control groups of the rod cluster control assemblies shown on Figure 4.3–36. All shutdown rod cluster control assemblies are withdrawn before withdrawal of the control banks is initiated. In going from zero to 100 percent power, control banks B, C, and D are sequentially withdrawn. The limits of rod positions and further discussion on the basis for rod insertion limits are provided in the Technical Specifications.

4.3.2.4.13 Reactor Coolant Temperature

Reactor coolant (or moderator) temperature control has added flexibility in reactivity control of the Westinghouse pressurized water reactor. This feature takes advantage of the negative moderator temperature coefficient inherent in a pressurized water reactor to:

1.   Maximize return to power capabilities.

2.   Provide ±5 percent power load regulation capabilities.

3.   Extend the time in cycle life to which daily load follow operations can be accomplished.

Reactor coolant temperature control supplements the dilution capability of the plant by lowering the reactor coolant temperature to supply positive reactivity through the negative moderator coefficient of the reactor. After the transient is over, the system returns the reactor coolant temperature to the programmed value.

Moderator temperature control of reactivity, like soluble boron control, has the advantage of not significantly affecting the core power distribution. However, unlike boron control, temperature control can be rapid enough to achieve reactor power change rates of 5 percent/minute.

4.3.2.4.14 Burnable Absorber Rods

The burnable absorber rods provide partial control of the excess reactivity available during the first fuel cycle. These rods prevent the moderator temperature coefficient from being positive at full power and exceeding a linear ramp of 0 pcm/°F at 100 percent power to +5.0 pcm/°F at 70 percent power, and +5.0 pcm/°F below 70 percent power. They perform this function by reducing the requirement for soluble boron in the moderator at the beginning of the fuel cycle, as previously described. For purposes of illustration, a typical burnable absorber rod pattern in the core, together with the number of rods per assembly, are shown on Figure 4.3–5a, while the arrangement within an assembly are displayed on Figure 4.3–4. The reactivity worth of these rods is shown in Table 4.3-1. The boron in the rods is depleted with burnup at a sufficiently slow rate so that the resulting critical concentration of soluble boron is such that the moderator temperature coefficient remains within the limits stated above at all times for power operating conditions.

4.3.2.4.15 Peak Xenon Startup

Compensation for the peak xenon buildup is accomplished using the boron control system. Startup from the peak xenon conditions is accomplished with a combination of rod motion and boron dilution. The boron dilution may be made at any time, including during the shutdown period, provided the shutdown margin is maintained.

4.3.2.4.16 Load Follow Control and Xenon Control

During load follow maneuvers, power changes are accomplished using control rod motion and dilution or boration by the boron system as required. Control rod motion is limited by the control rod insertion limits as provided in the Technical Specifications and discussed in Sections 4.3.2.4.12 and 4.3.2.4.13. The power distribution is maintained within acceptable limits through location of the control bank. Reactivity changes due to the changing xenon concentration can be controlled by rod motion and/or changes in the soluble boron concentration.

Late in cycle life, extended load follow capability is obtained by augmenting the limited boron dilution capability at low soluble boron concentrations by temporary moderator temperature reductions.

Rapid power increases (5 percent/min) from part power during load follow operation are accomplished with a combination of rod motion, moderator temperature reduction, and boron dilution. Compensation for the rapid power increase is initially accomplished by a combination of rod withdrawal and moderator temperature reduction. As the slower boron dilution takes effect after the initial rapid power increase, the moderator temperature is returned to the programmed value.

4.3.2.4.17 Burnup

Control of the excess reactivity for burnup is accomplished using soluble boron and/or burnable absorbers. The boron concentration must be limited during operating conditions to ensure that the moderator temperature coefficient is non-positive at 100 percent power, less than or equal to a linear ramp from 0 pcm/°F at 100 percent power to +5.0 pcm/°F at 70 percent power, and less than or equal to +5.0 pcm/°F below 70 percent power. Sufficient burnable absorbers are installed at the beginning of a cycle to give the desired cycle lifetime, without exceeding the boron concentration limit. The practical minimum boron concentration is in the range of 0 to 10 ppm.

4.3.2.5   Control Rod Patterns and Reactivity Worth

The rod cluster control assemblies are designated by function as the control groups and the shutdown groups. The terms "group" and "bank" are used synonymously throughout this report to describe a particular grouping of control assemblies. The rod cluster assembly pattern is displayed on Figure 4.3–36, which is not expected to change during the life of the plant. The control banks are labeled A, B, C, and D and the shutdown banks are labeled SA, SB, SC, SD, and SE. Each bank, although operated and controlled as a unit, is composed of two subgroups. The axial position of the rod cluster control assemblies may be manually or automatically controlled. The rod cluster control assemblies are all dropped into the core following actuation of reactor trip signals.

Two criteria have been employed for selection of the control groups. First, the total reactivity worth must be adequate to meet the requirements specified in Table 4.3-3. Second, in view of the fact that these rods may be partially inserted at power operation, the total power peaking factor should be low enough to ensure that the power capability requirements are met. Analyses indicate

that the first requirement can be met either by a single group or by two or more banks whose total worth equals at least the required amount. The axial power shape would be more peaked, following movement of a single group of rods worth 3 to 4 percent $\Delta\rho$. Therefore, four banks (described as A, B, C, and D on Figure 4.3–36) have been selected. Typical control bank worths are shown in Table 4.3-2.

The position of control banks for criticality under any reactor condition is determined by the concentration of boron in the coolant.

On an approach to criticality, boron is adjusted to ensure that criticality will be achieved with control rods above the insertion limit set by shutdown and other considerations (Technical Specifications). Early in the cycle, there may also be a withdrawal limit at low power to maintain the moderator temperature coefficient within allowed limits.

Ejected rod worths are given in Section 15.4.8 for several different conditions.

Allowable deviations due to misaligned control rods are discussed in the Technical Specifications.

A representative calculation for two banks of control rods simultaneously withdrawn (rod withdrawal accident) is given on Figure 4.3–37.

Calculation of control rod reactivity worth versus time following reactor trip involves both control rod velocity and differential reactivity worth. The rod position versus time of travel after rod release assumed is typified by Figure 4.3–38. For nuclear design purposes, the reactivity worth versus rod position is calculated by a series of steady state calculations at various control rod positions, assuming all rods out of the core as the initial position in order to minimize the initial reactivity insertion rate. Also, to be conservative, the rod of highest worth is assumed stuck out of the core, and the flux distribution (and thus reactivity importance) is assumed to be skewed to the bottom of the core. The result of these calculations is shown on Figure 4.3–39.

The shutdown groups provide additional negative reactivity to assure an adequate shutdown margin. Shutdown margin is defined as the amount by which the core would be subcritical at hot shutdown if all rod cluster control assemblies were tripped, but assuming that the highest worth assembly remains fully withdrawn and no changes in xenon or boron take place. The loss of control rod worth due to the material irradiation is negligible, since only bank D may be in the core under normal operating conditions (near full power).

The values given in Table 4.3-3 illustrate that the typical available reactivity in the withdrawn rod cluster control assemblies provides the design bases minimum shutdown margin. The highest worth control rod cluster is assumed to remain at its fully withdrawn position. Actual cycle specific values are contained in the Nuclear Design Report. An allowance for the uncertainty in the calculated worth of N-1 rods is made before determination of the shutdown margin.

4.3.2.6　Criticality of the Reactor during Refueling and Criticality of Fuel Assemblies

The basis for maintaining the reactor subcritical during refueling is presented in Section 4.3.1.5, and a discussion of how control requirements are met is given in Sections 4.3.2.4 and 4.3.2.5.

Criticality of fuel assemblies outside the reactor is precluded by adequate design of fuel transfer, shipping and storage facilities, and by administrative control procedures. The principal methods of preventing criticality are limiting the fuel assembly array size, limiting assembly interaction by fixing the minimum separation between assemblies, use of neutron poisons, and use of minimum fuel burnup requirements.

Spent Fuel Pool

The design basis for preventing criticality in the spent fuel pool is that, considering possible variations, there is a 95 percent probability at a 95 percent confidence level that the effective multiplication factor (K_{eff}) of the fuel assembly array will be less than 0.95 as required by 10 CFR 50.68(b)(4).

The following are conditions assumed in meeting the design basis spent fuel pool K_{eff} limit of 0.95:

1.　The criticality analysis considers the fuel assembly mechanical design of fuel stored in the spent fuel pool which will give the largest K_{eff}.

2.　The criticality analysis uses the fuel assembly reactivity for a particular Region of the spent fuel pool which is the maximum reactivity fuel assembly allowed for that Region of the spent fuel pool. The fuel assembly maximum reactivity is evaluated without credit for reduced enrichment axial blankets contained within the fuel. Credit for fuel burnup, fuel decay time (Region 3), control rods (Region 2), and Integral Fuel Burnable Absorber (IFBA) contained within the fuel (Region 1A) may be used.

3.　The moderator is water containing soluble boron at the temperature within the design limits which yields the largest reactivity.

4.　The array is either infinite in lateral extent, or is surrounded by a conservatively chosen reflector, whichever is appropriate to the design.

5.　Mechanical uncertainties are treated by either using "worst case" conditions, or by performing sensitivity studies and obtaining appropriate uncertainties and biases.

6.　Credit may be taken for the neutron absorption in some structural materials, and credit may be taken for solid materials added specifically for neutron absorption.

7. Credit for soluble boron is taken under normal and postulated accident conditions where the double contingency principle of ANSI N16.1-1975 is applied. This principle states that it shall require at least two unlikely, independent, and concurrent events to produce a criticality accident.

8. When credit is taken for fuel burnup, uncertainties and biases are considered for fuel assembly reactivity at a given burnup, uncertainty on measured fuel burnup, bias for fuel assembly dimensional changes with burnup, and a penalty is applied for fuel assembly reactivity changes due to axial and radial burnup variations.

9. Credit may be taken for the reactivity loss of irradiated fuel due to the time the fuel has decayed since last irradiated in the reactor.

The criticality design criteria are met when the calculated effective multiplication factor, plus the total uncertainty and bias, is in conformance to the design basis listed above.

The spent fuel pool criticality methods comply with:

(1) Code of Federal Regulations, Title 10, Part 50, Appendix A, General Design Criteria 62, Prevention of Criticality in Fuel Storage and Handling.

(2) USNRC Standard Review Plan, NUREG-0800, Section 9.1.2, Spent Fuel Storage, Rev 3, July 1981.

(3) USNRC letter of April 14, 1978 to all Power Reactor Licensees-OT Position for Review and Acceptance of Spent Fuel Storage and Handling Applications including modification letter dated January 18, 1979.

(4) ANSI N18.2-1973, "Nuclear Safety Criteria for the Design of Stationary Pressurized Water Reactor Plants," Section 5.7, Fuel Handling System.

(5) ANSI N210-1976, "Design Objectives for LWR Spent Fuel Storage Facilities at Nuclear Power Plants," Section 5.1.12.

(6) ANSI N16.9-1975, "Validation of Calculational Methods for Nuclear Criticality Safety."

(7) ANSI/ANS 57.2-1983, "Design Requirements for LWR Spent Fuel Storage Facilities at Nuclear Power Plants," Section 6.4.2.2.

(8) 10 CFR 50.68 Criticality Accident Requirements

New Fuel Storage Racks

For new fuel storage, the design basis for preventing criticality is that, considering possible variations, there is a 95 percent probability at a 95 percent confidence level that the effective

multiplication factor (K_{eff}) of the fuel assembly array when the new fuel racks are fully loaded with maximum reactivity fuel will be:

(1)   less than 0.95 when flooded with potential moderators; and

(2)   less than 0.98 when surrounded by optimum moderation.

This design basis is consistent with the guidance of the USNRC Standard Review Plan, NUREG-0800, Section 9.1.1, New Fuel Storage, Rev 2, July 1981.

The following are conditions assumed in meeting the design basis new fuel storage K_{eff} limit of 0.95 when flooded with potential moderators, and 0.98 when surrounded by optimum moderation:

1.   The criticality analysis uses the fuel assembly with the highest authorized enrichment. This does not take credit for reduced enrichment axial blankets, control rods, or burnable poisons contained within the fuel.

2.   For the K_{eff} limit of 0.95, the moderator is pure water at the temperature within the design limits which yields the largest reactivity.

3.   For the K_{eff} limit of 0.98, the optimum water density is calculated which yields the largest reactivity.

4.   The array is either infinite in lateral extent, or is surrounded by a conservatively chosen reflector, whichever is appropriate to the design.

5.   Mechanical uncertainties are treated by either using "worst case" conditions, or by performing sensitivity studies and obtaining appropriate uncertainties.

6.   Credit may be taken for solid materials added specifically for neutron absorption.

7.   Analyzed accident conditions must meet the same design basis criteria.

The criticality design criteria are met when the calculated effective multiplication factor, plus the total uncertainty, is in conformance to the design basis listed above.

The new fuel storage criticality methods comply with:

(1)   "Validation of Calculational Methods for Nuclear Criticality Safety," ANSI N16.9-1975, American Nuclear Society.

(2)   USNRC Standard Review Plan, NUREG-0800, Section 9.1.1, New Fuel Storage, Rev 2, July 1981.

(3)   USNRC letter of April 14, 1978 to all Power Reactor Licensees-OT Position for
         Review and Acceptance of Spent Fuel Storage and Handling Applications
         including modification letter dated January 18, 1979.

(4)   10 CFR 50.68 Criticality Accident Requirements

4.3.2.7   Stability

4.3.2.7.1   Introduction

The stability of the pressurized water reactor cores against xenon-induced spatial oscillations and
the control of such transients are extensively discussed in WCAP-7811 (Reference 4.3-6);
WCAP-3680-20 (Reference 4.3-13); WCAP-3680-21 (Reference 4.3-14); and WCAP-3680-22
(Reference 4.3-15). A summary of these reports is given in the following discussion, and the
design bases are given in Section 4.3.1.6.

In a large reactor core, xenon induced oscillations can take place with no corresponding change in
the total power of the core. The oscillation may be caused by a power shift in the core which
rapidly occurs by comparison with the xenon-iodine time constants. Such a power shift occurs in
the axial direction when a plant load change is made by control rod motion and results in a change
in the moderator density and fuel temperature distributions. Such a power shift could occur in the
diametral plane of the core as a result of abnormal control action.

Due to the negative power coefficient of reactivity, pressurized water reactor cores are inherently
stable to oscillations in total power. Protection against total power instabilities is provided by the
control and protection system, as described in Section 7.7. Hence, the discussion on the core
stability will be limited here to xenon-induced spatial oscillations.

4.3.2.7.2   Stability Index

Power distributions, either in the axial direction or in the X-Y plane, can undergo oscillations due
to perturbations introduced in the equilibrium distributions without changing the total core power.
The overtones in the current pressurized water reactors and the stability of the core against xenon
induced oscillations can be determined in terms of the eigenvalues of the first flux overtones.
Writing the eigenvalue of the first flux harmonic as:

$$\xi = b + ic \qquad\qquad (4.3\text{-}1)$$

then b is defined as the stability index and $T = 2\,\pi/c$ as the oscillation period of the first harmonic.
The time-dependence of the first harmonic $\delta\phi$ in the power distribution can now be represented
as:

$$\delta\phi(t) = A\,e^{\xi t} = ae^{bt}\cos ct \qquad\qquad (4.3\text{-}2)$$

where A and a are constants. The stability index can also be obtained approximately by:

$$b = (1/T) \text{ In } [(A_n + 1) \div (A_n)] \qquad\qquad (4.3\text{-}3)$$

where An and A_{n+1} are the successive peak amplitudes of the oscillation and T is the time period between the successive peaks.

4.3.2.7.3   Prediction of the Core Stability

The stability of the core described herein (i.e., with 17 x 17 fuel assemblies) against xenon-induced spatial oscillations is expected to be equal to or better than that of earlier designs for cores of similar size. The prediction is based on a comparison of the parameters which are significant in determining the stability of the core against the xenon-induced oscillations, namely:

1. the overall core size is unchanged and spatial power distributions will be similar,
2. the moderator temperature coefficient is expected to be similar to or slightly more negative, and
3. the Doppler coefficient of reactivity is expected to be equal to or slightly more negative at full power.

Analysis of both the axial and X-Y xenon transient tests, discussed in Section 4.3.2.7.5, shows that the calculational model is adequate for the prediction of core stability.

4.3.2.7.4   Stability Measurements

    1.   Axial measurements

        Two axial xenon transient tests conducted in a pressure water reactor with a core height of 12 feet and 121 fuel assemblies are reported in WCAP-7964 (Reference 4.3-16) and will be briefly discussed here. The tests were performed at approximately 10 percent and 50 percent of cycle life.

        Both a free-running oscillation test and a controlled test were performed during the first test. The second test at mid cycle consisted of a free-running oscillation test only. In each of the free-running oscillation tests, a perturbation was introduced to the equilibrium power distribution through an impulse motion of the control bank D and the subsequent oscillation was monitored to measure the stability index and the oscillation period. In the controlled test conducted early in the cycle, the part-length rods were used to follow the oscillations to maintain an axial offset within the prescribed limits. The axial offset of power was obtained from the excore ion chamber readings (which had been calibrated against the incore flux maps) as a function of time for both free-running tests, as shown on Figure 4.3–40.

        The total core power was maintained constant during these spatial xenon tests, and the stability index and the oscillation period were obtained from a least-square fit of the axial offset data in the form of Equation 4.3-2. The axial offset of power is the quantity that properly represents the axial stability in the sense that it

essentially eliminates any contribution from even-order harmonics, including the fundamental mode. The conclusions of the tests are:

a.   The core was stable against induced axial xenon transients, both at the core average burnups of 1,550 MWD/MTU and 7,700 MWD/MTU. The measured stability indices are -0.041 hr^{-1} for the first test (Curve 1 of Figure 4.3–40) and -0.014 hr^{-1} for the second test (Curve 2 of Figure 4.3–40). The corresponding oscillation periods are 32.4 and 27.2 hours, respectively.

b.   The reactor core becomes less stable as fuel burnup progresses and the axial stability index was essentially zero at 12,000 MWD/MTU. However, the movable control rod systems can control axial oscillations, as described in Section 4.3.2.7.

2.   Measurements in the X-Y plane

Two X-Y xenon oscillation tests were performed at a pressurized water reactor plant with a core height of 12 feet and 157 fuel assemblies. The first test was conducted at a core average burnup of 12,900 MWD/MTU. Both of the X-Y xenon tests show that the core was stable in the X-Y plane at both burnups. The second test shows that the core became more stable as the fuel burnup increased, and all Westinghouse pressurized water reactors with 121 and 157 assemblies are expected to be stable throughout their burnup cycles. The results of these tests are applicable to the 193 assembly Millstone 3 core, as discussed in Section 4.3.2.7.3.

In each of the two X-Y tests, a perturbation was introduced to the equilibrium power distribution through an impulse motion of one rod cluster control unit located along the diagonal axis. Following the perturbation, the uncontrolled oscillation was monitored, using the movable detector and thermocouple system and the excore power range detectors. The quadrant tilt difference (QTD) is the quantity that properly represents the diametral oscillation in the X-Y plane of the reactor core in that the differences of the quadrant average powers over two symmetrically opposite quadrants essentially eliminates the contribution to the oscillation from the azimuthal mode, The QTD data were fitted in the form of Equation 4.3-2 through least-square method. A stability index of -0.076 hr^{-1} with a period of 29.6 hours was obtained from the thermocouple data shown on Figure 4.3–41.

It was observed in the second X-Y xenon test that the pressurized water reactor core with 157 fuel assemblies had become more stable due to an increased fuel depletion, and the stability index was not determined.

4.3.2.7.5   Comparison of Calculations with Measurements

The analysis of the axial xenon transient tests was performed in an axial slab geometry, using a flux synthesis technique. The direct simulation of the axial offset data was carried out using the PANDA code (WCAP-7084, 7757, Reference 4.3-1). The analysis of the X-Y xenon transient tests was performed in an X-Y geometry, using a modified TURTLE code (WCAP-7213-A, 7758-A, Reference 4.3-10). Both the PANDA and TURTLE codes solve the two-group time dependent neutron diffusion equation with time dependent xenon and iodine concentrations. The fuel temperature and moderator density feedback is limited to a steady state model All the X-Y calculations were performed in an average enthalpy plane.

The basic nuclear cross-sections used in this study were generated from a unit cell depletion program which has evolved from the codes LEOPARD (WCAP-3269-26, Reference 4.3-17) and CINDER (WCAP-TM-334, Reference 4.3-18). The detailed experimental data during the tests, including the reactor power level, enthalpy rise, and the impulse motion of the control rod assembly, as well as the plant follow burnup data, were closely simulated in the study.

The results of the stability calculation for the axial tests are compared with the experimental data in Table 4.3-5. The calculations show conservative results for both of the axial tests with a margin of approximately -0.01 hr^{-1}, in the stability index.

An analytical simulation of the first X-Y xenon oscillation test shows a calculated stability index of -0.081 hr^{-1}, in good agreement with the measured value of -0.076 hr^{-1}. As indicated earlier, the second X-Y xenon test showed that the core had become more stable compared to the first test, and that no evaluation of the stability index was attempted. This increase in the core stability in the X-Y plane due to increased fuel burnup is due mainly to the increased magnitude of the negative moderator temperature coefficient.

Previous studies of the physics of xenon oscillations, including three dimensional analysis, are reported in the series of topical reports WCAP-3680-20 (Reference 4.3-13); WCAP-3680-21 (Reference 4.3-14); and WCAP-3680-22 (Reference 4.3-15). A more detailed description of the experimental results and analysis of the axial and X-Y xenon transient tests is presented in WCAP-7964 (Reference 4.3-16) and Section 1 of WCAP-8768 (Reference 4.3-19).

4.3.2.7.6   Stability Control and Protection

The excore detector system is utilized to provide indications of xenon-induced spatial oscillations. The readings from the excore detectors are available to the operator and also form part of the protection system.

1.   Axial power distribution.

For maintenance of proper axial power distributions, the operator is instructed to maintain an axial offset within a prescribed operating band, based on the excore detector readings. Should the axial offset be permitted to move far enough outside

this band, the protection limit will be reached, and the power will be automatically reduced.

Twelve-foot pressurized water reactor cores become less stable to axial xenon oscillations as fuel burnup progresses. However, free xenon oscillations are not allowed to occur, except for special tests. The full-length control banks are sufficient to dampen and control any axial xenon oscillations present. Should the axial offset be inadvertently permitted to move far enough outside the control band due to an axial xenon oscillation, or any other reason, the protection limit on axial offset will be reached and the power will be automatically reduced.

2. Radial power distribution.

The core described herein is calculated to be stable against X-Y xenon-induced oscillations at all times in life.

The X-Y stability of large pressurized water reactors has been further verified as part of the startup physics test program for pressurized water reactor cores with 193 fuel assemblies. The measured X-Y stability of the cores with 157 and 193 assemblies was in good agreement with the calculated stability, as discussed in Sections 4.3.2.7.4 and 4.3.2.7.5. In the unlikely event that X-Y oscillations occur, backup actions are possible and would be implemented, if necessary, to increase the natural stability of the core. This is based on the fact that several actions could be taken to make the moderator temperature coefficient more negative, which will increase the stability of the core in the X-Y plane.

Provisions for protection against non-symmetric perturbations in the X-Y power distribution that could result from equipment malfunctions are made in the protection system design. This includes control rod drop, rod misalignment, and asymmetric loss-of-coolant flow.

A more detailed discussion of the power distribution control in pressurized water reactor cores is presented in WCAP-7811 (Reference 4.3-6), WCAP-8385, 8403 (Reference 4.3-7) and VEP-NE-1-A (Reference 4.3-43).

4.3.2.8   Vessel Irradiation

A brief review of the methods and analyses used in the determination of neutron and gamma ray flux attenuation between the core and the pressure vessel is given below. A more complex discussion on the pressure vessel irradiation and surveillance program is given in Section 5.3.

The materials that serve to attenuate neutrons originating in the core and gamma rays from both the core and structural components consist of the core baffle, core barrel, neutron panels, and associated water annuli, all of which are within the region between the core and the pressure vessel.

In general, few group neutron diffusion theory codes are used to determine fission power density distributions within the active core, and the accuracy of these analysis is verified by incore measurements on operating reactors. Region and rodwise power-sharing information from the core calculations is then used as source information in two dimensional S_n transport calculations which compute the flux distributions throughout the reactor.

The neutron flux distribution and spectrum in the various structural components varies significantly from the core to the pressure vessel Representative values of the neutron flux distribution and spectrum are presented in Table 4.3-6. The values listed are based on time-average equilibrium cycle reactor core parameters and power distributions; and, thus, are suitable for long-term fluence projections and for correlation with radiation damage estimates.

As discussed in Section 5.3, the irradiation surveillance program utilizes actual test samples to verify the accuracy of the calculated fluxes at the vessel.

4.3.3   ANALYTICAL METHODS

Calculations required in nuclear design consist of three distinct types, which are performed in sequence:

      1.   Determination of effective fuel temperatures;

      2.   Generation of microscopic few-group parameters;

      3.   Space dependent, few-group diffusion calculations.

These calculations are carried out by computer codes which can be executed individually. Most of the codes required have been linked to form an automated design sequence which minimizes design time, avoids errors in transcription of data, and standardizes the design methods. The major analytical models currently approved for use in reload design and safety analysis are described in topical report VEP-FRD-42-A, Reference 4.3-45.

4.3.3.1   Fuel Temperature (Doppler) Calculations

The three dimensional fuel temperature distribution is evaluated in the Simulate5 thermal hydraulics module by solving the one-dimensional, annular heat conduction equation for the average fuel pin of each node. The radial distribution of the volumetric heat source in the pellet is dependent on the fuel depletion. The radial power profiles are computed using the Casmo5 code.

The Simulate5 fuel temperature model predictions were benchmarked against experimental measurements from the Halden boiling water reactor and showed good agreement.

4.3.3.2   Macroscopic Group Constants

The Casmo5 neutron data library is based on ENDG/B-VII data files (supplemented with TENDL-2012 data) and was processed with NJOY. The library contains cross sections for 586 energy groups. Additional details of the library are available in Reference 4.3-44.

Casmo5 is a multigroup two-dimensional transport theory code for burnup calculations on PWR assemblies or simple pin cells. The code handles a geometry consisting of cylindrical fuel rods of varying composition in a square pitch array with allowance for absorber-loaded fuel rods, Integral Fuel Burnable Absorber (IFBA), burnable absorber rods, cluster control rods, in-core instrument channels, and water gaps.

To generate the neutronic data needed for use in Simulate5, a series of Casmo5 depletions and branch cases are required. This series of calculations is defined within the CMS5 system as the "Simulate5 Case Matrix." This case matrix consists of a series of depletions and instantaneous branch cases versus exposure as a function of varied boron concentrations, moderator temperature, fuel temperature, and shutdown cooling time as well as cases with control rods and without removable burnable poison in the guide tube locations.

4.3.3.2.1   Cross Section Representation

Cmslink5 is a linking code that processes Csmo5 Card Image files into a binary formatted nuclear data library for use by Simulate5. The library functionalization used for the macroscopic cross sections is used for the fission product data and discontinuity factors as well. The pin library which includes pin peaking, kinetics, isotopic, and detector data is written for each fuel segment by default. The one-dimensional tables of these parameters are determined by the program.

4.3.3.3   Spatial Few-Group Diffusion Calculations

Simulate5 is a multi-group analytical nodal code for the steady-state analysis of both PWRs and BWRs. Simulate5 cross section input is provided from Casmo5 with linkage through Cmslink5. Cross sections are described in Simulate5 by a hybrid microscopic-macroscopic model that includes 50 isotopes (17 actinides and 30+ fission products and burnable absorbers).

The CMS5 code system was benchmarked using 63 cycles of measured plant data to demonstrate its predictive capabilities versus measured difference data for various physics parameters. In addition, several operational transients are modeled to demonstrate Doppler/xenon response, fixed source neutron multiplication/ex-core detector response, overall code fidelity. Based on the comparisons with measured data, CMS5 Nuclear Reliability Factors (NRF) have been developed for Millstone Unit 3 according to the methodology in Reference 4.3-44.

4.3.4   REFERENCES FOR SECTION 4.3

4.3-1   WCAP-7084-P-A (Proprietary) and WCAP-7757-A (Non-proprietary) 1975 Barry, R. F. and Minton, G, "The PANDA Code."

4.3-2   WCAP-7308-L-P-A (Proprietary), and WCAP-7308-L-A (Non-proprietary), E.M. Spier, June 1988, "Evaluation of Hot Channel Factor Uncertainties."

4.3-3   WCAP-13589-A, March 1995, Davidson, S. L., Oelrich, R. L., Kersting, P. J., "Assessment of Clad Flattening and Densification Power Spike Factor Elimination in Westinghouse Nuclear Fuel."

4.3-4   Reference Deleted

4.3-5   Reference Deleted

4.3-6   WCAP-7811, 1971, "Power Distribution Control of Westinghouse Pressurized Water Reactors."

4.3-7   WCAP-8385 (Proprietary) and WCAP-8403 (Non-proprietary), 1974, Morita, T. et al., "Power Distribution Control and Load Following Procedures."

4.3-8   WCAP-7912-P-A (Proprietary) and WCAP-7912-A (Non-proprietary), 1975, McFarlane, A.F., "Power Peaking Factors."

4.3-9   WCAP-8498, 1975, Meyer, C.E. and Stover, R.L., "Incore Power Distribution Determination in Westinghouse Pressurized Water Reactors."

4.3-10   WCAP-7213-A (Proprietary) and WCAP-7758-A (Non-proprietary) 1975, Barry, R.F. and Altomare, S, "The TURTLE 24.0 Diffusion Depletion Code."

4.3-11   Reference Deleted

4.3-12   WCAP-3969-8 (EURAEC-2074), 1968, Cermak, J.O. et al., "Pressurized Water Reactor pH-Reactivity Effect Final Report."

4.3-13   WCAP-3680-20 (EURAEC-1974) 1968, Poncelet, C.G. and Christie, A.M., "Xenon--Induced Spatial Instabilities in Large Pressurized Water Reactors."

4.3-14   WCAP-3680-21 (EURAEC-2111), 1969 Skogen, F.B. and McFarlane, A.F., "Control Procedures for Xenon-Induced X-Y Instabilities in Large Pressurized Water Reactors."

4.3-15   WCAP-3680-22 (EURAEC-2116), 1969 Skogen, F.B. and McFarlane, A.F. "Xenon-Induced Spatial Instabilities in Three-Dimensions."

4.3-16   WCAP-7964, 1971 Lee, J.C., et al., "Axial Xenon Transient Tests at the Rochester Gas and Electric Reactor."

4.3-17   WCAP-3269-26, 1963 Barry, R.F, "LEOPARD - A Spectrum Dependent Non-spatial Depletion Code for the IBM-7094."

4.3-18 WAPD-TM-334, 1962 England, T.R., "CINDER - A One-Point Depletion and Fission Product Program."

4.3-19 WCAP-8768, Revision 2, 1978 Eggleston, F. R., "Safety-Related Research Development for Westinghouse Pressurized Water Reactors, Program Summaries -Winter 1977 - Summer 1978."

4.3-20 Reference Deleted

4.3-21 Reference Deleted

4.3-22 Reference Deleted

4.3-23 Reference Deleted

4.3-24 Reference Deleted

4.3-25 Reference Deleted

4.3-26 Reference Deleted

4.3-27 Reference Deleted

4.3-28 Reference Deleted

4.3-29 Reference Deleted

4.3-30 Reference Deleted

4.3-31 Reference Deleted

4.3-32 Reference Deleted

4.3-33 Reference Deleted

4.3-34 Reference Deleted

4.3-35 Reference Deleted

4.3-36 Reference Deleted

4.3-37 Reference Deleted

4.3-38 Reference Deleted

4.3-39 Reference Deleted

4.3-40 WCAP-8330, 1974, "Westinghouse Anticipated Transients without Reactor Trip Analysis."

4.3-41 WCAP-14441, Rev. 0, August 1995, G. J. Corpora, "BORDER Code Methodology."

4.3-42 Reference Deleted

4.3-43 VEP-NE-1-1, Revision 0, Minor Revision 3, "Relaxed Power Distribution Control Methodology and Associated FQ Surveillance Technical Specifications," October 2017.

4.3-44 SSP-14-P01/028-TR-P-A, Revision 0, "Generic Application of the Studsvik Scandpower Core Management System to Pressurized Water Reactors," September 2017.

4.3-45 VEP-FRD-42-A, Revision 2, Minor Revision 2, "Reload Nuclear Design Methodology," October 2017.

TABLE 4.3-1 REACTOR CORE DESCRIPTION (FIRST CYCLE)

Active Core	
Equivalent diameter (in)	132.7
Active fuel height, first core (in)	144
Height-to-diameter ratio	1.09
Total cross section area (ft^2)	96.04
H$_2$O/U molecular ratio, lattice (cold)	2.39
Reflector Thickness and Composition	
Top - water plus steel (in)	~10
Bottom - water plus steel (in)	~10
Side - water plus steel (in)	~15
Fuel Assemblies	
Number	193
Rod array	17 x 17
Rods per assembly	264
Rod pitch (in)	0.496
Overall transverse dimensions (in)	8.426 x 8.426
Fuel weight, as UO$_2$ (lb)	222,645
Zircaloy weight (lb)	46,993
Number of grids per assembly	8-Type R
Composition of Grids	Inconel-718
Weight of seven grids, seven grids in active core (lb)	1842
Number of guide thimbles per assembly	24
Composition of guide thimbles	Zircaloy-4
Diameter of guide thimbles, upper part (in)	0.450 I.D. x 0.482 O.D.

TABLE 4.3-1 REACTOR CORE DESCRIPTION (FIRST CYCLE) (CONTINUED)

Diameter of guide thimbles, lower part (in)	0.397 I.D. x 0.429 O.D.
Diameter of instrument guide thimbles (in)	0.450 I.D. x 0.482 O.D.
Fuel Rods	
Number	50,952
Outside diameter (in)	0.374
Diameter gap (in)	0.0065
Clad thickness (in)	0.0225
Clad material	Zircaloy-4
Fuel Pellets	
Material	UO_2 Sintered
Density (percent of theoretical)	95
Fuel enrichments (weight percent)	
Region 1	2.40
Region 2	2.90
Region 3	3.40
Diameter (in)	0.3225
Length (in)	0.530
Mass of UO_2 per foot of fuel rod (lb/ft)	0.364
Rod Cluster Control Assemblies	
Neutron Absorber	Hafnium or Ag-In-Cd
Diameter (in)	0.341
Density (lb/in^3)	Hafnium 0.454
Cladding material	Type 304, cold worked stainless steel
Clad thickness (in)	0.0185
Number of clusters, full length	61
Number of absorber rods per cluster	24

TABLE 4.3-1 REACTOR CORE DESCRIPTION (FIRST CYCLE) (CONTINUED)

Burnable Poison Rods (First Core)	
Number	1846
Material	Borosilicate Glass
Outside diameter (in)	0.381
Inner tube, O.D. (in)	0.1815
Clad material	Stainless Steel
Inner tube material	Stainless Steel
Boron loading (w/o B_2O_3 in glass rod)	12.5
Weight of boron-10 per foot of rod (lb/ft)	0.00419
Initial reactivity worth (percent $\Delta\rho$)	8.1 (hot)
	5.7 (cold)
Excess Reactivity	
Maximum fuel assembly k ∞ (cold, clean unborated water)	1.41
Maximum core reactivity (cold, zero power, beginning of cycle, zero soluble boron)	1.24

TABLE 4.3-2 NUCLEAR DESIGN PARAMETERS (FIRST CYCLE)

	Design Limits	Best Estimate
Core average linear power, including densification effects (kW/ft)		5.45
Total heat flux hot channel factor, F_Q		32
Nuclear enthalpy rise hot channel factor, $F^N_{\Delta H}$		1.55
Reactivity Coefficients [1]		
Doppler-only power coefficients, (pcm/percent power) [1]		
Upper curve	-19.4 to -12.6	-15 to -10
Lower curve	-10 to -6.7	-13 to -8
Doppler temperature coefficient (pcm/°F) [1]	-2.9 to -1.0	-2.2 to -1.3
Moderator temperature coefficient (pcm/°F) [1]	0 to -40	0 to -35
Boron coefficient (pcm/ppm) [1]	-16 to -7	-11.2 to -7.5
Rodded moderator density (pcm/gm/cc) [1]	$\leq 0.43 \times 10$	$\leq 0.38 \times 10$
Delayed Neutron Fraction and Lifetime		
β_{eff}BOL, (EOL)	0.0075 (0.0044)	
l^*, BOL, (EOL) µsec	19.4 (18.1)	

TABLE 4.3-2 NUCLEAR DESIGN PARAMETERS (FIRST CYCLE) (CONTINUED)

Control Rods

Rod requirements

See Table 4.3-3

Maximum bank worth (pcm)

Maximum ejected rod worth

< 2000

Bank worth HZP no overlap (pcm)

	BOL, Xe free	EOL Eq. Xe
Bank D	600	640
Bank C	1240	1160
Bank B	1240	1000
Bank A	1120	1180

Radial Factor HZP (BOL to EOL)

	Best Estimate
Unrodded	1.43 to 1.26
D bank	1.69 to 1.41
D + C banks	1.63 to 1.41
D + C + B banks	1.68 to 1.64

Boron Concentrations (ppm)

Zero power, $K_{eff} = 0.99$, cold [2], rod cluster control assemblies out	1690
Zero power, $K_{eff} = 0.99$, hot [3], rod cluster control assemblies out	1660
Design basis refueling boron concentration	2000
Zero power, $K_{eff} \leq 0.95$, cold [2], rod cluster control assemblies in	1492

TABLE 4.3-2 NUCLEAR DESIGN PARAMETERS (FIRST CYCLE) (CONTINUED)

Zero power, $K_{eff} = 1.00$, hot [3], rod cluster control assemblies out	1543
Full power, no xenon, $K_{eff} = 1.0$, hot, rod cluster control assemblies out	1398
Full power, equilibrium xenon, $K_{eff} = 1.0$ hot rod cluster control assemblies out	1038
Reduction with fuel burnup	
First cycle (ppm/GWD/MTU) [4]	See Figure 4.3–3
Reload cycle (ppm/GWD/MTU)	~100

Bounding lower value used for safety analysis.

NOTES:

1. 1 pcm = (percent mille) 10^{-5} $\Delta\rho$ where $\Delta\rho$ is calculated from two statepoint values of K_{eff} by ln (k_2/k_1)

2. Cold means 68°F, 14.7 psia.

3. Hot means 557°F, 2250 psia.

4. Gigawatt day (GWD) = 1000 megawatt day (1000 MWD). During the first cycle, fixed burnable poison rods are present which significantly reduce the boron depletion rate compared to reload cycles.

5. Uncertainties are given in Section 4.3.3.3.

Bounding lower value used for safety analysis.

TABLE 4.3-3 TYPICAL REACTIVITY REQUIREMENTS FOR ROD CLUSTER CONTROL ASSEMBLIES

	Reactivity Effects (Percent)	Beginning of Life (First Cycle)	End of Life (First Cycle)	End of Life (Representative Equilibrium Cycle)
1.	Control requirements			
	Fuel temperature, Doppler (percent Δρ)	1.35	1.13	1.01
	Moderator temperature (percent Δρ)*	0.20	1.14	1.17
	Redistribution (percent Δρ)	0.50	0.89	0.98
	Rod insertion allowance (percent Δρ)	0.50	0.50	0.50
2.	Total control (percent Δρ)	2.55	3.61	3.75
3.	Estimated rod cluster control assembly worth (61 rods)			
	a. All full-length assemblies inserted (percent Δρ)	8.95	8.49	7.91
	b. All but one (highest worth) assemblies inserted (percent Δρ)	7.64	7.35	6.68
4.	Estimated rod cluster control assembly credit with 10 percent adjustment to accommodate uncertainties, Item 3b minus 10 percent (percent Δρ)	6.88	6.62	6.01
5.	Shutdown margin available Item 4 minus Item 2 (percent Δρ)	4.33	3.01	2.26

NOTES:
Includes void effects.
The design basis minimum shutdown is 1.3 percent Δρ.

TABLE 4.3-4 OMITTED

TABLE 4.3-5 AXIAL STABILITY INDEX PRESSURIZED WATER REACTOR CORE WITH A 12-FOOT HEIGHT

Burnup (MWD/MTU)	F_Z	C_B(ppm)	Stability Index (hr^{-1})	
			Exp	Calc
1550	1.34	1065	-0.041	-0.032
7700	1.27	700	-0.014	-0.006
5090 *			-0.0325	-0.0255
		RADIAL STABILITY INDEX		
2250 **			-0.068	-0.07

NOTES:

*   4-loop plant, 12-foot core in Cycle 1, axial stability test

**   4-loop plant, 12-foot core in Cycle 1, radial (X-Y) stability test

TABLE 4.3-6 TYPICAL NEUTRON FLUX LEVELS (n/cm^2-sec) AT FULL POWER

	E >1.0 MeV	0.111 Mev < E	0.3 eV ≤ E	
		< 1.0 MeV	< 0.111 MeV	< E 0.3 eV
Core center	9.98 x 10^{13}	1.11 x 10^{14}	2.17 x 10^{14}	5.36 x 10^{13}
Core outer radius at mid-height	4.24 x 10^{13}	4.85 x 10^{13}	9.52 x 10^{13}	2.21 x 10^{13}
Core top, on axis	2.62 x 10^{13}	2.13 x 10^{13}	1.31 x 10^{14}	4.35 x 10^{13}
Core bottom, on axis	2.70 x 10^{13}	2.25 x 10^{13}	1.33 x 10^{14}	4.74 x 10^{13}
Pressure vessel inner diameter aximuthal peak, core mid-height	2.08 x 10^{10}	2.83 x 10^{10}	6.18 x 10^{10}	1.20 x 10^{11}

**TABLE 4.3-7 TYPICAL COMPARISON OF MEASURED AND CALCULATED
DOPPLER DEFECTS**

Plant	Fuel Type	Core Burnup (MWD/MTU)	Measured (pcm) *	Calculated (pcm)
1	Air-filled	1800	1700	1710
2	Air-filled	7700	1300	1440
3	Air and helium-filled	8460	1200	1210

NOTE:

* $pcm = 10^{-5} \times \ln (K_2/K_1)$

TABLE 4.3-8 OMITTED

TABLE 4.3-9 OMITTED

TABLE 4.3-10 TYPICAL COMPARISON OF MEASURED AND CALCULATED AG-IN-CD ROD WORTH

2-Loop Plant, 121 Assemblies 10 Foot Core	Measured (pcm)	Calculated (pcm)
Group B	1885	1893
Group A	1530	1649
Shutdown group	3050	2917
ESADA Critical, 0.69" Pitch, 2 w/o Pu0$_2$, 8 percent Pu-240, 9 Control Rods		
6.21" rod separation	2250	2250
2.07" rod separation	4220	4160
1.38" rod separation	4100	4019
Benchmark Critical Experiment Hafnium Control Rod Worth		

Control Rod Configuration	No. of Fuel Rods	Measured * Worth (Dppm B-10)	Calculated * Worth (Dppm B-10)
9 Hafnium Rods	1192	138.3	141.0

NOTE:

*   Calculated and measured worths are given in terms of an equivalent change in B-10 concentration.

TABLE 4.3-11 TYPICAL COMPARISON OF MEASURED AND CALCULATED MODERATOR COEFFICIENTS AT HZP, BOL

Plant Type/ Control Bank Configuration	Measured α_{iso} * (pcm/°F)	Calculated α_{iso} (pcm/°F)
3-loop, 157 assemblies,		
12 foot core		
D at 160 steps	-0.50	-0.50
D in, C at 190 steps	-3.01	-2.75
D in, C at 28 steps	-7.67	-7.02
B, C, and D in	-5.16	-4.45
2-loop, 121 assemblies		
12 foot core		
D at 180 steps	+0.85	+1.02
D in, C at 180 steps	-2.40	-1.90
C and D in, B at 165 steps	-4.40	-5.58
B, C and D in, A at 174 steps	-8.70	-8.12
4-loop, 193 assemblies		
12-foot core		
ARO	-0.52	-1.2
D in	-4.35	-5.7
D and C in	-8.59	-10.0
D, C, and B in	-10.14	-10.55
D, C, B, and A in	-14.63	-14.45

NOTE:

*   Isothermal coefficients, which include the Doppler effect in the fuel.

$$\alpha_{iso} = 10^5 \; ln \; \frac{k_2}{k_1} / \; \Delta T°F$$

FIGURE 4.3–1 FUEL LOADING ARRANGEMENT
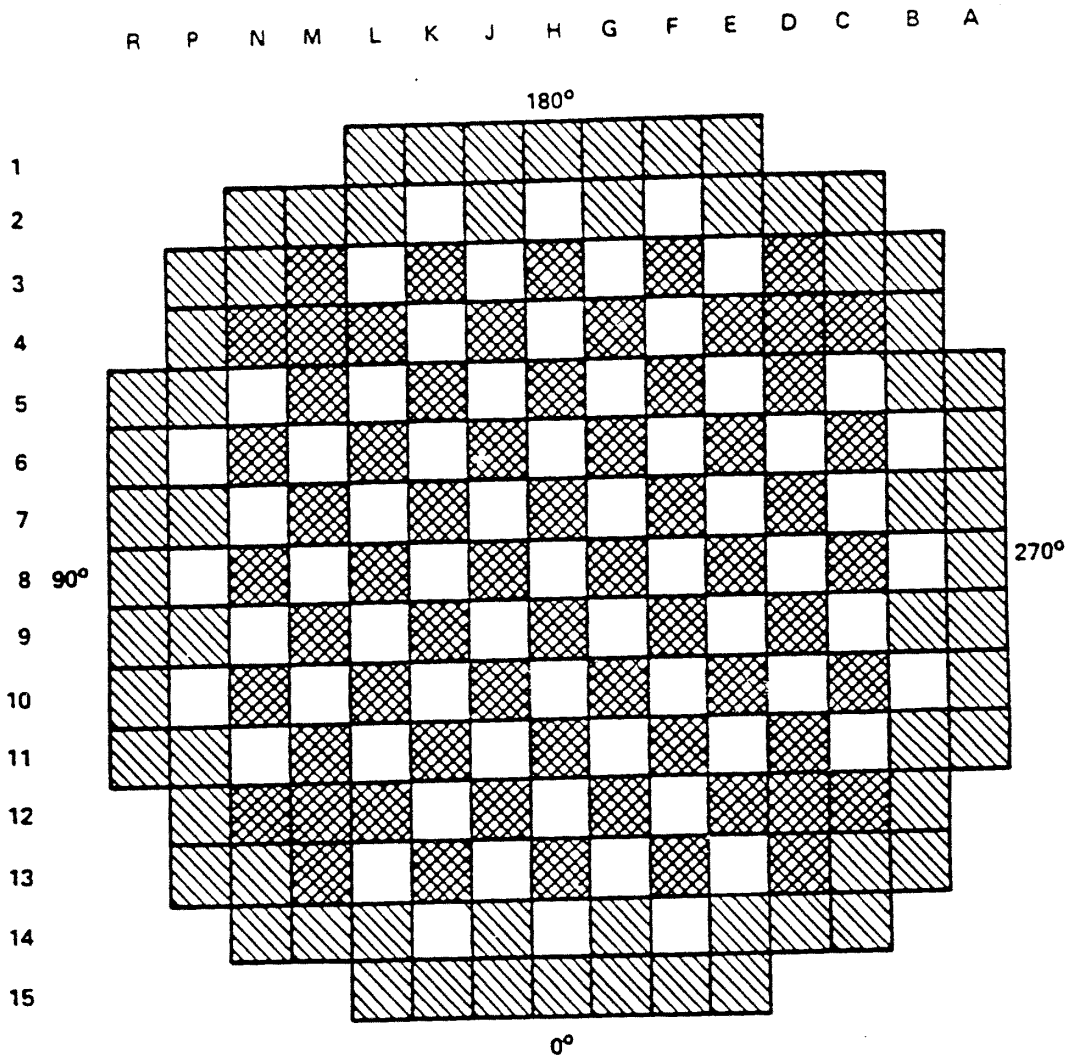
FIGURE 4.3-1
FUEL LOADING ARRANGEMENT
MILLSTONE NUCLEAR POWER STATION
UNIT 3
FINAL SAFETY ANALYSIS REPORT

FIGURE 4.3–2 TYPICAL PRODUCTION AND CONSUMPTION OF HIGHER ISOTOPES
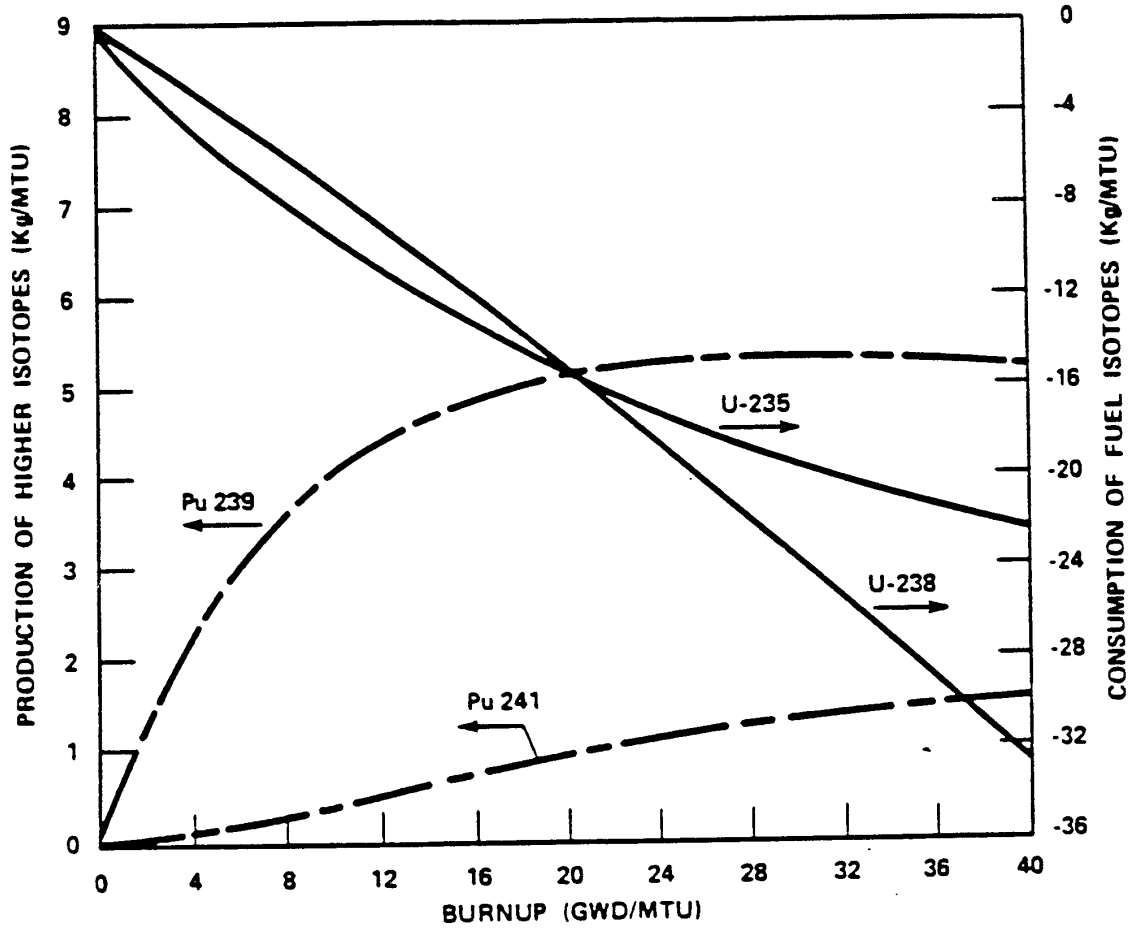
FIGURE 4.3–3 TYPICAL BORON CONCENTRATION VERSUS FIRST CYCLE BURNUP WITH AND WITHOUT BURNABLE ABSORBER RODS
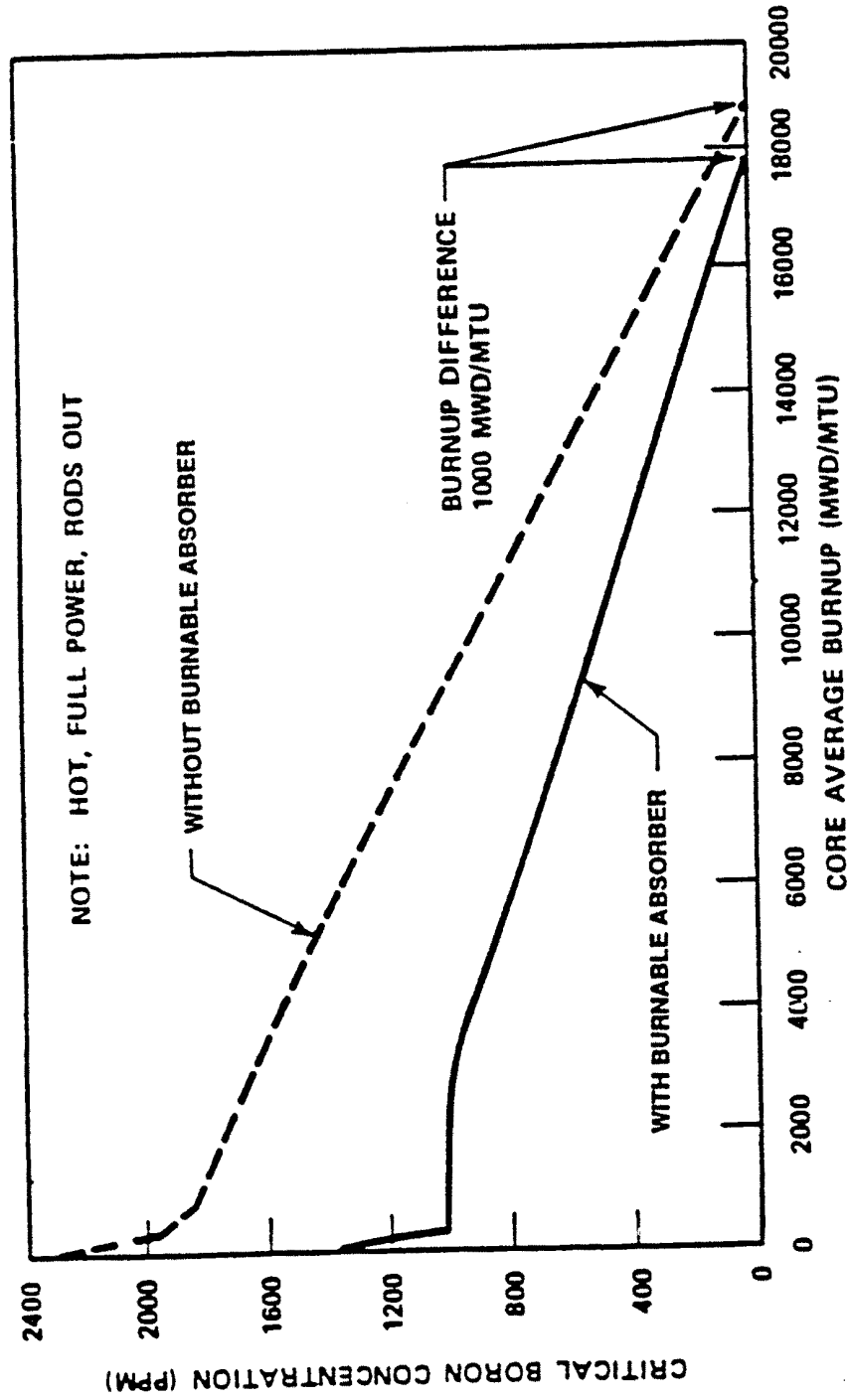
FIGURE 4.3–4 TYPICAL INTEGRAL FUEL BURNABLE ABSORBER ROD ARRANGEMENT WITHIN AN ASSEMBLY
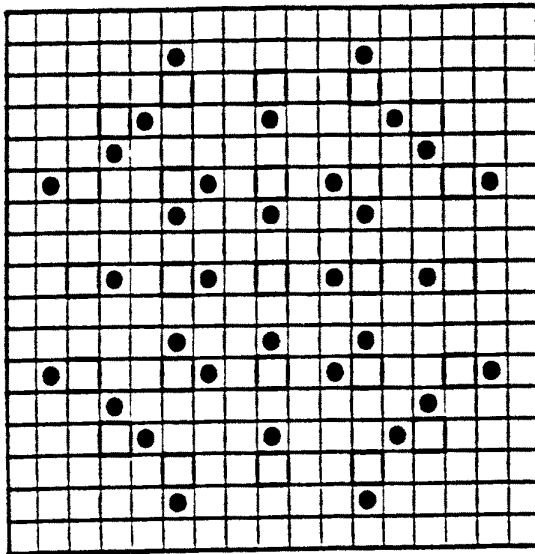
32 IFBA Rods
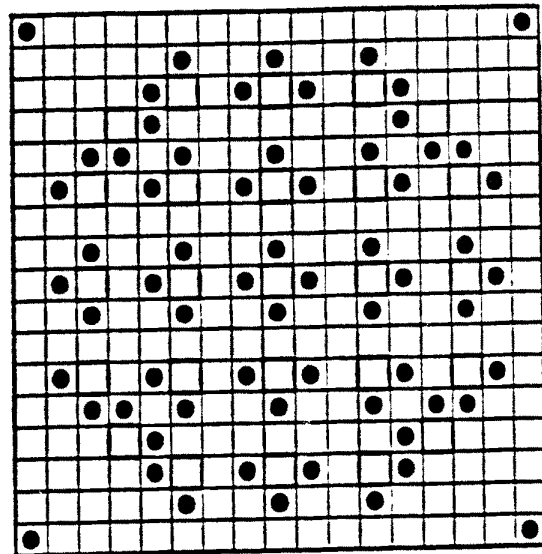
64 IFBA Rods
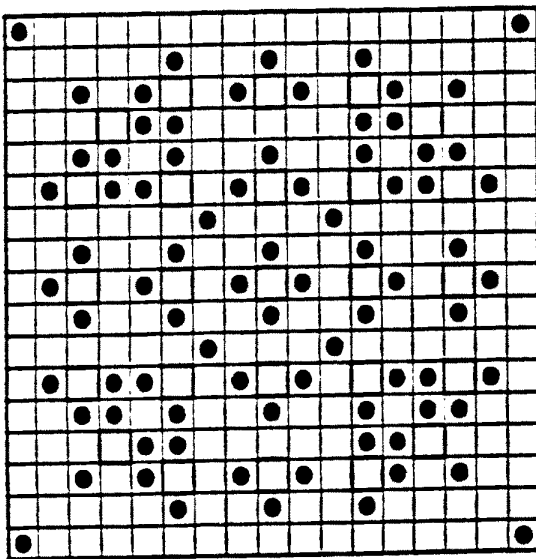
80 IFBA Rods
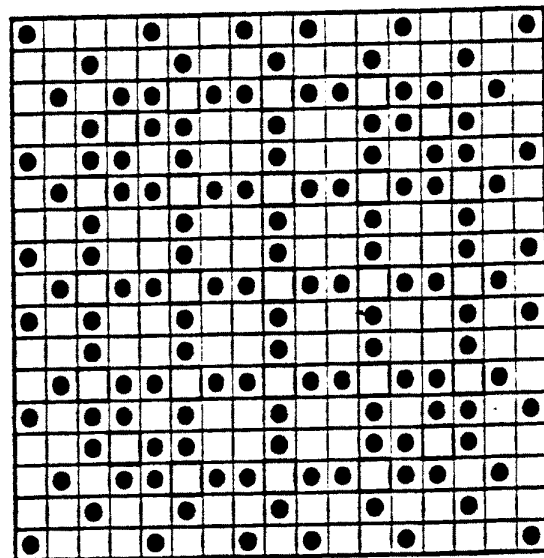
128 IFBA Rods

LEGEND

☐ Fuel Rod

☐ Guide Tube or Instrumentation Tube

☑ IFBA Rod

Fuel Assembly Orientation

• Reference Hole
O Core Pin Hole
∕ Holddown Bar

NOTE: All Figures are Top

FIGURE 4.3–5 BURNABLE ABSORBER LOADING PATTERN (TYPICAL)

R　P　N　M　L　K　J　H　G　F　E　D　C　B　A

180°

							6							
1														
2		6		20		24		23 1S		20		6		
3	6		24		24		20		24		24		6	
4		24		24	4S	24		24		24		24	
5		20		24		24		24		24		24		24	
6		24		24		24		24		24		24	
7		24		24		24		24		24		24		24	
8	6		20		24		24		24		24		20		6
9		24		24		24		24		24		24		24	
10		24		24		24		24		24		24	
11		20		24		24		24		24		24		20	
12		24		24		24		24	4S	24		24	
13	6		24		24		20		24		24		6	
14		6		20		24		23 1S		20		6		
15								6							

90°

27

0°
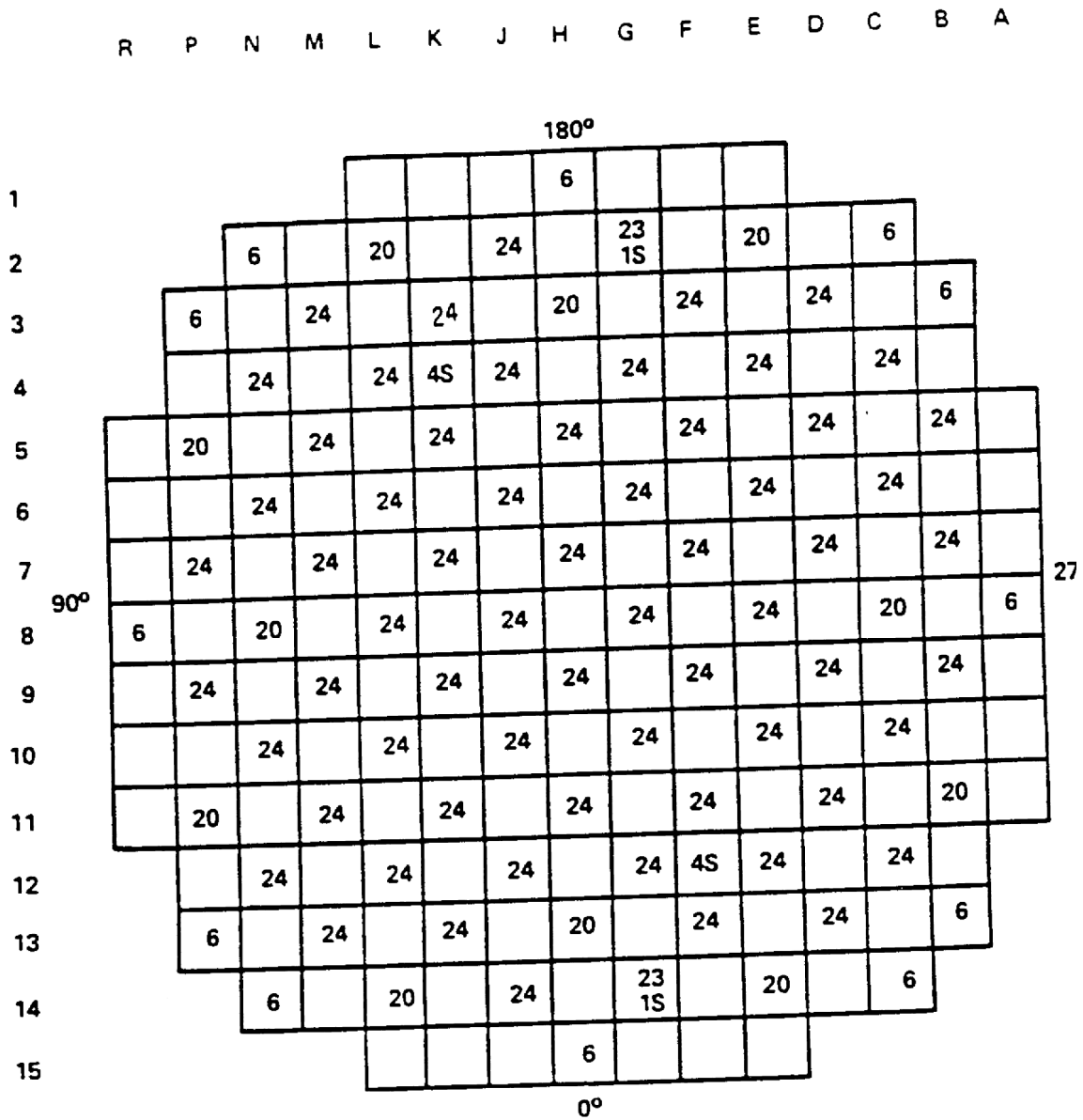
NUMBER INDICATES NUMBER OF BURNABLE ABSORBER RODS
S INDICATES SOURCE ROD

FIGURE 4.3–5A INTEGRAL FUEL BURNABLE LOADING PATTERN (CYCLE 7)

	R	P	N	M	L	K	J	H	G	F	E	D	C	B	A
1															
2					48I	64I	64I	128I	64I	64I	48I				
3			48I	64I	128I			6SSA			128I	64I	48I		
4			64I		128I			128I		128I			64I		
5		48I	128I		128I						128I		128I	48I	
6		64I		128I		128I		128I		128I		128I		64I	
7		64I					128I		128I					64I	
8		128I	6SSA	128I		128I				128I		128I	6SSA	128I	
9		64I					128I		128I					64I	
10		64I		128I		128I		128I		128I		128I		64I	
11		48I	128I		128I						128I		128I	48I	
12			64I				128I		128I		128I		64I		
13			48I	64I	128I			6SSA			128I	64I	48I		
14					48I	64I	64I	128I	64I	64I	48I				
15															

90°   0°

TYPE		TOTAL
##I	(TOTAL NUMBER OF FRESH IFBA RODS)	7232
#SSA	(NUMBER OF SECONDARY SOURCE RODLETS)	24

FIGURE 4.3-5A
INTEGRAL FUEL BURNABLE ABSORBER AND SOURCE ROD LOCATIONS (TYPICAL)

FIGURE 4.3–6 NOT USED

FIGURE 4.3–7 NOT USED

FIGURE 4.3–8 NOT USED

FIGURE 4.3–9 NOT USED

FIGURE 4.3–10 NOT USED

FIGURE 4.3–11 NOT USED

FIGURE 4.3–12 NOT USED

FIGURE 4.3–13 NOT USED

FIGURE 4.3–14 NOT USED

FIGURE 4.3–15 NOT USED

FIGURE 4.3–16 NOT USED

FIGURE 4.3–17 COMPARISON OF A TYPICAL ASSEMBLY AXIAL POWER DISTRIBUTION WITH CORE AVERAGE AXIAL DISTRIBUTION BANK D SLIGHTLY INSERTED
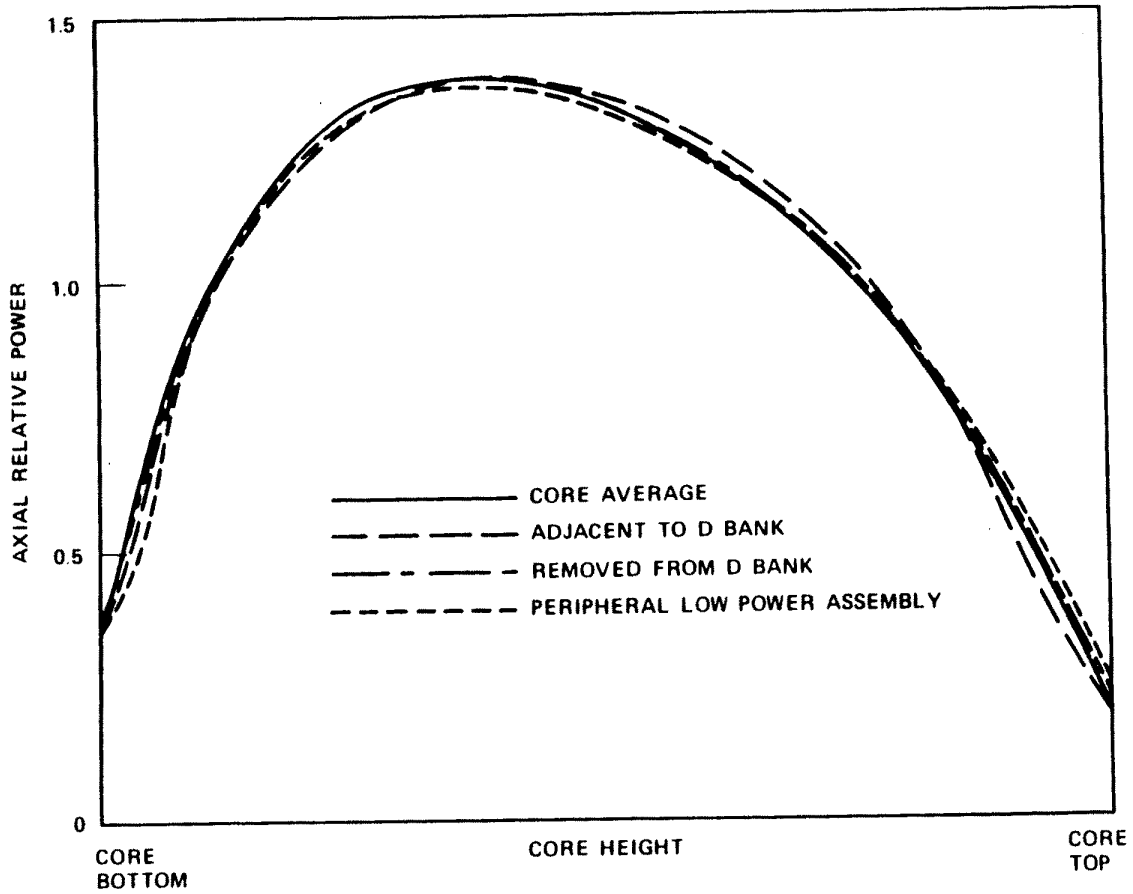
FIGURE 4.3–18 NOT USED

FIGURE 4.3–19 NOT USED

FIGURE 4.3–20 NOT USED

FIGURE 4.3–21 TYPICAL MAXIMUM NORMALIZED FQ X POWER VERSUS AXIAL HEIGHT
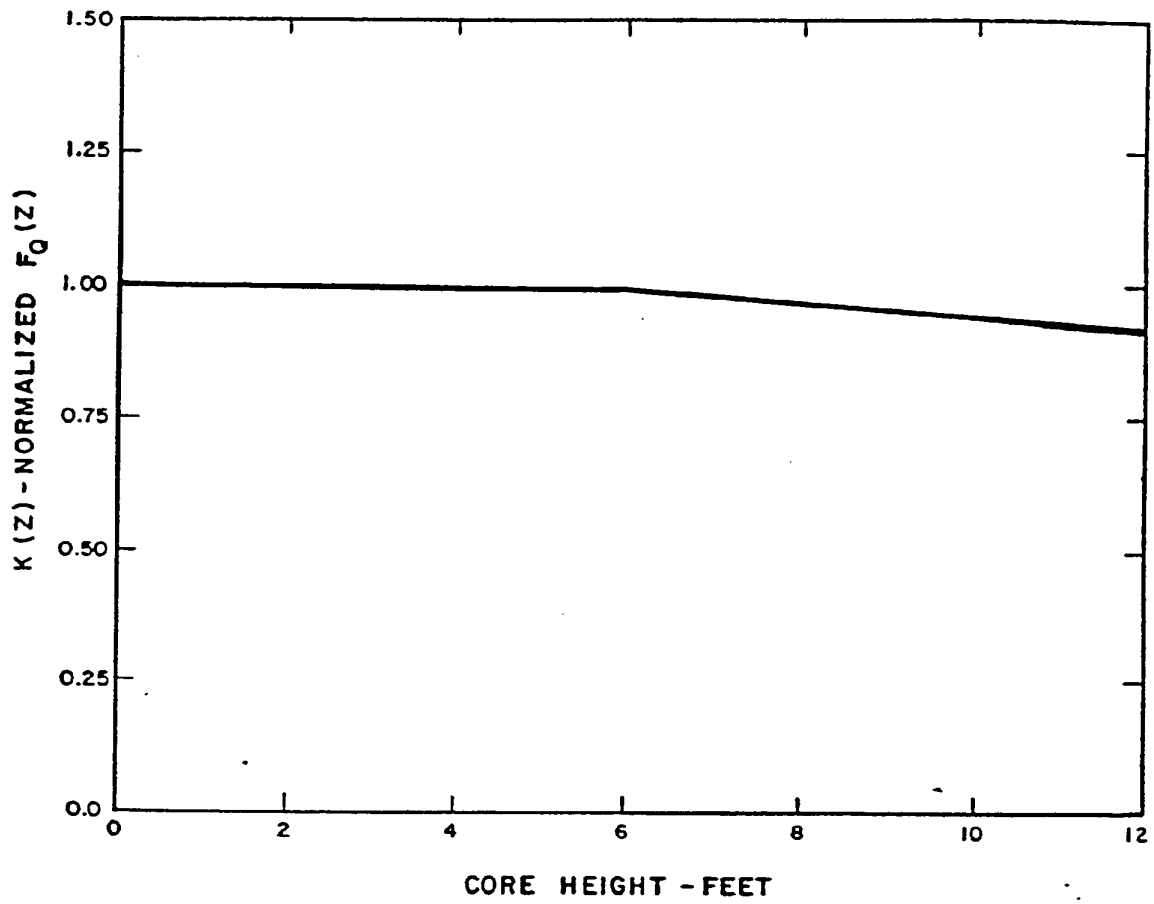
TOTAL F_Q = 2.60

CORE HEIGHT	K (Z)
0.0	1.000
6.0	1.000
12.0	0.925

FIGURE 4.3–22 NOT USED

FIGURE 4.3–23 NOT USED

FIGURE 4.3–24 TYPICAL COMPARISON BETWEEN CALCULATED AND MEASURED RELATIVE FUEL ASSEMBLY POWER DISTRIBUTION
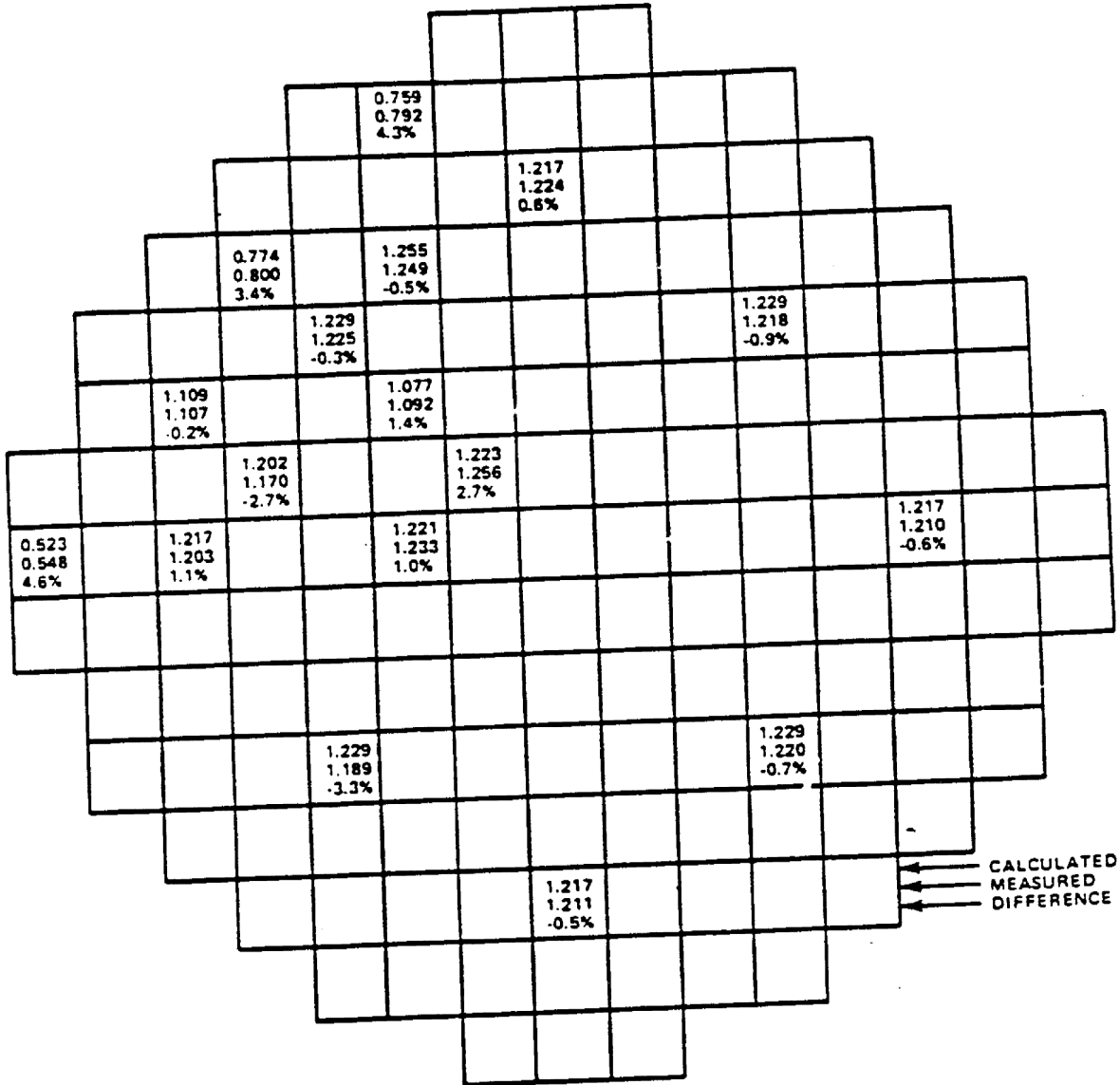
PEAKING FACTORS

$$\overline{F}_Z = 1.5$$

$$F_{\Delta H}^N = 1.357$$

$$F_Q^N = 2.07$$

FIGURE 4.3–25 COMPARISON OF TYPICAL CALCULATED AND MEASURED AXIAL SHAPES
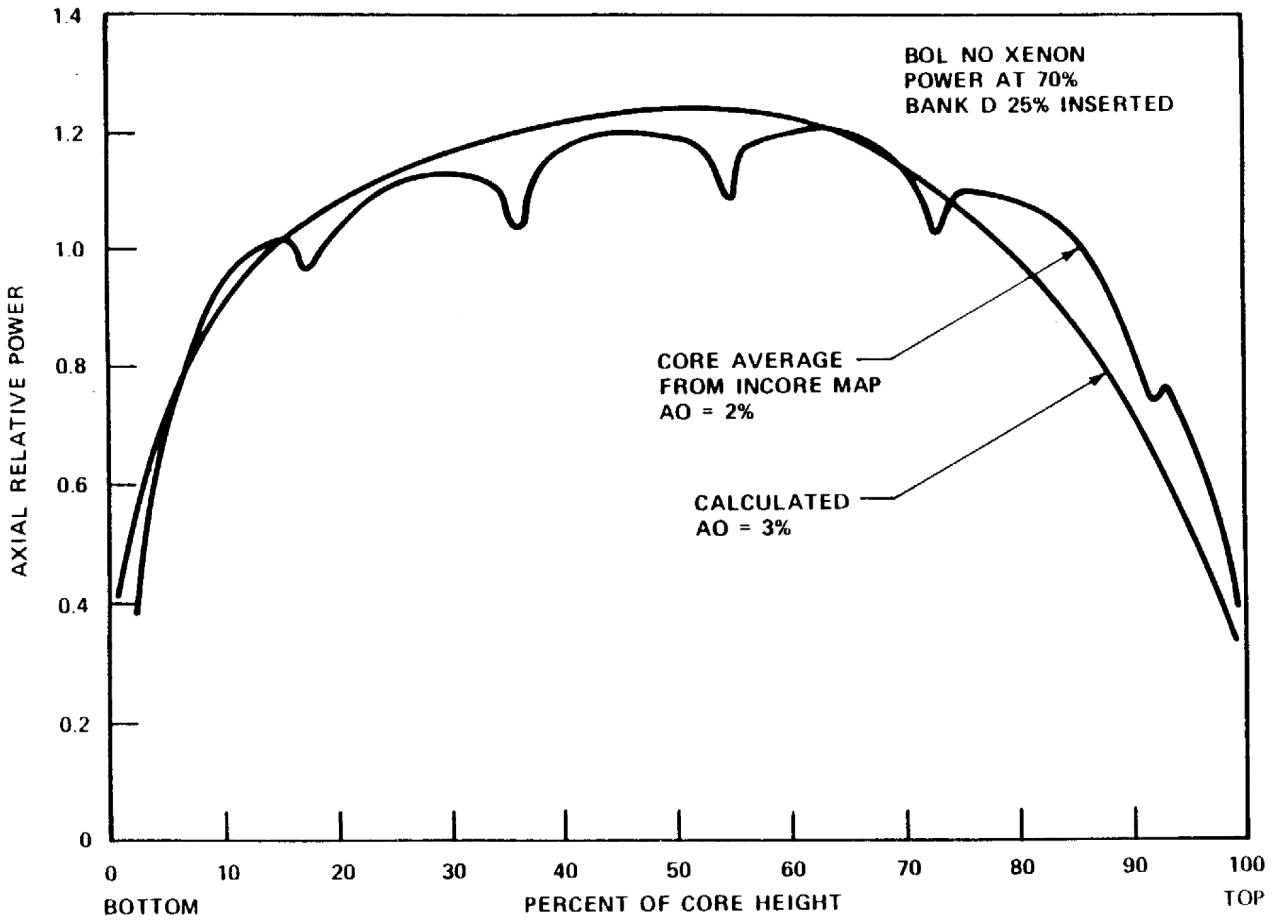
FIGURE 4.3–26 TYPICAL MEASURED VALUES OF FQ FOR FULL POWER ROD CONFIGURATIONS
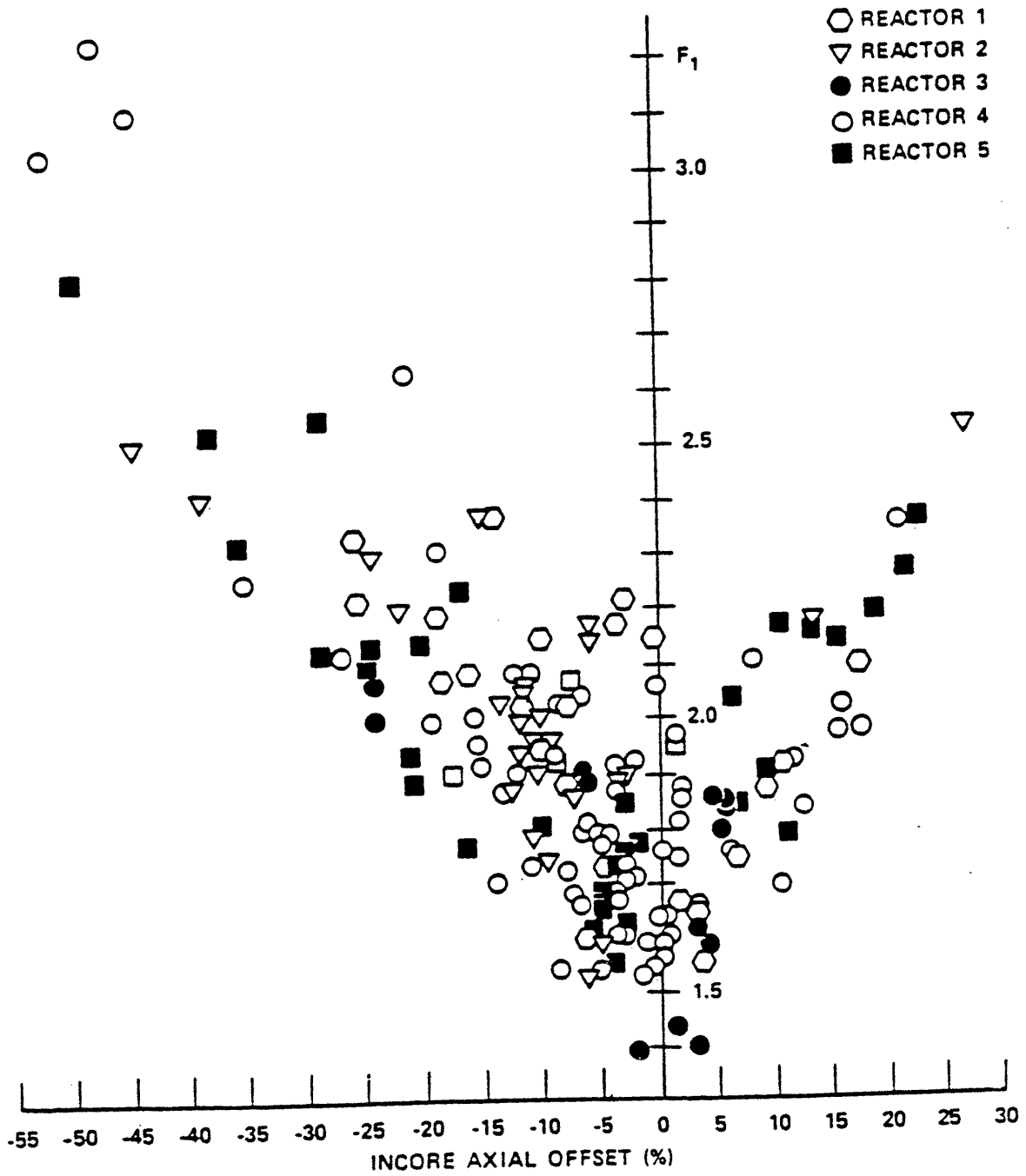
FIGURE 4.3–27 TYPICAL DOPPLER TEMPERATURE COEFFICIENT AT BEGINNING-OF-LIFE AND END-OF-LIFE, CYCLE 1
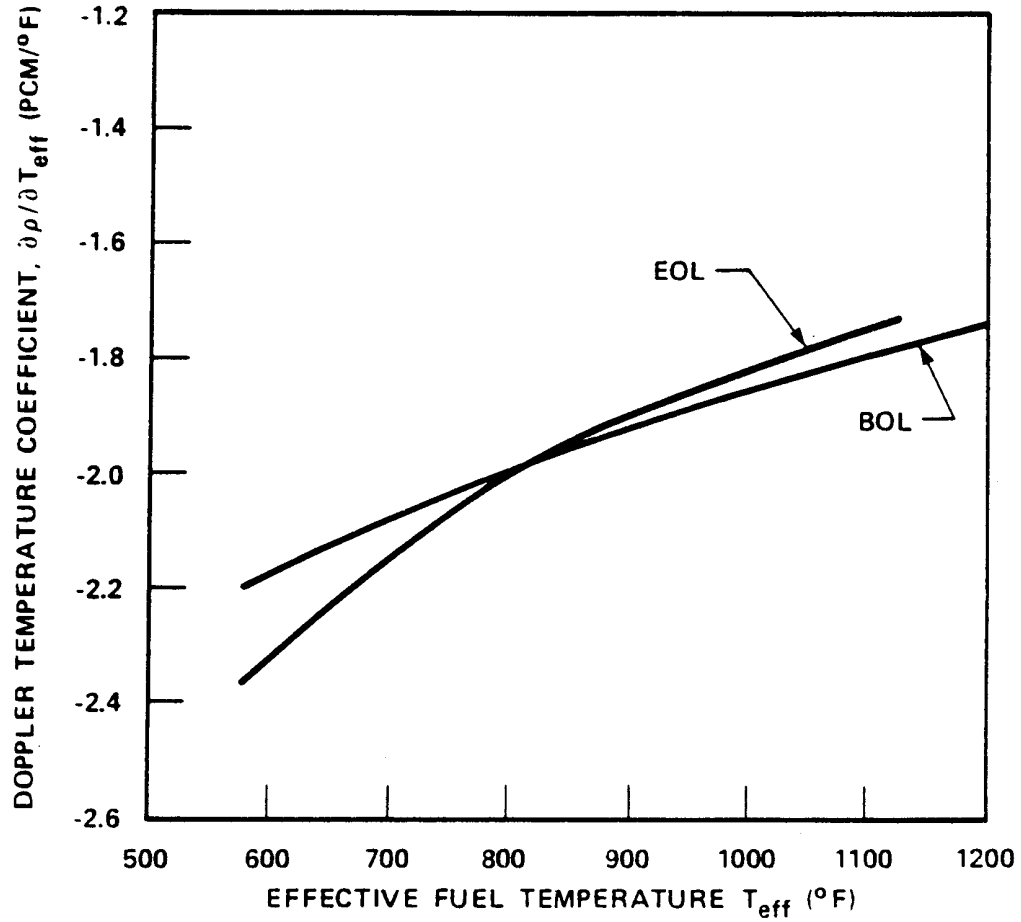
**FIGURE 4.3–28 TYPICAL DOPPLER - ONLY POWER COEFFICIENT AT
BEGINNING-OF-LIFE AND END-OF-LIFE, CYCLE 1**
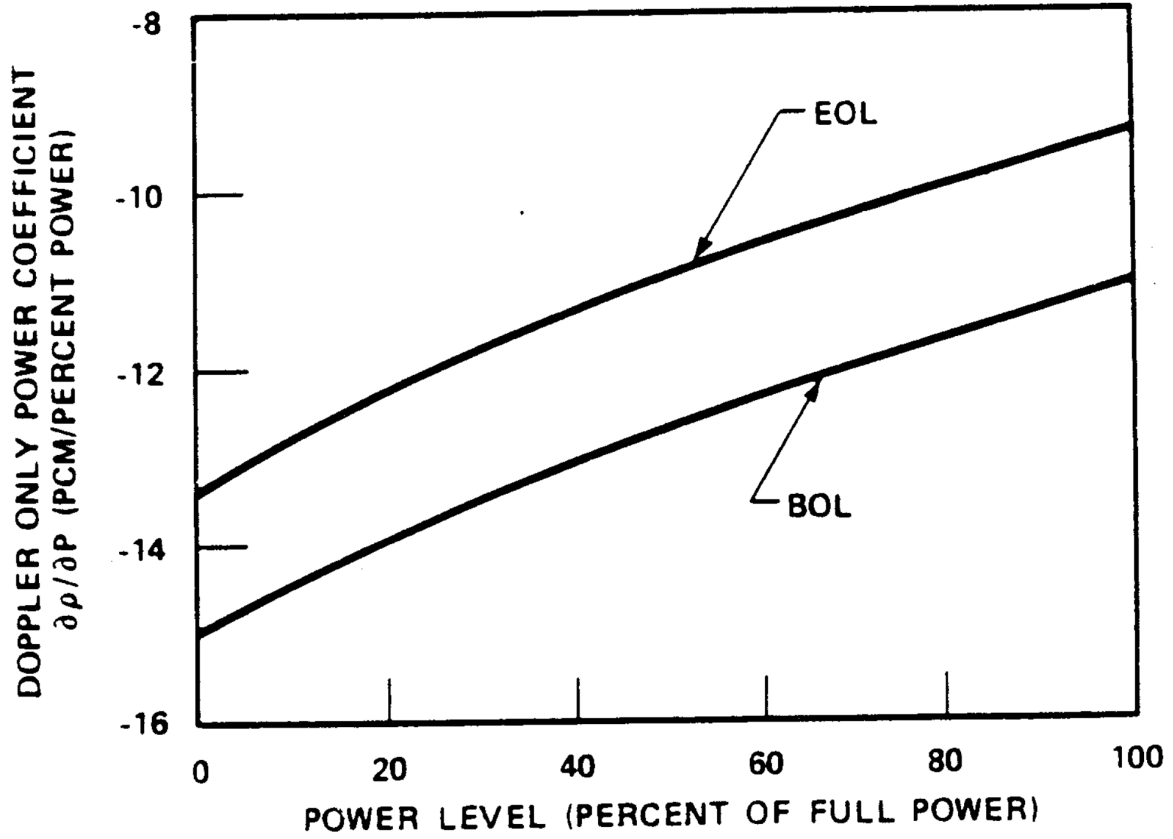
FIGURE 4.3–29 TYPICAL DOPPLER - ONLY POWER DEFECT AT BEGINNING-OF-LIFE AND END-OF-LIFE, CYCLE 1
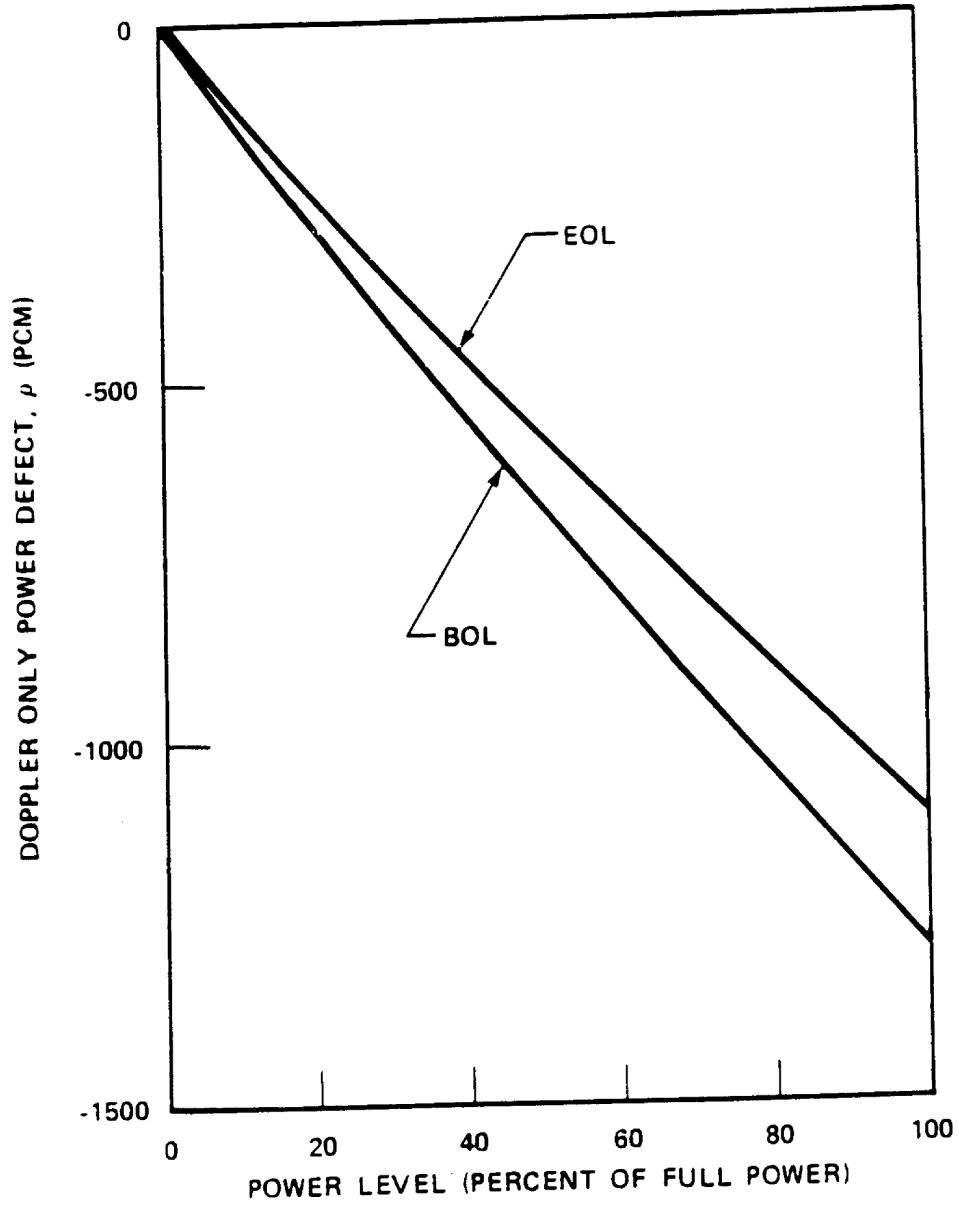
FIGURE 4.3–30 TYPICAL MODERATOR TEMPERATURE COEFFICIENT AT BEGINNING-OF-LIFE, CYCLE 1, NO RODS
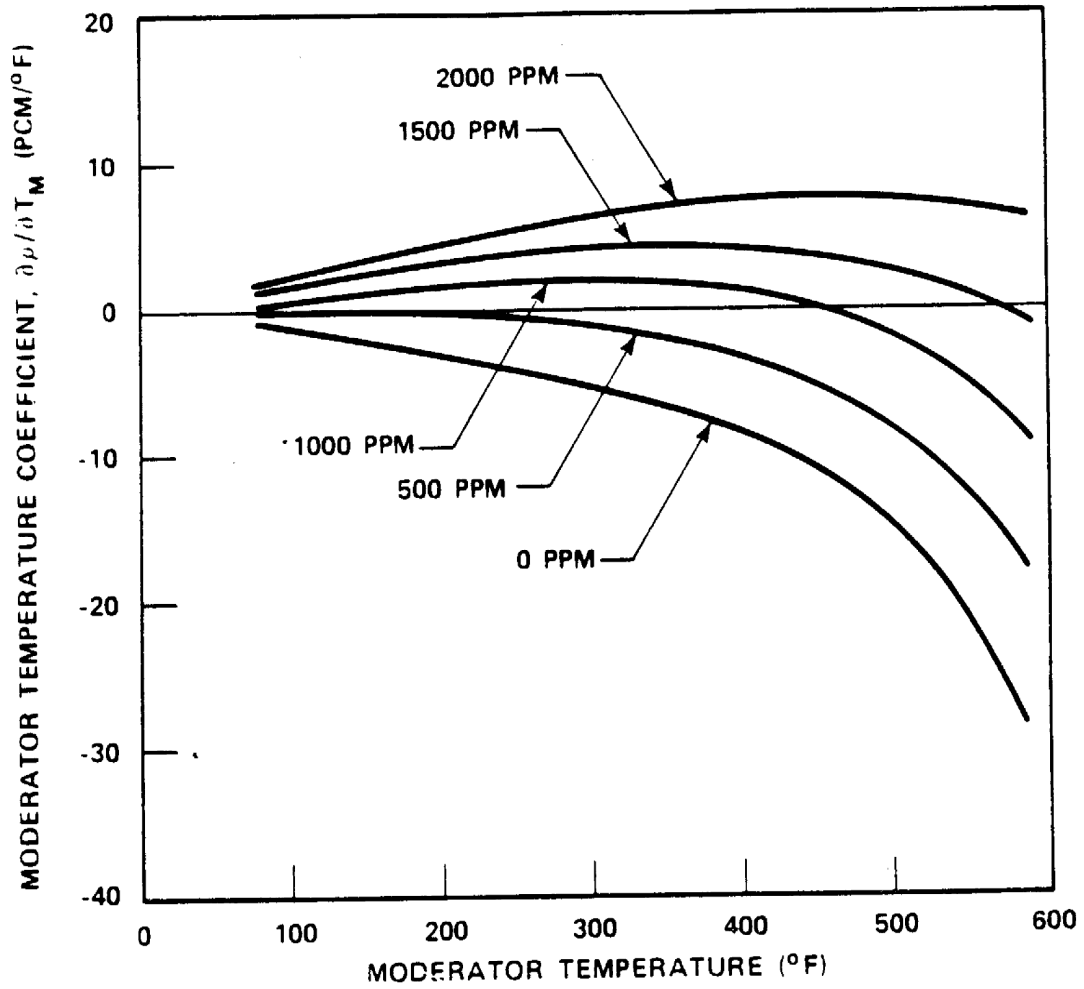
FIGURE 4.3–31 TYPICAL MODERATOR TEMPERATURE COEFFICIENT AT END-OF-LIFE, CYCLE 1
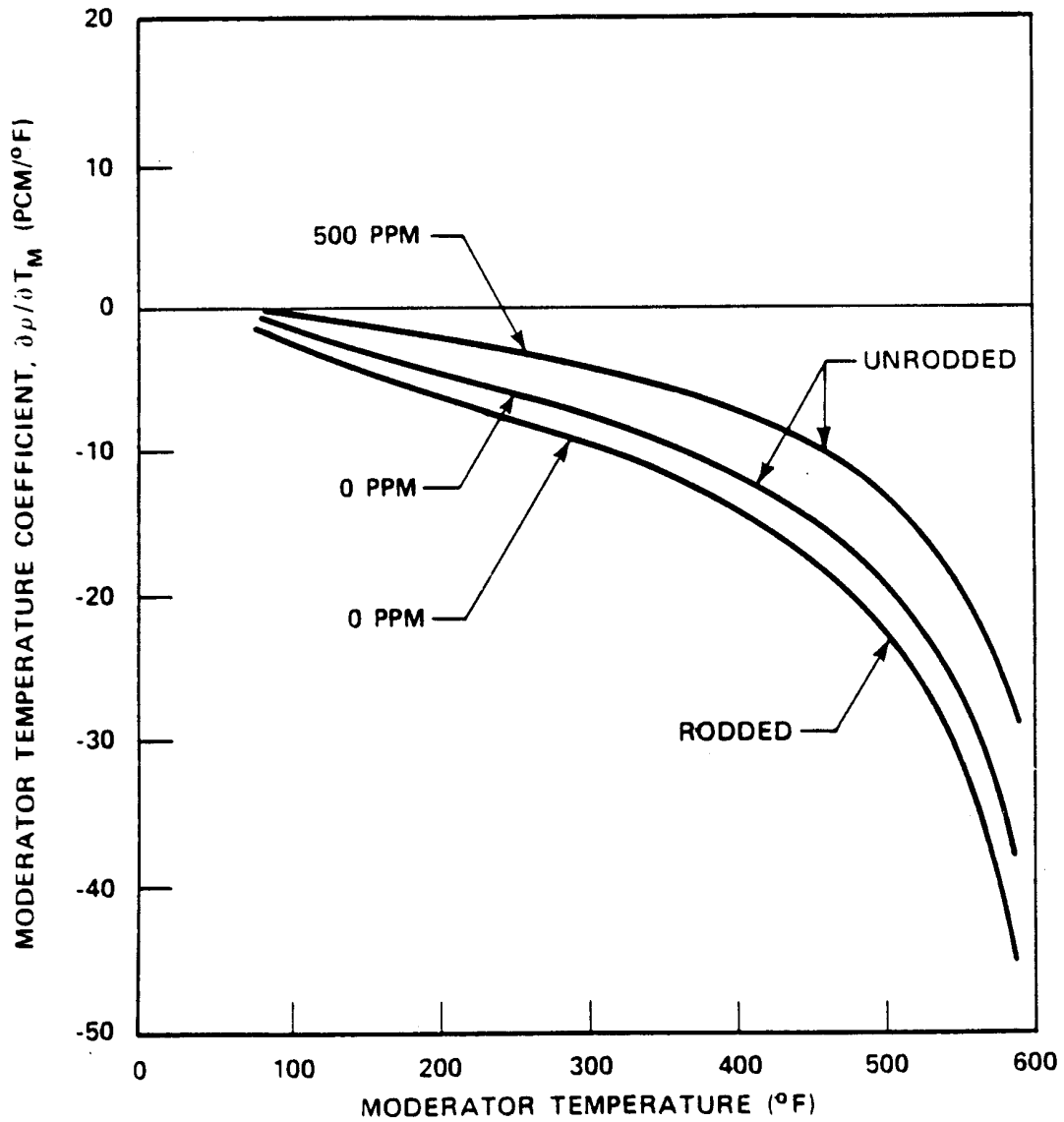
FIGURE 4.3–32 TYPICAL MODERATOR TEMPERATURE COEFFICIENT AS A FUNCTION OF BORON CONCENTRATION AT BEGINNING-OF-LIFE, CYCLE 1, NO RODS
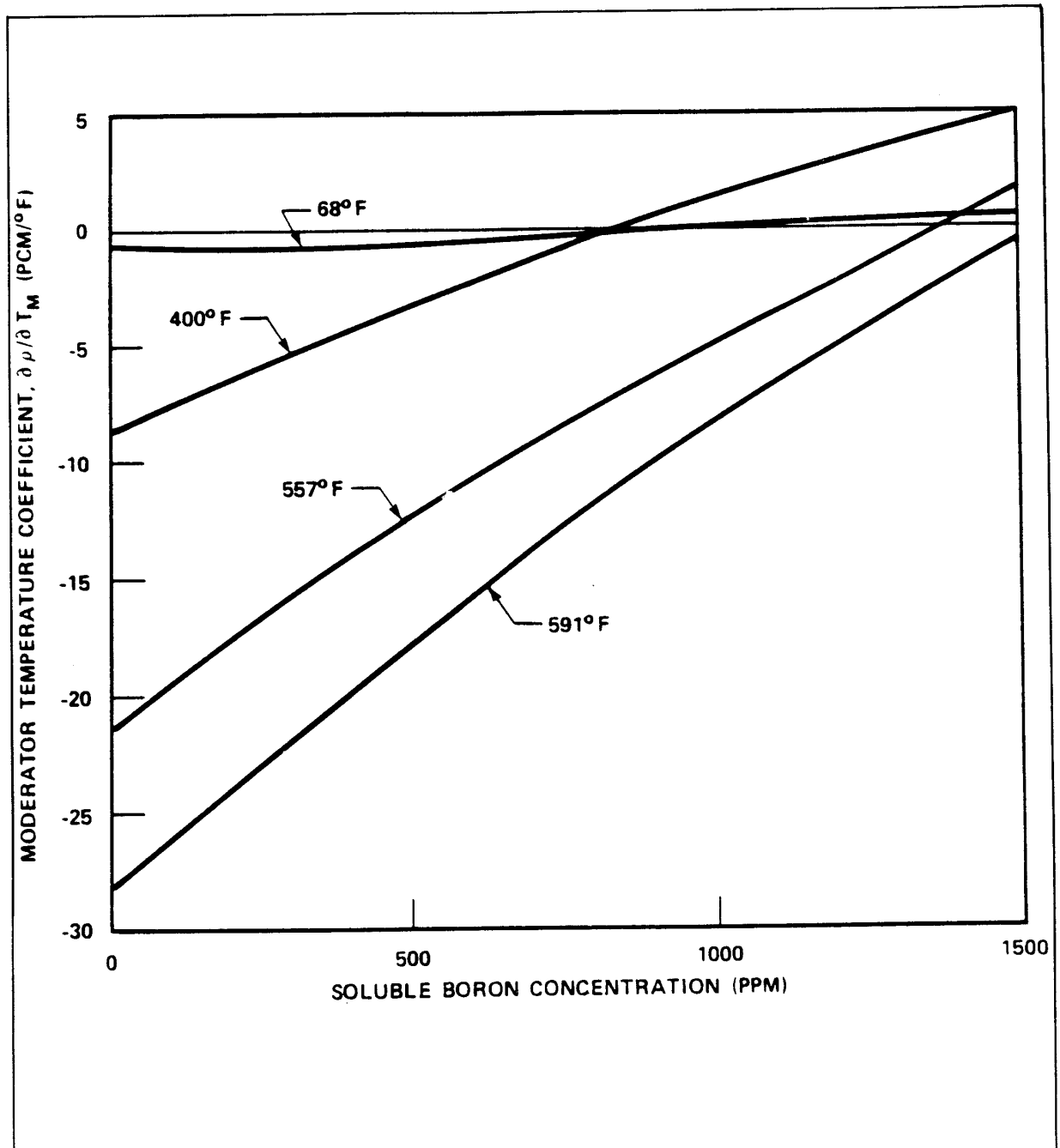
FIGURE 4.3–33 TYPICAL HOT FULL POWER TEMPERATURE COEFFICIENT DURING CYCLE 1 FOR THE CRITICAL BORON CONCENTRATION
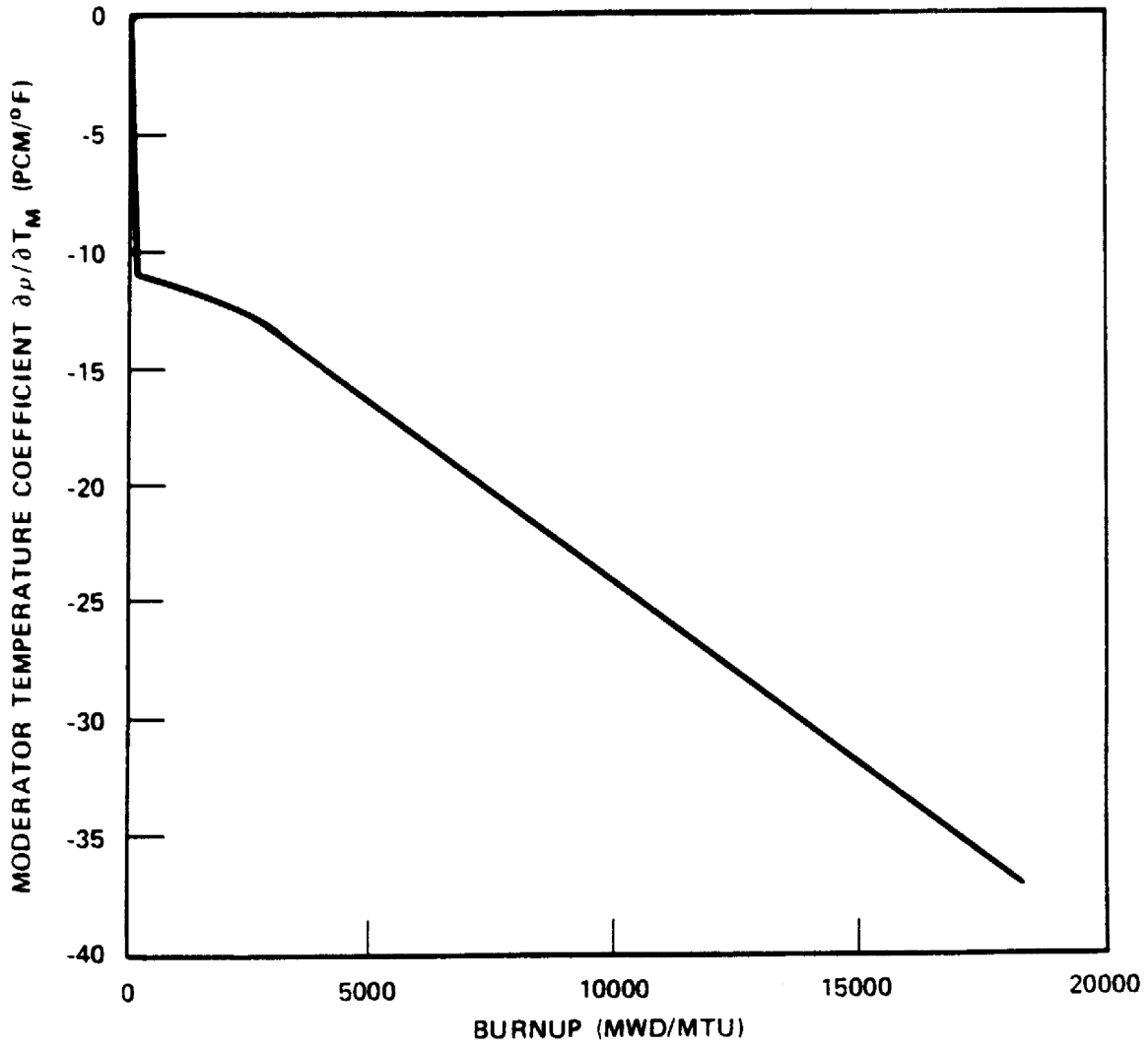
FIGURE 4.3–34 TYPICAL TOTAL POWER COEFFICIENT AT BEGINNING-OF-LIFE AND END-OF-LIFE, CYCLE 1
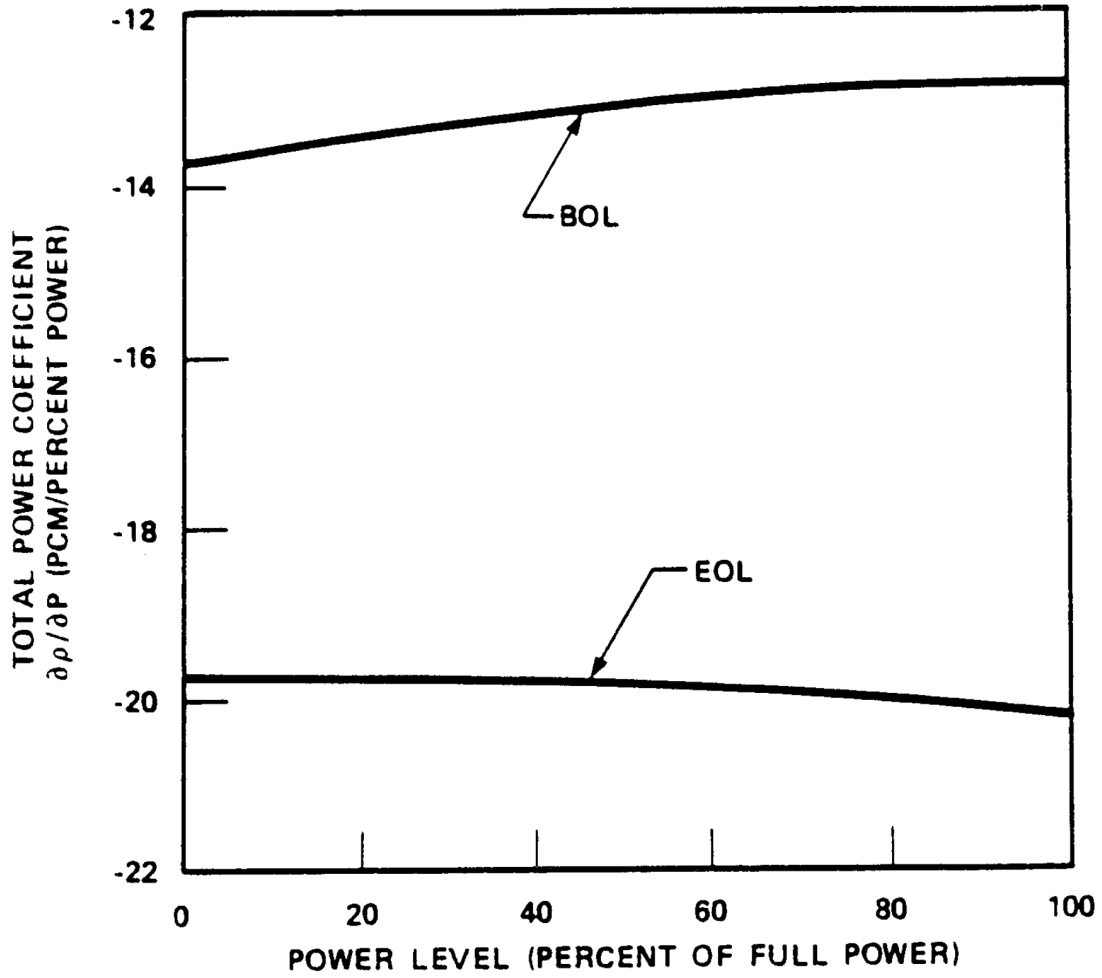
FIGURE 4.3–35 TYPICAL TOTAL POWER DEFECT AT BEGINNING-OF-LIFE AND END-OF-LIFE, CYCLE 1
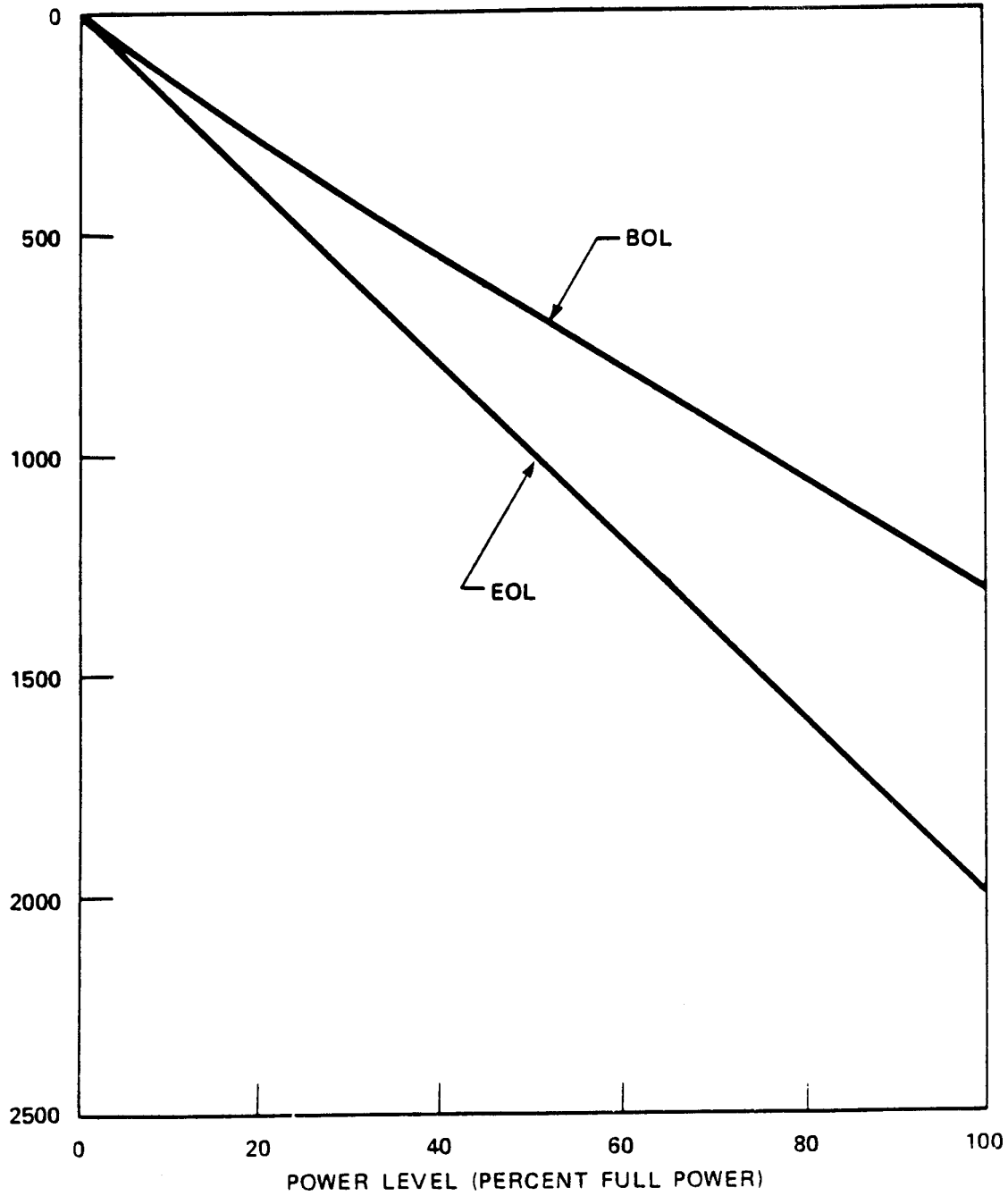
FIGURE 4.3–36 ROD CLUSTER CONTROL ASSEMBLY PATTERN
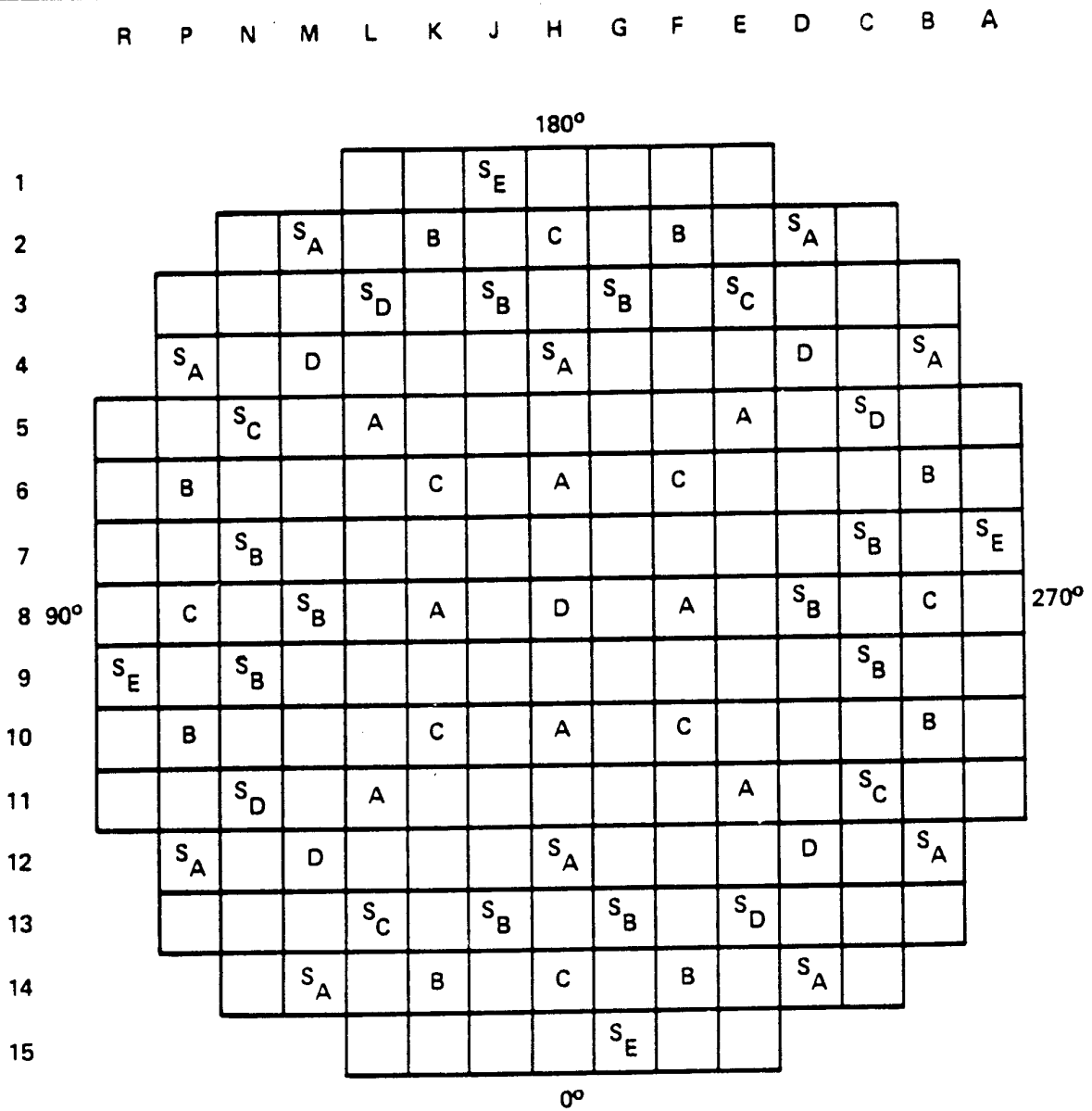
CONTROL BANK	NUMBER OF RODS		SHUTDOWN BANK	NUMBER OF RODS
A	8		S_A	10
B	8		S_B	10
C	8		S_C	4
D	5		S_D	4
TOTAL	29		S_E	4
			TOTAL	32

FIGURE 4.3–37 TYPICAL ACCIDENTAL SIMULTANEOUS WITHDRAWAL OF TWO CONTROL BANKS AT EOL, HZP, BANK D AND B MOVING IN THE SAME PLANE
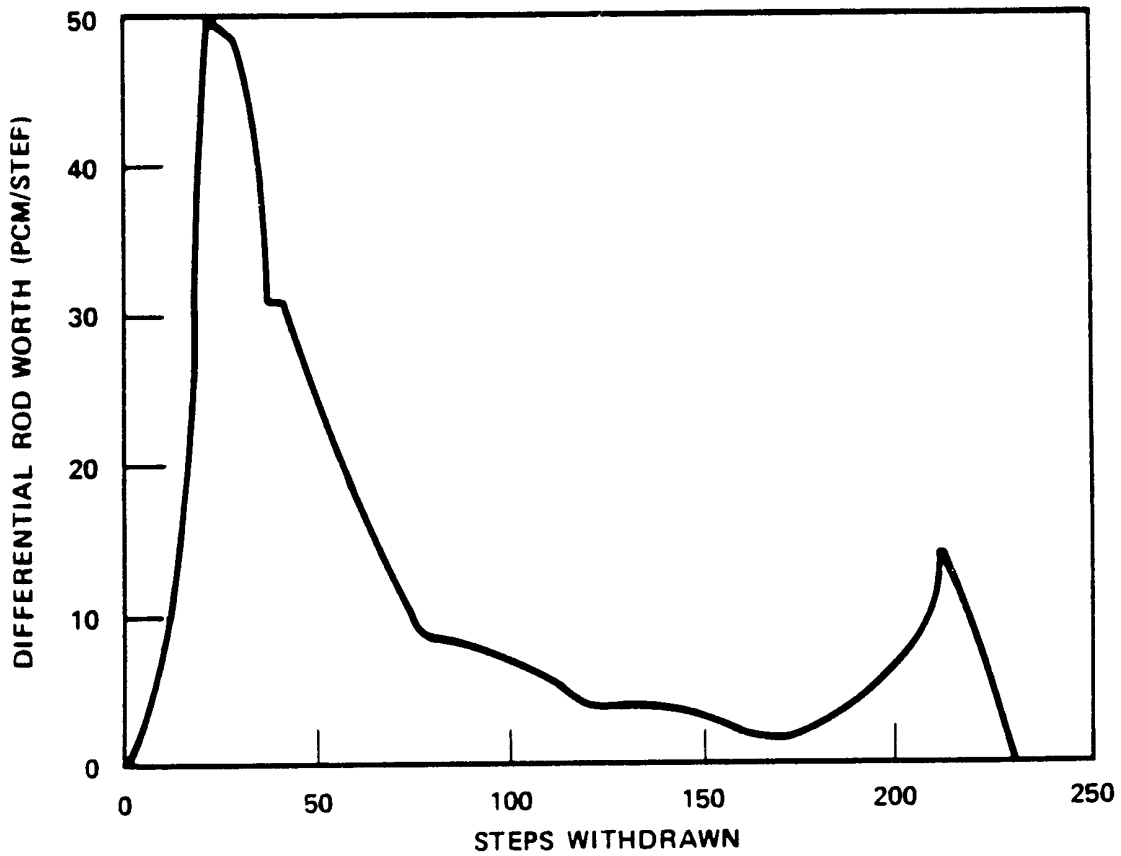
FIGURE 4.3–38 DESIGN TRIP CURVE (TYPICAL)
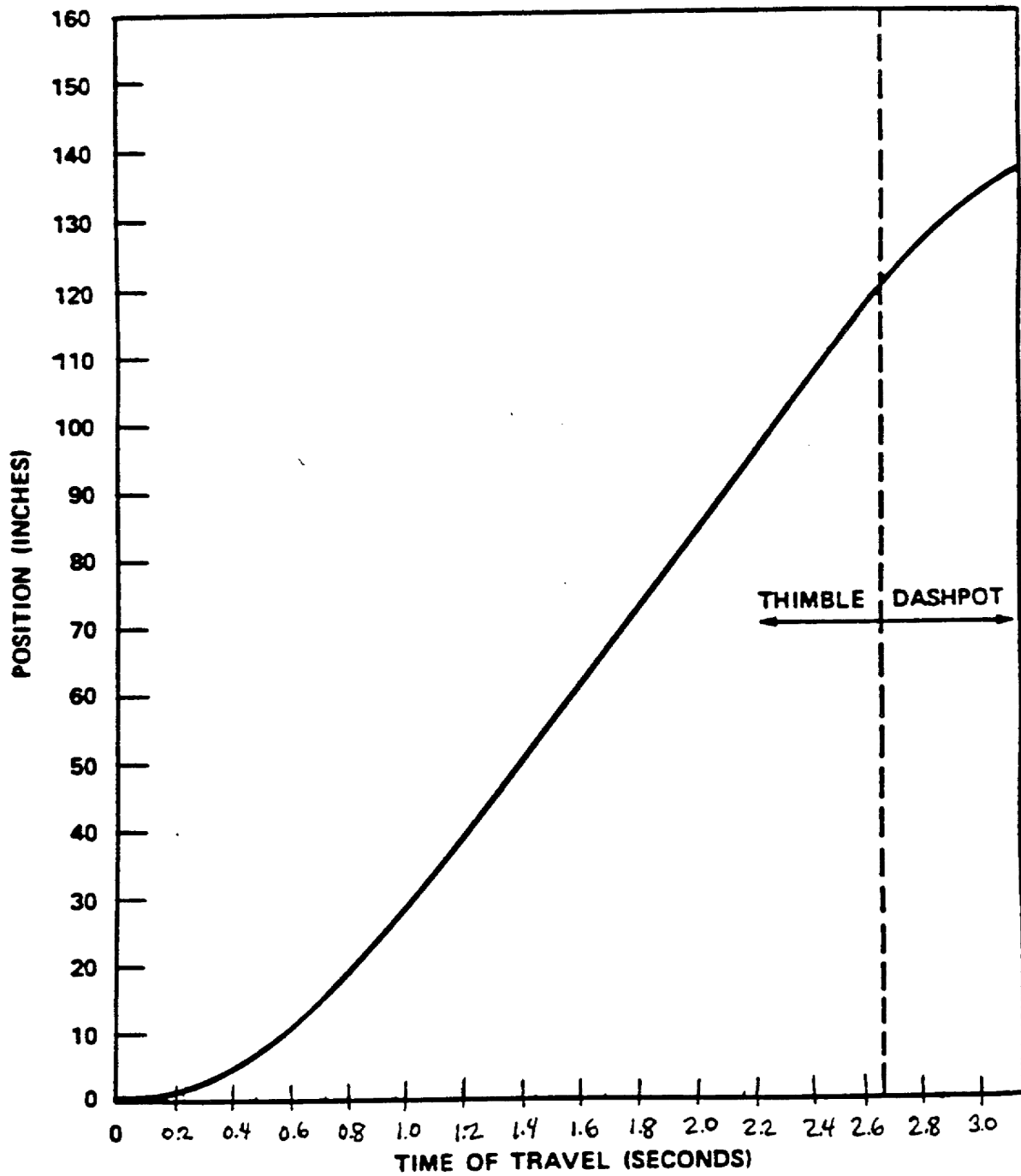
FIGURE 4.3–39 TYPICAL NORMALIZED ROD WORTH VERSUS PERCENT INSERTION, ALL RODS OUT BUT ONE
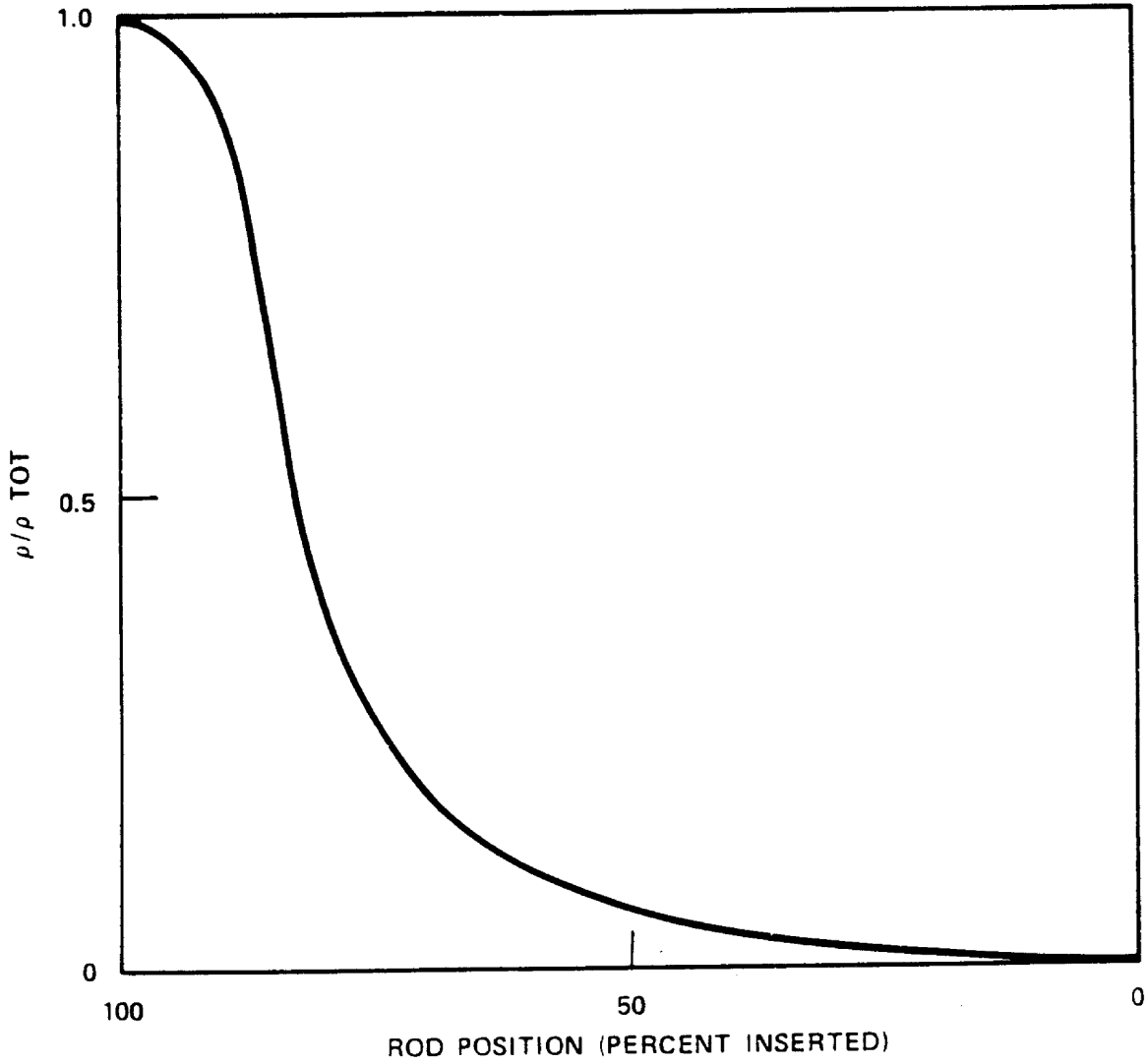
FIGURE 4.3-40 TYPICAL AXIAL OFFSET VERSUS TIME, PWR CORE WITH A 12 FOOT HEIGHT AND 121 ASSEMBLIES

CURVE	BURNUP (MWD/MTU)	PERIOD (HOURS)	STABILITY INDEX (HOURS-1)
1	1550	32.4	-0.041
2	7700	27.2	-0.014
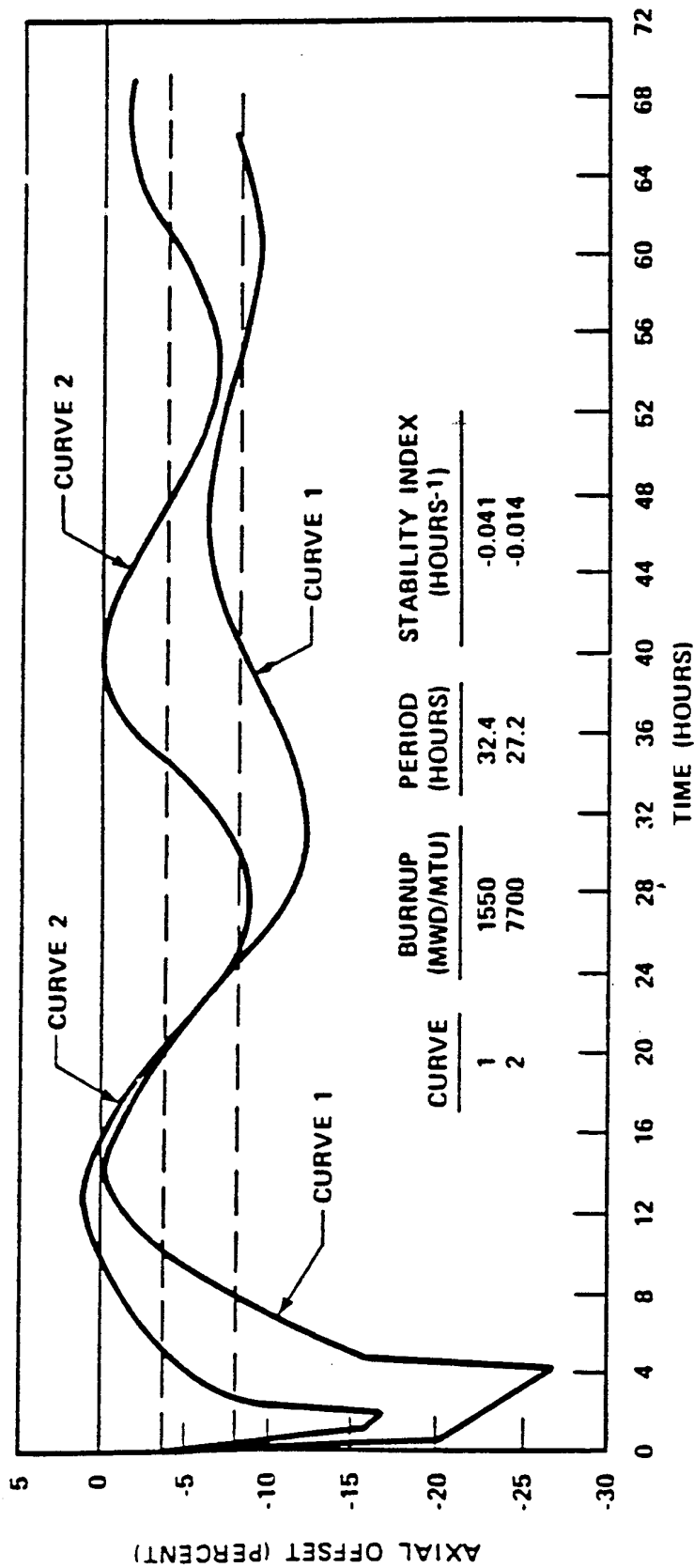
FIGURE 4.3–41 TYPICAL X-Y XENON TEST THERMOCOUPLE RESPONSE QUADRANT TILT DIFFERENCE VERSUS TIME
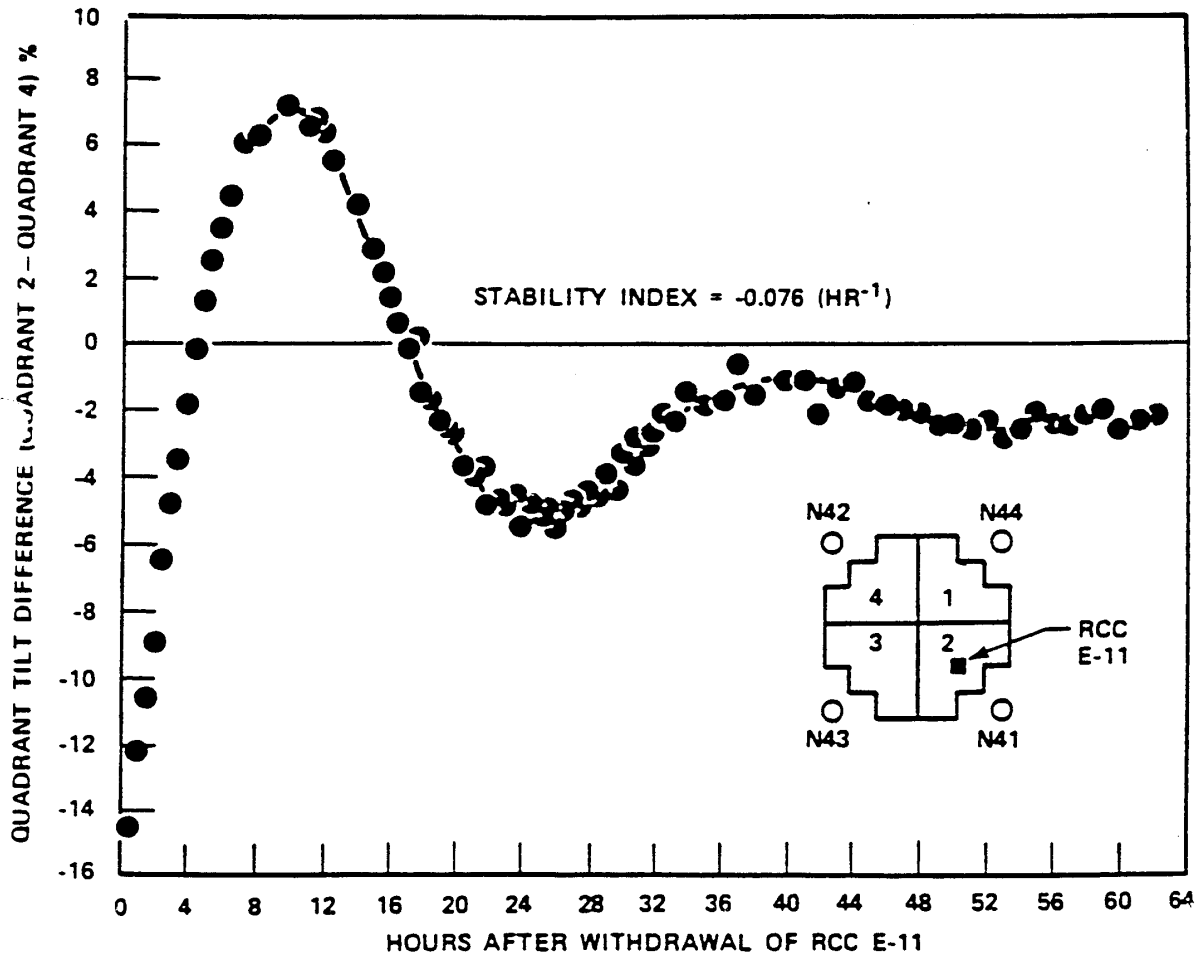
FIGURE 4.3–42 TYPICAL CALCULATED AND MEASURED DOPPLER DEFECT AND COEFFICIENTS AT BOL, 2-LOOP PLANT, 121 ASSEMBLIES, 12 FOOT CORE
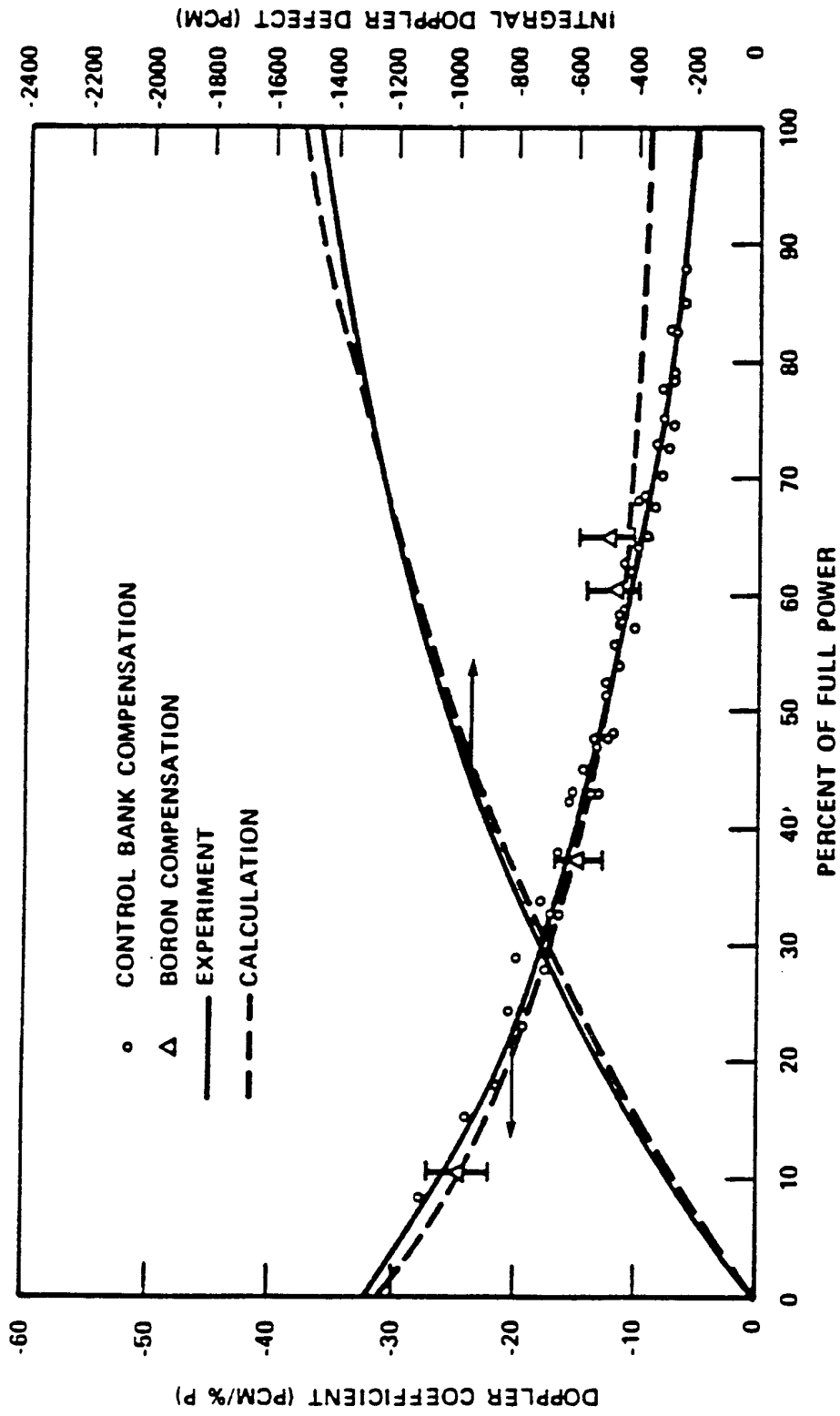
4.4   THERMAL AND HYDRAULIC DESIGN

4.4.1   DESIGN BASES

The overall objective of the thermal and hydraulic design of the reactor core is to provide adequate heat transfer compatible with the heat generation distribution in the core such that heat removal by the reactor coolant system (RCS) or the emergency core cooling system (ECCS) (when applicable) assures that the following performance and safety criteria requirements are met:

1.   Fuel damage (defined as penetration of the fission product barrier, i.e., the fuel rod clad) is not expected during normal operation and operational transients (Condition I) or any transient conditions arising from faults of moderate frequency (Condition II). It is not possible, however, to preclude a very small number of rod failures. These will be within the capability of the plant cleanup system and are consistent with the plant design bases.

2.   The reactor can be brought to a safe state following a Condition III event with only a small fraction of fuel rods damaged (see above definition) although sufficient fuel damage might occur to preclude resumption of operation without considerable outage time.

3.   The reactor can be brought to a safe state and the core can be kept subcritical with acceptable heat transfer geometry following transients arising from Condition IV events.

In order to satisfy the above requirements, the following design bases have been established for the thermal and hydraulic design of the reactor core.

4.4.1.1   Departure from Nucleate Boiling Design Basis

Basis

There will be at least a 95 percent probability that departure from nucleate boiling (DNB) will not occur on the limiting fuel rods during normal operation and operational transients and any transient conditions arising from faults of moderate frequency (Condition I and II events), at a 95 percent confidence level.

For this application, design limit DNBR (departure from nucleate boiling ratio) values are established that meet the 95/95 DNB design criterion. For use in the DNB safety analysis, the limit DNBR is conservatively increased to a DNBR safety analysis limit to provide DNB margin to offset the effect of rod bow and any other DNB penalties that may occur and to provide flexibility in design and operation of the plant. The DNBR limits are listed in Table 4.4-4.

Discussion

By preventing DNB, adequate heat transfer is assured between the fuel clad and the reactor coolant, thereby preventing clad damage as a result of inadequate cooling. Maximum fuel rod surface temperature is not a design basis, as it will be within a few degrees of coolant temperature during operation in the nucleate boiling region. Limits provided by the nuclear control and protection systems are such that this design basis will be met for transients associated with Condition II events, including overpower transients. There is an additional large DNBR margin at rated power operation and during normal operating transients.

The WRB-2M DNB correlation is the primary correlation used for the analysis of the 17 x 17 RFA-2 fuel assemblies. This correlation has a DNBR limit of 1.14 based on the NRC evaluation and approval (DOM-NAF-2-P-A), including the WRB-2M adjustment factor (WCAP-15025-P-A). The NRC has approved the use of the ABB-NV and WLOP DNB correlations as alternates to the W-3 DNB correlation. The WLOP correlation is only used when operating conditions are outside the range of validity of the WRB-2M and ABB-NV correlations and is used deterministically with a DNBR limit of 1.22. The ABB-NV DNB correlation is applicable to the fuel region below the first mixing vane grid and has a DNBR limit of 1.14 (DOM-NAF-2-P-A).

The W-3 correlation with a 95/95 limit DNBR of 1.30 can be used below the fuel assembly first mixing vane grid. The W-3 correlation with a 95/95 limit DNBR of 1.45 can be used for analyses at low pressure (DOM-NAF-2-P-A).

Under Dominion Energy's Statistical DNBR Evaluation Methodology (VEP-NE-2-A), variations in plant operating parameters, nuclear and thermal parameters, fuel fabrication parameters, as well as VIPRE-01, transient code, and DNB correlation predictions are combined statistically to obtain the overall DNBR uncertainty factor which is used to define the design limit DNBR that satisfies the DNB design criterion. This criterion is that the probability that DNB will not occur on the most limiting fuel rod is at least 95 percent (at 95 percent confidence level) for any Condition I or II event. Plant parameter uncertainties are used to determine the plant DNBR uncertainty, combined with the DNBR limit, establishes the statistical design limit (SDL) which must be met in plant safety analyses. Since the parameter uncertainties are considered in determining the SDL, the plant safety analyses are performed using values of input parameters without uncertainties. A deterministic methodology is applied when conditions are outside the range of statistical methods. It should be noted that a more restrictive safety analysis limit (SAL) is employed in all safety analyses. A summary of the applicable DNBR limits are provided in Table 4.4-4.

Statistical DNB analyses use the minimum measured flow (MMF) which is equal to thermal design flow (TDF) plus a flow uncertainty. Analyses by deterministic methods continue to use TDF.

4.4.1.2   Fuel Temperature Design Basis

Basis

During modes of operation associated with Condition I and Condition II events, there is at least a 95 percent probability that the peak kW/ft fuel rods will not exceed the UO_2 melting temperature at the 95 percent confidence level. The melting temperature of UO_2 is taken as 5080°F (WCAP-6065), unirradiated and decreasing 58°F per 10,000 MWD/MTU. By precluding UO_2 melting, the fuel geometry is preserved and possible adverse effects of molten UO_2 on the cladding are eliminated. To preclude center melting and as a basis for overpower protection system setpoints, a calculated centerline fuel temperature of 4700°F has been selected as the overpower limit. This provides sufficient margin for uncertainties in the thermal evaluations as described in Section 4.4.2.9.1.

Discussion

Fuel rod thermal evaluations are performed at rated power, maximum overpower, and during transients at various burnups. These analyses assure that this design basis, as well as the fuel integrity design bases given in Section 4.2, are met. They also provide input for the evaluation of Condition III and IV events described in Chapter 15.

4.4.1.3   Core Flow Design Basis

Basis

With the thimble plug assemblies removed, a minimum of 91.4 percent of the thermal flow rate will pass through the fuel rod region of the core and be effective for fuel rod cooling. The DNB analyses are conservatively based on thimble plugs removed. With the thimble plug assemblies installed, a minimum of 93.4 percent of the thermal flow rate will pass through the fuel region of the core and be effective for fuel rod cooling. Coolant flow through the thimble tubes, as well as the leakage from the core barrel-baffle region into the core, are not considered effective for heat removal. If installed, the thimble plug assemblies limit bypass flow through the rod cluster control guide thimbles in fuel assemblies which do not contain either control rods, neutron source rods or burnable absorber rods. The thimble plug assemblies are described in Section 4.2.2.3.4.

Discussion

Core cooling evaluations are based on the thermal flow rate (minimum flow) entering the reactor vessel. A maximum of 8.6 percent (with the thimble plug assemblies removed) or 6.6 percent (with the thimble plug assemblies installed) of the thermal flow rate is allotted as bypass flow. The bypass flow fraction includes rod cluster control guide thimble cooling flow, head cooling flow, baffle leakage and leakage to the vessel outlet nozzle.

4.4.1.4   Hydrodynamic Stability Design Basis

Basis

Modes of operation associated with Condition I and II events shall not lead to hydro-dynamic instability.

4.4.1.5   Other Considerations

The above design bases, together with the fuel clad and fuel assembly design bases given in Section 4.2.1, are sufficiently comprehensive so additional limits are not required.

Fuel rod diametral gap characteristics, moderator-coolant flow velocity and distribution, and moderator void are not inherently limiting. Each of these parameters is incorporated into the thermal and hydraulic models used to ensure the above mentioned design criteria are met. For instance, the fuel rod diametral gap characteristics change with time (Section 4.2.3.3) and the fuel rod integrity is evaluated on that basis. The effect of the moderator flow velocity and distribution (Section 4.4.2.2) and moderator void distribution (Section 4.4.2.4) are included in the core thermal evaluation and thus affect the design bases.

Meeting the fuel clad integrity criteria covers possible effects of clad temperature limitations. As noted in Section 4.2.3.3, the fuel rod conditions change with time. A single clad temperature limit for Condition I or Condition II events is not appropriate since, of necessity, it would be overly conservative. A clad temperature limit is applied to the loss-of-coolant accident (Section 15.6.5), control rod ejection accident, and locked rotor accident.

4.4.2   DESCRIPTION

4.4.2.1   Summary Comparison

Values of pertinent parameters, along with critical heat flux ratios, fuel temperatures, and linear heat generation rates, are presented in Table 4.4-1. In power capability evaluation, there has not been any change in this design criteria. The reactor is still designed to meet the DNB design criterion of Section 4.4.1.1, as well as no fuel centerline melting during normal operation, operational transients, and faults of moderate frequency.

All DNB analyses were performed such that the DNBR margins are available for offsetting rod bow penalties, and any other DNB penalties that may exist, and for flexibility in design.

Fuel densification has been considered in the DNB and fuel temperature evaluations utilizing the methods and models described in WCAP-8218, WCAP-10851 and WCAP-13589.

4.4.2.2   Critical Heat Flux Ratio or Departure from Nucleate Boiling Ratio and Mixing
Technology

The minimum DNBR in the limiting flow channel will be downstream of the peak heat flux
location (hot spot) due to the increased downstream enthalpy rise.

DNBRs are calculated by using the correlation and definitions described in Sections 4.4.2.2.1 and
4.4.2.2.2. The VIPRE-D computer code (discussed in Section 4.4.4.5.1) is used to determine the
flow distribution in the core and the local conditions in the hot channel for use in the DNB
correlation. The use of hot channel factors is discussed in Section 4.4.4.3.1 (nuclear hot channel
factors) and in Section 4.4.2.2.4 (engineering hot channel factors).

4.4.2.2.1   Departure from Nuclear Boiling Technology

The WRB-2M, ABB-NV, WLOP, and W-3 Correlations are used to evaluate critical heat flux in
the RFA-2 fuel assemblies. All correlations are tested against measured heat flux data in order to
establish a correlation limit which satisfies the DNB design basis stated in Section 4.4.1.1.

The WRB-2M correlation takes advantage of the improvement in the accuracy of critical heat flux
predictions over previous DNBR correlations to establish a lower correlation limit of 1.14.

The ABB-NV correlation is only used below the first mixing grid and the WLOP correlation is
only used when the operations conditions are outside the range of validity of the WRB-2M and
ABB-NV CHF correlations, such as the main steam-line break evaluation, where there are
reduced temperature and pressure conditions. The WLOP CHF correlation is used
deterministically. The W-3 correlation can also be used, within its limits applicability.

4.4.2.2.2   Definition of Departure from Nuclear Boiling Ratio

The DNB heat flux ratio (DNBR), as applied to this design when all flow cell walls are heated, is:

$$DNBR = \frac{q''_{DNB,\,N}}{q''_{loc}} \qquad\qquad\qquad (4.4.\text{-}1)$$

where:

$$q''_{DNB,\,N} = \frac{q''_{DNB,\,EU}}{F} \qquad\qquad\qquad (4.4.\text{-}2)$$

and $q''_{DNB,EU}$ is the uniform DNB heat flux as predicted by the WRB-2M, ABB-NV, WLOP, or
W-3 DNB correlation. For the WRB-2M correlation, the WRB-2M adjustment factor (Collins
2006) is used with the Tong Factor for CHF predictions. The ABB-NV correlation is applied
using the same Tong Factor as the primary DNB correlation, consistent with DOM-NAF-2-P-A.

F is the flux shape factor to account for nonuniform axial heat flux distributions (Tong 1967) with the "C" term modified as in Tong (1972).

q''_{loc} is the actual local heat flux.

4.4.2.2.3 Mixing Technology

The rate of heat exchange by mixing between flow channels is proportional to the difference in the local mean fluid enthalpy of the respective channels, the local fluid density and the flow velocity. The proportionality is expressed by the dimensionless thermal diffusion coefficient (TDC) which is defined as:

$$\text{TDC} = \frac{\dot{w}}{pVa} \tag{4.4-3}$$

where:

$\dot{w}$ = Flow exchange rate per unit length (lbm/ft-sec)

p = Fluid density (lbm /ft^3)

V = Fluid velocity (ft/sec)

a = Lateral flow area between channels per unit length, (ft^2 /ft)

Various mixing tests have been performed at Columbia University (WCAP-7941). These series of tests, using the "R" mixing vane grid design on 13-, 26-, and 32-inch grid spacing, were conducted in pressurized water loops at Reynolds numbers similar to that of a pressurized water reactor core under the following single and two phase (subcooled boiling) flow conditions:

Pressure 1,500 to 2,400 psia
Inlet temperature 332 to 642°F
Mass velocity 1.0 to 3.5 x 10^6 lbm/hr-ft^2
Reynolds number 1.34 to 7.45 x 10^5
Bulk outlet quality -52.1 to -13.5 percent

TDC was determined by comparing the VIPRE-01 Code predictions with the measured subchannel exit temperatures. Data for 26 inch axial grid spacing is presented on Figure 4.4–2; where the TDC is plotted versus the Reynolds number. TDC is found to be independent of Reynolds number, mass velocity, pressure, and quality over the ranges tested. The two-phase data (local, subcooled boiling) fell within the scatter of the single phase data. The effect of two-phase flow on the value of TDC has been demonstrated by (WCAP-7667), Rowe and Angle (1967; 1969), and Gonzalez-Santalo et al. In the subcooled boiling region, the values of TDC were indistinguishable from the single phase values. In the quality region, Rowe and Angle show that in the case with rod spacing similar to that in pressurized water reactor core geometry, the value of

TDC increased with quality to a point and then decreased, but never below the single phase value. Gonzalez-Santalo and Griffith showed that the mixing coefficient increased as the void fraction increased.

The data from these tests on the "R" grid showed that a design TDC value of 0.038 (for 26 inch grid spacing) could be used in determining the effect of coolant mixing in the VIPRE-01 analysis.

A mixing test program similar to the one described above was conducted at Columbia University for the current 17 by 17 geometry and mixing vane grids on 26 inch spacing (WCAP-8298). The mean value of TDC obtained from these tests was 0.059 and all data were well above the current design value of 0.038.

Since the actual reactor grid spacing is approximately 20 inches, approximately 10 inches in the IFM region of the RFA/RFA-2 fuel, additional margin is available for this design, as the value of TDC increases as grid spacing decreases (WCAP-7941).

4.4.2.2.4   Hot Channel Factors

The total hot channel factors for heat flux and enthalpy rise are defined as the maximum-to-core average ratios of these quantities. The heat flux hot channel factor considers the local maximum linear heat generation rate at a point (the hot spot), and the enthalpy rise hot channel factor involves the maximum integrated value along a channel (the hot channel).

Each of the total hot channel factors is composed of a nuclear hot channel factor (Section 4.4.4.3) describing the neutron power distribution and an engineering hot channel factor, which allows for variations in flow conditions and fabrication tolerances. The engineering hot channel factors are made up of subfactors which account for the influence of the variations of fuel pellet diameter, density, enrichment, and eccentricity; fuel rod diameter pitch and bowing; inlet flow distribution; flow redistribution; and flow mixing.

Heat Flux Engineering Hot Channel Factor (F^E_Q)

The heat flux engineering hot channel factor evaluates the maximum linear heat generation rate in the core. This subfactor is determined by statistically combining the fabrication variations for fuel pellet diameter, density, and enrichment, and has a value of 1.03 at the 95 percent probability level with 95 percent confidence. As shown in WCAP-8174 and WCAP-8296, no DNB penalty need be taken for the short relatively low intensity heat flux spikes caused by variations in the above parameters, as well as fuel pellet eccentricity and fuel rod diameter variation.

Enthalpy Rise Engineering Hot Channel Factor ($F^E_{\Delta H}$)

The effect of variations in flow conditions and fabrication tolerances on the hot channel enthalpy rise is directly considered in the VIPRE-D core thermal subchannel analysis (Section 4.4.4.5.1) under any reactor operating condition. The items considered contributing to the enthalpy rise engineering hot channel factor are discussed below:

1.   Pellet diameter, density, and enrichment

Design values employed in the VIPRE-D analysis related to the above fabrication variations are based on applicable limiting tolerances such that these design values are met for 95 percent of the limiting channels at a 95 percent confidence level. Measured manufacturing data on Westinghouse 17 by 17 fuel show that the tolerances used in this evaluation are conservative. In addition, each fuel assembly is checked to ensure that the channel spacing design criteria are met. The effect of variations in pellet diameter, enrichment, and density is employed in the VIPRE-D analysis as a direct multiplier on the hot channel enthalpy rise for analyses using deterministic methods. For analyses using statistical methods these variations are considered statistically when defining the DNBR limits.

2.   Inlet flow maldistribution

The consideration of the inlet flow maldistribution in core thermal performances is discussed in Section 4.4.4.2.2. A design basis of 5 percent reduction in coolant flow to the hot assembly is used in the VIPRE-D analysis.

3.   Flow redistribution

The flow redistribution accounts for the reduction in flow in the hot channel resulting from the high flow resistance in the channel due to the local or bulk boiling. The effect of the nonuniform power distribution is inherently considered in the VIPRE-D analysis for every operating condition which is evaluated.

4.   Flow mixing

The subchannel mixing model incorporated in the VIPRE-D Code and used in reactor design is based on experimental data (WCAP-7667) discussed in Sections 4.4.2.2.3 and 4.4.4.5.1. The mixing vanes incorporated in the spacer grid design induce additional flow mixing between the various flow channels in a fuel assembly, as well as between adjacent assemblies. This mixing reduces the enthalpy rise in the hot channel resulting from local power peaking or unfavorable mechanical tolerances.

4.4.2.2.5   Effects of Rod Bow on DNBR

The phenomenon of fuel rod bowing as described in WCAP-8691, must be accounted for in the DNBR safety analysis of Condition I and Condition II events for each plant application. The methodology described in WCAP-8691 has been accepted by the NRC for use in design applications (Thomas, 1982) and is used in the analysis of fuel rod bowing.

The maximum rod bow penalties accounted for in the design safety analysis are based on an assembly average burnup of 24,000 MWD/MTU. At burnups greater than 24,000 MWD/MTU, credit is taken for the effect of $F^N_{\Delta H}$ burndown due to the decrease in fissionable isotopes and the

buildup of fission product inventory, and no additional rod bow penalty is required (Berlinger, 1986). The safety analysis for MPS-3 maintained sufficient DNBR margin, as discussed in Section 4.4.1.1, to accommodate the full and low flow DNBR penalties for RFA-2 fuel.

For the upper spans of the RFA-2 fuel assembly, where additional restraint is provided with the intermediate flow mixer (IFM) grids, the grid-to-grid spacing in those spans with the IFM grids is approximately 10 inches compared to approximately 20 inches in the other spans. Using the NRC- approved scaling factor results in predicted channel closure in the 10 inch spans of less than 50-percent closure. Therefore, no rod bow DNBR penalty is required in the 10 inch spans in the RFA-2 safety analyses.

4.4.2.2.6   Effects of Lower Plenum Flow Anomaly on DNBR

In addition to the rod bow DNBR penalty discussed in Section 4.4.2.2.5, a DNBR penalty was computed to account for the lower plenum flow anomaly. Sufficient DNBR margin was retained, as discussed in Section 4.4.1.1, to offset this additional penalty.

4.4.2.2.7   High Quality Threshold on WRB-2M and WRB-2

Use of the WRB-2M and WRB-2 CHF correlations has been conservatively modified to utilize a penalty above a certain high quality threshold within approved correlation ranges.

4.4.2.3   Linear Heat Generation Rate

The core average and maximum linear heat generation rates are given in Table 4.4-1. The method of determining the maximum linear heat generation rate is given in Section 4.3.2.2.

4.4.2.4   Void Fraction Distribution

The calculated core average and the hot subchannel maximum and average void fractions are presented in Table 4.4-2 for operation at full power with design hot channel factors. The void models used in the VIPRE-D Code are described in Section 4.4.2.7.3. Normalized core flow and enthalpy rise distributions are shown on Figures 4.4–3 through 4.4–5 for an early core design.

4.4.2.5   Core Coolant Flow Distribution

Assembly average coolant mass velocity and enthalpy at various radial and axial core locations are given on Figures 4.4–3 through 4.4–5. Typical coolant enthalpy rise and flow distributions for the 4-foot elevation (1/3 of core height) are shown on Figure 4.4–3, for the 8 foot elevation (two thirds of core height) on Figure 4.4–4, and at the core exit on Figure 4.4–5. The analysis for this case utilized a uniform core inlet enthalpy and inlet flow distribution. No orificing is employed in the reactor design.

4.4.2.6   Core Pressure Drops and Hydraulic Loads

4.4.2.6.1   Core Pressure Drops

The analytical model and experimental data used to calculate the pressure drops shown in
Table 4.4-1 are described in Section 4.4.2.7. The core pressure drop includes the fuel assembly,
lower core plate, and upper core plate pressure drops. The full power operation pressure drop
values shown in Table 4.4-1 are the unrecoverable pressure drops across the vessel, including the
inlet and outlet nozzles, and across the core. Uncertainties associated with the core pressure drop
values are discussed in Section 4.4.2.9.2.

4.4.2.6.2   Hydraulic Loads

The fuel assembly hold down springs (Figure 4.2–2) keep the fuel assemblies in contact with the
lower core plate under all Condition I and II events with the exception of the turbine overspeed
transient associated with a loss of external load. The hold down springs are designed to tolerate
the possibility of an over deflection associated with fuel assembly liftoff for this case and provide
contact between the fuel assembly and the lower core plate following this transient. More adverse
flow conditions occur during a loss-of-coolant accident. These conditions are presented in
Section 15.6.5.

Hydraulic loads at normal operating conditions are calculated considering the best estimate flow
and accounting for the best estimate core bypass flow assuming thimble plug insertion which is
more conservative than thimble plug removal for lift force calculations based on manufacturing
tolerances. Core hydraulic loads at cold plant startup conditions are based on the cold best
estimate flow, but are adjusted to account for the coolant density difference. Conservative core
hydraulic loads for a pump overspeed transient, which could possibly create flow rates 18 percent
greater than the best estimate flow, are evaluated to be approximately twice the fuel assembly
weight. Applicable uncertainties are applied to these results.

4.4.2.7   Correlation and Physical Data

4.4.2.7.1   Surface Heat Transfer Coefficients

Forced convection heat transfer coefficients are obtained from the familiar Dittus-Boelter
correlation (Dittus et al., 1930), with the properties evaluated at bulk fluid conditions:

$$\frac{hD_e}{K} = 0.023\left(\frac{D_e G}{\mu}\right)^{0.8}\left(\frac{C_p \mu}{K}\right)^{0.4} \tag{4.4-4}$$

where:

   h = Heat transfer coefficient (Btu/hr-ft^2-°F)

   D_e = Equivalent diameter (feet)

K = Thermal conductivity (Btu/hr-ft^2 -°F)

G = Mass velocity (lb /hr-ft^2)

μ = Dynamic viscosity (lb /ft-hr)

C_p = Heat capacity (Btu/lb -°F)

This correlation has been shown to be conservative (Weisman 1959) for rod bundle geometries with pitch to diameter ratios in the range used by pressurized water reactors.

The onset of nucleate boiling occurs when the clad wall temperature reaches the amount of superheat predicted by Thom's (Thom et al., 1965-1966) correlation. After this occurrence, the outer clad wall temperature is determined by:

$$\Delta T_{sat} = 0.072 \exp(-P/1260)\,(q'')^{0.5} \qquad\qquad (4.4\text{-}5)$$

where:

ΔT_{sat} = Wall superheat, T_w - T_{sat} (°F)

q" = Wall heat flux (Btu/hr-ft^2)

P = Pressure (psia)

T_w = Outer clad wall temperature (°F)

T_{sat} = Saturation temperature of coolant at P (°F)

4.4.2.7.2　Total Core and Vessel Pressure Drop

Unrecoverable pressure losses occur as a result of viscous drag (friction) and/or geometry changes (form) in the fluid flow path. The flow field is assumed to be incompressible, turbulent, single- phase water. These assumptions apply to the core and vessel pressure drop calculations for the purpose of establishing the primary loop flow rate. Two-phase considerations are neglected in the vessel pressure drop evaluation because the core average void is negligible (Table 4.4-2). Two-phase flow considerations in the core thermal subchannel analyses are considered and the models are discussed in Section 4.4.4.2.3. Core and vessel pressure losses are calculated by equations of the form:

$$\Delta P_L = \left(K + F\frac{L}{D_e}\right)\frac{pV^2}{2\,g_c(144)} \qquad\qquad (4.4\text{-}6)$$

where:

ΔP_L = Unrecoverable pressure drop (lb /in^2)

p = Fluid density (lb /ft^3)

L = Length (feet)

D_e = Equivalent diameter (feet)

V = Fluid velocity (ft/sec)

g_c = 32.174 (lbm-ft/lbf-sec^2)

K = Form loss coefficient, dimensionless

F = Friction loss coefficient, dimensionless

Fluid density is assumed to be constant at the appropriate value for each component in the core and vessel. Because of the complex core and vessel flow geometry, precise analytical values for the form and friction loss coefficients are not available. Therefore, experimental values for these coefficients are obtained from geometrically similar models.

Values are quoted in Table 4.4-1 for unrecoverable pressure loss across the reactor vessel, including the inlet and outlet nozzles, and across the core. The results of full scale tests of core components and fuel assemblies were utilized in developing the core pressure loss characteristic. The pressure drop for the vessel was obtained by combining the core loss with correlation of one-seventh scale model hydraulic test data on a number of vessels (Hetsroni 1965 and WCAP-3269-8) and form loss relationships (Idel'chik 1960). Moody (1944) curves were used to obtain the single-phase friction factors.

Tests of the primary coolant loop flow rates were made (Section 4.4.5.1) prior to initial criticality to verify that the flow rates used in the design, which were determined in part from the pressure losses calculated by the method described here, are conservative.

4.4.2.7.3   Void Fraction Correlation

There are several empirical correlations available in VIPRE-D (DOM-NAF-2-P-A) to calculate both subcooled and bulk boiling void fractions. However, the EPRI models are used in thermal-hydraulic analyses using the VIPRE-D code.

4.4.2.8   Thermal Effects of Operational Transients

DNB core safety limits are generated as a function of coolant temperature, pressure, core power, and axial power imbalance. Steady state operation within these safety limits ensures that the minimum DNBR is not less than the safety analysis limit. The Reactor Core Safety Limit curves in the COLR show the loci points of thermal power, Reactor Coolant System pressure, and average temperature below which the calculated DNBR is no less than the design DNBR value or the average enthalpy at the vessel exit is less than the enthalpy of saturated liquid. This system provides adequate protection against anticipated operational transients that are slow with respect to fluid transport delays in the primary system. In addition, for fast transients, e.g., uncontrolled rod bank withdrawal at power incident (Section 15.4.2), specific protection functions are

provided as described in Section 7.2 and the use of these protection functions is described in Chapter 15.

4.4.2.9   Uncertainties in Estimates

4.4.2.9.1   Uncertainties in Fuel and Clad Temperatures

As discussed in Section 4.4.2.11, the fuel temperature is a function of crud, oxide, clad, pellet-clad gap, and pellet conductances. Uncertainties in the fuel temperature calculation are essentially of two types: fabrication uncertainties, such as variations in the pellet and clad dimensions and the pellet density; and model uncertainties, such as variations in the pellet conductivity and the gap conductance. These uncertainties have been quantified by comparison of the thermal model to the in-pile thermocouple measurements (Kjaerheim and Rolstad 1967; Kjaerheim 1969; Cohen et al., 1960; Clough and Sayers 1964; Stora et al., 1964; Devold 1968; WCAP-2923) by out-of-pile measurements of the fuel and clad properties (Howard and Gulvin 1960; Lucks and Deem 1961; Daniel et al., 1962; Feith 1962; Vogt et al., 1964; Nishijima et al., 1965; Ainscough and Wheeler 1968; Godfrey et al., 1964; Stora et al., 1964; Bush 1965; Asamoto 1968; Kruger 1968), and by measurements of the fuel and clad dimensions during fabrication. The resulting uncertainties are then used in all evaluations involving the fuel temperature. The effect of densification on fuel temperature is presented in WCAP-8218 and WCAP-10851. Other models that affect uncertainties in fuel temperature calculations, such as the clad creep model, are discussed in WCAP-15063.

In addition to the temperature uncertainty described above, the measurement uncertainty in determining the local power, and the effect of density and enrichment variations on the local power are considered in establishing the heat flux hot channel factor. These uncertainties are described in Section 4.3.2.2.1.

Reactor trip set points, as specified in the Technical Specifications, include allowance for instrument and measurement uncertainties, such as calorimetric error, instrument drift and channel reproducibility, temperature measurement uncertainties, noise, and heat capacity variations.

Uncertainty in determining the cladding temperature results from uncertainties in the crud and oxide thicknesses. Because of the excellent heat transfer between the surface of the rod and the coolant, the film temperature drop does not appreciably contribute to the uncertainty.

4.4.2.9.2   Uncertainties in Pressure Drops

Core and vessel pressure drops are listed in Table 4.4-1. The uncertainties are based on the uncertainties in both the test results and the analytical extension of these values to the reactor application.

A major use of the core and vessel pressure drops is to determine the primary system coolant flow rates as discussed in Section 5.1. In addition, as discussed in Section 4.4.5.1, tests on the primary

system prior to initial criticality were made to verify that a conservative primary system coolant flow has been used in the design and analyses of the plant.

4.4.2.9.3   Uncertainties due to Inlet Flow Maldistribution

The effects of uncertainties in the inlet flow maldistribution criteria used in the core thermal analyses are discussed in Section 4.4.4.2.2.

4.4.2.9.4   Uncertainty in DNB Correlation

The uncertainty in the DNB correlation (Section 4.4.2.2) can be written as a statement on the probability of not being in DNB based on the statistics of the DNB data. This is discussed in Section 4.4.2.2.2.

4.4.2.9.5   Uncertainties of DNBR Calculations

The uncertainties in the DNBRs calculated by VIPRE-D analysis (Section 4.4.4.5.1) with the Statistical DNBR Evaluation Methodology are accounted for as discussed in Section 4.4.1.1. For those transients that do not use the Statistical DNBR Evaluation Methodology, the uncertainties are applied directly to the VIPRE-D parameters. The results of a sensitivity study (WCAP-8054) show that the minimum DNBR in the hot channel is relatively insensitive to variations in the core-wide radial power distribution (for the same value of $F^N_{\Delta H}$).

The ability of the VIPRE-D Code to accurately predict flow and enthalpy distributions in rod bundles is discussed in Section 4.4.4.5.1.

4.4.2.9.6   Uncertainties in Flow Rates

The uncertainties associated with loop flow rates are discussed in Section 5.1. For use in core thermal performance evaluations, a minimum loop flow is used which is less than the best estimate loop flow. In addition, a fraction of the thermal design flow is assumed to be ineffective for core heat removal capability because it bypasses the core through the various available vessel flow paths. With the thimble plug assemblies removed, the bypass fraction is assumed to be 8.6 percent and with the thimble plug assemblies installed the bypass fraction is assumed to be 6.6 percent. The flow paths considered in calculating the bypass flow fraction are described in Section 4.4.4.2.1.

4.4.2.9.7   Uncertainties in Hydraulic Loads

As discussed in Section 4.4.2.6.2, hydraulic loads on the fuel assembly are evaluated for a pump overspeed transient which creates flow rates 18 percent greater than the best estimate flow. Applicable uncertainties are applied to these results.

4.4.2.9.8   Uncertainty in Mixing Coefficient

The value of the mixing coefficient, TDC, used in VIPRE-D analyses for this application is 0.038. The mean value of TDC obtained in the "R" grid mixing tests described in Section 4.4.2.2.3 was 0.042 (for 26 inch grid spacing). The value 0.038 is one standard deviation below the mean value; approximately 90 percent of the data gives values of TDC greater than 0.038 (WCAP-7941-P-A).

The results of the mixing tests done on 17 x 17 geometry, as discussed in Section 4.4.2.2.3, had a mean value of TDC of 0.059 and standard deviation of equal to 0.007. Hence, the current design value of TDC is almost three standard deviations below the mean 26 inch grid spacing.

4.4.2.10 Flux Tilt Considerations

Significant quadrant power tilts are not anticipated during normal operation, since this phenomenon is caused by some asymmetric perturbation. A dropped or misaligned rod cluster control assembly could cause changes in hot channel factors; however, these events are analyzed separately in Chapter 15.

Other possible causes for quadrant power tilts include X-Y xenon transients, inlet temperature mismatches and enrichment variations within tolerances.

In addition to unanticipated quadrant power tilts as described above, other readily explainable asymmetries may be observed during calibration of the excore detector quadrant power tilt alarm. During operation, incore maps are taken at least once per month and, periodically, additional maps are obtained for calibration purposes. Each of these maps is reviewed for deviations from the expected power distributions. Asymmetry in the core, from quadrant to quadrant, is frequently a consequence of the design when assembly and/or component shuffling and rotation requirements do not allow exact symmetry preservation. In each case, the acceptability of an observed asymmetry, planned or otherwise, depends solely on meeting the required accident analyses assumptions. In practice, once acceptability has been established by review of the incore maps, the quadrant power tilt alarms and related instrumentation are adjusted to indicate zero Quadrant Power Tilt (Quadrant Power Tilt Ratio Normalized to 1.0) as the final step in the calibration process. This action ensures that the instrumentation is correctly calibrated to alarm in the event an unexplained or unanticipated change occurs in the quadrant-to-quadrant relationships between calibration intervals. Proper functioning of the quadrant power tilt alarm is significant because no allowances are made in the design for increased hot channel factors due to unexpected developing flux tilts since all likely causes are prevented by design or procedures or specifically analyzed. Finally, in the event that unexplained flux tilts do occur, the Technical Specifications (Section 3/4.2.4) provide appropriate corrective actions to ensure continued safe operation of the reactor.

4.4.2.11 Fuel and Cladding Temperatures

Consistent with the thermal-hydraulic design bases described in Section 4.4.1, the following discussion pertains mainly to fuel pellet temperature evaluation. A discussion of fuel clad integrity is presented in Section 4.2.3.1.

The thermal-hydraulic design assures that the maximum fuel temperature is below the melting point of UO_2 (Section 4.4.1.2). To preclude center melting and as a basis for overpower protection system set points, a calculated centerline fuel temperature of 4,700°F has been selected as the overpower limit. This provides sufficient margin for uncertainties in the thermal evaluations, as described in Section 4.4.2.9.1. The temperature distribution within the fuel pellet is predominantly a function of the local power density and the UO_2 thermal conductivity. However, the computation of radial fuel temperature distributions combines crud, oxide, clad gap, and pellet conductances. The factors which influence these conductances, such as gap size (or contact pressure), internal gas pressure, gas composition, and radial power distribution within the pellet, etc., have been combined into a semi empirical thermal model (Section 4.2.3.3) with the model modifications for phenomena such as time dependent fuel densification given in WCAP-8218 and WCAP-10851 and clad creep as given in WCAP-15063. This thermal model enables the determination of these factors and their net effects on temperature profiles. The temperature predictions have been compared to in-pile fuel temperature measurements (Kjaerheim and Rolstad 1967; Kjaerheim 1969; Cohen et al., 1960; Clough and Sayers 1964; Stora et al., 1964; Devold 1968; WCAP-2923) and melt radius data (Duncan 1962; Nelson et al., 1964) with good results.

As described in WCAP-8218, WCAP-10851, WCAP-13589 and WCAP-15063, fuel rod thermal evaluations (fuel centerline, average, and surface temperatures) are determined throughout the fuel rod lifetime with consideration of properties such as time dependent fuel densification and clad creep. To determine the maximum fuel temperatures, various burnup rods, including the highest burnup rod, are analyzed over the rod linear power range of interest.

The principal factors which are employed in the determination of the fuel temperature are discussed below.

4.4.2.11.1 UO_2 Thermal Conductivity

The thermal conductivity of uranium dioxide was evaluated from data reported by Howard et al. (1960); Lucks et al. (1961); Daniel et al. (1962); Feith (1962); Vogt et al. (1964); Nishijima et al. (1965); Godfrey et al. (1964); Stora et al. (1964); Bush (1965); Ainscough et al. (1968); Asamoto et al. (1968); Kruger (1968); and Gyllander (1971).

At the higher temperatures, thermal conductivity is best obtained by utilizing the integral conductivity to melt which can be determined with more certainty. From an examination of the data, it has been concluded that the best estimate from the value of

$$\int_{0}^{2800°C} KdT \qquad\qquad (4.4\text{-}7)$$

is 93 watts/cm. This conclusion is based on the integral values reported by Gyllander (1971); Lyons et al. (1966); Coplin et al. (1968); Duncan (1962); Bain (1962); and Stora (1970).

The design curve for the thermal conductivity is shown on Figure 4.4–7. The section of the curve at temperatures between 0°C and 1,300°C is in excellent agreement with the recommendation of the IAEA panel (1966). The section of the curve above 1,300°C is derived for an integral value of 93 watts/cm (Duncan 1962; Gyllander 1971; Stora 1970).

Thermal conductivity for UO_2 at 95 percent theoretical density can be represented best by the following equation:

$$K = \frac{1}{11.8 + 0.0238\,T} + 8.775 \text{ x } 10^{-13}\,T^3 \tag{4.4-8}$$

where:

K = watts/cm°C

T = °C

4.4.2.11.2 Radial Power Distribution on UO_2 Fuel Rods

An accurate description of the radial power distribution as a function of burnup is needed for determining the power level for incipient fuel melting and other important performance parameters, such as pellet thermal expansion, fuel swelling, and fission gas release rates. Radial power distribution in UO_2 fuel rods is determined with the neutron transport theory code, LASER. The LASER Code has been validated by comparing the code predictions on radial burnup and isotopic distributions with measured radial microdrill data (WCAP-6069 and WCAP-3385-56). A "radial power depression factor," f, is determined using radial power distributions predicted by LASER. The factor f enters into the determination of the pellet centerline temperature, T_c, relative to the pellet surface temperature, T_s, through the expression:

$$\int_{T_s}^{T_c} K(t)\,dT = \frac{q'F}{4\pi} \tag{4.4-9}$$

where:

K(t) = The thermal conductivity for UO_2 with a uniform density distribution

q' = The linear power generation rate

4.4.2.11.3 Gap Conductance

The temperature drop across the pellet-clad gap is a function of the gap size and the thermal conductivity of the gas in the gap. The gap conductance model is selected such that when combined with the UO_2 thermal conductivity model, the calculated fuel centerline temperatures

reflect the in-pile temperature measurements. A more detailed discussion of the gap conductance model is presented in WCAP-10851.

4.4.2.11.4 Surface Heat Transfer Coefficients

The fuel rod surface heat transfer coefficients during subcooled forced convection and nucleate boiling are presented in Section 4.4.2.7.1.

4.4.2.11.5 Fuel Clad Temperatures

The outer surface of the fuel rod at the hot spot operates at a temperature of approximately 660°F for steady state operation at rated power throughout core life due to the onset of nucleate boiling. Initially (beginning of life), this temperature is that of the clad metal outer surface.

During operation over the life of the core, the buildup of oxides and crud on the fuel rod surface causes the clad surface temperature to increase. Allowance is made in the fuel center melt evaluation for this temperature rise. Since the thermal-hydraulic design basis limits DNB, adequate heat transfer is provided between the fuel clad and the reactor coolant so that the core thermal output is not limited by considerations of clad temperature.

4.4.2.11.6 Treatment of Peaking Factors

The total heat flux hot channel factor, F_Q, is defined by the ratio of the maximum to core average heat flux. The design value of F_Q, as presented in Table 4.3-2 and discussed in Section 4.3.2.2.6, is 2.548 for normal operation. This results in a peak linear power of 15.09 kW/ft at full power conditions.

The peak linear power resulting from overpower transients/operator errors (assuming a maximum overpower of 121 percent) is less than 22.6 kW/ft. The centerline fuel temperature must be below the UO_2 melt temperature over the lifetime of the rod, including allowances for uncertainties. The fuel temperature design basis is discussed in Section 4.4.1.2 and results in a maximum allowable calculated centerline temperature of 4,700°F. The peak linear power for prevention of centerline melt is 22.6 kW/ft. The centerline temperature at the peak linear power resulting from overpower transients/operator errors (assuming a maximum power of 121 percent) is below that required to produce melting.

4.4.3   DESCRIPTION OF THE THERMAL AND HYDRAULIC DESIGN OF THE REACTOR COOLANT SYSTEM

4.4.3.1   Plant Configuration Data

Plant configuration data for the thermal-hydraulic and fluid systems external to the core are provided, as appropriate, in Chapters 5, 6, and 9. Implementation of the emergency core cooling system (ECCS) is discussed in Chapter 6. Some specific areas of interest are the following:

1.   Total coolant flow rates for the reactor coolant system (RCS) and each loop are provided in Table 5.1–1. Flow rates employed in the evaluation of the core are presented throughout Section 4.4.

2.   Total RCS volume, including pressurizer and surge line; RCS liquid volume, including pressurizer water at steady state power conditions are given in Table 5.1–1.

3.   The flow path length through each volume may be calculated from physical data provided in the above referenced tables.

4.   The height of fluid in each component of the RCS may be determined from the physical data presented in Section 5.4. The components of the RCS are water filled during power operation with the pressurizer being approximately 60 percent water filled.

5.   Components of the ECCS are to be located so as to meet the criteria for net positive suction head described in Section 6.3.

6.   Line lengths and sizes for the safety injection system are determined so as to guarantee a total system resistance which provides, as a minimum, the fluid delivery rates assumed in the safety analyses described in Chapter 15.

7.   The parameters for components of the RCS are presented in Section 5.4.

8.   The steady state pressure drops and temperature distributions through the RCS are presented in Table 5.1–1.

4.4.3.2   Operating Restrictions on Pumps

The minimum net positive suction head (NPSH) and minimum seal injection flow rate must be established before operating the reactor coolant pumps. With the minimum 6 gpm labyrinth seal injection flow rate established, the operator verifies that the system pressure satisfies net positive suction head requirements.

4.4.3.3   Power-Flow Operating Map (BWR)

Not applicable to Millstone 3.

4.4.3.4   Temperature-Power Operating Map

RCS temperatures increase linearly with power as shown in Figure 4.4–8, for a core power of 3709 MWt and a full power T_{ave} of 589.5°F.

The effects of reduced core flow, due to inoperative pumps, are discussed in Sections 5.4.1, 15.2.6, and 15.3. Natural circulation capability of the system is shown in Table 15.2–2.

4.4.3.5   Load Following Characteristics

Load following using control rod motion and dilution or boration by the boron system is discussed in Section 4.3.2.4.16.

The RCS is designed on the basis of steady state operation at full power heat load. The reactor coolant pumps utilize constant speed drives as described in Section 5.4 and the reactor power is controlled to maintain average coolant temperature at a value which is a linear function of load, as described in Section 7.7.

4.4.3.6   Thermal and Hydraulic Characteristics Summary Table

The thermal and hydraulic characteristics are given in Tables 4.1-1 and 4.4-1.

4.4.4   EVALUATION

4.4.4.1   Critical Heat Flux

The critical heat flux correlations utilized in the core thermal analysis are explained in detail in Section 4.4.2.2.

4.4.4.2   Core Hydraulics

4.4.4.2.1   Flow Paths Considered in Core Pressure Drop and Thermal Design

The following flow paths for core bypass flow are considered:

1.   Flow through the spray nozzles into the upper head for head cooling purposes

2.   Flow entering into the rod cluster control guide thimbles to cool the control rods

3.   Leakage flow from the vessel inlet nozzle directly to the vessel outlet nozzle through the gap between the vessel and the barrel

4.   Flow introduced between the baffle and the barrel for the purpose of cooling these components and which is not considered available for core cooling

5.   Flow in the gaps between the fuel assemblies on the core periphery and the adjacent baffle wall

The above contributions are evaluated to confirm that the design value of the core bypass flow is met. The design value of core bypass flow for the Millstone 3 plant is equal to 8.6 percent of the total vessel flow with the thimble plug assemblies removed and 6.6 percent with the thimble plug assemblies inserted.

Of the total allowance, 4.1 percent (with thimble plug assemblies removed) or 2.1 percent (with the thimble plug assemblies inserted) is associated with the core (item 2 above). The remainder of the core bypass flow is associated with the reactor vessel internals (items 1, 3, 4 and 5 above). Calculations have been performed using drawing tolerances in the worst direction and accounting for uncertainties in pressure losses. Based on these calculations, the core bypass is no greater than the design values quoted above.

Flow model test results for the flow path through the reactor are discussed in Section 4.4.2.7.2.

4.4.4.2.2   Inlet Flow Distributions

Data have been considered from several 1/7-scale hydraulic reactor model tests (WCAP-3269-8; Hetsroni and in sensitivity studies (WCAP-8054)) in arriving at the core inlet flow maldistribution criteria to be used in the VIPRE-D analyses (Section 4.4.4.5.1). The design basis of 5 percent reduction to the hot assembly inlet is used in VIPRE-D analyses.

The experimental error estimated in the inlet velocity distribution has been considered, as outlined in WCAP-8054, where the sensitivity of changes in inlet velocity distributions to hot channel thermal performance is shown to be small.

The effect of the total flow rate on the inlet velocity distribution was studied in the experiments of WCAP-3269-8. As was expected, on the basis of the theoretical analysis, no significant variation could be found in inlet velocity distribution with reduced flow rate.

4.4.4.2.3   Empirical Friction Factor Correlations

Two empirical friction factor correlations are used in the VIPRE-D Code (Section 4.4.4.5.1).

The friction factor in the axial direction, parallel to the fuel rod axis, is evaluated using the McAdams correlation as discussed in DOM-NAF-2-P-A.

The flow in the lateral directions, normal to the fuel rod axis, views the reactor core as a large tube bank. Thus, the lateral friction factor proposed by Idel'chik (1960) is applicable. This correlation is of the form:

$$F_L = A Re_L^{-0.2} \tag{4.4-10}$$

where:

   A = A function of the rod pitch and diameter as given in Idel'chik (1960)

   Re_L = The lateral Reynolds number based on the rod diameter

4.4.4.3　Influence of Power Distribution

The core power distribution, which is largely established at beginning of life by fuel enrichment, loading pattern, and core power level is also a function of variables, such as control rod worth and position, and fuel depletion throughout lifetime. Radial power distributions in various planes of the core are often illustrated for general interest, however, the core radial enthalpy rise distribution as determined by the integral of power up each channel is of greater importance for DNB analyses. These radial power distributions, characterized by $F^N_{\Delta H}$ (Section 4.3.2.2.1) as well as axial heat flux profiles, are discussed in the following two sections.

4.4.4.3.1　Nuclear Enthalpy Rise Hot Channel Factor, $F^N_{\Delta H}$

Given the local power density q' (kW/ft) at a point x, y, z in a core with N fuel rods and height H:

$$F^N_{\Delta H} = \frac{\text{hot rod power}}{\text{average rod power}} = \frac{Max\int_o^H q'(x_o, y_o, z_o)dz}{\frac{1}{N} \sum_{\substack{all \\ rods}} \int_o^H q'(x, y, z)dz} \qquad (4.4\text{-}11)$$

The way in which $F^N_{\Delta H}$ is used in the DNB calculation is important. The location of minimum DNBR depends on the axial profile and the value of DNBR depends on the enthalpy rise to that point. Basically, the maximum value of the rod integral is used to identify the most likely rod for DNBR. An axial power profile is obtained which, when normalized to the design value of $F^N_{\Delta H}$, recreates the axial heat flux along the limiting rod. The surrounding rods are assumed to have the same axial profile with rod average powers, which are typical distributions found in hot assemblies. In this manner, worst case axial profiles can be combined with worst case radial distributions for reference DNB calculations.

It should be noted again that $F^N_{\Delta H}$ is an integral and is used as such in DNB calculations. Local heat fluxes are obtained by using hot channel and adjacent channel explicit power shapes, which take into account variations in horizontal power shapes throughout the core.

For operation at a fraction of full power (P), the design $F^N_{\Delta H}$ used is given by the equation in Table 4.4-1 (Radial Power Distribution Parameters). The value of $F^{RTP}_{\Delta H}$, which is the limit of $F^N_{\Delta H}$ at Rated Thermal Power (RTP), is specified in the COLR.

The permitted relaxation of $F^N_{\Delta H}$ is included in the DNB protection set points and allows radial power shape changes with rod insertion to the insertion limits (WCAP-7912), thus allowing greater flexibility in the nuclear design.

4.4.4.3.2   Axial Heat Flux Distributions

As discussed in Section 4.3.2.2, the axial heat flux distribution can vary as a result of rod motion, power change, or due to spatial xenon transients which may occur in the axial direction. Consequently, it is necessary to measure the axial power imbalance by means of the excore nuclear detectors (Section 4.3.2.2.4) and protect the core from excessive axial power imbalance. The reference axial shape used in establishing core DNB limits, and performing DNB analysis of Chapter 15 accidents, is a chopped cosine with a peak to average value of 1.78. The reactor trip system provides automatic reduction of the trip set points on excessive axial power imbalance. To determine the magnitude of the set point reduction, the reference shape is supplemented by other axial shapes skewed to the bottom and top of the core.

The initial conditions for the accidents for which DNB protection is required are assumed to be those permissible within the specified axial offset control limits described in Section 4.3.2.2.6. The course of those accidents in which DNB is a concern is analyzed in Chapter 15, assuming that the protection set points have been set on the basis of these shapes. In many cases, the axial power distribution in the hot channel changes throughout the course of the accident, due to rod motion, coolant temperature, and power level changes.

4.4.4.4   Core Thermal Response

A general summary of the steady state thermal-hydraulic design parameters, including thermal output, flow rates, etc., is provided in Table 4.4-1.

As stated in Section 4.4.1, the design bases of the application are to prevent DNB and to prevent fuel melting for Condition I and II events. The protective systems described in Chapter 7 are designed to meet these bases. The response of the core to Condition II transients is given in Chapter 15.

4.4.4.5   Analytical Techniques

4.4.4.5.1   Core Analysis

The objective of reactor core thermal design is to determine the maximum heat removal capability in all flow subchannels and to show that the core safety limits are not exceeded using the most conservative power distribution. The thermal design takes into account local variations in dimensions, power generation, flow redistribution, and mixing. VIPRE-D is a three-dimensional subchannel code that has been developed to account for hydraulic and nuclear effects on the enthalpy rise in the core and hot channels (DOM-NAF-2-P-A). VIPRE-D modeling of a PWR core is based on a one-pass modeling approach, wherein hot channels and their adjacent channels are modeled in detail, while the rest of the core is modeled simultaneously on a relatively coarse mesh. The behavior of the hot assembly is determined by superimposing the power distribution upon the inlet flow distribution, while allowing for flow mixing and flow distribution between flow channels. Local variations in fuel rod power, fuel rod and pellet fabrication, and turbulent mixing are also considered in determining conditions in the hot channels. Conservation equations

of mass, axial and lateral momentum, and energy are solved for the fluid enthalpy, axial flow rate, lateral flow, and pressure drop.

The behavior of the hot assembly is determined by superimposing the power distribution among the assemblies upon the inlet flow distribution while allowing for flow mixing and flow distribution between assemblies. The boundary flow and enthalpy distributions for the hottest assembly are obtained from the core-wide, assembly-by-assembly analysis. The local variations in power, fuel rod and pellet fabrication, and mixing within the hottest assembly are combined with the boundary conditions of the hottest assembly, in order to determine the conditions in the hot channel.

4.4.4.5.2   Steady State Analysis

The VIPRE-D computer program, as approved by the NRC, in DOM-NAF-2-P-A, is used to determine coolant density, mass velocity, enthalpy, vapor void, static pressure, and DNBR distributions along parallel flow channels within a reactor core under all expected operating conditions.

Estimates of uncertainties are discussed in Section 4.4.2.9.

4.4.4.5.3   Experimental Verification

Extensive experimental verification of VIPRE-01 is presented in Stewart (1989). The Dominion version of VIPRE-01, VIPRE-D, was modified by Dominion to fit the specific needs of Millstone 3 and its fuel products by adding vendor specific CHF correlations and customizing its input and output. The NRC-approved constitutive models and algorithms in VIPRE-01 are unchanged in VIPRE-D.

4.4.4.5.4   Transient Analysis

The approved VIPRE-D methodology, DOM-NAF-2-P-A, was shown to be conservative for transient thermal hydraulic analysis.

4.4.4.6   Hydrodynamic and Flow Power Coupled Instability

Boiling flow may be susceptible to thermohydrodynamic instabilities (Boure et al., 1973). These instabilities are undesirable in reactors since they may cause a change in thermohydraulic conditions that may lead to a reduction in the DNB heat flux relative to that observed during a steady flow condition or to undesired forced vibrations of core components. Therefore, a thermohydraulic design criterion was developed which states that modes of operation under Condition I and II events shall not lead to thermohydrodynamic instabilities.

Two specific types of flow instabilities are considered for Westinghouse PWR operation. These are the Ledinegg or flow excursion type of static instability and the density wave type of dynamic instability.

A Ledinegg instability involves a sudden change in flow rate from one steady state to another. This instability occurs (Boure et al., 1973) when the slope of the reactor coolant system pressure drop-flow rate curve ($\partial \Delta P \div \partial G_{internal}$) becomes algebraically smaller than the loop supply (pump head) pressure drop-flow rate curve ($\partial \Delta P \div \partial G_{external}$). The criterion for stability is thus ($\partial \Delta P \div \partial G_{internal}$) > ($\partial \Delta P \div \partial G_{external}$).

The Westinghouse pump head curve has a negative slope ($\partial \Delta P \div \partial G_{external}$) < 0 whereas the reactor coolant system pressure drop-flow curve has a positive slope ($\partial \Delta P \div \partial G_{internal}$) > 0 over the Condition I and Condition II operational ranges. Thus, the Ledinegg instability will not occur.

The mechanism of density wave oscillations in a heated channel has been described by Lahey and Moody (1977). Briefly, an inlet flow fluctuation produces an enthalpy perturbation. This perturbs the length and the pressure drop of the single phase region and causes quality or void perturbations in the two-phase regions which travel up the channel with the flow. The quality and length perturbations in the two-phase region create two-phase pressure drop perturbations. However, since the total pressure drop across the core is maintained by the characteristics of the fluid system external to the core, then the two-phase pressure drop perturbation feeds back to the single- phase region. These resulting perturbations can be either attenuated or self-sustained.

A simple method has been developed by Ishii (Saha et al., 1976) for parallel closed channel systems to evaluate whether a given condition is stable with respect to the density wave type of dynamic instability. This method had been used to assess the stability of typical Westinghouse reactor designs under Condition I and II operation. The results indicate that a large margin to density wave instability exists, e.g., increases on the order of 150 to 200 percent of rated reactor power would be required for the predicted inception of this type of instability.

The application of the method of Ishii (Saha et al., 1976) to Westinghouse reactor designs is conservative due to the parallel open channel feature of Westinghouse PWR cores. For such cores, there is little resistance to lateral flow leaving the flow channels of high power density. There is also energy transfer from channels of high power density to lower power density channels. This coupling with cooler channels has led to the opinion that an open channel configuration is more stable than the above closed channel analysis under the same boundary conditions. Flow stability tests (Kakac et al., 1974) have been conducted where the closed channel systems were shown to be less stable than when the same channels were cross connected at several locations. The cross connections were such that the resistance to channel cross flow and enthalpy perturbations would be greater than that which would exist in PWR core which has a relatively low resistance to cross flow.

Flow instabilities which have been observed have occurred almost exclusively in closed channel systems operating at low pressures relative to the Westinghouse PWR operating pressures. Kao, Morgan, and Parker (1973) analyzed parallel closed channel stability experiments simulating a reactor core flow. These experiments were conducted at pressures up to 2200 psia. The results showed that for flow and power levels typical of power reactor conditions, no flow oscillations could be induced above 1200 psia.

Additional evidence that flow instabilities do not adversely affect thermal margin is provided by the data from the rod bundle DNB tests. Many Westinghouse rod bundles have been tested over wide ranges of operating conditions with no evidence of premature DNB or of inconsistent data which might be indicative of flow instabilities in the rod bundle.

In summary, it is concluded that thermohydrodynamic instabilities will not occur under Condition I and II modes of operation for Westinghouse PWR reactor designs. A large power margin, greater than doubling rated power, exists to predicted inception of such instabilities. Analysis has been performed which shows that minor plant to plant differences in Westinghouse reactor designs, such as fuel assembly arrays, core power flow ratios, fuel assembly length, etc., will not result in gross deterioration of the above power margins.

4.4.4.7   Fuel Rod Behavior Effects from Coolant Flow Blockage

Coolant flow blockages can occur within the coolant channels of a fuel assembly or external to the reactor core. The effects of fuel assembly blockage within the assembly on fuel rod behavior are more pronounced than external blockages of the same magnitude. In both cases, the flow blockages cause local reductions in coolant flow. The amount of local flow reduction, where it occurs in the reactor, and how far along the flow stream the reduction persists, are considerations which will influence the fuel rod behavior. The effects of coolant flow blockages, in terms of maintaining rated core performance, are determined both by analytical and experimental methods. The experimental data are usually used to augment analytical tools such as computer programs similar to VIPRE-D. Inspection of the DNB correlation (Section 4.4.2.2 and Tong 1967) shows that the predicted DNBR is dependent upon the local values of quality and mass velocity.

The thermal hydraulic codes are capable of predicting the effects of local flow blockages on DNBR within the fuel assembly on a subchannel basis, regardless of where the flow blockage occurs. In WCAP-8054, it is shown that for a fuel assembly similar to the Westinghouse design, the flow distribution within the fuel assembly when the inlet nozzle is completely blocked can be accurately predicted. Full recovery of the flow was found to occur about 30 inches downstream of the blockage. With the reactor operating at the nominal full power conditions specified in Table 4.4-1, the effects of an increase in enthalpy and decrease in mass velocity in the lower portion of the fuel assembly would not result in the reactor reaching a minimum DNBR below the safety analysis limit.

From a review of the open literature, it is concluded that flow blockage in "open lattice cores" similar to the Westinghouse cores causes flow perturbations which are local to the blockage. For instance, Ohtsubo et al. (1972) show that the mean bundle velocity is approached asymptotically about 4 inches downstream from a flow blockage in a single flow cell. Similar results were also found for two and three cells completely blocked. Basmer et al. (1972) tested an open lattice fuel assembly in which 41 percent of the subchannels were completely blocked in the center of the test bundle between spacer grids. Their results show that the stagnant zone behind the flow blockage essentially disappears after 1.65 L/De or about 5 inches for their test bundle. They also found that leakage flow through the blockage tended to shorten the stagnant zone or, in essence, the complete recovery length. Thus, local flow blockages within a fuel assembly have little effect on subchannel enthalpy rise. The reduction in local mass velocity is then the main parameter which

affects the DNBR. If the plants were operating at full power and nominal steady state conditions, as specified in Table 4.4-1, a reduction in local mass velocity of approximately 50 percent would be required to reduce the DNBR from the nominal value to the safety analysis limit. The above mass velocity effect on the DNBR correlation was based on the assumption of fully developed flow along the full channel length.

In reality, a local flow blockage is expected to promote turbulence and thus would likely not affect DNBR at all.

Coolant flow blockages induce local cross flows, as well as promote turbulence. Fuel rod behavior is changed under the influence of a sufficiently high cross flow component. Fuel rod vibration could occur, caused by this cross flow component, through vortex shedding or turbulent mechanisms. If the cross flow velocity exceeds the limit established for fluid elastic stability, large amplitude whirling results. The limits for a controlled vibration mechanism are established from studies of vortex shedding and turbulent pressure fluctuations. The cross flow velocity required to exceed fluid elastic stability limits is dependent on the axial location of the blockage and the characterization of the cross flow (jet flow or not). These limits are greater than those for vibratory fuel rod wear. Cross flow velocity above the established limits can lead to mechanical wear of the fuel rods at the grid support locations. Fuel rod wear due to flow induced vibration is considered in the fuel rod fretting evaluation (Section 4.2).

4.4.5   TESTING AND VERIFICATION

4.4.5.1   Test Prior to Initial Criticality

A reactor coolant flow test is performed following fuel loading, but prior to initial criticality. Coolant loop pressure drop data are obtained in this test. These data, in conjunction with coolant pump performance information, allow determination of the coolant flow rates at reactor operating conditions. This test verifies that conservative coolant flow rate assumptions have been used in the core thermal and hydraulic analysis.

4.4.5.2   Initial Power and Plant Operation

Core power distribution measurements are made at several core power levels (Chapter 14). These tests are used to implicitly confirm the validity of the core design inputs in the safety analysis.

4.4.5.3   Component and Fuel Inspections

Inspections performed on the manufactured fuel are described in Section 4.2.4. Fabrication measurements critical to thermal and hydraulic analysis are obtained to verify that the engineering hot channel factors in the design analyses (Section 4.4.2.2.4) are met.

4.4.6   INSTRUMENTATION REQUIREMENTS

4.4.6.1   Incore Instrumentation

Instrumentation is located in the core so that by correlating movable neutron detector information with fixed thermocouple information, radial, axial, and azimuthal core characteristics may be obtained for all core quadrants.

The incore instrumentation system is comprised of thermocouples, which are positioned to measure fuel assembly coolant outlet temperatures at preselected positions and fission chamber detectors positioned in guide thimbles which run the length of selected fuel assemblies to measure the neutron flux distribution. Figure 4.4–10 shows the number and location of instrumented assemblies in the core. The core-exit thermocouples provide a backup to the flux monitoring instrumentation for monitoring power distribution. The routine, systematic, collection of thermocouple readings provides a data base. From this data base, abnormally high or abnormally low readings, quadrant temperature tilts, or systematic departures from a prior reference map can be deduced.

The movable incore neutron detector system would be used for more detailed mapping if the thermocouple system were to indicate an abnormality. These two complimentary systems are more useful when taken together than either system alone would be. The incore instrumentation system is described in more detail inSection 7.7.1.9.

The incore instrumentation is provided to obtain data from which fission power density distribution in the core, coolant enthalpy distribution in the core, and fuel burnup distribution may be determined.

4.4.6.2   Overtemperature and Overpower ΔT Instrumentation

The Overtemperature ΔT trip protects the core against low DNBR. The Overpower ΔT trip protects against excessive power (fuel rod rating protection).

As discussed in Section 7.2.1.1.2, factors included in establishing the Overtemperature ΔT and Overpower ΔT trip set points include the reactor coolant temperature in each loop and the axial distribution of core power through the use of the two section excore neutron detectors.

4.4.6.3   Instrumentation to Limit Maximum Power Output

The output of the three ranges (source, intermediate, and power) of detectors, with the electronics of the nuclear instruments, is used to limit the maximum power output of the reactor within their respective ranges.

There are six radial locations containing a total of eight neutron flux detectors installed around the reactor in the primary shield. Two proportional counters for the source range are installed on opposite "flat" portions of the core containing the primary startup sources at an elevation approximately one-quarter of the core height. Two compensated ionization chambers for the

intermediate range, located in the same instrument wells and detector assemblies as the source range detectors, are positioned at an elevation corresponding to one-half of the core height. Four dual section uncompensated ionization chamber assemblies for the power range are installed vertically in wells located within the reactor neutron shield tank and adjacent to the wall closest to the reactor vessel to minimize neutron flux pattern distortions. These wells are located at the four corners of the core and equidistant from the reactor vessel at all points. Each power range detector provides two signals corresponding to the neutron flux in the upper and in the lower sections of a core quadrant. The three ranges of detectors are used as inputs to monitor neutron flux from a completely shutdown condition to 120 percent of full power with the capability of recording overpower excursions up to 200 percent of full power.

The output of the power range channels is used for:

1.   The rod speed control function

2.   Alerting the operator to an excessive power imbalance between the quadrants

3.   Protecting the core against the consequences of rod ejection accidents

4.   Protecting the core against the consequences of adverse power distributions resulting from dropped rods.

Details of the neutron detectors and nuclear instrumentation design and the control and trip logic are given in Chapter 7. The limits on neutron flux operation and trip set points are given in the Technical Specifications.

4.4.6.4   Loose Parts Monitoring System

The Loose Parts Monitoring System (LPMS) is a system provided for the detection of loose metallic parts in the primary system during power operation modes. The LPMS, together with the associated programmatic procedures, comprise the Millstone 3 Loose Part Detection Program described in Regulatory Guide 1.133, Revision 1.

A detailed comparison of the LPMS with each specific positions of Section C of Regulatory Guide 1.133, Revision 1 is presented below:

Regulatory Guide Position	Discussion
C.1.a, C.1.b, and C.4.a	A total of twelve loose parts sensors are provided to detect loose parts impacts with a kinetic energy of 0.5 ft-lb of parts weighing between 0.25 pounds and 30 pounds in the vicinity of six natural collection areas
	1. Two sensors are located under the reactor vessel. Each sensor is stud-mounted to a clamp which is clamped to a thimble guide tube.
	2. Two sensors are located on the reactor vessel head. Each is stud-mounted to a reactor vessel head lifting lug.
	1. Two sensors are located under the reactor vessel. Each sensor is stud-mounted to a clamp which is clamped to a thimble guide tube.
	2. Two sensors are located on the reactor vessel head. Each is stud mounted to a reactor vessel head lifting lug.
	3. Two sensors are stud-mounted on each steam generator. Both sensors are located approximately in the same vertical plane equal distant above and below the steam generator tubesheet centerline.
C.1.c	Two independent sensors are provided at each natural collection region. Each of these channels is physically separated from each other at the sensors up to and including the charge preamplifiers. The output of the preamplifiers is routed by individual shielded cables through seismically qualified conduit and cable trays and a penetration transition box to a containment penetration.
C.1.d and C.1.e	The data acquisition system of the LPMS continuously compares the active channel's outputs with predetermined alarm setpoints and software algorithm and alerts the control room operators via an audible alarm when a potential loose part condition exists. All 12 channels' outputs are digitally recorded upon receiving an alarm condition for analysis.
C.1.f	The LPMS has the capability for periodic on-line channel checks and channel functional tests in addition to on-line and off-line channel calibration.
C.1.g	See Table 1.8-1.

Regulatory Guide Position	Discussion
C.1.h	The LPMS will be included in the Millstone surveillance and maintenance program. Any components that are not qualified for 40 years will be replaced prior to the end of their service life. Maintenance actions will be performed in accordance with approved procedures. The documented maintenance history results will be maintained and evaluated over the life of the plant.
C.1.i	Recognition of a faulty channel is easily identified with a CPU Trouble condition alarm. All instrument rack room electronics are rack-mounted, designed for the ease of replacement or repair in the event of a malfunctioning channel.
C.2 and C.4.e	The Alert Level setpoints were determined by simulating impact at locations with impact energies specified by the Regulatory Guide 1.133. These simulated impacts were compared to background amplitudes at various plant conditions to determine if the alarm circuitry can distinguish between the two levels. This is used to determine an alarm setpoint which will give an indication of an impact but will not cause excessive false alarms due to background noise.
C.3, C.4.b, and C.4.e	The procedures for performing channel check, channel functional test, and background noise measurements are available at the Millstone station. In the event an alert level is exceeded or if the weekly audio monitoring or quarterly measurements indicate the presence or possibility of a loose part, diagnostic steps will be taken within 72 hours to determine whether a loose part is present and its safety significance.
C.4.c	Anticipated major sources of external and internal noises are pump starts, reactor trips, and control rod stepping. The alarm is automatically bypassed during rod stepping.
C.4.d	Meeting the Regulatory Guide 1.133 criteria in position C.3, the acquisition of data is assured.
C.4.f	Functionality and surveillance requirements for the LPMS are included in the Technical Requirements Manual.
C.4.g	Millstone procedures provide a diagnostic program using information from other plant systems and operating history to confirm the presence of a loose part.

Regulatory Guide Position	**Discussion**
C.4.i	Radiation protection procedures have been developed to provide guidance and direction to station personnel for minimizing radiation exposure during maintenance, calibration, and diagnostics activities and are available at the Millstone station.
C.4.j	Millstone's non-licensed training program provides pertinent training for plant personnel involved with the system operation and maintenance. Loose part diagnosis is performed by an organization qualified to interpret loose part data.
C.4.k	The equipment inside containment has been demonstrated to be functional following an OBE.
C.6	If the presence of a loose part is confirmed and is evaluated to have safety significance, it will be reported to the NRC in accordance with 10 CFR 50.72.

4.4.6.5   Instrumentation for Detection of Inadequate Core Cooling

The ICC Monitoring System integrates the processing and display of:

1.   Subcooled/Superheat Monitor,

2.   Core Exit Thermocouples, and

3.   Reactor Vessel Level Monitoring (Heated Junction Thermocouple) (HJTC).

The information provided by this system allows the plant operators to monitor the reactor status during abnormal plant conditions. The operator uses this information to take corrective action as needed and/or confirm that actions taken produce the desired result. Thus, the approach to, existence of, and recovery from inadequate core cooling conditions can be monitored consistent with the requirements of NUREG 0737, Section II.F.2. The Millstone 3 ICC System is designed as Category 1 (Class IE) with redundant trains (Train A and Train B). Each train contains stand alone processing electronics and displays, which monitors, alarms, and trends ICC, as shown in Figure 4.4–11.

Subcooled/superheat monitors use RCS temperatures and pressures to calculate the degree of subcooling or superheat in the reactor coolant either in terms of temperature or pressure. The calculation is based upon the most conservative input temperature and pressures.

Core exit thermocouples (CET) are provided with required cold junction temperature compensation. All core exit temperatures are displayed on a digital panel meter, selectable from a switch panel.

4.4.6.5.1   CE-Heated Junction Thermocouple System

System Purpose

A typical small break LOCA illustrates the progression of an event which causes the approach to Inadequate Core Cooling. Figure 4.4–12 shows a representative behavior of reactor coolant level, reactor coolant system pressure, and core exit temperature vs. time after break. During the progression of the event, a variety of monitoring instruments must be available to properly inform the operator of the status of the nuclear system at any given time. C-E has determined that inadequate core cooling monitoring requirements can be met by appropriately measuring the displaying margin to saturation, reactor vessel water level above the core, and reactor core exit temperatures. In order to accomplish these functions, ICC utilizes three instruments: (1) the Subcooled Margin Monitor to measure saturation/superheat margin, (2) the Heated Junction Thermocouple (HJTC) System to monitor level/temperature in the region of the upper portion of the reactor vessel, and (3) Core Exit Thermocouples to measure the temperature of the reactor coolant as it leaves the reactor core.

It is the function of the HJTC System to monitor reactor coolant inventory during saturation conditions. The reactor coolant system is at saturation conditions until sufficient coolant is lost to uncover the top of the active core. During this interval, instrumentation to measure coolant inventory loss has not previously been available. The HJTC System provides measurement of the collapsed liquid level above the upper core alignment plate.

During these types of events the reactor coolant exists in a saturated two-phase mixture of liquid and voids. The HJTC System is designed with a shield to separate the voids from the liquid to give a more accurate indication of water inventory, defined as collapsed water level. The collapsed water level is obtained in all operating and accident conditions as indicated in Figure 4.4–12, including the recovery period when the reactor coolant has risen above the fuel alignment plate. Therefore, the HJTC System is designed to survive the high steam temperatures occurring during the preceding uncovery of the core.

The level range extends from the top of the vessel down to just above the upper core alignment plate. Based on a generic study done for Westinghouse plants, the response time is short enough to track the level during small break LOCA events. The resolution is sufficient to show the initial level drop, the key locations near the hot leg elevation, and the lowest levels just above the upper core alignment plate. This provides the operator with information to track the event and to detect the consequences of his mitigating actions or the functionality of automatic equipment.

The Heated Junction Thermocouple System (HJTCSP) is a reactor vessel measuring system that meets the NRC recommendations and requirements outlined in NUREG-0578. The HJTCSP monitors coolant inventory in the vessel region above the core. Redundant strings of heated junction thermocouples are arranged in the reactor vessel head area to provide indication of conditions at eight distinct levels. The system is a two-channel system, each consisting of a string of eight sensors.

The HJTCSP is provided by Combustion Engineering. Because the system requires access to the vessel, Westinghouse provides the hardware to implement its installation.

System Description

The overall system functional configuration is shown in Figure 4.4–13. As indicated in the figure, the system consists of two independent safety channels. Each channel consists of one probe assembly, signal processing equipment, and an operator interface. Probe assemblies are located in the upper core support structure of the reactor vessel. Signal processing equipment and operator interfaces are located outside of containment.

Probe Assemblies

The HJTC System measures reactor coolant liquid inventory with discrete HJTC sensors located at different levels within a separator tube running from the top of the core to the reactor vessel head. The basic principle of system operation is the detection of a temperature difference between adjacent heated and unheated thermocouples.

As pictured in Figures 4.4–14 and 4.4–15, the HJTC sensor consists of a Chromel-Alumel thermocouple near a heater (or heated junction) and another Chromel-Alumel thermocouple positioned away from the heater (or unheated junction). In a fluid with relatively good heat transfer properties, the temperature difference between the adjacent thermocouples is very small. In a fluid with relatively poor heat transfer properties, the temperature difference between the thermocouples is large.

Two design features are provided to improve operation of the HJTC System. First, each HJTC is shielded to avoid overcooling due to direct water contact during two-phase liquid conditions. The HJTC with the splash shield is referred to as the HJTC sensor (see Figure 4.4–15). Second, a string of HJTC sensors is enclosed in a tube that separates the liquid and gas phases that surround it.

The separator tube creates a collapsed liquid level that the HJTC sensors measure. The collapsed liquid level can be related to the average liquid fraction of the fluid in the reactor head volume above the fuel alignment plate. This mode of direct in-vessel sensing reduces spurious effects due to pressure, fluid properties, and non homogeneities of the fluid medium. The string of HJTC sensors and the separator tube are referred to as the HJTC probe assembly.

Signal Processing

The heated and unheated thermocouples in the HJTC are connected in such a way that absolute and differential temperature signals are available. This is shown in Figure 4.4–16. When water surrounds the thermocouples, their temperature and voltage outputs are approximately equal. $V_{(A-C)}$ on Figure 4.4–16 is, therefore, approximately zero. In the absence of liquid, the thermocouple temperature and output voltages become unequal, causing $V_{(A-C)}$ to rise.

The voltage output for each HJTC is processed by a microprocessor-based system performing the following signal processing, surveillance, and heater power control functions:

- Provides indication of the collapsed liquid level above the upper core alignment plate.

- Provides a level output signal.

- Provides temperature indications of coolant in the upper plenum.

- Provides test features for performing HJTCS operability and diagnostics.

- Provides on-line surveillance of HJTCS to assess operability.

- Provides control of heater voltage to minimize HJTC internal heating after uncovery.

Operator Interface

The HJTCS operator interface, located in each of the ICC cabinets, consists of an output indicator, and alarms output to the plant annunciator system. The level indication consists of a panel insert for a digital panel meter that is capable of displaying the percent level of the steam-water interface above the fuel alignment plate as indicated by the HJTC Probe assembly. The plant annunciator system alerts the operator that reactor vessel water level has decreased below a preset level when activated by HJTCS contact outputs.

Hardware Design

A diagram showing the HJTCS hardware configuration for a single channel is provided in Figure 4.4–17. The hardware consists of the following major components: (a) sensing equipment, (b) signal processing equipment, (c) heater power controllers, and (d) indicators.

Sensing Equipment

The HJTC System is composed of two channels of HJTC instruments. Each HJTC instrument channel is manufactured into a probe assembly consisting of eight (8) HJTC sensors, a seal plug, and electrical connectors (Figure 4.4–18). The eight (8) HJTC sensors are physically independent and located at eight levels from the reactor vessel head to the fuel alignment plate.

The probe assembly is housed in a stainless steel structure that protects the sensors from flow loads and serves as the guide path for the sensors. Figure 4.4–19 describes the locations of the HJTC probe assemblies.

Signal Processing Equipment

Signal processing is performed by a microprocessor system. The system also controls heater power and performs on-line surveillance to determine thermocouple opens and heater operability. The signal processor receives millivolt inputs from each of the eight (8) HJTCs. The device then

processes these inputs and provides the following outputs: (a) level and temperature signals to the panel insert, (b) a level signal output to the plant computer, (c) a signal to the plant annunciator system, (d) a signal to the heater controllers to modulate heater voltage after uncovery, and (e) signal to the subcooled margin calculator.

Heater Power Controllers

In each channel, a heater controller supplies power to the HJTC heaters. The heater controller is divided into two separate power supplies, each serving four (4) probe sensors.

Indicators

The outputs of the signal processor are sent to the Safety Parameter Display System (SPDS), which is a subset of the plant computer system. This information can be viewed on one of the control room or board mounted plant computer monitors. The control room or board mounted computer monitors will display percent level (head/plenum), provide for alarm indication, and upon operator request, can display the temperatures of each individual unheated thermocouple.

HJTC Probe Holder Support Tube

The probe holder support tubes provide the guidance and support for the HJTC probe assemblies. They are located in two (2) guide path shrouds.

The guide path shrouds are located in spare control rod drive mechanism (CRDM) Penetrations 22 and 26. The probe holder support tubes are attached to the interior of the guide path shroud structure that is conceptually identical to an existing Rod Cluster Control Guide Tube. The two (2) Probe Holder Assemblies (see Figure 4.4–19) consisting of the Guide Path Shroud and the probe holder are installed in the Upper Core Support Structure. This was accomplished by first removing a cover plate from the Upper Core Support Plate. The installed Probe Holder Assembly is held in place utilizing the bolting and locking arrangement employed in the original design of the Upper Core Support Structure. The Probe Holder Assembly in essence simply replaces the Rod Cluster Control Guide Tube and Rod Cluster Control Drive Shaft.

The Probe Holder Assemblies have been judiciously located remote from the outlet nozzles to reduce normal and postulated accident loadings on the Probe Holder. The Probe Holder is defined as an Internal Structure in accordance with ASME Boiler and Pressure Code Subsection NG requirements and is fabricated to adhere to these requirements.

Reactor Pressure Boundary Modifications

Modification of the reactor vessel head pressure boundary at two spare CRDM locations was required to form a penetration for each of the two HJTC probe assemblies. At the two locations selected for the HJTC probe assemblies, the pressure housing was cut and a section removed and replaced with new components containing a quick disconnect type flange and extension tube (see Figure 4.4–20). Provisions are made in the assembly to capture the probe within the flange and effect a pressure tight seal.

The design of the high pressure seal for each of the HJTC probes, consists of a Grayloc Assembly, Grafoil Packing Rings, and a Drive Nut. This high pressure seal assembly is located just above the Reactor Vessel Head Seismic Support Platform which provides ease of accessibility.

HJTC Handling Canister Design

The HJTC probe handling hardware configuration is shown on Figure 4.4–21. The Grayloc flange is disassembled and a protective bullet nose assembly is screwed onto the HJTC probe seal plug. The hub adapter is lowered over the bullet nose onto the Grayloc seal ring and secured (hand tight) using the Grayloc clamp assembly. The handling canister is then positioned over the bullet nose assembly and a cable is attached to the bullet nose assembly. The handling canister is then lowered over the bullet nose assembly with the weight of the handling canister supported by the overhead crane. The cable assembly supporting the HJTC Probe is then tied off to a lanyard attached to the canister. The winch at the base of the canister is removed with quick disconnect pins. The handling canister assembly, with the HJTC probe inside, is then removed to the storage area using the overhead crane. The operation is then repeated for the other HJTC probe location with a second handling canister. After the reactor vessel head has been reinstalled, the above procedure is reversed to reinsert the HJTC probes. Some of the specific features for the design of the handling hardware are as follows:

• The bottom zone of the canister contains sealed attenuating material such that exposure to personnel from the HJTC probe will be kept reasonably low. Estimated radiation levels are provided in Table 4.4-3.

• The attenuating material is encapsulated in stainless steel.

• A winch, attached to the base of the canister with quick release pins, is operated by one man. The man would be standing on a work platform above the control rod drive mechanism housings. (Work would be done in parallel with other normal head area work.)

• Modifications to the head lift rig or any head area components are not required for probe handling.

• The reactor head area/control rod drive mechanism area is left completely unencumbered and servicing of the drive mechanisms and underside of the head may be performed without increased personnel radiation exposure and without risk of damage to the probes.

• The weight of a handling canister is maintained at 1100 pounds, including the attenuating material.

• A support bracket is provided on the handling canister compatible with the storage location. The storage location is on the south wall of Steam Generator "B" Cubicle.

• A removable drop catcher is provided on the bottom of the handling canister to prevent water dripping while the canister is being transported from the reactor vessel to the storage area.

- A Hub Adapter is provided to protect the Grayloc seal ring surface and to pilot the lower end of the handling canister.

Equipment required to install the HJTCSP consists of (1) a probe holder shroud, (2) a modified thermal sleeve, and (3) an upper probe housing.

There are two probe holder shrouds located in the upper internals assembly and they are similar in design to control rod drive mechanism guide tubes. The shrouds support, vent, and shroud the CE HJTCSP probe and probe holder and minimize the coolant flow between the upper head and upper plenum inside the probe holder shroud assembly. The shroud consists of a lower and upper assembly that are bolted together. A probe holder, provided by CE, is inserted into the center of the probe holder shroud. The probe holder is held in place at two (2) points. At the bottom of the probe holder there is an interference fit between the shroud and the probe holder. At the top of the probe holder the probe holder is welded to the upper assembly of the shroud. The shroud, with the CE-supplied probe holder, is installed into the upper internals in a manner similar to the CRDM guide tubes.

The shroud is bolted to the upper support plate and has a support pin type arrangement at the bottom.

The modified thermal sleeve is similar to the other thermal sleeves attached to the Vessel Head. It is inserted into the CRDM housing of the Reactor Vessel closure head and has a guide thread on the bottom end. Its purpose is to aid during head insertion after a refueling operation and protect the probe from flows in the upper head region.

The upper probe housing consists of a tube with a CRDM housing adapter welded on one end and a Grayloc butt weld hub (provided by CE) on the other end. The adapter can be threaded onto the CRDM housing and seal-welded. The upper probe housing is part of the primary pressure boundary and extends from just above the seismic support platform to the reactor vessel head. The upper probe housing provides the HJTCSP access into the vessel.

Each ICC cabinet (Train A and B) has a qualified Class IE display system that includes the following ICC information.

- Subcooled/superheat in °F (300°F subcooling to 45°F superheat).
- Core exit temperatures (200°F to 2300°F).
- Percent level in the plenum and head areas.

The primary means of displaying all the ICC information is provided via the safety parameter display system (SPDS). SPDS receives all the ICC transmitted data with optical isolation provided by ICC. SPDS has the capability to calculate subcooling/superheat based on primary coolant temperatures, T_{hot}, T_{cold}, CET, unheated junction temperatures of HJTC, and RCS pressure. Signal validation techniques are utilized in the SPDS to ensure the quality of the input variables. SPDS displays are designed to incorporate accepted human factors principles so that the displayed ICC information can be readily perceived and understood by plant operators during normal and abnormal plant conditions.

Alarms are provided on main control boards from the ICC cabinets. There are four alarms, saturation/superheat trouble alarm, CET high alarm, plenum percent level alarm, and head percent level alarm.

4.4.7   REFERENCES FOR SECTION 4.4

4.4-1   Ainscough, J. B. and Wheeler, M. J. 1968. Thermal Diffusivity and Thermal Conductivity of Sintered Uranium Dioxide. In: Proceedings of the Seventh Conference of Thermal Conductivity, p 467, National Bureau of Standards, Washington, D.C.

4.4-2   Asamoto, R. R.; Anselin, F. L.; and Conti, A. E. 1968. The Effect of Density on the Thermal Conductivity of Uranium Dioxide. GEAP-5493.

4.4-3   ASME OMa-S/G-1991 Addenda to ASME OM-S/G-1990 Standards and Guides for Operation and Maintenance of Nuclear Power Plants, Part 12.

4.4-4   Bain, A. S. 1962. The Heat Rating Required to Produce Center Melting in Various UO_2 Fuels. ASTM Special Technical Publication, Number 306, p 30-46, Philadelphia, Penn.

4.4-5   Basmer, P.; Kirsh, D.; and Schultheiss, G. F. 1972. Investigation of the Flow Pattern in the Recirculation Zone Downstream of Local Coolant Blockages in Pin Bundles. Atomwirtschaft, 17, Number 8, 416-417 (In German).

4.4-6   Berlinger, C. (NRC) 1986. Letter to Rahe, Jr., E. P. (Westinghouse). Request for Reduction in Fuel Assembly Burnup Limit for Calculation of Maximum Rod Bow Penalty.

4.4-7   Boure, J. A.; Bergles, A. E.; and Tong, L. S. 1973. Review of Two-Phase Flow Instability. Nuclear Engineering Design 25, p 165-192.

4.4-8   Bush, A. J. 1965. Apparatus for Measuring Thermal Conductivity to 2500°C. Westinghouse Research Laboratories Report 64-1P6-401-43 (Proprietary).

4.4-9   Byron/Braidwood FSAR, Docket No. 50-456.

4.4-10 Clough, D.J. and Sayers, J. B. 1964. The Measurement of the Thermal Conductivity of UO_2 Under Irradiation in the Temperature Range 150°−1600°C. AERE-R-4690, UKAEA Research Group, Harwell.

4.4-11 Cohen, I.; Lustman, B.; and Eichenberg, D. 1960. Measurement of the Thermal Conductivity of Metal-clad Uranium Oxide Rods during Irradiation. WAPD-228.

4.4-12 Coplin, D. H. et al., 1968. The Thermal Conductivity of UO_2 by Direct In-reactor Measurements. GEAP-5100-6.

4.4-13 Daniel, J. L.; Matolich, Jr., J.; and Deem, H. W. 1962. Thermal Conductivity of UO_2. HW-69945.

4.4-14 Devold, I. 1968. A Study of the Temperature Distribution in UO_2 Reactor Fuel Elements. AE-318, Aktiebolaget Atomenergi, Stockholm, Sweden.

4.4-15 Dittus, F. W. and Boelter, L. M. K. 1930. Heat Transfer in Automobile Radiators of the Tubular Type. Calif. Univ. Publication in Eng., 2, No. 13, 443461.

4.4-16 Duncan, R. N. 1962. Rabbit Capsule Irradiation of UO_2. CVTR Project, CVNA-142.

4.4-17 Feith, A. D. 1962. Thermal Conductivity of UO_2 by a Radial Heat Flow Method. TID-21668.

4.4-18 Godfrey, T. G.; Fulkerson, W.; Killie, T. G.; Moore, J. P.; and McElroy, D. L. 1964. Thermal Conductivity of Uranium Dioxide and Armco Iron by an Improved Radial Heat Flow Technique. ORNL-3556.

4.4-19 Gonzalez-Santalo, J. M. and Griffith, P. Two-phase Flow Mixing in Rod Bundle Subchannels. ASME Paper 72-WA/NE-19.

4.4-20 Griffith, P.; Clark, J. A.; and Rohsenow, W. M. Void Volumes in Subcooled Boiling Systems. AMSE Paper No. 58-HT-19.

4.4-21 Gyllander, J. A. 1971. In-pile Determination of the Thermal Conductivity of UO_2 in the Range 500-2500°C. AE-411.

4.4-22 Hetsroni, G. 1965. Studies of the Connecticut-Yankee Hydraulic Model. NYO-3252-2.

4.4-23 Howard, V. C. and Gulvin, T. G. 1960. Thermal Conductivity Determinations on Uranium Dioxide by a Radial Flow Method. UKAEA IG- Report 51.

4.4-24 Idel'chik, I. E. 1960. Handbook of Hydraulic Resistance. AEC-TR-6630.

4.4-25 International Atomic Energy Agency 1966. Thermal Conductivity of Uranium Dioxide. Report of the Panel Held in Vienna, April 1965, IAEA Technical Reports Series, Number 59, Vienna, The Agency, 1966.

4.4-26 Kakac, S.; Veziroglu, T. N.; Akyuzlu, K.; and Berkol, O. 1974. Sustained and Transient Boiling Flow Instabilities in a Cross-Connected Four-Parallel-Channel Upflow System. Proc. of 5th International Heat Transfer Conference, Tokyo, September 3-7, 1974.

4.4-27 Kao, H. S.; Morgan, T. D.; and Parker, W. B. 1973. Prediction of Flow Oscillation in Reactor Core Channel. Trans. ANS, Vol. 16, 1973, p 212-213.

4.4-28　Kjaerheim, G. and Rolstad, E. 1967. In-pile Determination of UO_2 Thermal Conductivity, Density Effects and Gap Conductance. HPR-80.

4.4-29　Kjaerheim, G. 1969. In-pile Measurements of Centre Fuel Temperatures and Thermal Conductivity Determination of Oxide Fuels. Paper IFA-175, presented at the European Atomic Energy Society Symposium on Performance Experience of Water-Cooled Power Reactor Fuel, Stockholm, Sweden, October 21-22, 1969.

4.4-30　Kruger, O. L. 1968. Heat Transfer Properties of Uranium and Plutonium Dioxide. Paper 11-N-68F, presented at the Fall Meeting of Nuclear Division of the American Ceramic Society, Pittsburgh, Penn.

4.4-31　Lahey, R. T. and Moody, F. J. 1977. The Thermal Hydraulics of a Boiling Water Reactor. American Nuclear Society.

4.4-32　Lucks, C. F. and Deem, H. W. 1961. Thermal Conductivity and Electrical Conductivity of UO_2. In: Progress Reports Relating to Civilian Applications, BMI-1448 (Rev) for June 1960; BMI-1489 (Rev) for December 1960; and BMI-1518 (Rev) for May 1961.

4.4-33　Lyons, M. F. et al., 1966. UO_2 Powder and Pellet Thermal Conductivity During Irradiation. GEAP-5100-1.

4.4-34　Moody, L. F. 1944. Friction Factors for Pipe Flow. Transaction of the American Society of Mechanical Engineers, 66, 671-684.

4.4-35　Nelson, R. C.; Coplin, D. H.; Lyons, M. F.; and Weidenbaum, B. 1964. Fission Gas Release from UO_2 Fuel Rods with Gross Central Melting. GEAP-4572.

4.4-36　Nishijima, T.; Kawada, T.; and Ishihata, A. 1965. Thermal Conductivity of Sintered UO_2 and $A1_2O_3$ at High Temperatures. J. American Ceramic Society, 48, 31 34.

4.4-37　Ohtsubo, A. and Urawashi, S. 1972. Stagnant Fluid due to Local Flow Blockage. J. Nuclear. Science Technology, 9 No. 7, 433-434.

4.4-38　Rowe, D. S. and Angle, C. W. 1967. Crossflow Mixing between Parallel Flow Channels during Boiling, Part II Measurements of Flow and Enthalpy in Two Parallel Channels. BNWL-371, Part 2.

4.4-39　Rowe, D. S. and Angle, C. W. 1969. Crossflow Mixing between Parallel Flow Channels during Boiling, Part III Effect of Spacers on Mixing between Two Channels. BNWL-371, Part 3.

4.4-40　Saha, P.; Ishii, M.; and Zuber, N. 1976. An Experimental Investigation of the Thermally Induced Flow Oscillations in Two-Phase Systems. J. of Heat Transfer, p 616-612.

4.4-41 Stora, J. P. 1970. In-reactor Measurements of the Integrated Thermal Conductivity of UO_2 - Effect of Porosity. Trans. ANS, 13, 137-138.

4.4-42 Stora, J. P.; Debernardy, DeSigoyer, B.; Delmas, R.; Deschamps, P.; Ringot, C.; and Lavaud, B. 1964. Thermal Conductivity of Sintered Uranium Oxide under In–pile Conditions. EURAEC-1095.

4.4-43 South Texas FSAR, Docket No. 50-498.

4.4-44 Deleted

4.4-45 Thom, J. R. S.; Walker, W. M.; Fallon, T. A.; and Reising, G. F. S. 1965-66. Boiling in Subcooled Water during Flowup Heated Tubes or Annuli. Prc. Instn. Mech. Engrs., 180, Pt. C, 226-46.

4.4-46 Tong, L. S. 1967. Prediction of Departure from Nucleate Boiling for an Axially Nonuniform Heat Flux Distribution. J. Nuclear Energy, 21, 241-248.

4.4-47 Tong, L. S. 1972. Boiling Crisis and Critical Heat Flux. AEC Critical Review Series, TID-25887.

4.4-48 Virgil C. Summer FSAR, Docket No. 50-395.

4.4-49 Vogt, J.; Grandell, L.; and Runfors, U. 1964. Determination of the Thermal Conductivity of Unirradiated Uranium Dioxide. AB Atomenergi Report RMB-527, 1964, Quoted by IAES Technical Report Series No. 59, "Thermal Conductivity of Uranium Dioxide."

4.4-50 Weisman, J. 1959. Heat Transfer to Water Flowing Parallel to Tube Bundles. Nuclear Science Engineering, 6,78-79. 26.45.

4.4-51 WCAP-2923, 1966, Balfour, M. G.; Christensen, J. A.; and Ferrari, H. M. "Inpile Measurement of UO_2 Thermal Conductivity."

4.4-52 WCAP-3269-8, 1964, Hetsroni, G., "Hydraulic Tests of San Onofre Reactor Model."

4.4-53 WCAP-3385-56, 1970, Nodvick, R. J., "Saxton Core II Fuel Performance Evaluation. Part, II, Evaluation of Mass Spectrometric and Radio- Chemical Analyses of Irradiated Saxton Plutonium Fuel."

4.4-54 WCAP-6065, 1965, Christensen, J. A.; Allio, R.J.; and Biancheria, A., "Melting Point of Irradiated UO_2."

4.4-55 WCAP-6069, 1965, Poncelet, C. G., "Burnup Physics of Heterogeneous Reactor Lattices."

4.4-56 WCAP-7667-P-A (Proprietary) and WCAP-7755-A (Non-proprietary), January 1975, Cadek, F. F., "Interchannel Thermal Mixing with Mixing Vane Grids."

4.4-57 WCAP-7912-P-A (Proprietary) and WCAP-7912-A (Non-proprietary), January 1975, 'McFarlane, A. F. Power Peaking Factors."

4.4-58 WCAP-7941-P-A (Proprietary) and WCAP-7959-A (Non-proprietary), 1975, Cadek, F. F., et al.," Effect of Axial Spacing on Interchannel Thermal Mixing with the R Mixing Vane Grid."

4.4-59 WCAP-8054-P-A (Proprietary) and WCAP-8195-a (Non-proprietary), February 1989, Hochreiter, L. E. "Application of the THINC-IV Program to PWR Design."

4.4-60 WCAP-8174-P-A (Proprietary) and WCAP-8202-A (Non-proprietary), February 1975, Hill, K. W.; Motley, F. E.; and Cadek, F. F., "Effect of Local Heat Flux Spikes on DNB in Non-uniformly Heated Rod Bundles."

4.4-61 WCAP-8218-P-A (Proprietary) and WCAP-8219-A (Non-proprietary), March 1975, Hellman, J. M. (Ed.) "Fuel Densification Experimental Results and Model for Reactor Application."

4.4-62 WCAP-8296-P-A (Westinghouse Proprietary) and WCAP-8297 (Non- proprietary), 1975, Hill, K. W.; Motley, F. E.; Cadek, F. F.; and Wenzel, A. H., "Effect of 17 x 17 Fuel Assembly Geometry on DNB."

4.4-63 WCAP-8298-P-A (Proprietary) and WCAP-8299-A (Non-proprietary), 1975, Motley, F. E.; Wenzel, A. H.; and Cadek, F. F., "The Effect of 17 x 17 Fuel Assembly Geometry on Interchannel Thermal Mixing."

4.4-64 Deleted by MP3-UCR-2014-013.

4.4-65 WCAP-8691, Revision 1 (Proprietary) and WCAP-8692, Revision 1 (Non-proprietary), July 1979, Skaritka, J., (Ed.), "Fuel Rod Bow Evaluation"

4.4-66 WCAP-10851-P-A (Proprietary) and WCAP-11873-A (Non-proprietary) August 1988, Weiner, R. A. et al.," Improved Fuel Performance Models for Westinghouse Fuel Rod Design and Safety Evaluations.'

4.4-67 Deleted

4.4-68 Kitchen, T. J., "Generic Safety Evaluation for 17x17 Standard Robust Fuel Assembly (17x17 STD RFA)," SECL-98-056, Revision 0, September 30, 1998.

4.4-69 Deleted (PKG FSC MP3-UCR-2013-005)

4.4-70   WCAP-15025-P-A, April 1999, Smith, L.D.III, et al., "Modified WRB-2 Correlation, WRB-2M, for Predicting Critical Heat Flux in 17x17 Rod Bundles with Modified LPD Mixing Vane Grids."

4.4-71   Delete

4.4-72   WCAP-14565-P-A, October 1999, Suny, Y., et al., "VIPRE-01 Modeling and Qualification for Pressurized Water Reactor Non-LOCA Thermal-Hydraulic Safety Analysis."

4.4-73   WCAP-13589-A, March 1995, Kersting, P. J., et al., "Assessment of Clad Flattening and Densification Power Spike Factor Elimination in Westinghouse Nuclear Fuel."

4.4-74   WCAP-15063-P-A, Revision 1, July 2000, Slagle, W. H., et al., "Westinghouse Improved Performance Analysis and Design Model (PAD 4.0)."

4.4-75   Stewart, C. W., et al., "VIPRE-01: A Thermal-Hydraulic Code for Reactor Cores," Volume 1 - 3 (Revision 3, August 1989), Volume 4 (April 1987), NP-2511-CCMA, Electric Power Research Institute.

4.4-76   Delete

4.4-77   Delete

4.4-78   DOM-NAF-2-P-A, Revision 0, Minion Revision 3, "Reactor Core Thermal-Hydraulics Using the VIPRE-D Computer Code," September 2014.

4.4-79   VEP-NE-2-1, "Statistical DNBR Evaluation Methodology," June 1987.

TABLE 4.4-1 THERMAL AND HYDRAULIC DESIGN PARAMETERS [1]

Thermal and Hydraulic Design Parameters

Reactor Core Heat Output, MWt	3709[5]
Reactor Core Heat Output, 10^6 Btu/hr	12,656[5]
Heat Generated in Fuel, %	97.4
System Pressure, Nominal, psia	2,250
Radial Power Distribution [2]	1.65 [1 + 0.3 (1 - P)]

HFP Nominal Coolant Conditions

Vessel Thermal Design Flow Rate (Including Bypass), 10^6 lbm/hr	135.5
Vessel Thermal Design Flow Rate (Including Bypass), gpm	363,200

Core Flow Rate [3] (Excluding Bypass, Based on TDF):

10^6 lbm/hr	123.9
gpm	331,965

Core Flow Area, square feet:

RFA/RFA-2 (for full core of RFA/RFA-2 fuel)	51.1

Core Inlet Mass Velocity 10^6 lbm/hr, ft^2 (Based on TDF):

RFA/RFA-2 (for full core of RFA/RFA-2 fuel)	2.42
Pressure Drop Across Core (psi) [4]	21.6 +/- 2.2
Nominal Vessel/Core Inlet Temperature, for TDF °F	555.8
Vessel Average Temperature, °F	589.5
Core Average Temperature, °F	594.7
Vessel Outlet Temperature, °F	623.2
Average Temperature Rise in Vessel °F	67.4
Average Temperature Rise in Core °F	72.9

Heat Transfer

Active Heat Transfer Surface Area, ft^2:

    (RFA/RFA-2)   59,700

Average Heat Flux, Btu/hr, ft^2:

    (RFA/RFA-2)   206,500

Average Linear Power, kW/ft   5.92

Peak Linear Power for Normal Operation, [5] kW/ft   15.09

Temperature at Peak Linear Power for Prevention of Centerline Melt, °F   4700

(1)   1.65 represents the value of $F^N_{\Delta H}$ used in deterministic Safety Analysis. The $F^N_{\Delta H}$ surveillance limit at Rated Thermal Power is specified in the COLR as 1.586. Statistical DNB analyses use an $F^N_{\Delta H}$ of 1.587.

(2)   Based on design bypass flow of 8.6% without thimble plug assemblies.

(3)   Based on best estimate flow and thimble plugs removed.

(4)   Based on maximum F_Q of 2.548.

(5)   Thermal-hydraulic analyses considered core heat output of 3712 MWt. This bounds the actual operating power for Millstone Unit 3 (3709 MWt).

TABLE 4.4-2 VOID FRACTIONS AT NOMINAL REACTOR CONDITIONS WITH DESIGN HOT CHANNEL FACTORS

	Average	Maximum
Core (% void)	0.0	--
Hot subchannel (% void)	≤ 2.6	≤ 9.1

TABLE 4.4-3 RADIATION LEVELS FROM HJTC PROBE (R/HR)

	Dose Rates		
	Crud Contribution	**Activation Contribution**	**Total**
Surface of Canister Zone A	.0007-.02	+.20	= 0.22
Surface of Canister Zone B	.007-.25	+0	= 0.25
Surface of Canister Zone C	.07-2.5	+0	= 2.5
1 Foot From Surface Zone A	Insignificant	+.05	= 0.05
1 Foot From Surface Zone B	.125	+0	= 0.125
1 Foot From Surface Zone C	.5-1.25	+0	= 0.51-1.25

NOTES:

See Figure 4.4–21 for definition of zones.

Worker dose in Shielded Zone for ten minutes $= \dfrac{10}{60}(.125R/\text{hr}) = \begin{array}{l} .021\text{R} \\ 21mR \end{array}$

TABLE 4.4-4 DNB LIMITS FOR WESTINGHOUSE 17X17 RFA-2 FUEL

Correlation	Limit Type	Limit Value
WRB-2M	DDL	1.14
	SDL	1.23
	SAL	1.45
WLOP	DDL	1.22
	SAL	1.45
ABB-NV	DDL	1.14
	SDL	1.19
	SAL	1.45

FIGURE 4.4–1 DELETED BY FSARCR PKG FSC 07-MP3-040

FIGURE 4.4-2 TDS VERSUS REYNOLDS NUMBER FOR 26 INCH GRID SPACING
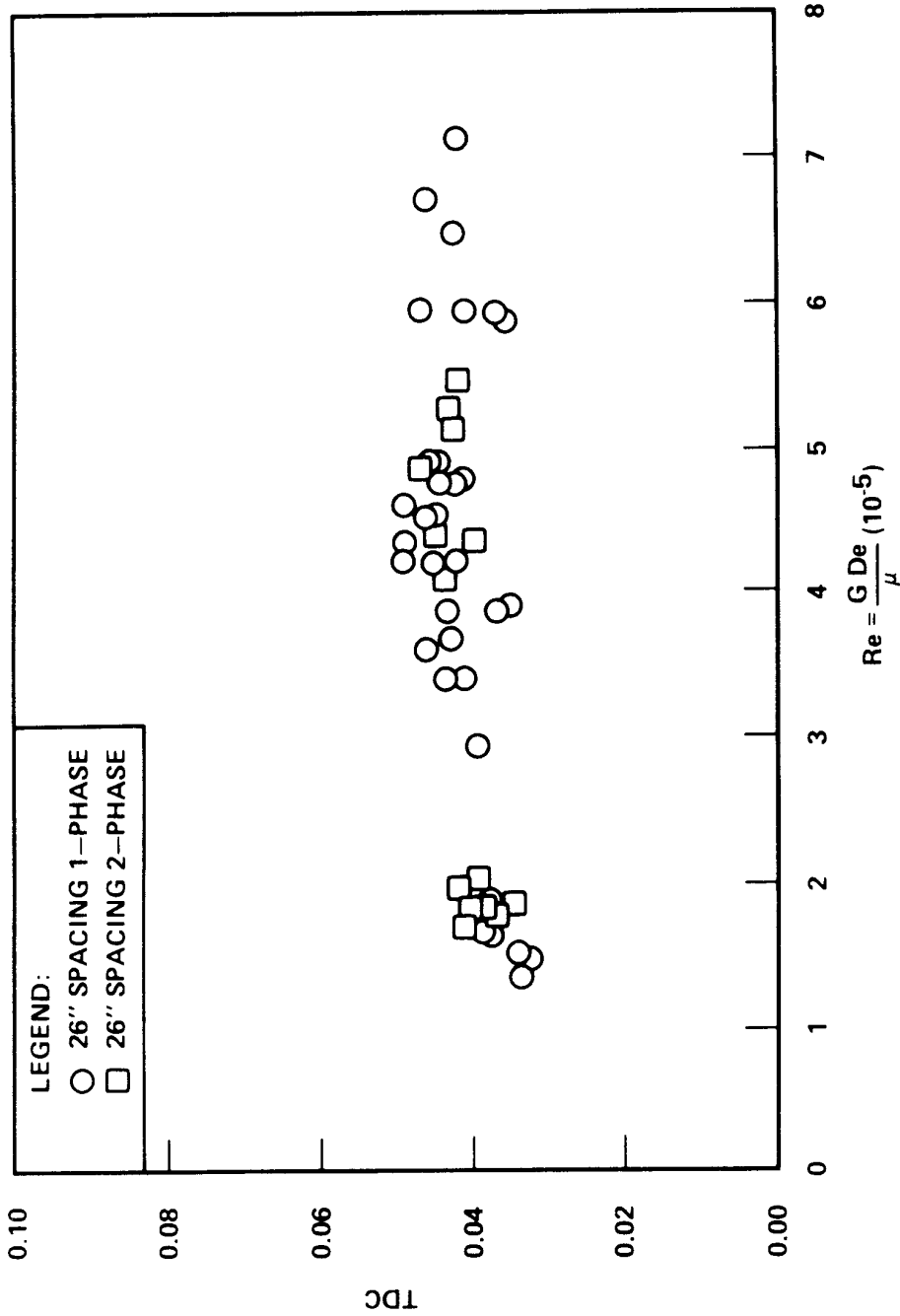
FIGURE 4.4–3 TYPICAL NORMALIZED RADIAL FLOW AND ENTHALPY DISTRIBUTION AT 4 FOOT ELEVATION

KEY
$\Delta h / \Delta \bar{h}$
$G / \bar{G}$

1.090 / 0.999							
0.968 / 1.001	1.094 / 0.999						
1.099 / 0.999	0.977 / 1.001	1.104 / 0.999					
0.987 / 1.001	1.111 / 0.999	0.988 / 1.001	1.121 / 0.999				
1.141 / 0.998	1.005 / 1.000	1.119 / 0.999	0.998 / 1.000	1.227 / 0.997			
1.086 / 0.999	1.156 / 0.998	0.996 / 1.000	1.087 / 0.999	0.910 / 1.001	1.038 / 1.000		
1.139 / 0.998	1.076 / 0.999	1.093 / 0.999	0.939 / 1.001	0.861 / 1.001	0.556 / 1.003		
0.895 / 1.001	0.936 / 1.001	0.907 / 1.001	0.636 / 1.003				

FOR RADIAL POWER DISTRIBUTION NEAR BEGINNING OF LIFE

CALCULATED $F_{\Delta H}^{N} = 1.36$

FIGURE 4.4–4 TYPICAL NORMALIZED RADIAL FLOW AND ENTHALPY DISTRIBUTION AT 8 FOOT ELEVATION

1.091 / 0.997							KEY: Δh/Δh̄ G/Ḡ
0.968 / 1.001	1.095 / 0.997						
1.100 / 0.997	0.977 / 1.001	1.105 / 0.997					
0.987 / 1.000	1.112 / 0.996	0.988 / 1.000	1.123 / 0.996				
1.144 / 0.994	1.005 / 1.000	1.121 / 0.996	0.999 / 1.000	1.231 / 0.988			
1.087 / 0.998	1.159 / 0.993	0.997 / 1.000	1.088 / 0.998	0.911 / 1.003	1.038 / 1.000		
1.142 / 0.994	1.077 / 0.998	1.095 / 0.998	0.939 / 1.002	0.859 / 1.005	0.555 / 1.015		
0.894 / 1.003	0.936 / 1.002	0.906 / 1.003	0.634 / 1.013				

KEY: $\Delta h / \Delta \bar{h}$, $G / \bar{G}$

FOR RADIAL POWER DISTRIBUTION NEAR BEGINNING OF LIFE

CALCULATED $F_{\Delta H}^{N} = 1.36$

FIGURE 4.4–5 TYPICAL NORMALIZED RADIAL FLOW AND ENTHALPY DISTRIBUTION AT 12 FOOT ELEVATION-CORE EXIT

KEY:
Δh/Δh̄
G/Ḡ

1.091 0.995							KEY: Δh/Δh̄ G/Ḡ
0.968 1.002	1.095 0.995						
1.101 0.994	0.977 1.001	1.106 0.994					
0.987 1.001	1.113 0.994	0.988 1.001	1.124 0.993				
1.145 0.992	1.006 1.000	1.122 0.993	0.999 1.000	1.233 0.987			
1.088 0.995	1.160 0.991	0.997 1.000	1.088 0.995	0.911 1.004	1.037 0.998		
1.143 0.992	1.078 0.996	1.095 0.995	0.939 1.003	0.859 1.008	0.557 1.026		
0.894 1.006	0.936 1.003	0.906 1.005	0.634 1.021				

FOR RADIAL POWER DISTRIBUTION NEAR BEGINNING OF LIFE

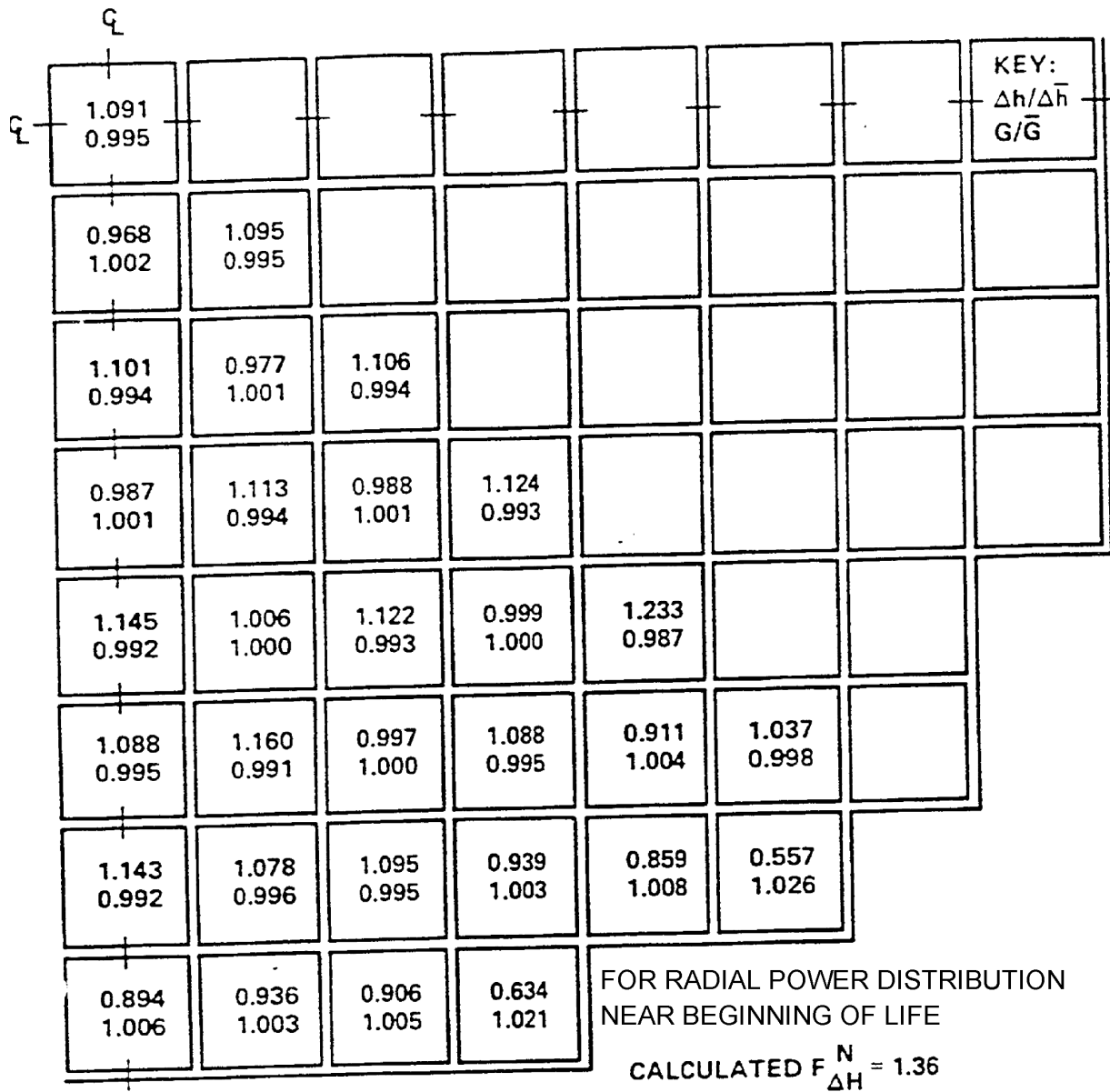CALCULATED $F_{\Delta H}^{N} = 1.36$

FIGURE 4.4–6 DELETED BY FSARCR PKG FSC 07-MP3-040

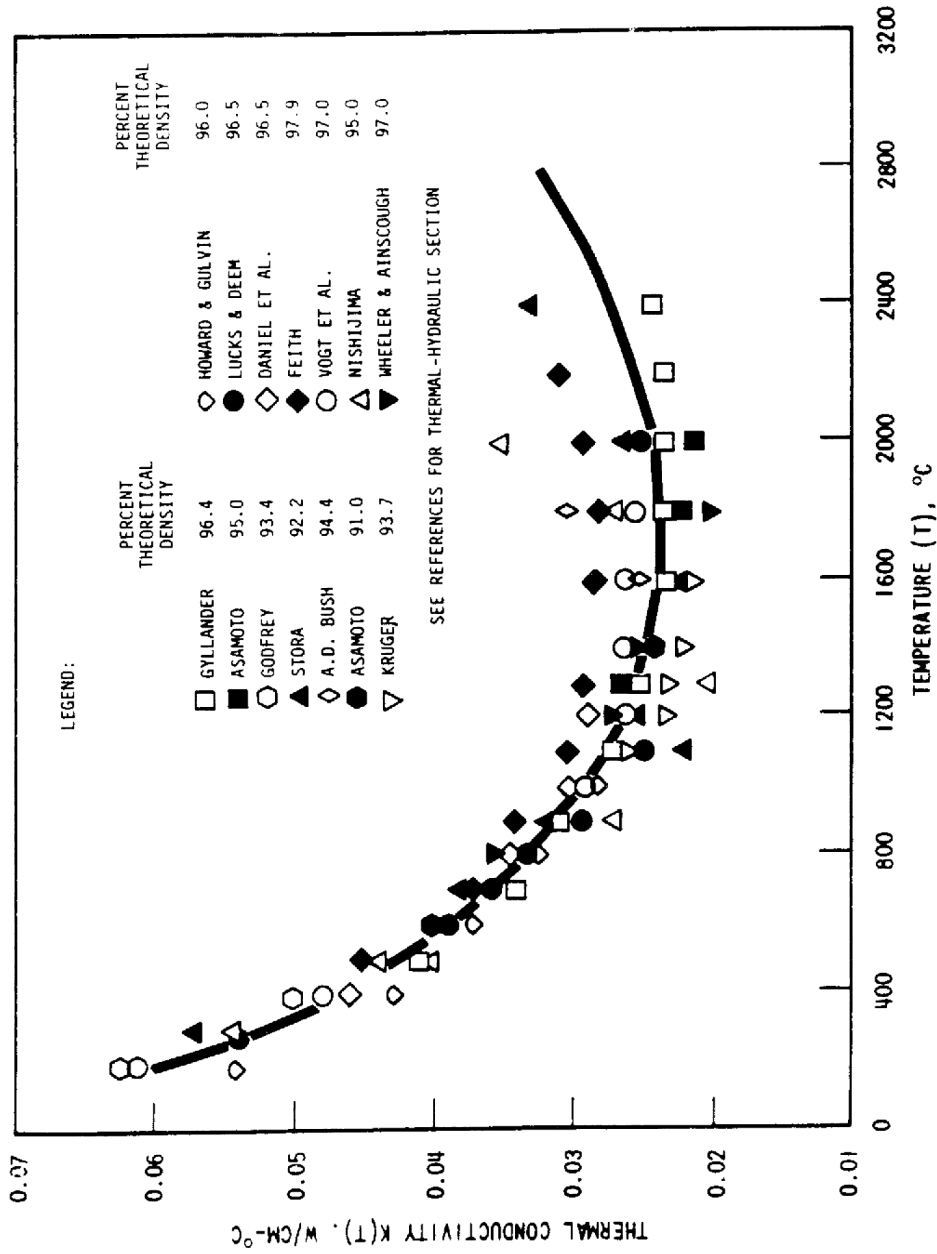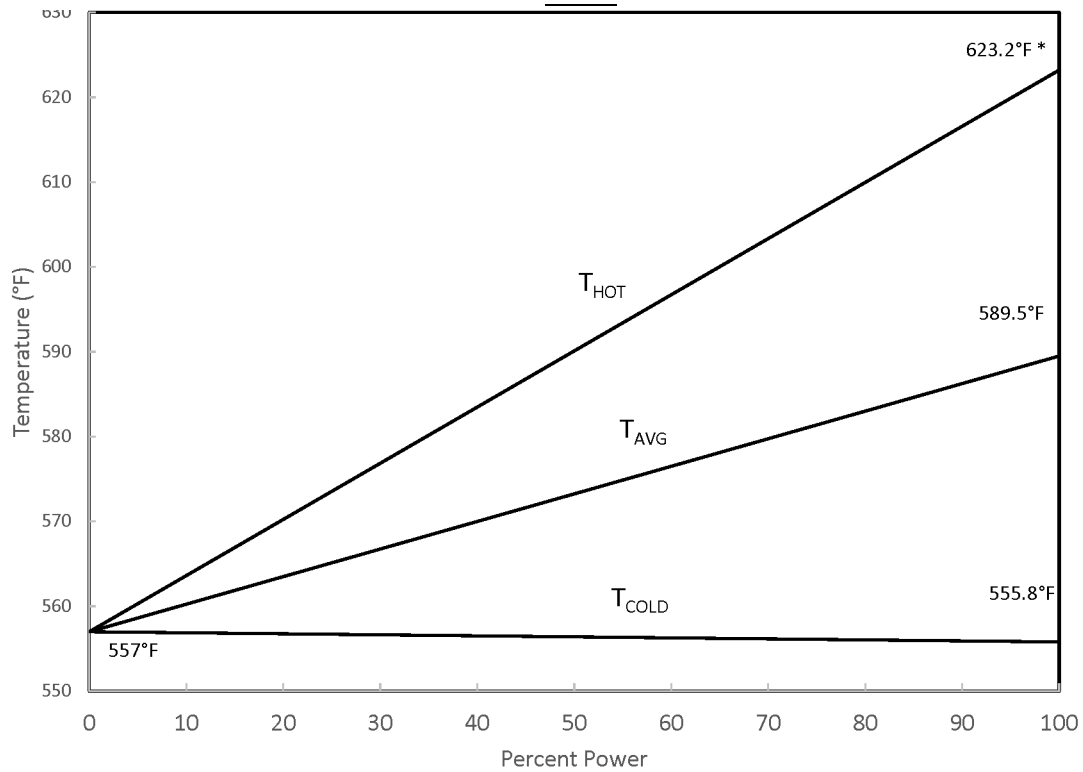FIGURE 4.4-7 THERMAL CONDUCTIVITY OF UO2 (DATA CORRECTED TO 95 PERCENT THEORETICAL DENSITY)

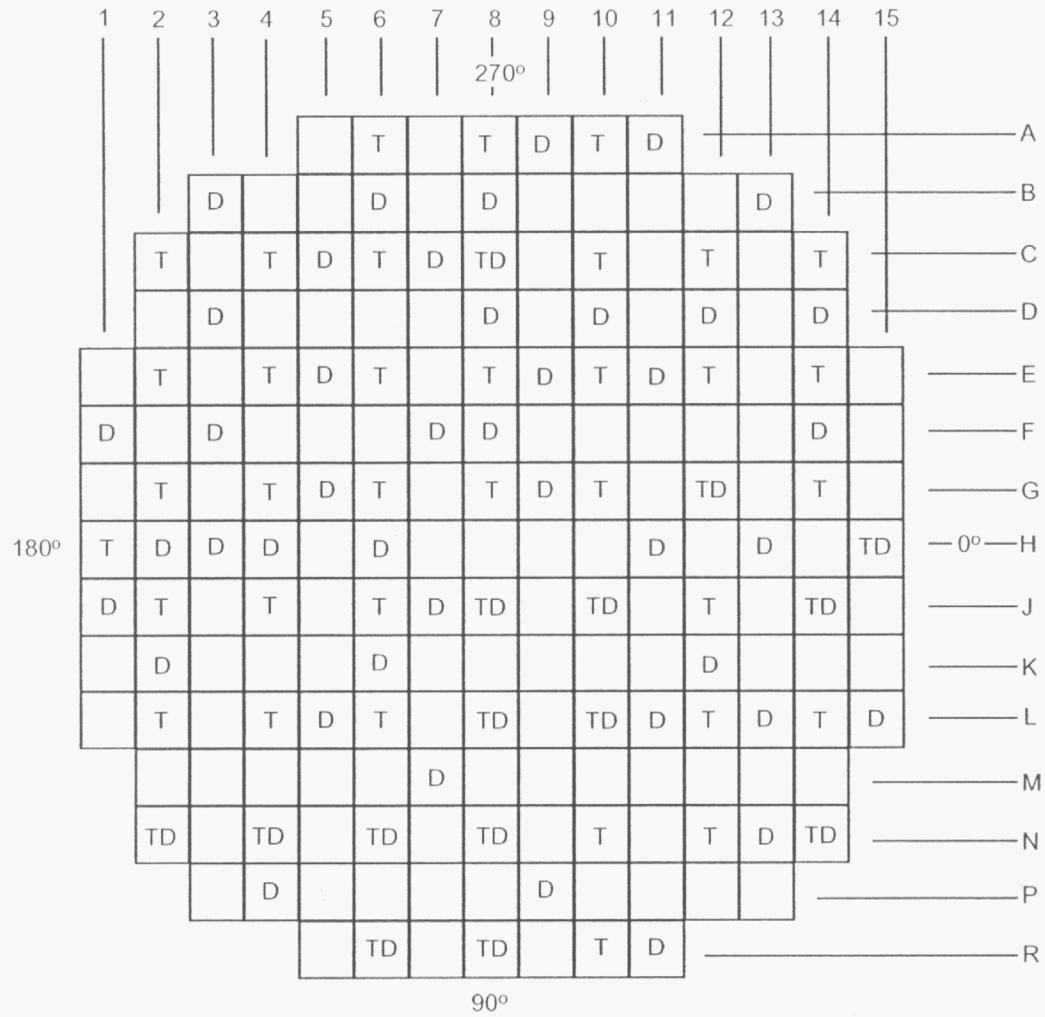## FIGURE 4.4–8 REACTOR COOLANT SYSTEM TEMPERATURE-PERCENT POWER MAP

*Millstone Unit 3 is limited to a Thot of 622.6°F. T_{avg} and Tcold values would be adjusted accordingly to maintain the rated power level of 3709 MWt. The values in this figure are retained to represent conditions at the high end of the T_{avg} operating window.

FIGURE 4.4–9 NOT USED

FIGURE 4.4–10 DISTRIBUTION OF INCORE INSTRUMENTATION

	1	2	3	4	5	6	7	8	9	10	11	12	13	14	15
A						T		T	D	T	D				
B		D				D		D					D		
C		T		T	D	T	D	TD		T		T		T	
D		D						D		D		D		D	
E		T		T	D	T		T	D	T	D	T		T	
F	D		D					D	D					D	
G		T		T	D	T		T	D	T		TD		T	
H	T	D	D	D		D				D		D		TD	
J	D	T		T		T	D	TD		TD		T		TD	
K		D				D						D			
L		T		T	D	T		TD		TD	D	T	D	T	D
M							D								
N		TD		TD		TD		TD		T		T	D	TD	
P			D						D						
R						TD		TD		T	D				

270° (top)   180° (left)   0° (right, row H)   90° (bottom)

T = THERMOCOUPLE (50 LOCATIONS)
D = MOVABLE INCORE DETECTOR (58 LOCATIONS)
(DETECTOR LOCATIONS MAY BE CAPPED AND
REMOVED FROM SERVICE BASED ON DEGRADATION)

FIGURE 4.4–11 ICC FUNCTIONAL BLOCK DIAGRAM (TRAIN A-TRAIN B SIMILAR)
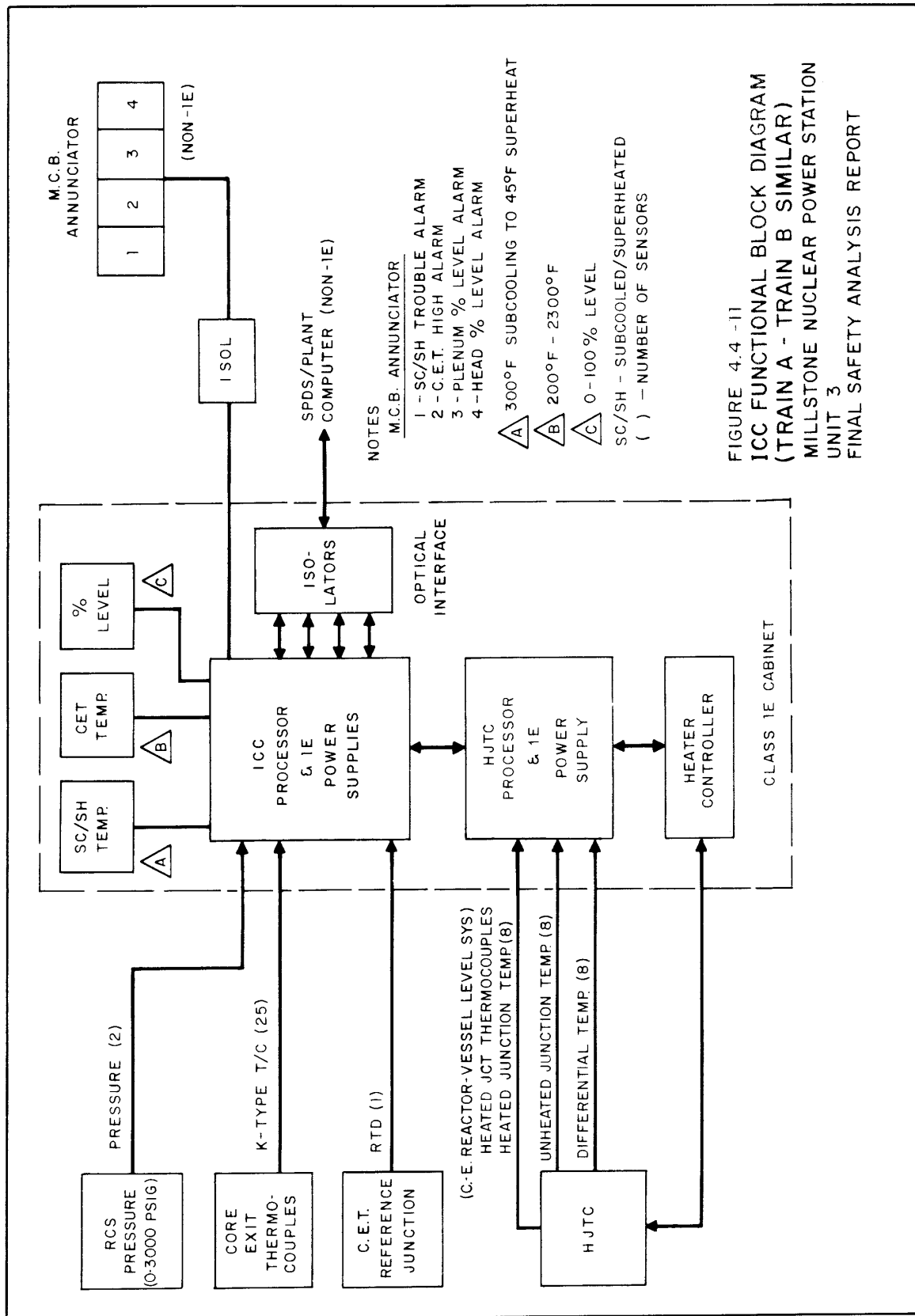
FIGURE 4.4-11
ICC FUNCTIONAL BLOCK DIAGRAM
(TRAIN A - TRAIN B SIMILAR)
MILLSTONE NUCLEAR POWER STATION
UNIT 3
FINAL SAFETY ANALYSIS REPORT

FIGURE 4.4–12 TYPICAL REACTOR COOLANT PARAMETERS FOLLOWING SMALL BREAK LOCA

USEFUL OPERATING RANGE OF C-E ICC MONITORING INSTRUMENTS*
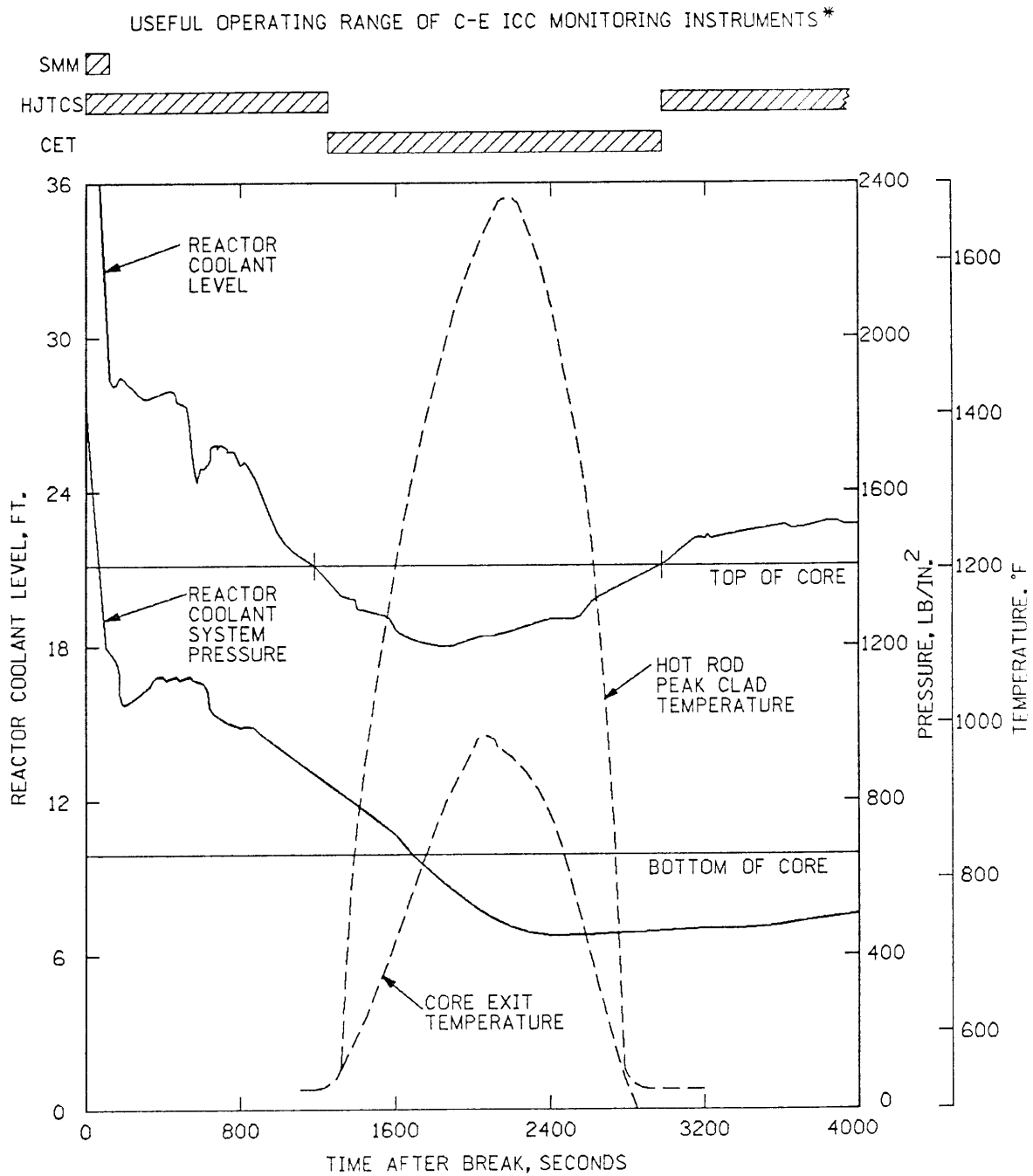
*SMM - SUBCOOLED MARGIN MONITOR
HJTCS - HEATED JUNCTION THERMOCOUPLE SYSTEM
CET - CORE EXIT THERMOCOUPLE

FIGURE 4.4-12
TYPICAL REACTOR COOLANT PARAMETERS
FOLLOWING SMALL BREAK LOCA
MILLSTONE NUCLEAR POWER STATION
UNIT 3
FINAL SAFETY ANALYSIS REPORT
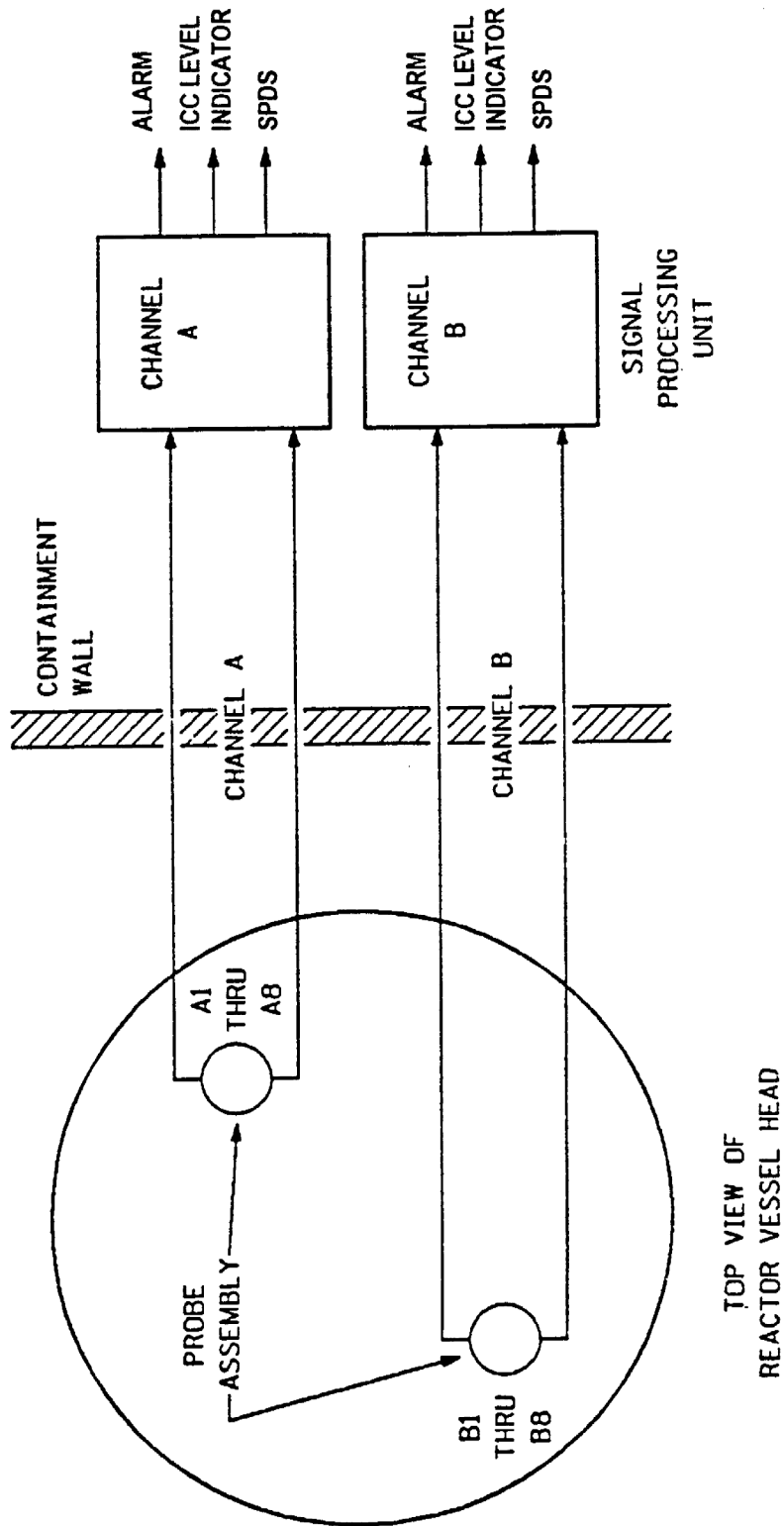
FIGURE 4.4–13 HJTCS FUNCTIONAL CONFIGURATION

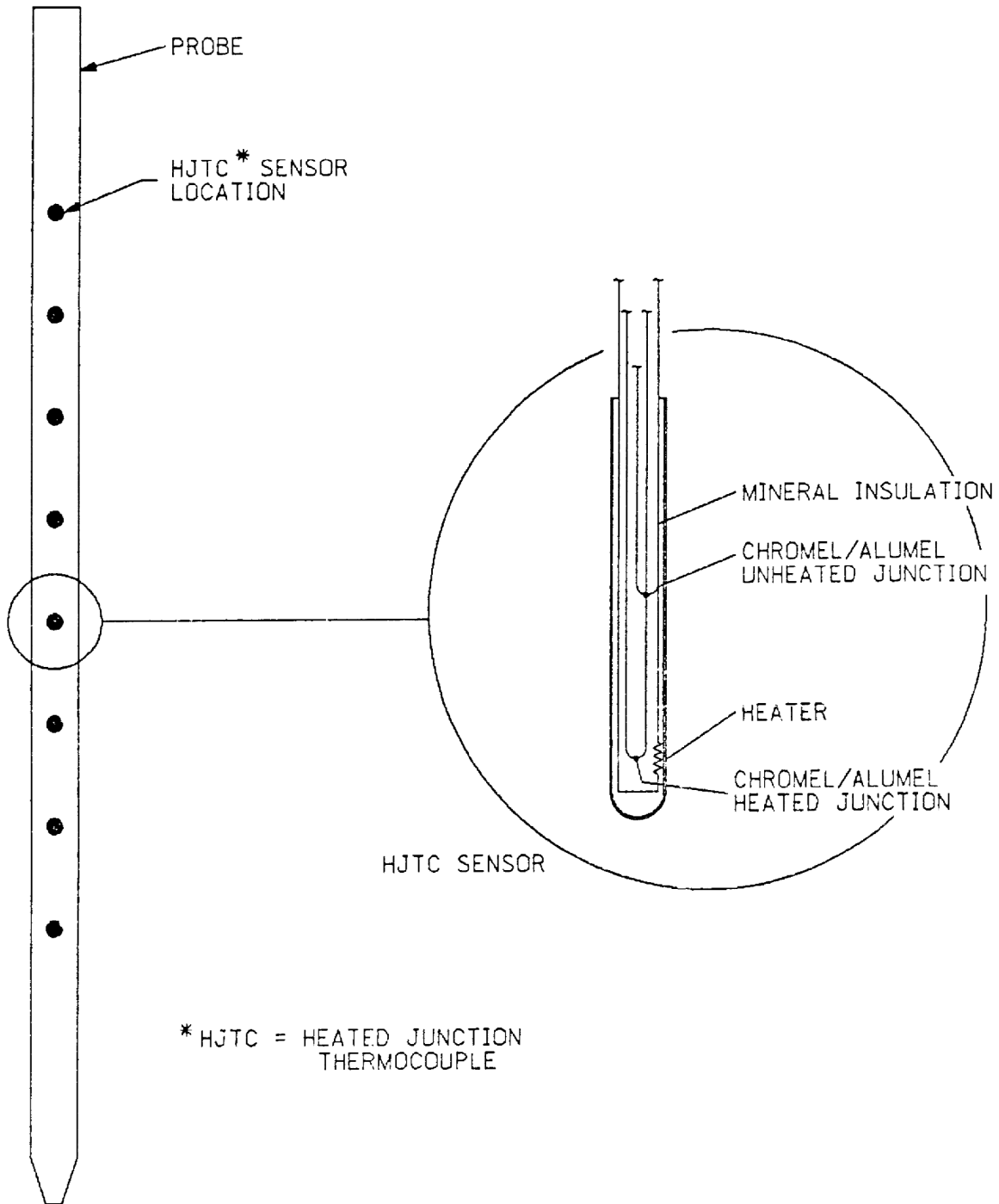# FIGURE 4.4–14 TYPICAL PROBE/SENSOR CONFIGURATION

FIGURE 4.4–15 HJTC SENSOR - HJTC/SPLASH SHIELD

REFERENCE
T/C LOCATION

HEATER
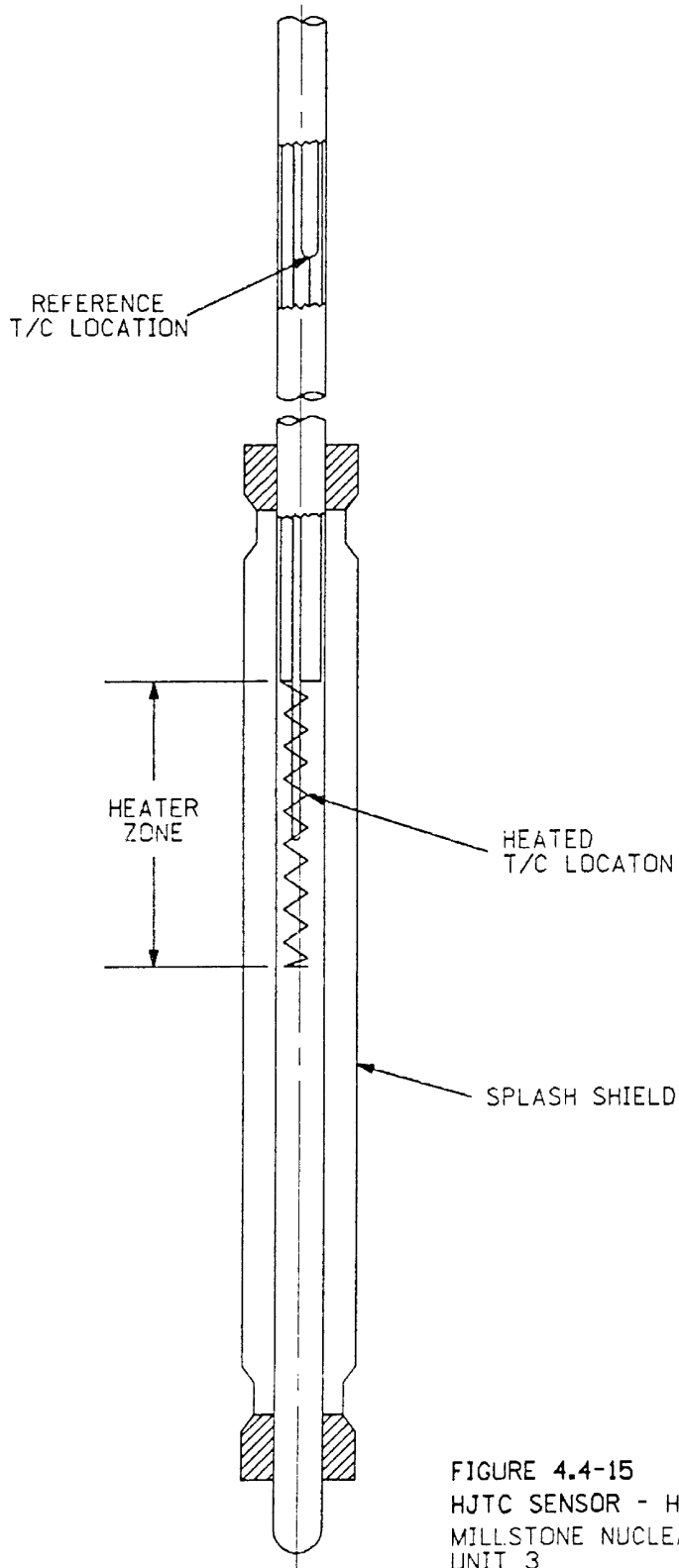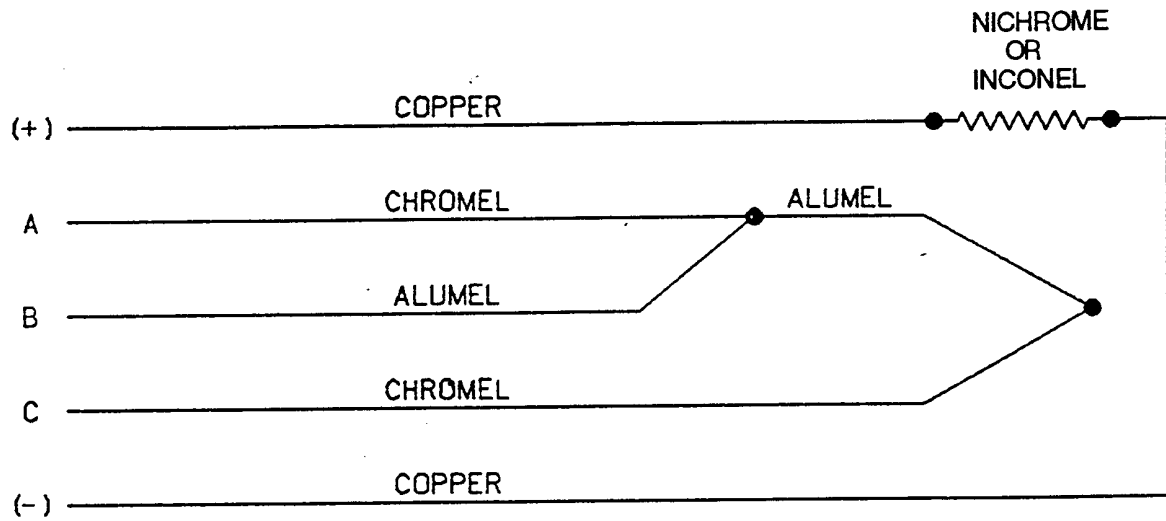ZONE

HEATED
T/C LOCATON

SPLASH SHIELD

FIGURE 4.4-15
HJTC SENSOR - HJTC/SPLASH SHIELD
MILLSTONE NUCLEAR POWER STATION
UNIT 3
FINAL SAFETY ANALYSIS REPORT

FIGURE 4.4–16 ELECTRICAL DIAGRAM OF HJTC


```
V( A - B )= ABSOLUTE TEMPERATURE, UNHEATED JUNCTION
V( C - B )= ABSOLUTE TEMPERATURE, HEATED JUNCTION
V( A - C )= DIFFERENTIAL TEMPERATURE
```
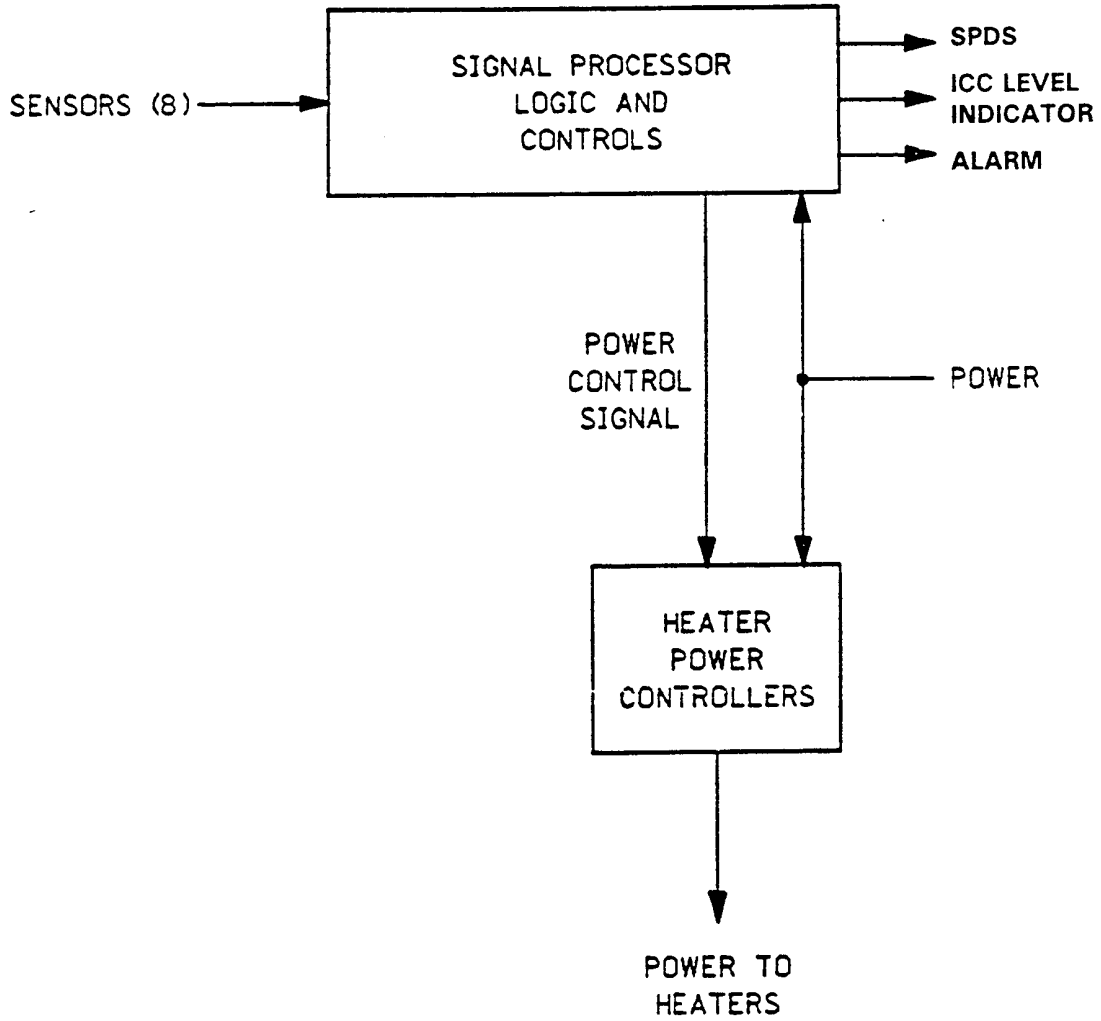
FIGURE 4.4–17 TYPICAL CONFIGURATION (ONE CHANNEL)

SENSORS (8) ──────▶ SIGNAL PROCESSOR LOGIC AND CONTROLS

──▶ SPDS

──▶ ICC LEVEL INDICATOR

──▶ ALARM

POWER CONTROL SIGNAL

POWER

HEATER POWER CONTROLLERS

POWER TO HEATERS

FIGURE 4.4–18 HEATED JUNCTION THERMOCOUPLE PROBE ASSEMBLY

ELECTRICAL CONNECTORS
(ONE PER SENSOR)

SEAL PLUG

SEPARATOR TUBE

HJTC SENSOR
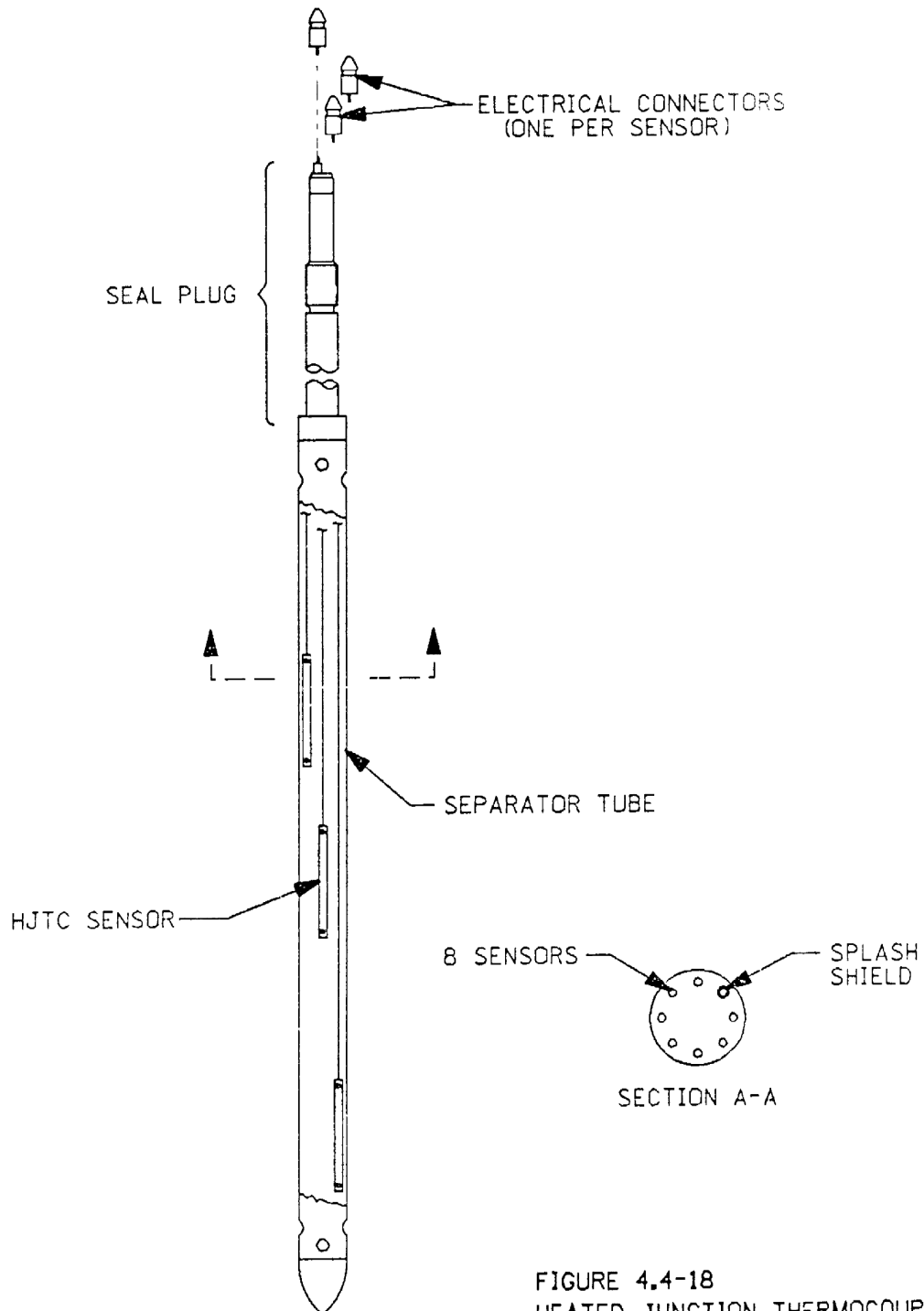
8 SENSORS — SPLASH SHIELD

SECTION A-A

FIGURE 4.4-18
HEATED JUNCTION THERMOCOUPLE
PROBE ASSEMBLY
MILLSTONE NUCLEAR POWER STATION
UNIT 3
FINAL SAFETY ANALYSIS REPORT

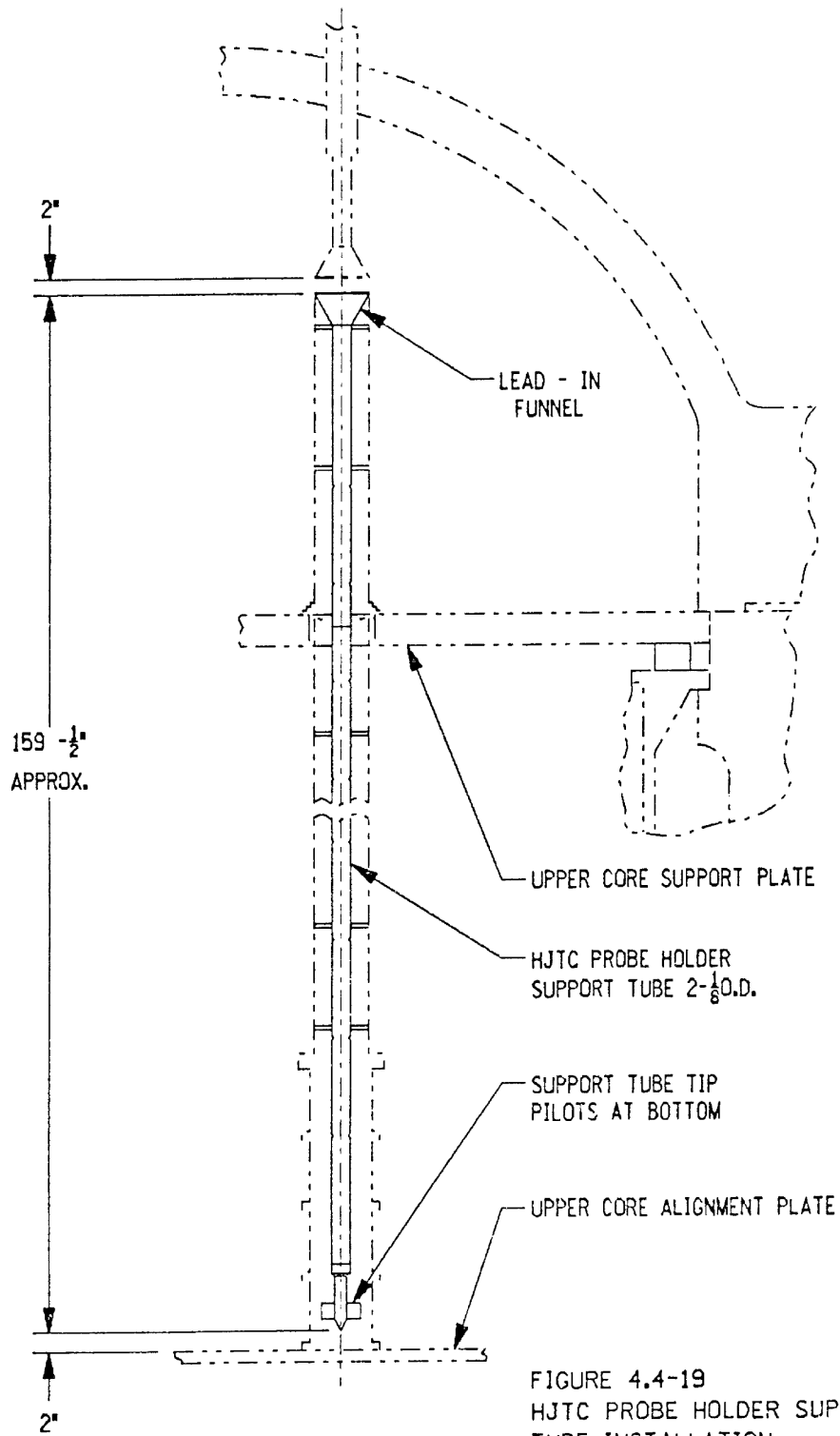# FIGURE 4.4–19 HJTC PROBE HOLDER SUPPORT TUBE INSTALLATION

FIGURE 4.4-19
HJTC PROBE HOLDER SUPPORT
TUBE INSTALLATION
MILLSTONE NUCLEAR POWER STATION
UNIT 3
FINAL SAFETY ANALYSIS REPORT

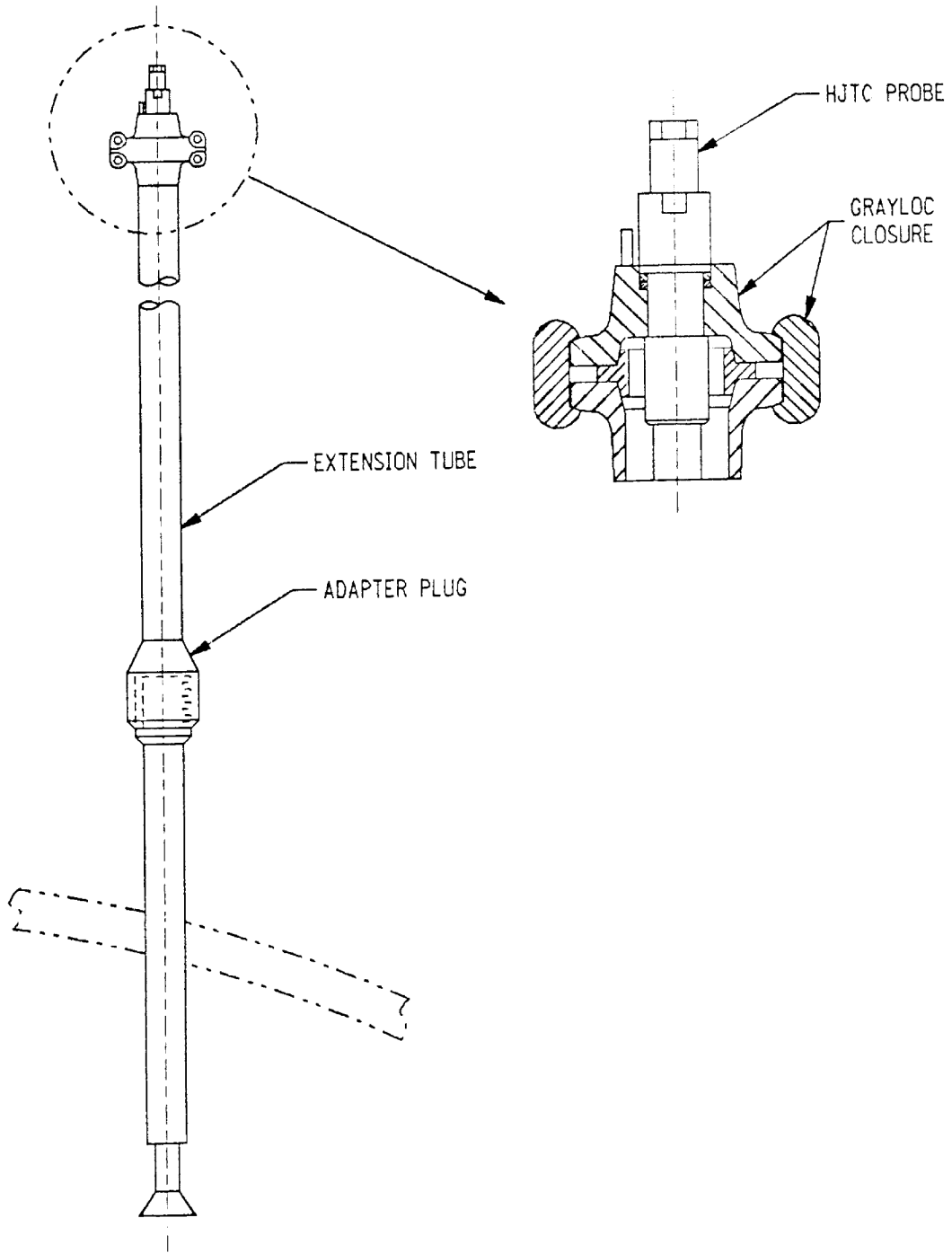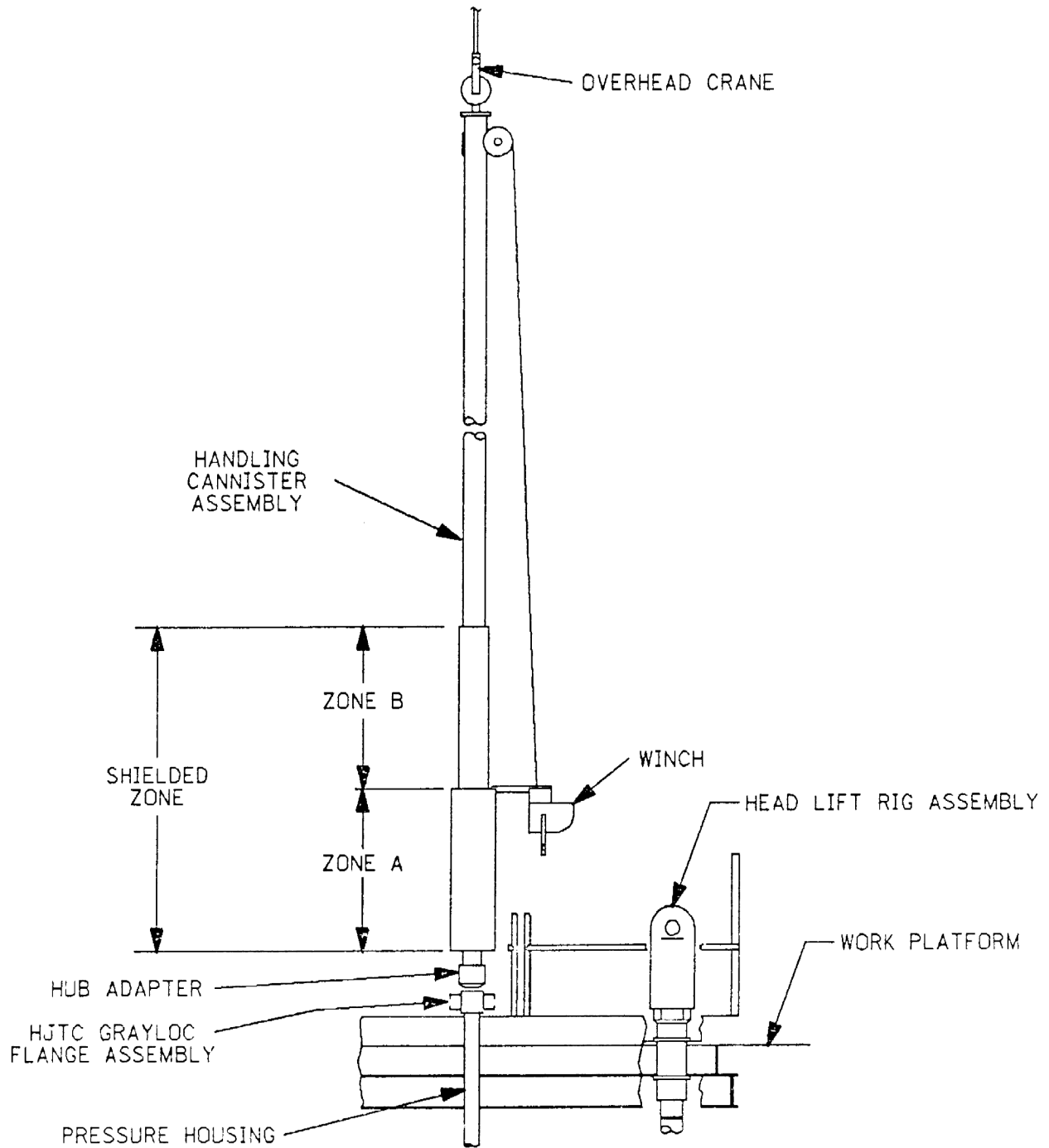## FIGURE 4.4–20 HJTC PROBE PRESSURE BOUNDARY INSTALLATION

FIGURE 4.4–21 PROBE HANDLING HARDWARE CONFIGURATION

4.5   REACTOR MATERIALS

Section 4.5 provides a discussion of the materials employed in the control rod drive system (CRDS) and for the reactor internals.

A more detailed evaluation of the reactor internals and reactivity control systems indicating the degree of conformance with the recommendations of the applicable Regulatory Guides is presented in Section 1.8:

4.5.1   CONTROL ROD SYSTEM STRUCTURAL MATERIALS

4.5.1.1   Materials Specifications

All parts exposed to reactor coolant are made of metals which resist the corrosive action of the borated water. Three types of metals are used exclusively: Stainless steels, nickel-chromium-iron, and cobalt-based alloys. In the case of stainless steels, only austenitic and martensitic stainless steels are used. For pressure boundary parts, martensitic stainless steels are not used in the heat treated conditions which cause susceptibility to stress corrosion cracking or accelerated corrosion in the Westinghouse pressurized water reactor water chemistry.

<u>Pressure boundary</u>

All pressure retaining materials comply with Section III of the ASME Boiler and Pressure Vessel Code, and are fabricated from austenitic (300 series) stainless steel and Nickel-Chromium-Iron alloys.

<u>Coil stack assembly</u>

The coil housings require magnetic material. Both low carbon cast steel and ductile iron have been successfully tested for this application. On the basis of performance, ductile iron was selected for the control rod drive mechanism (CRDM). The finished housings are zinc plated or flame sprayed to provide corrosion resistance.

Coils are wound on bobbins of glass reinforced silicon thermoset molding material, with double glass-insulated copper wire. Coils are then vacuum impregnated with silicon resin. A wrapping of mica sheet is secured to the coil outside diameter. The result is a well-insulated coil capable of sustained operation at 200°C.

<u>Latch assembly</u>

Magnetic pole pieces are fabricated from Type 410 stainless steel. All nonmagnetic parts, except pins and springs, are fabricated from Type 304 stainless steel. Haynes 25 is used to fabricate link pins. Springs are made from nickel-chromium-iron alloy (Inconel 750). Latch arm tips are clad with Stellite-6 to provide improved wearability. Hard chrome plate and Stellite-6 are used selectively for bearing and wear surfaces.

Drive rod assembly

The drive rod assembly utilizes a Type 410 stainless steel drive rod and Type 304 stainless steel disconnect rod assembly. The coupling is machined from Type 403 stainless steel. Other parts are Type 304 stainless steel with the exception of the springs, which are nickel-chromium-iron alloy, and the locking button, which is Haynes 25.

Material specifications for Class 1 components of the CRDM are as follows:

CRDM, upper head	SB-167 and SA-182, Grade F304
Latch housing	SA-182, Grade F304 or SA-351, Grade CF8
Rod travel housing	SA-182, Grade F304 or SA-336, Class F8
Cap	SA-479, Type 304

Welding materials EWth-2, ERN:Cr-3; and EN:CrFe-3

4.5.1.2   Austenitic Stainless Steel Components

Controls

All austenitic stainless steel materials used in the fabrication of CRDM components are processed, inspected, and tested to avoid sensitization and prevent intergranular stress corrosion cracking.

The rules covering these controls are stipulated in Westinghouse process specifications. As applicable, these process specifications supplement the equipment specifications and purchase order requirements of every individual austenitic stainless steel component regardless of the ASME Code Classification.

Westinghouse practice is that austenitic stainless steel materials of product forms with simple shapes need not be corrosion tested provided that the solution heat treatment is followed by water quenching. Simple shapes are defined as all plates, sheets, bars, pipe and tubes, as well as forgings, fittings and other shaped products which do not have inaccessible cavities or chambers that would preclude rapid cooling when water quenched. When testing is required, the tests are performed in accordance with ASTM A 262, Practice A or E, as amended by Westinghouse Process Specification 84201 MW.

If, during the course of fabrication, the steel is inadvertently exposed to the sensitization temperature range (800 to 1,500°F), the material may be tested in accordance with ASTM A 262, as amended by Westinghouse Process Specification 84201 MW to verify that it is not susceptible to intergranular attack, except that testing is not required for:

1.   Cast metal or weld metal with a ferrite content of 5 percent or more

2. Material with carbon content of 0.03 percent or less that is subjected to temperatures in the range of 800 to 1,500°F for less than 1 hour

3. Material exposed to special processing provided the processing is properly controlled to develop a uniform product and provided that adequate documentation exists of service experience and/or test data to demonstrate that the processing will not result in increased susceptibility to intergranular stress corrosion.

   If it is not verified that such material is not susceptible to intergranular attack, the material will be resolution annealed and water quenched or rejected.

Welding

The welding of austenitic stainless steel is controlled to mitigate the occurrence of microfissuring or hot cracking in the weld.

Available data indicates that a minimum delta ferrite level expressed in ferrite number (FN), above which the weld metals commonly used by Westinghouse are not prone to hot cracking, lies somewhere between O FN and 3 FN. The undiluted weld deposits of the starting welding materials are required to contain a minimum of 5 FN.

4.5.1.3   Other Materials

The CRDMs are cleaned prior to delivery in accordance with the guidance of ANSI N45.2.2 edition in effect at time of manufacture. Westinghouse personnel do conduct surveillance to ensure that manufacturers and installers adhere to appropriate requirements.

Haynes 25 is used in small quantities to fabricate link pins. The material is ordered in the solution treated and cold-worked condition. Stress corrosion cracking has not been observed in this application over the last 35 years.

The CRDM springs are made from nickel-chromium-iron alloy (Inconel 750) ordered to MIL-S-23192 Class A and D drawn wire. Operating experience has shown that springs made of this material are not subject to stress-corrosion cracking.

4.5.1.4   Cleaning and Cleanliness Control

The CRDMs are cleaned prior to delivery in accordance with the guidance of ANSI N45.2.2 edition in effect at time of manufacture. Measures are taken, as appropriate, to apply packaging requirements to procurement orders, to review supplier packaging procedures, to apply proper cleaning requirements, marking and identification and to provide protection to equipment from physical or weather damage, to apply special handling precautions and to define storage requirements. Westinghouse Energy Systems Business Unit quality assurance procedures are described in the "ESBU Quality Management System."

4.5.2   REACTOR INTERNALS MATERIALS

4.5.2.1   Materials Specifications

All the major material for the reactor internals is Type 304 stainless steel. Parts not fabricated from Type 304 stainless steel include bolts and dowel pins, which are fabricated from Type 316 stainless steel, and reactor vessel clevis insert bolts, and dowel pins which are fabricated from Inconel 750.

Material specifications for reactor vessel internals for emergency core cooling systems are shown in Table 5.2–3.

There are no other materials used in the reactor internals or core support structures which are not otherwise supplied to the intent of the ASME Code, Section III, Appendix I.

4.5.2.2   Controls on Welding

The discussions provided in Section 4.5.1 are applicable to the welding of reactor internals and core support components.

4.5.2.3   Nondestructive Examination of Wrought Seamless Tubular Products and Fittings

The nondestructive examination of pressure retaining wrought seamless tubular products and fittings is in accordance with Section III of the ASME Code.

4.5.2.4   Fabrication and Processing of Austenitic Stainless Steel Components

Cleaning of reactor internals and core support structures is in accordance with ANSI 45.2.2 edition in effect at time of manufacture.

4.6   FUNCTIONAL DESIGN OF REACTIVITY CONTROL SYSTEMS

4.6.1   INFORMATION FOR CONTROL ROD DRIVE SYSTEM (CRDS)

The CRDS includes the Control Rod Drive mechanisms (CRDMs) discussed in Section 3.9N.4.1, the Rod Control System discussed in Section 7.7.1.2 and the Reactor Trip Switchgear discussed in Section 7.2.1.1.

Figure 4.2–8 provides the layout of CRDS. The CRDS is a magnetically operated jack with no hydraulic system associated with its functioning. The CRDM consists of four separate subassemblies.

1.   The pressure vessel which includes the latch housing and rod travel housings

2.   The coil stack assembly which includes three operating coils: stationary gripper coil, movable gripper coil, and lift coil

3.   The latch assembly which includes the guide tube, the stationary and the movable pole pieces, and the stationary and movable gripper latches

4.   The drive rod assembly which includes the coupling system and the drive rod Rod Cluster Control Assembly (RCCA)

4.6.2   EVALUATION OF THE CRDS

The CRDS has been analyzed in detail in a failure mode and effects analysis in WCAP-8976. Changes to the results of this analysis to account for timing changes to the Rod Control System are described in WCAP-13864. These studies and the analyses presented in Chapter 15.0, demonstrate that the CRDS performs its intended safety function, reactor trip, by putting the reactor in a subcritical condition when a safety system setting is approached, with any assumed credible failure of a single active component. The essential elements of the CRDS (those required to ensure reactor trip) are isolated from nonessential portions of the CRDS (the Rod Control System).

Despite the extremely low probability of a common mode failure impairing the ability of the reactor trip system to perform its safety function, analyses have been performed in accordance with the requirements of WASH-1270. These analyses, documented in WCAP-7706-L and WCAP-8330 (1977), have demonstrated that acceptable safety criteria would not be exceeded even if the CRDS were rendered incapable of functioning during a reactor transient for which their function would normally be expected.

The design of the control rod drive mechanism is such that failure of the control rod drive mechanism cooling system will, in the worst case, result in an individual control rod drop or a full reactor trip.

4.6.3   TESTING AND VERIFICATION OF THE CRDS

The CRDS is extensively tested prior to its operation. These tests may be subdivided into five categories: (1) prototype tests of components, (2) prototype CRDS tests, (3) production tests of components following manufacture and prior to installation, (4) onsite preoperational and, (5) initial startup tests. In addition, the CRDS is subject to periodic inservice tests. These tests which are described in Sections 3.9N.4.4, 4.2, and 14.2, and 16.3/4.1.3 (of the Technical Specifications) are conducted to verify the operability of the CRDS when called upon to function.

4.6.4   INFORMATION FOR COMBINED PERFORMANCE OF REACTIVITY SYSTEMS

As is indicated in Chapter 15, the only postulated events which assume credit for reactivity control systems other than a reactor trip to render the plant subcritical are the steam line break, feedwater line break, and loss-of-coolant accident. The reactivity control systems for which credit is taken in these accidents are the reactor trip system and the safety injection system (SIS). Note that no credit is taken for the boration capabilities of the chemical and volume control system (CVCS) as a system in the analysis of transients presented in Chapter 15. The adverse boron dilution possibilities due to the operation of the CVCS are investigated in Chapter 15. Prior proper operation of the CVCS has been presumed as an initial condition to evaluate transients, and appropriate technical specifications have been prepared to ensure the correct operation or remedial action.

4.6.5   EVALUATION OF COMBINED PERFORMANCE

The evaluations of the steam line break, feedwater line break, and the loss-of-coolant accident, which presume the combined actuation of the reactor trip system to the CRDS and the SIS, are presented in Chapter 15. Reactor trip signals and safety injection signals for these events are generated from functionally independent and diverse sensors and actuate diverse means of reactivity control, i.e., control rod insertion or injection of soluble poison.

Nondiverse but redundant types of equipment are utilized only in the processing of the incoming sensor signals into the Solid State Protection System logic, which initiates the appropriate protective action. In particular, note that protection from equipment failures is provided by redundant equipment and periodic testing. Effects of failures of this equipment have been extensively investigated as reported in WCAP-8330 Westinghouse letter NS-TMA-2182 to the NRC and WCAP-8584. The failure mode and effects analyses described in these references verify that any single failure will not have a deleterious effect on the engineered safety features actuation system.

4.6.6   REFERENCES FOR SECTION 4.6

4.6-1   WCAP-7706-L (Proprietary) and WCAP-7706 (Nonproprietary), July 1971, Gangloff, W.C. and Loftus, W.D., "An Evaluation of Solid State Logic Reactor Protection in Anticipated Transients."

4.6-2   WCAP-8330, Salvatore, R., August 1974. "Westinghouse Anticipated Transients Without Trip Analysis."

4.6-3   WCAP-8584 (Proprietary) and WCAP-8760 (Nonproprietary), April 1976, Eggleston, F.T., Rawlins, D.H. and Petrow, J.R., "Failure Mode and Effects Analysis (FMEA) of the Engineering Safeguard Features Actuation System," and Revision 1, February 1980, Mesneringer, J. C.

4.6-4   WCAP-8976, August 1977, Shopsky, W.E., "Failure Mode and Effects Analysis (FMEA) of the Solid State Full Length Rod Control System."

4.6-5   WCAP-13864, September 1993. Baker T., "Rod Control System Evaluation Program" and Revision 1A, November 1994.

4.6-6   Anderson, T. M., "ATWS Submittal," Westinghouse letter NS-TMA-2182 to S. H. Hanauer of the NRC, December 1979.